University of Stavanger

Faculty of Science and Technology

MASTER'S THESIS

Study program/ Specialization: Petroleum Engineering/Drilling Technology	Spring semester, 2016 Open
Writer: Stanislaw Wrobel	…… (Writer's signature)
Faculty supervisor: Mesfin Belayneh	
Thesis title: **Development of an improved Nanoparticle-modified Water Based Drilling Fluid**	
Credits (ECTS): 30	
Key words: WBM, Nanoparticles, Rheology, Friction, Simulations, Experimental	Pages: 127 (+ 45 enclosure) Stavanger, 15.06.2016

Acknowledgements

I like to express my deepest gratitude and appreciation to Mesfin Belayneh Agonafir for allocating this very interesting subject to me. His guidance, enthusiasm, encouragement and advice have supported me in the understanding of this subject. His contribution to the success of this work has been inevitable. I could never have made it to see the day that I finish my thesis, without his support.

Additionally, I would like to thank my family and my friends for supporting me in every endeavor.

Stavanger, June 2016

Stanislaw Wrobel

Abstract

The objective was to improve conventional water based drilling fluid systems by the addition of nanoparticles. Experiments were conducted to evaluate whether addition of nanoparticles to the drilling fluid could improve rheological, lubricating, viscoelastic and filtrate loss properties. The rheological properties were measured using av Fanning-VG viscometer. The lubricating properties of the fluid were determined through friction coefficient measurements using a CSM DIN 50324 Tribometer at varying temperatures, while filtrate loss was measured using standard API filtrate loss test setup. The tested nanoparticle additives were MoS_2, Graphene, TiO_2 and TiN.

The results show that nanoparticle additives to the drilling fluid can improve the rheological properties. Addition of 0.1 g MoS_2 per 500 ml at ambient temperature, improved the Bingham Yield Strength (YS) of the drilling fluid by 183 % relative to the reference fluid. Similar experiments with higher concentration in the range of 0.2 g to 0.4 g per 500 mL, showed that increasing the nanoparticle concentration leads to a reduction in Bingham YS at ambient temperature. The same added concentrations showed that Graphene, TiO_2 and TiN did not have a significant impact on the fluid rheological properties. Nanoparticle composition and size may therefore impact the potential for drilling property improvement.

In terms of lubricating properties, the experiments show that nanoparticles can improve the lubricity of the drilling fluid by reducing the friction coefficient. MoS_2 showed a reduction in friction coefficient of up to 53 %, while Graphene modified fluid systems showed up to 56 % reduction. TiO_2 and TiN did not show lubricating effects, in some cases increasing the friction coefficient of the drilling fluid. Experiments at temperatures ranging from 20-70 °C showed that MoS_2 and Graphene yield improved lubricity at all tested temperatures.

Based on experimental results Hydraulic, Cuttings transport and Torque & Drag simulations were conducted. Simulations suggested that 0.4g MoS_2 added to the drilling fluid could reduce the bed height by 45%, improving cuttings transport capacity significantly. Torque & drag simulations suggest that the improved lubricity of graphene and MoS_2 addition could extend drilling reach by as much as 26.3%.

1 Table of Contents

1 Introduction

This thesis presents the effect of different Nanoparticles in conventional (nano-free) bentonite drilling fluid. The reference fluid (nano-free) is prepared with bentonite clay, polymers (carboxymethyl cellulose (CMC), polyanionic cellulose (PAC) and Xanthan Gum(XG)) and KCl salt. The primary objective of the study was to formulate a nano-modified drilling fluid with enhanced parameters. The evaluation of the fluid systems was through experimental and simulation studies. For the characterization of the fluid systems, their rheology, filtrate volume, viscoelasticity, and tribology attributes were measured.

The best fluid systems have been selected based on rheological and tribological properties and their performances have been evaluated through simulation studies. These are hydraulics, cuttings transport and torque & drag.

1.1 Background

A drilling operation is about connecting the surface environment with a reservoir with the objective to gain access hydrocarbons. For this, the drilling fluid plays many important roles. The main function of drilling fluid among many others is to lift cuttings, maintain well pressure and cool the bit.

If drilling fluid is not appropriately designed, several drilling problems could occur, which cost the oil industry a lot.

The static mud density and the friction loss when circulating determine the circulation mud density, (i.e equivalent circulation density, ECD), which is a function of rheology and density of drilling fluid.

Equivalent circulating density is determined by [1]

$$ECD = \rho_{st} + \frac{\Delta P_{annulus}}{0.052.TVD} \tag{1.1}$$

Where:

ρ_{st} - Static mud weight [ppg]

$\Delta P_{annulus}$ - Pressure loss in the annulus [psi]

TVD - True vertical depth [ft]

When the well pressure is higher than the fracture strength of the formation, the formation fractures and that results in a huge mud loss. On the other hand, when the well pressure lower than the fracture collapse gradient, the borehole wall will collaps and formation will fall into the well. That can cause a pack-off and/or sticking of the drillstring. In a worset case scenario the drillstring has to be cut, milled and a sidetrack operation has to be conducted to continue drilling the well.

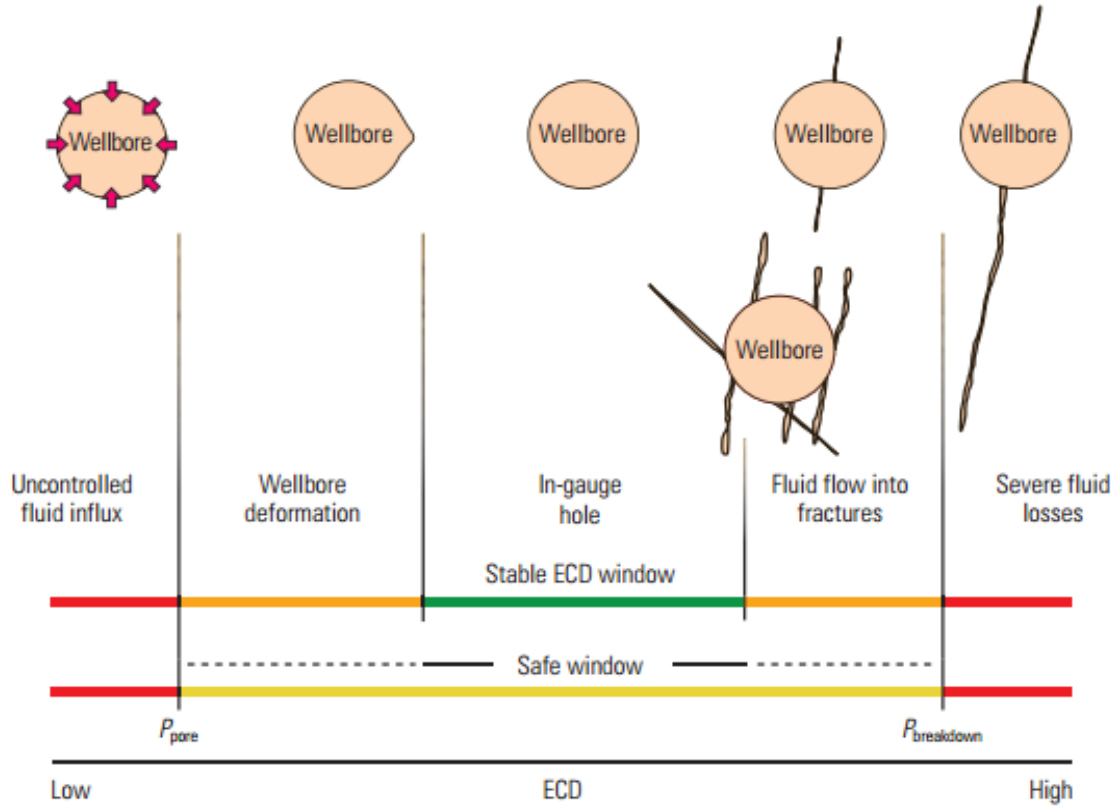

Figure 1-1 : Description of the ECD window [2]

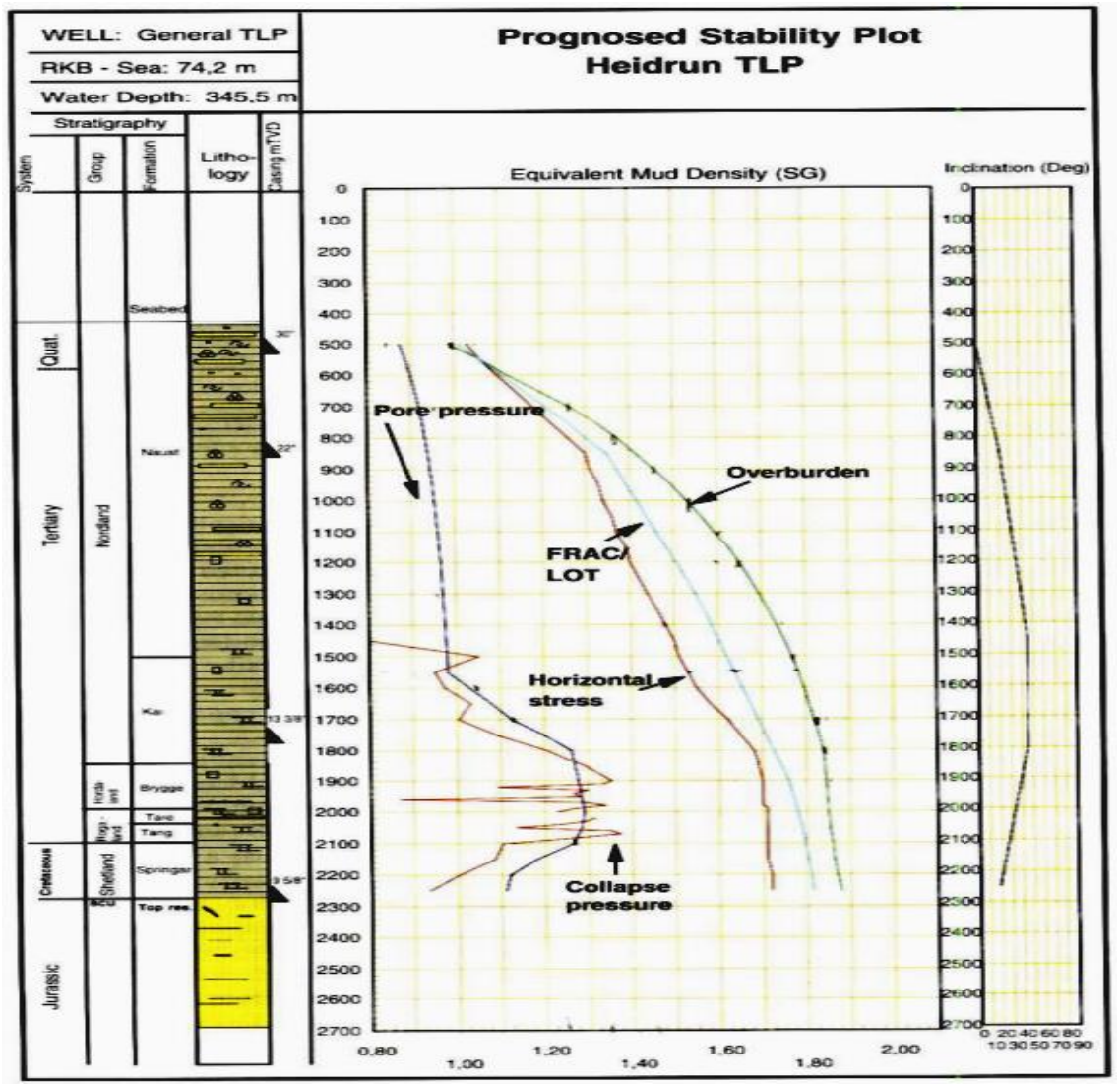

Figure 1-2 Prognosis stability plot for a typical Heidrun TLP well [3]

Recent research has shown that the addition of nano reduces the lubricity of drilling fluids. [4] In this thesis, several nano in drilling fluid will be investigated their degree of friction reduction. Oil based drilling fluids have lower lubricity relative to water based drilling fluid [5]. WBM is an ionic fluid and is naturally charged, which influences the lubrication property. Due to this reason water is by nature a less suitable lubricant. However, WBM is environmental friendly and cost effective. On the Norwegian continental shelf, the first top hole section are required to be drilled with WBM and it is commonly used as long as borehole conditions allow it. Therefore, it is of particular of interest to investigate and improve lubrication behavior of WBM, with the help of nanoparticles.

1.2 Problem definition

Oil based drilling fluid is better than water based mud systems in terms of higher lubricity and shale stability. However, in some cases (e.g. drilling top section) oil based drilling fluid systems are not allowed to be used in a country where environmental policy is very strict such as in Norway. The common practice is to change the drilling operation to water based drilling fluid. However, water based drilling fluids can not replace the oil based mud system and are less effective in terms of the mentioned parameters.

The application of nanomaterials have been documented in literature showing positive performance in drilling fluids, cement and enhanced oil recovery. [4] [6] [7]

This thesis addresses issues such as:

- The effect of different nanoparticles with different concentrations on conventional WBM in terms of rheology, viscoelasticity and lubricity
- Issues regarding pump pressure and ECD management
- Potential extended reach drilling by drilling fluid modification with nanoparticles
- Effect of different nanoparticles in terms of borehole cleaning

1.3 Objective

The primary objective of this thesis is to formulate nanoparticle-modified drilling fluids and characterize their properties through experimental work and simulation studies. The main activities are:

- Literature studies on the theory of rheology, hydraulics, and well friction model used to analyze the drilling fluids.
- Review of drilling fluid's chemical ingredients properties used for the formulation of a nanoparticle-modified drilling drilling fluid
- Characterization of the formulated drilling fluids through experimental evaluations
- Evaluation of the best formulated nanoparticle treated drilling fluids through simulation studies.

1.4 Methodology

The research methodology employed in the thesis is categorized in to two parts:

1. The first part investigates experimental measurement and modelling of measured results the measurement consists of rheology, filtrate loss, pH, lubricity and viscoelasticity of the formulated drilling fluids.
2. The second part will simulate the performance of best drilling fluids selected from part 1. The performance simulation studies the drilling fluids evaluated by simulating cutting transport, hydraulics and torque and drag in a well.

Figure 1-3 summarized the detail activities of the thesis work.

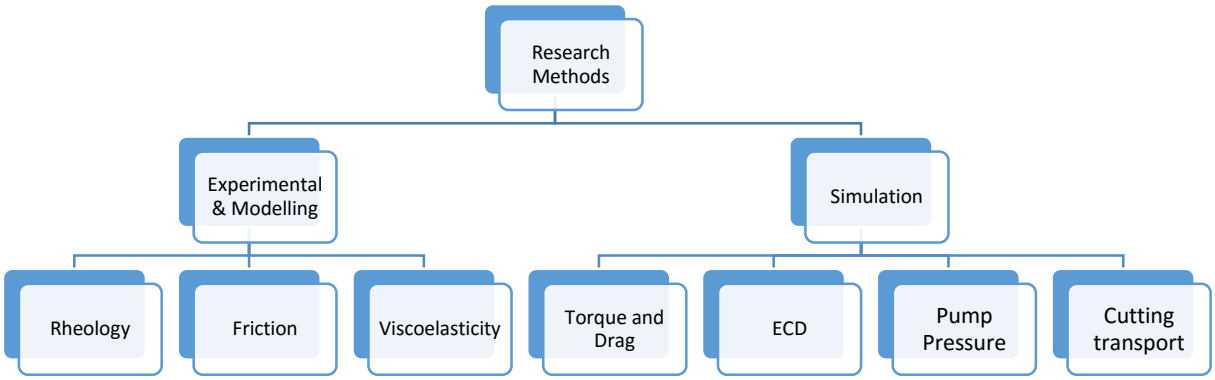

Figure 1-3 Overview of thesis methodology

2 Literature study

This chapter presents the description of the drilling fluid additives used for the formulation in chapter 4.

2.1 Loss of Circulation

Lost circulation is the loss of drilling fluid into drilling formation. The loss increases drilling cost directly and indirectly by increasing nonproductive time. The fluid loss into formation also damages the formation. [2]

As illustrated on Figure 2-1, lost circulation occurs in drilling formation through several means such as [8]

A. Unconsolidated or highly permeable formations (such as loose gravels)
B. Cavernous formations (crevices and channels)
C. Natural fractures
D. Drilling induced fractures

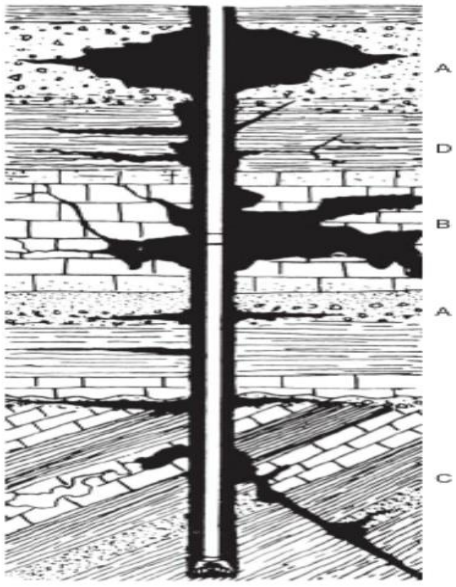

Figure 2-1 Lost circulation formations [18]

Depending on the degree and severity of loss, operators use loss circulation materials to cure huge mud loses. Among other Messenger has studied the performance of various loss circulation materials to gain control of loss circulation scenarios. [8]

Figure 2-2 illustrates the four strategies used to take prevention and remediation measures.

The prevention action comprises of three elements, namely:

- Best drilling practices
- Fluid selection having proper rheological properties
- Materials used for wellbore strengthening.

The remediation action is to use loss circulation material in order to cure or stop losses.

Experience showed that prevention of loss circulation occurrence is more beneficial than to stop/cure or reduce the problem once they already have occurred. [2].

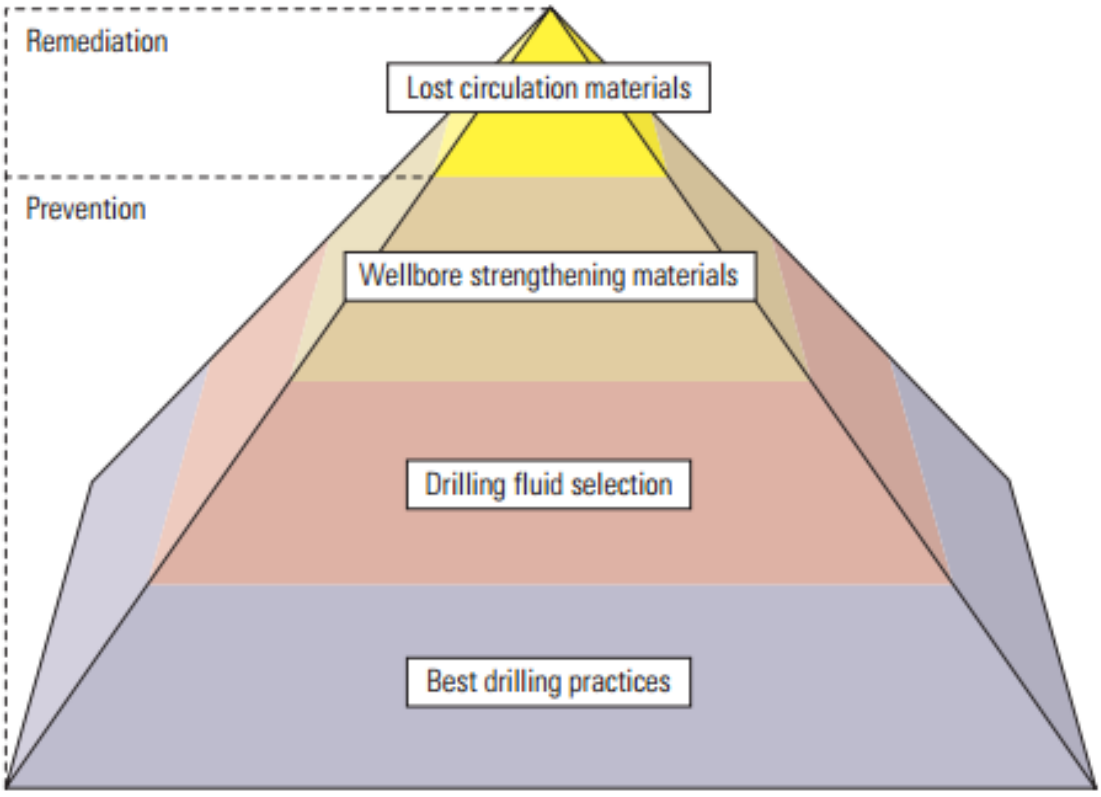

Figure 2-2 Four-tiered strategy consisting of both prevention and remediation measures for lost circulation [2]

2.2 Function, Characterization and Composition of Drilling Fluids

Drilling fluids are the essential part of drilling operation. Among several functions, it provides: [9].

- **Hole cleaning :** Drilling fluids lift cuttings from downhole all the way to the surface
- **Maintain well pressure:** Drilling fluids control well pressure in order to avoid well instability.
- **Buoyancy effect:** Drilling fluids reduce the hook load by reducing the effective weight of the submerged drillstring.
- **Lubricity :** Drilling fluids provide lubricity between the drill string and formations, reducing torque, drag and perhaps wear.
- **Cooling effect :** Drilling fluids cooling the drillbit and wellbore.
- **Well stability (chemical)** : Drilling fluids control the **shale swelling** effect if properly designed.
- **Medium for signal transfer** for real time measurements and/or logging data.

2.3 Filter cake-bridging process

As shown on Figure 2-3, drilling through formation may ended up with partial or heavy mud losses.

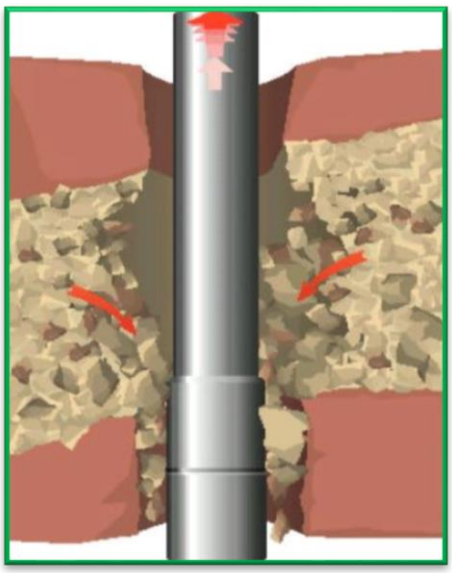

Figure 2-3 Sketch of loose formation

Properly designed drilling fluid forms a good mud cake and seals the pores spaces at the wall of the wellbore. This will reduce fluid seepage and hence reduces formation damage.

For instance, drilling through unconsolidated formation leads to wall fragments fall into the wellbore. To prevent this problem, drilling fluids should be designed which have good filter cake forming by being strong and low permeable type. These properties of the filter cake can stabilize the weak formation.

Figure 2-4 is also another problematic formation, which is reactive shale. Drilling through this formation with oil based mud or ‘’inhibitive’’ KCL treated water based mud are the best solutions for stability of shale swelling. However, the water base inhibitive drilling cannot completely solve swelling problems.

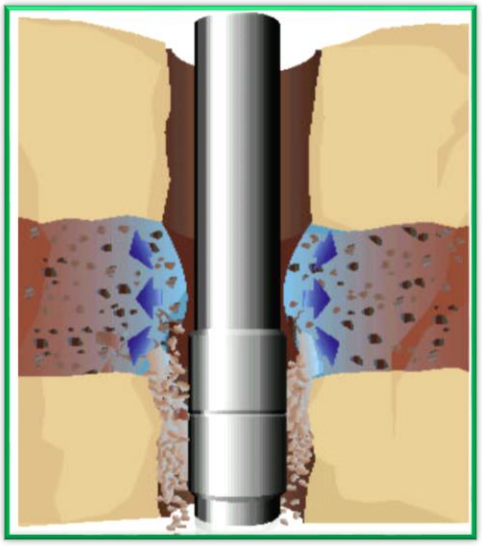

Figure 2-4 Sketch of reactive shale

In recent years, the application of nano on improving the filter cake property has shown a promising results for developing nano-fluid in water based system. This thesis also deals with the performance of nano in water based fluid.

Figure 2-5 shows the process of formation of filter cake. As shown, as mud fluid in the wellbore, particles and deposited at forming filter cake externally at the face of the wellbore and internally inside the pore spaces of the formation. During spur loss process, fine particles and chemicals also have been flushed into the invaded section of the wellbore. [10]

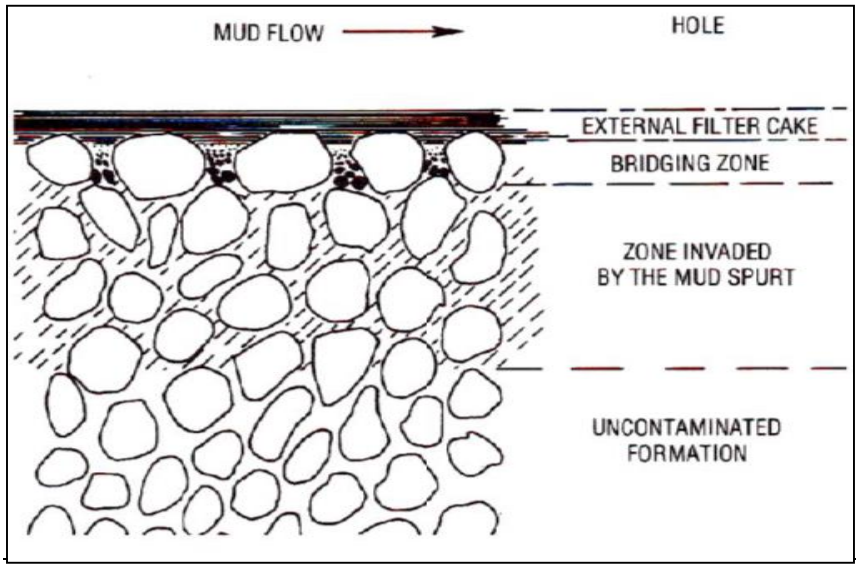

Figure 2-5 Mud cake formation and invasion of spurt loss through a permeable formation [10]

This shows the appropriately designed fluids system performance on reducing formation damage and improving mechanical strength of weak formation as well.

2.3.1 Components of water drilling fluids

This section presents the the description of chemical additives used to prepare drilling fluid in section 4. These are tap water, bentonite, KCl salt, polymers (CMC, Xanthan gum and PAC) and nano particles.

2.3.1.1 Fresh water

Tap water was used to prepare bentonite based drilling fluid. The chemistry of the tap water is not documented here since no data available.

2.3.1.2 Clays - Bentonite

Bentonite clay is used in drilling fluid to provide a desired viscosity. Structurally, the clay minerals are of a crystalline nature. Clays composed of tiny crystal platelets, normally stacked together. The unit layer is formed from an octahedral sheet and one or two silica tetrahedral sheets. The sheets tie together by covalent bonds, which are tied by Oxygen atoms. Figure 2-6 shows an illustration of clay crystal structure (montmorillonite). The spacing between the layers is an exchangeable cation and water. [11]

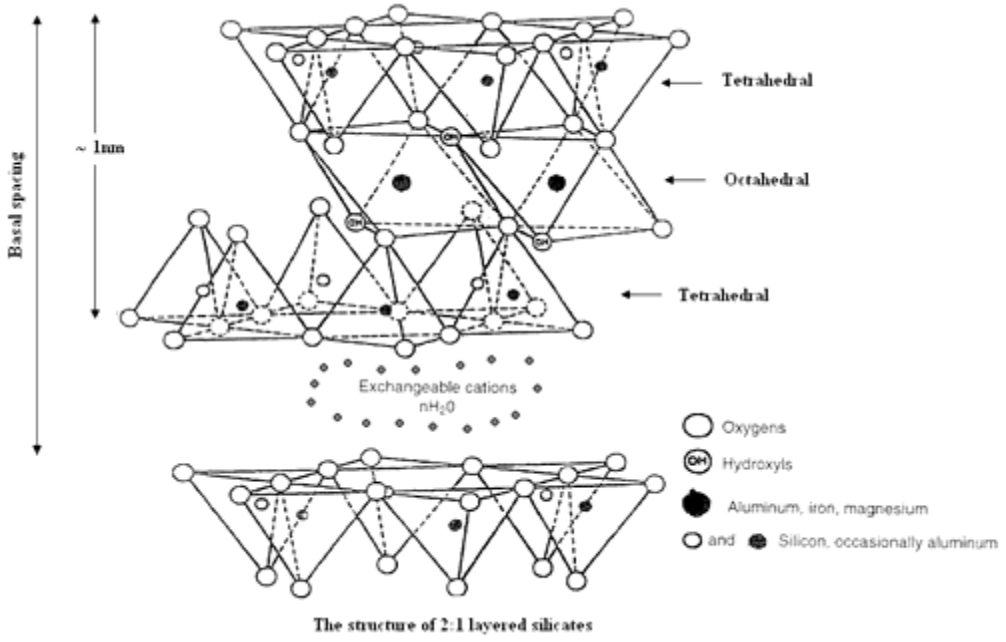

Figure 2-6 Illustration of montmorillonite layer structure [12]

2.3.1.3 Particle associations

The rheological properties and fluid losses behaviors are affected by the particle arrangement of clay. The particle arrangement in general are categorized into four and illustrated as in Figure 2-7.

Dispersed system

When the aggregated clay particles are break down, the particles exist in as single platelets. This system is known as a Dispersed system. The particle systems could be in a deflocculated and flocculated state and yet dispersed.

Flocculated system

This system describe the clay particles are connected, but exist in the form of loose structure. This system is due the positive change on the surface of clay, which allows to create a 3D network system. Flocculated systems result in a higher viscosity, yield strength and filter loss.

Deflocculated system

Due to the repulsive force between particles, the platelets the aggregated clay platelets will be separated as illustrated on Figure 2-7. The repulsion force is due to the same changes of the particles.

Aggregated system

As shown on Figure 2-7, the aggregate system is formed when the clay platelets are bounded together. The system could be in flocculated and deflocculated condition.

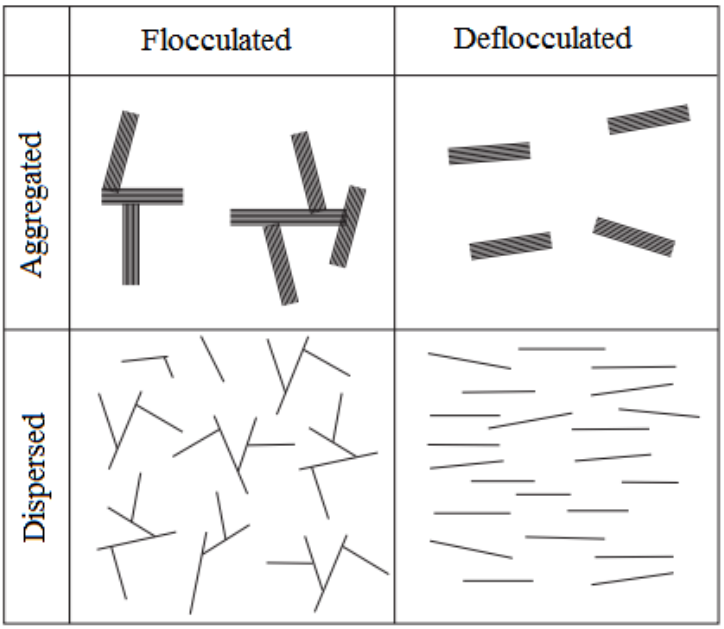

Figure 2-7 Arrangement of clay particles in drilling fluid

2.3.2 Polymers

Polymers are used in drilling fluid in order to control viscosity, and fluid loss. There are different types of polymer which are classified by their origin. Figure 2-8 illustrates the liner, branched and crosslinked structure of polymers. [13]

The three types of polymers were used in this thesis. They are:

- Carboxymethyl Cellulose Sodium (CMC),
- Polyanionic Cellulose (PAC)
- Xantham Gum, all are modified natural polymers.

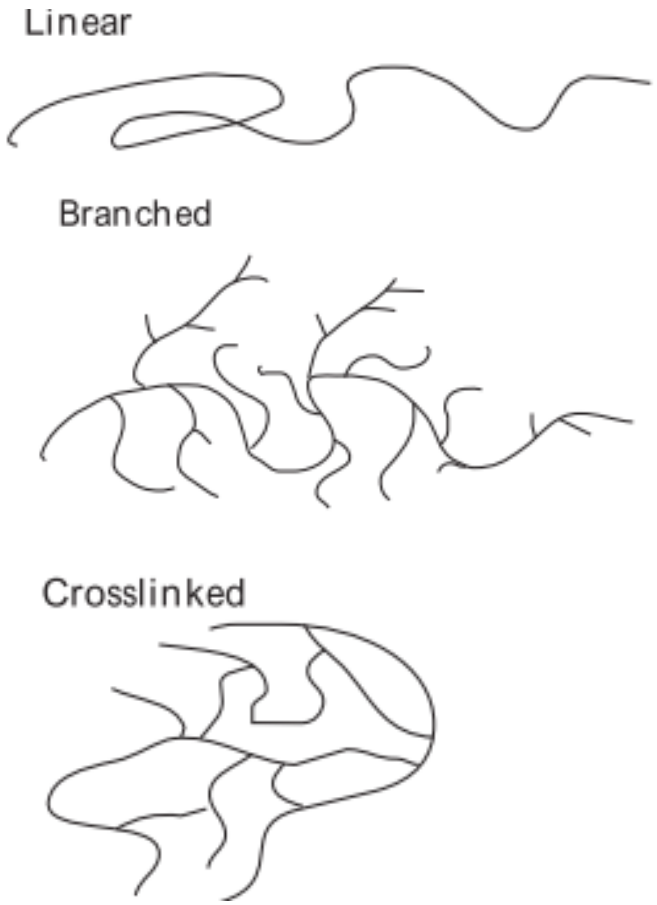

Figure 2-8 Polymers structures: linear, branched and crosslinked

2.3.2.1 Carboxymethyl Cellulose Sodium (CMC)

CMC is Carboxymethyl Cellulose Sodium derived by the reaction of sodium salt with cellulose. The structure is linear and polyaniuc. Figure 2-9 illustrate the CMC polymer As mentioned earlier, CMC is used as viscosity and fluid loss control additives. [14]

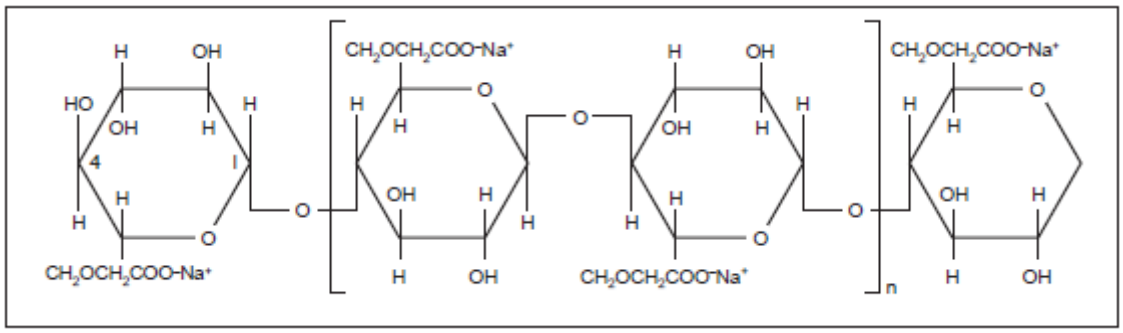

Figure 2-9 Structure of Sodium CMC [14]

2.3.3 Polyanionic Cellulose (PAC)

PAC is viewed upon as the modified version of CMC with lower viscosity. It has the same chemical formula as CMC, $[C_6H_7O_2(OH)_2CH_2COONa]_n$.

Like CMC; PAC is also used to control and filtrate. However, the performance of CMC and PAC in drilling fluids are different in terms of rheology. The difference is due to the uniformity of the substitution along the chain. [15]

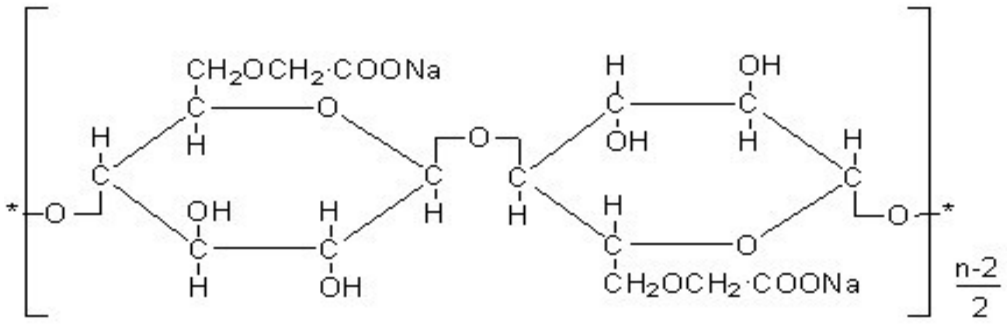

Figure 2-10 Structure of PAC [16]

2.3.4 KCl

Salt are used in WBMs for shale swelling control. Potassium chloride salt is used in drilling fluid to drill water sensitive shales. The K^+ ions are attracted to the surface of clay and this allows shale stability by inhibition of shale swelling and disintegration [17] [1]

Figure 2-11 illustrates the effect of salt on CMC. As shown the addition salt has a capacity to break down the CMC chains into smaller pieces. For the stability, it is important to optimize the right amount of salt additive. [15]

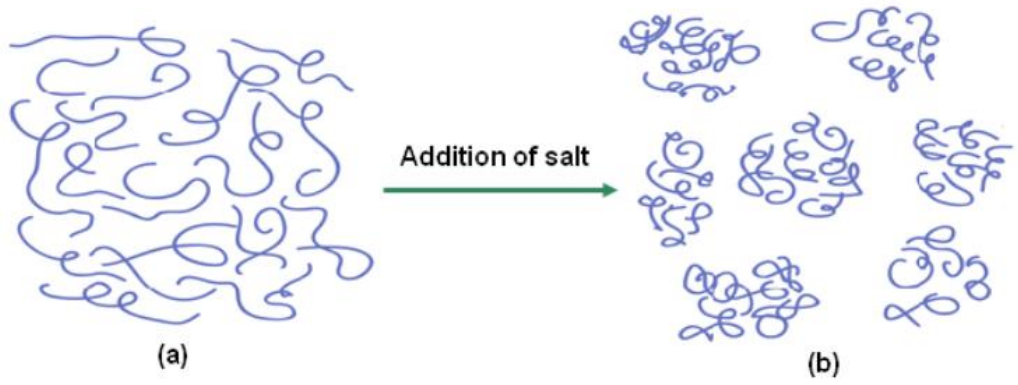

Figure 2-11 Structure of CMC (a) Only CMC (b) CMC + Salt [[15]

3 Theory

This chapter presents the review theories used for the evaluation of the drilling fluids formulated in chapter 4.

3.1 The Rheology of Drilling Fluids

Rheology is the study of fluid deformation and flow. The rheological characterization of fluid is important. The hole cleaning, and hydraulics performance of drilling fluid is a function of the fluids physical and viscosity properties. [18]

There are two types of rheology models, namely Newtonian and non-Newtonian. The rheology parameters extracted from the models are used for borehole cleaning, and hydraulics model. Therefore selecting the right model is indirectly getting the right input parameters for the models. [19] Figure 3-1 Rheological models illustrating typical behaviour for each model Figure 3-1 illustrates the different rheological models describing typical behaviour for each model.

3.1.1 Newtonian Fluids

Newtonian liquids have a viscosity which is independent of shear rate. They are simple and clean liquids containing no particles larger than molecules. The Newtonian model does not describe fluid systems that contain solid particles. For instance liquids such as water, oil, and glycol, that do not contain solids behave, as Newtonian fluids [20]

Given as Eq. the shear stress is directly proportional to shear rate:

$$\tau = \mu \cdot \gamma \qquad (1)$$

where τ is shear stress, μ is viscosity and γ is shear rate.

3.1.2 Non-Newtonian Fluids

Unlike the Newtonian fluids, the viscosity for non-Newtonian fluids depends on shear rate. These are divided into three main categories: Plastic liquids, pseudo plastic fluids and dilatant fluids. It follows that the assortment of drilling fluids will be either having plastic or pseudo plastic characteristics. In short, the main difference between plastic and pseudo plastic fluids are that plastic fluids have yield strength and a pseudo plastic

do not. Still, both are simultaneously shear thinning, i.e. Apparent viscosity (AV) decreases with increasing shear rate. [19]

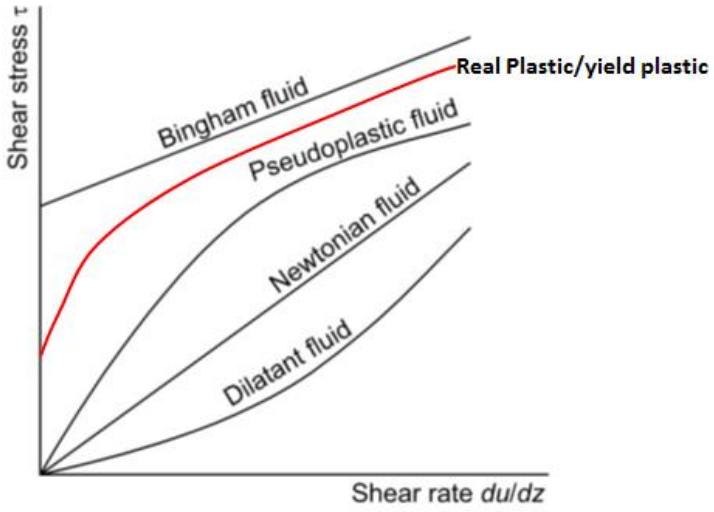

Figure 3-1 Rheological models illustrating typical behaviour for each model [20]

3.1.3 Rheological models

3.1.3.1 Bingham-Plastic model

The Bingham model displays a linear function of shear rate, which has slope and intercept. The slope of the curve is called Bingham plastic viscosity (PV or **μp**), and the intercept is called Bingham yield stress (YS or **τy**). According to the model, fluids require a minimum shear stress overcome the yield strength in order to set the fluid in motion. Most drilling fluids behave as shear thinning. Their apparent viscosity decreases as shear rate increase. This phenomenon is not described by the Bingham model, which rather says that the apparent viscosity is constant for any applied shear rate. The model is given as [22] [23]:

$$\tau = \tau_y + \mu_p \gamma \qquad (2)$$

where

- τ_y (YP) [lbf /100ft^2]=yield point
- μ_p (PV) – [cP]= plastic viscosity,

- $(\gamma[1/\text{sec}])$ =the shear rate

The plastic viscosity is calculated as:

$$\mu_P\ [cP] = \theta_{600} - \theta_{300} \quad (3)$$

The yield strength is calculated as:

$$\tau_y\ [lbs/100ft^2] = \theta_{300} - \mu_P = 2 \cdot \theta_{300} - \theta_{600} \quad (4)$$

3.1.3.2 Power Law Model

Unlike the Bingham model, the Power-law fluid model describes that the apparent viscosity decreases as the shear rate increases, as it does for most drilling fluids. The aspect of yield stress is not included in this model. The shear stress and shear rate behavior is described in the power law model and it is two parameter model. The shear stress is given by [23] [22]

$$\tau = k \cdot \gamma^n \quad (5)$$

Where

- k [lbf/100sqft] = consistency index
- n = flow behaviour index.

The Power-law parameters computed from the following equations:

$$n = 3.32 \log\left(\frac{R_{600}}{R_{300}}\right) \quad (6)$$

$$k = \frac{R_{300}}{511^n} = \frac{R_{600}}{1022^n} \quad (7)$$

The flow index parameter describe the fluid as::

- n < 1 a shear thinning fluid
- n = 1 a Newtonian fluid
- n > 1 a shear thickening or dilatant fluid

3.1.3.3 Herschel-Bulkley model

The Herschel-Bulkley model is described by three parameters. One disadvantage of the power law model is that it describes that fluid can flow at zero shear rate without the applied external pressure. However, this is not observed in real fluids. Herschel-Bulkley enhanced the Power Law model by including yield stress τ_0. This model describes the measured drilling fluid data more exceptional accuracy. The model is defined by the equation below [21] [22]

$$\tau = \tau_0 + K(\gamma)^n \qquad (8)$$

where

$$\tau_0 = \frac{\tau^{*2} - \tau_{min} \cdot \tau_{max}}{2 \cdot \tau^* - \tau_{min} - \tau_{max}}$$

where $\tau*$ is determined by interpolation from the shear rate, $\gamma*$.

$$\gamma^* = \sqrt{\gamma_{min} \cdot \gamma_{max}} \qquad (9)$$

3.1.3.4 Robertson-Stiff model

The Robertson-Stiff model is the more generalized model. It describes the rheology behavior of drilling fluids and cement slurries. The model reads [21]

$$\tau = A\,(\gamma + C)^B \qquad (10)$$

where *A* and *B* are model parameters, these are similar to *n* and *K values in the power law and* in the Herschel-Bulkley model. The yield stress is determined from the zero shear stress, which yields:.

$$\tau_0 = AC^B \qquad (11)$$

$$C = \frac{\gamma_{min} \cdot \gamma_{max} - \gamma^{*2}}{2 \cdot \gamma^* - \gamma_{min} - \gamma_{max}}$$

where $\gamma*$ is the shear rate value which is determined by interpolation from the shear stress, $\tau*$,

$$\tau^* = \sqrt{\tau_{min} \cdot \tau_{max}} \quad (12)$$

3.1.3.5 Unified Model

The unified model is also a modified version of the Power law model. The difference between the Herschel-Bulkley model is based on the determination of the yield strength.

In addition, the way the flow index and the consistency indexes are determined are different from the Herschel-Bulkley modes. The model reads as [21]:

$$\tau = \tau_{yL} + k \cdot \gamma^n \quad (13)$$

Where:

$$\tau_{yL} = (2R_3 - R_6) * 1.066 \quad (14)$$

Pipe flow:

$$n_p = 3.32 \log\left(\frac{2\mu_p + \tau_y}{\mu_p + \tau_y}\right) \quad (15)$$

$$k_p = 1.066\left(\frac{\mu_p + \tau_y}{511^{n_p}}\right) \quad (16)$$

Annular flow:

$$n_a = 3.32 \log\left(\frac{2\mu_p + \tau_y - \tau_y}{\mu_p + \tau_y - \tau_y}\right) \quad (17)$$

$$k_a = 1.066\left(\frac{\mu_p + \tau_y - \tau_y}{511^{n_a}}\right) \quad (18)$$

Where:

τ_{yL} - Lower shear yield stress [lbf /100ft^2]

n_p -Flow index in the pipe

n_a -Flow index in the annulus

k_p -Pipe flow consistency index [lbf*sec^n/100ft^2]

k_a - annulus flow consistency index [lbf*sec^n/100ft^2]

3.2 Hydraulics

As drilling fluid is circulated through/past various parts of the circulating system it experiences a frictional pressure loss, due to obstacles in the flow path. The pump pressure should overcome all the pressure losses to circulate mud back to the surface. Figure 3-2 describes different regions of the flow path where the flow parameters vary for inner and outer conduit. Therefore, pump pressure is the sum of all pressure loses these are [24]:

- In surface equipment such as Kelly, swivel, standpipe. (ΔP_s)
- Inside the drillstring (drillpipe, ΔP_{dp} and drill collar, ΔP_{dc}).
- Across the bit, ΔP_b.
- In the annulus around the drillstring, ΔP_a.

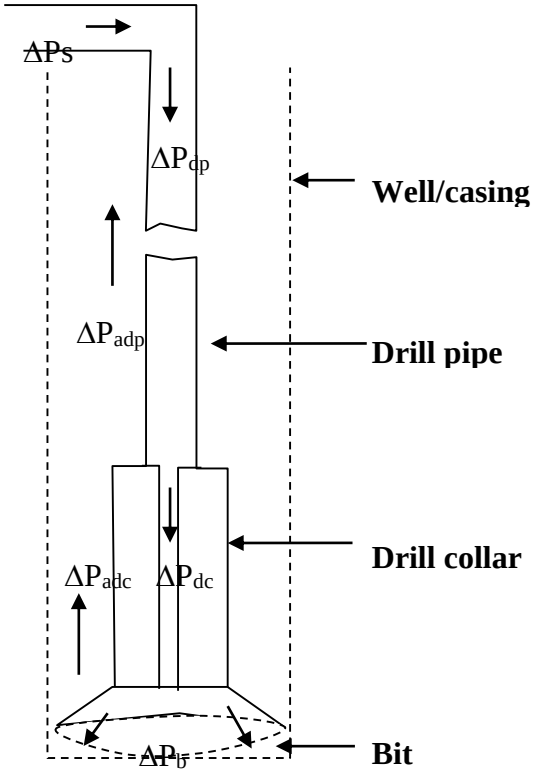

Figure 3-2 Entities of fluid circulation system with different diameters

The pump pressure can be written as [21]:

$$\Delta Pp = \Delta Ps + \Delta Pds + \Delta Pb + \Delta Pa \quad (19)$$

The drilling fluids formulated in this thesis will be analyzed their hydraulics performance. For this, the Unified hydraulic model has been selected and summarized in Table 3-1 [24]

Sagidov [24] has analyzed the predictive power of several models. He has shown that the Unified model predicted most of the field and experimental data very well. Therefore, the selection of this model in this thesis is based on the previous studies performed by Sagidov work.

Table 3-1 Rheological and hydraulics equations for Unified model [21]

Unified model	
Pipe Flow	Annular flow
$\boldsymbol{\mu_p = R_{600} - R_{300}, [cP]}$ $\quad \boldsymbol{\tau_y = R_{300} - \mu_p, [lbf/100ft^2]}$ $\quad \boldsymbol{\tau_0 = 1.066 \cdot (2 \cdot R_3 - R_6)}$	
$\boldsymbol{n_p = 3.32 \cdot log\left(\frac{2 \cdot \mu_p + \tau_y}{\mu_p + \tau_y}\right)}$ $\boldsymbol{k_p = 1.066\left(\frac{\mu_p + \tau_y}{511^{n_p}}\right)}$	$n_a = 3.32 \cdot log\left(\frac{2 \cdot \mu_p + \tau_{y-\tau_y}}{\mu_p + \tau_{y-\tau_y}}\right)$ $k_a = 1.066\left(\frac{\mu_p + \tau_y - \tau_0}{511^{n_a}}\right)$ $k = [lbf \cdot sec^n/100ft^2]$
$\boldsymbol{G = \left(\frac{(3-\alpha)n+1}{(4-\alpha)n}\right) \cdot \left(1 + \frac{\alpha}{2}\right)}$ $\boldsymbol{\alpha = 1\ for\ pipe}$ $\quad \boldsymbol{\alpha = 1\ for\ annuli}$	
$\boldsymbol{v_p = \frac{24.51 \cdot q}{D_P^2}}$	$v_a = \frac{24.51 \cdot q}{D_2^2 - D_1^2}$ $v = [ft/min]$

$$\gamma_w = \frac{1.6 \cdot G \cdot v}{D_R} = [sec^{-1}]$$

$$\tau_w = \left[\left(\frac{4-\alpha}{3-\alpha}\right)^n \tau_0 + (k \cdot \gamma_w^n)\right] = [lbf/100ft^2]$$

$N_{Re} = \frac{\rho \cdot v_p^2}{19.36 \cdot \tau_w}$	$N_{Re} = \frac{\rho \cdot v_a^2}{19.36 \cdot \tau_w}$
$f_{laminar} = \frac{16}{N_{Re}}$ $f_{transient} = \frac{16 \cdot N_{Re}}{(3470 - 1370 \cdot n_p)^2}$ Turbulent: $f_{turbulent} = \frac{a}{N_{Re}^b}$ $a = \frac{\log(n) + 3.93}{50}$ $b = \frac{1.75 - \log(n)}{7}$	$f_{laminar} = \frac{24}{N_{Re}}$ $f_{transient} = \frac{16 \cdot N_{Re}}{(3470 - 1370 \cdot n_a)^2}$ Turbulent: $f_{turbulent} = \frac{a}{N_{Re}^b}$ $a = \frac{\log(n) + 3.93}{50}$ $b = \frac{1.75 - \log(n)}{7}$

$$f_{partial} = (f_{transient}{}^{-8} + f_{turbulent}{}^{-8})^{-1/8}$$

$f_p = (f_{partial}{}^{12} + f_{laminar}{}^{12})^{1/12}$	$f_a = (f_{partial}{}^{12} + f_{laminar}{}^{12})^{1/12}$
$\left(\frac{dp}{dL}\right) = 1.076 \cdot \frac{f_p \cdot v_p^2 \cdot \rho}{10^5 \cdot D_p} = [psi/ft]$ $\Delta p = \left(\frac{dp}{dL}\right) \cdot \Delta L = [psi]$	$\left(\frac{dp}{dL}\right) = 1.076 \cdot \frac{f_a \cdot v_a^2 \cdot \rho}{10^5 \cdot (D_2 - D_1)} = [psi/ft]$ $\Delta p = \left(\frac{dp}{dL}\right) \cdot \Delta L = [psi]$

$$\Delta p_{Nozzles} = \frac{156 \cdot \rho \cdot q^2}{\left(D_{N1}{}^2 - D_{N2}{}^2 - D_{N3}{}^2\right)^2} = [psi]$$

3.3 Viscoelasticity

Drilling fluids can display viscous and elastic responses during deformation. This is called viscoelastic behavior. It is a time-dependent attribute, which is used to evaluate the gel strength and internal gel structure of drilling fluid. [25] The elastic property has an effect on the flow behavior and pressure drop during circulation of drilling fluid.

The viscoelastic properties are quantified by measuring the elastic (storage) modulus (G') and viscous (loss) modulus (G'')

Viscoelasticity is measured with oscillatory methods using rheometer, which applies sinusoidally varying strain (deformation) to the fluid sample. As shown on Figure 3-4, the she stress and strain sine waves are in phase for elastic material whereas the stress and strain will be 90° out of phase for viscous fluid specimen. For the phase angle values between 0° and 90° it is a viscoelastic material (Figure 3-4). [25] [26]

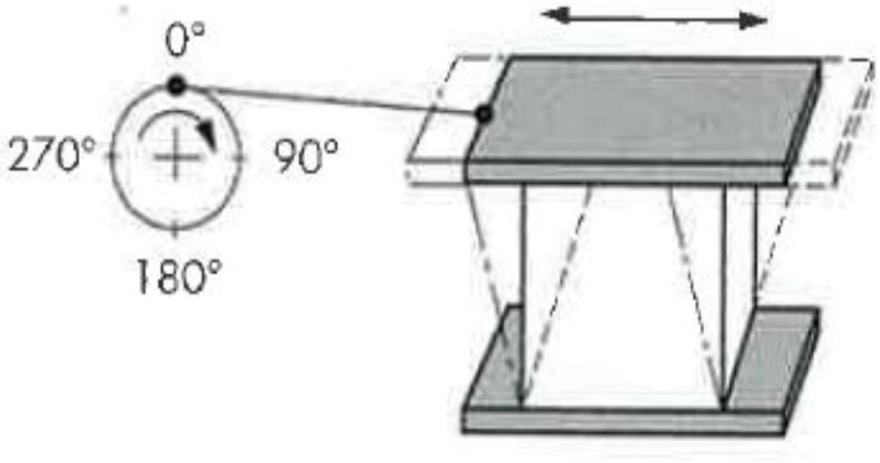

Figure 3-3 Periodic oscillations illustrated by two plate model [25]

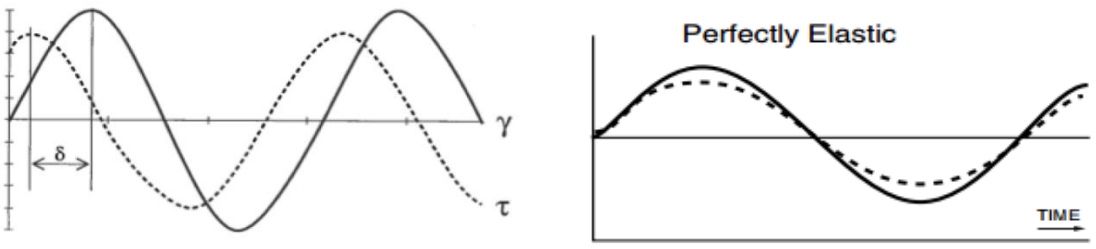

Figure 3-4 Viscous and elastic responses to an applied strain. Graph to left showing the stress (solid line) and strain (dashed line) are 90° out of phase. Graph to right showing the two lines in phase [25]

During testing, the fluid sample is exposed to time varying sinusoidal shear force, which causes deformation. The stress is written as:

$$\tau(t) = \gamma_o \left[\left(\frac{\tau_o}{\gamma_o} \cos\delta \right) \sin(\omega t) + \left(\frac{\tau_o}{\gamma_o} \sin\delta \right) \cos(\omega t) \right] \quad (20)$$

$$\tau(t) = \gamma_o \left[G' \sin(\omega t) + G'' \cos(\omega t) \right] \quad (21)$$

The Storage Modulus describes energy stored per cycle. Whereas, loss modulus describes the energy loss per cycle . These are given respectively as:

$$G' = \left(\frac{\tau_o}{\gamma_o} \cos\delta \right) \quad (22)$$

$$G'' = \left(\frac{\tau_o}{\gamma_o} \sin\delta \right) \quad (23)$$

The ratio of the viscous and elastic deformation, one can compute the damping factor tanδ as:

$$\tan\delta = \frac{G''}{G'} \quad (24)$$

Where δ is the phase angle. The phase angle is equal to 90^o for fluid which behaves perfectly viscous. For perfectly elastic fluid, the phase angle is equal to 0^o. when the phase angle is between < 0^o and 90^o , the fluid behaves viscoelastic. [25] In this thesis the 45° angle is evaluated. That point is called the *flow point* where the fluid is as viscous as it is elastic.

3.3.1 Oscillatory Test: Amplitude Sweep

During amplitude test the fluid specimen will be exposed to an oscillatory load that has varying the amplitude of the shear force while keeping the frequency constant.

The deformation shows a linear and nonlinear deformation, which measures the storage modulus and loss modules during the entire testing phase. For the analysis, we normally are interested in the linear viscoelastic region (LVER). The LVER describes the structure stability of the internal structure of the fluid systems can determine the stability of a suspension. The longer the LVER is the better dispersed and stable is structure of the fluid.

Figure 3-5 illustrates the amplitude sweep test responses showing the storage modulus G' and the loss modulus G" plotted against the deformation. Drawing a horizontal line along the measured G', the point where it deviates is known as the yield point. The shear yield strength is determined from the corresponding shear rate.

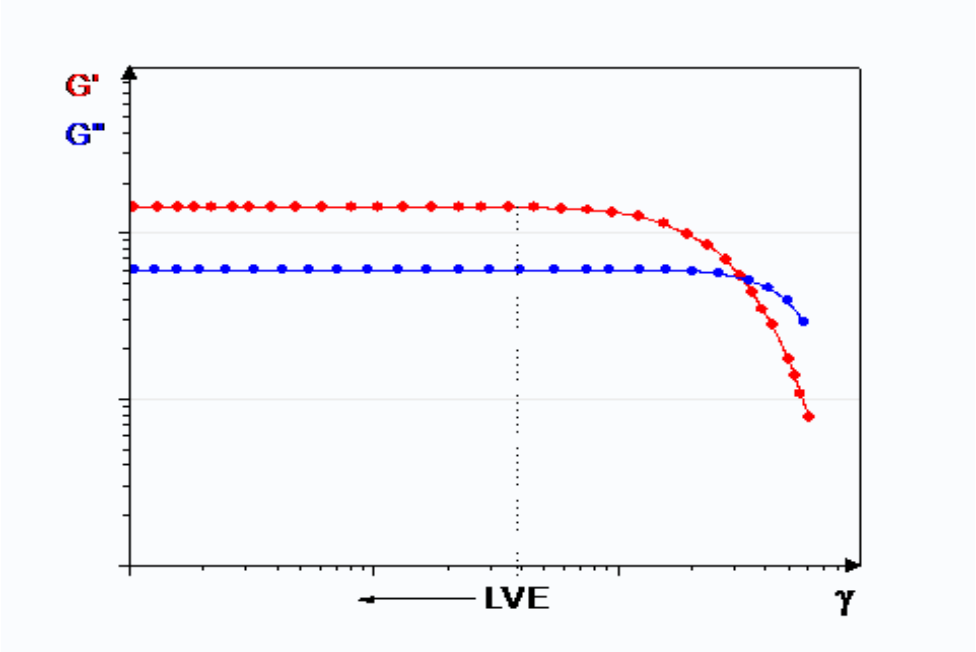

Figure 3-5 An illustration of amplitude test

The horizontal (constant) G' and G" in the LEVL is an indication that the system is undisturbed. After the yield point the curve deviates from the horizontal line, which is an indication that the internal structure is disturbed.

As shown on Figure 3-5, the point where the storage modulus and loss modulus cross each other (G'=G''), the fluid behavior starts to flow. This point is known as the flow point of the fluid. This means that the fluid is behaves both viscous and elastic equally. After the flow point the viscous behavior is more dominating than the elastic behavior. At the flow point, the phase angle is 45°, but in the drilling industry yield point is a more common

3.4 Drill string mechanics

Prior to drilling, during the design phase, the drill string mechanics simulation is study is very important to conduct. This allow us to predict if one can drill and hit the desired target formation. In addition, it yields an investigation of the sensitivity of important parameters.

The torque drag simulation, hookload and stress in the drill string are the most commonly encountered issues to be studied during simulation

3.4.1 Drag

As we drill or during a tripping operation, the drill string-formaton/casing interaction generates a friction force. This force is in the direction of the self weight as tripping out and in the opposite direction when tripping in.

There are several torque and drag models documented in literature (Aadnøy. Johansickk)

In this thesis, the Johansic model is reviewed since the model is implemented in WellPlanTM software.

Figure 3-6 illustrate a drill string inclied at an angle (q) and having azith angle (f). the drill string is discretized into small element.

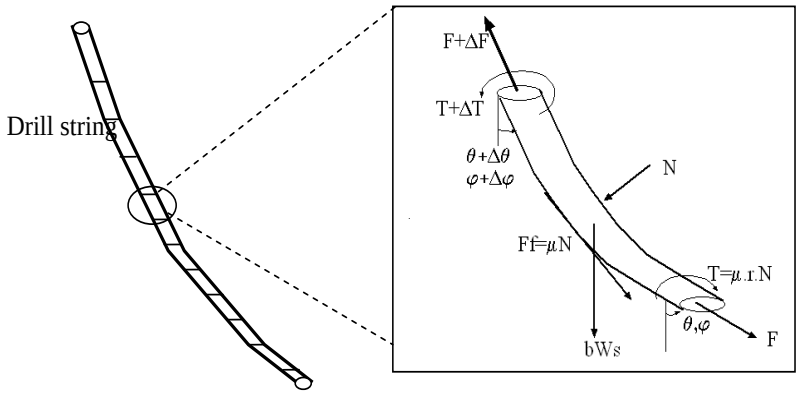

Figure 3-6 Loads on the segmented drill string

The drag force is given by the equation [22]

$$F_{i+1} = F_i + \sum_{i=1}^{n} \left[\beta w_i \cos\left(\frac{\theta_{i+1}+\theta_i}{2}\right) \pm \mu_{ai} N_i\right](S_{i+1} - S_i) \qquad (25)$$

The contact force, N_i is given by the equation [22]

$$N_i = \sqrt{\left[\beta w_i \sin\left(\frac{\theta_{i+1}+\theta_i}{2}\right) + F_i\left(\frac{\theta_{i+1}-\theta_i}{S_{i+1}-S_i}\right)\right]^2 + \left[F_i \sin\left(\frac{\theta_{i+1}+\theta_i}{2}\right)\left(\frac{\alpha_{i+1}-\alpha_i}{S_{i+1}-S_i}\right)\right]^2} \qquad (26)$$

where

$F_i = Weigth\ on\ bit\ (WOB)$

$\beta = Buoyance\ factor$

$w_i = Weight\ per\ unit\ length$

$\theta_i = Inclination$

$\mu_{ai} = Axial\ coefficient\ of\ friction$

$N_i = Contact\ force$

$S_i = Length$

As shown in Equation 25, the plus sign is as drilling string is tripping out and the minus sign is as a drill string is tripping in.

3.4.2 Torque

As drill string is rotating, it experience torque due to friction. The applier toque should overcome all the resistance toques due to string and formation induced frictional force.

It is important to note that applied surface torque should not overcome the maximum allowable makeup torque. Therefore, during planning phase, simulation studies delineates the allowable working window.

Referring to the force balance free body diagram shown in Figure 3-6, the toque for simple geometry that string is varies in inclination only is given as: [22]

$$T = \mu w \Delta sr \ \sin\alpha \qquad (27)$$

where

$\mu = Friction\ factor$

$w\Delta sr = Normal\ moment$

$\alpha = Angle\ of\ deviation$

Torque for any inclination and azimuth can be generalized as [22]

$$T_{i+1} = T_i + \sum_{i=1}^{n} \mu_t r_i N_i (S_{i+1} - S_i) \qquad (28)$$

where

$T_i = Torque\ at\ bit$

$\mu_t = Tangential\ coefficient\ of\ friction$

$r_i = Radius\ of\ string$

$N_i = Contact\ force$

$S_i = Length$

4 Experimental evaluation of nano-modified bentonite based drilling fluid

Several fluids systems were formulated and prepared to investigate the effect of nano, polymers and salt in bentonite treated WBM systems. The effect of temperature was also evaluated.

The primary objective of the research work is to design nano based drilling fluid system, which improve the performance of a conventional nano-free water based drilling fluid. The performance of the newly formulated fluid would be characterized in terms of lower filtrate loss, suitable viscosity and reduce friction. Finally the fluid system also used in a simulation well in order to evaluate its performance in terms of torque and drag, hydraulics.

At first, screening tests were performed to establish the right amount of polymer to add in the fluid system. Previous students [27] [28] [29] have established the concentration ratios between polymers, bentonite and salt for optimal effect of mud by conducting several screening tests. However, in this thesis work, a screening test for performed for every nano in question with polymer, salt and bentonite concentrations kept constant. The polymer varied between PAC, CMC and XG. The salt was at all times KCl.

4.1 Description of equipment

Fann35 viscometer

The drilling fluids were first measured with the Fann35 viscometer (Figure 4-1). For rheology measurement and filter loss testing the temperature was kept at ambient temperature, to not damage the polymer. Rheology models such as Bingham rheology model was used to calculate plastic viscosity and yield strength, while Power Law rheology model was used for consistency index (k) and flow behavior index (n).

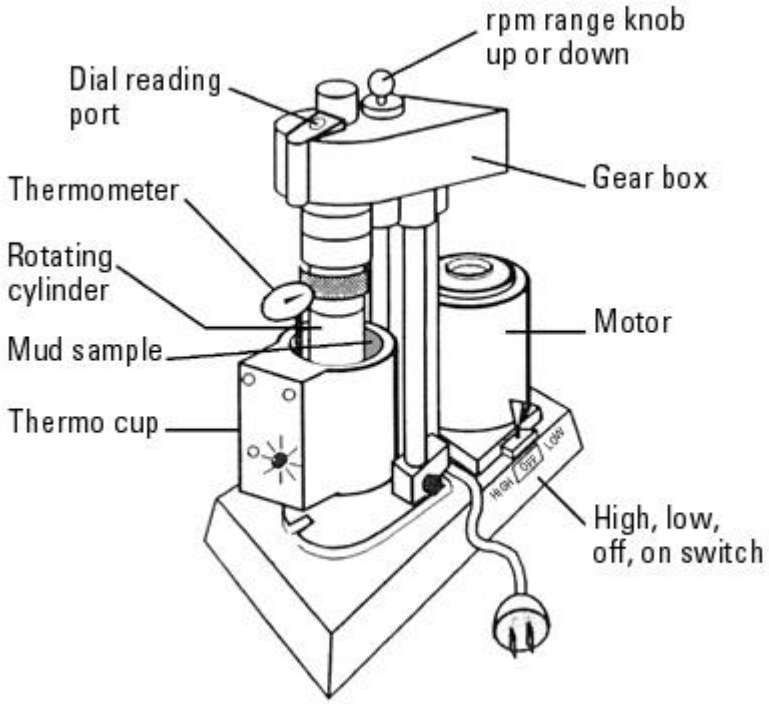

Figure 4-1 Illustration of Fann35 viscometer

Filtrate loss

API filter press with 100psig (7 bar) working pressure was used to characterize the the filtration properties of drilling fluids. The filtering area is 7.1-in^2. The specification is documented in *API Recommended Practice 13B-1 and 13B-2*. Figure 4-2 is a photograph picture of the filter press.

Figure 4-2 Filtrate loss measurement system

pH

In addition to rheology and filtrate, pH measurement is fundamental to drilling fluid control. Additionally bentonite interaction, solubility of additives and the overall effectiveness of chemical additives in drilling fluid are all affected by pH level. The acidity and the alkalinity of the fluids are measured with portable pH test meter apparat shown in Figure 4-3.

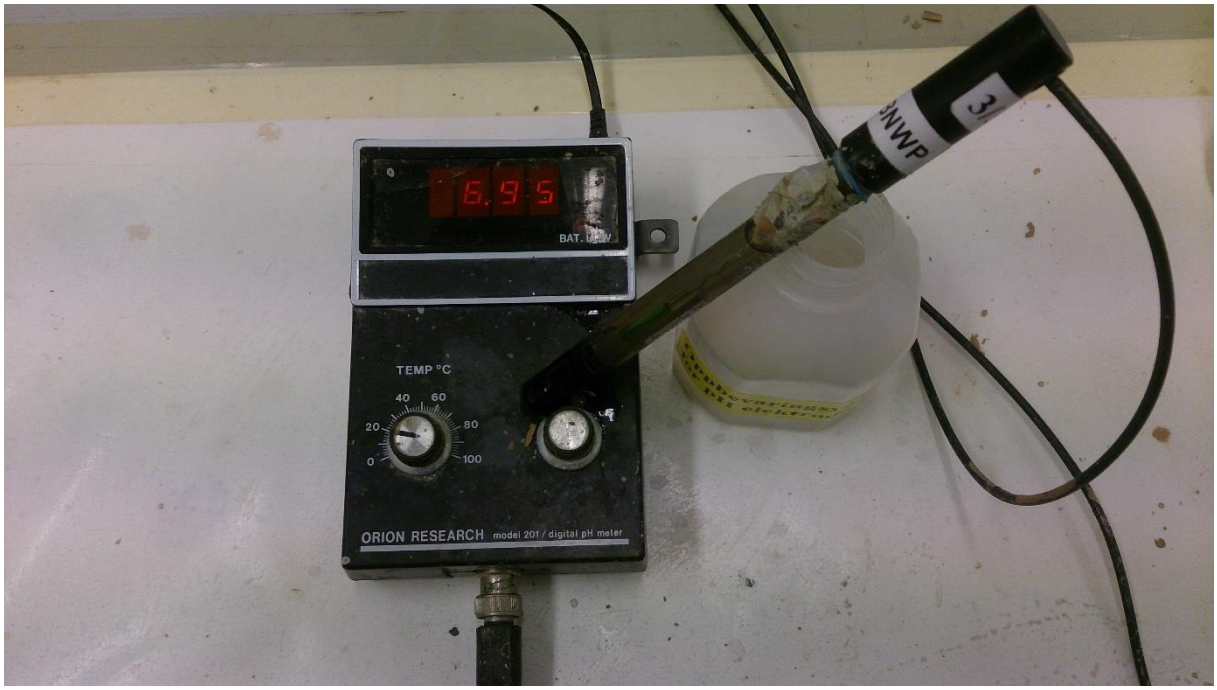

Figure 4-3 Picture of Orion pH meter model 201

Friction test

The friction test was performed on a CSM DIN 50324 Tribometer (Figure 4-4) at different temperatures with 10N normal force at 4 cm/s for 8 minutes. Based on the friction data, temperature dependent coefficient of friction were developed. The surface of the pin-on-disk tribometer were cleaned properly before each measurement. More details are mentioned in section 4.

Figure 4-4 CSM DIN 50324 Tribometer with nano-fluid lubricant

Visco-elasticity Test

The drilling fluid system that showed the best result was selected for simulation work and Viscoelastic behaviors of the fluids has been measured and characterized by using Anton Paar MCR 301 Rheometer (Figure 4-5). During this thesis work, only the Oscillatory Amplitude Sweep Test was performed.

Figure 4-5 Illustration of the Anton Paar MCR 301 Rheometer

4.2 Description of the drilling fluid systems

Except for the chemical ingredients, all drilling fluids have the same mixing, aging and testing procedure. The common additives are 500g H_2O, 25g bentonite, 2.5g KCl and 0.5g Polymer. The fluid without nano-additiv is refered to as the reference/base fluid or control fluid. The ingredients in a fluid system were mixed in a specific order as it affects fluid behavior. After mixing the fluid system, it was aged for two days in order to let the bentonite clay swell very well. Afterwards, viscometer responses, API static filtrate and pH of the fluids were measured. Last the friction coefficient on the tribometer and viscoelasticity on the Anton Paar rheometer were measured.

Four different fluid systems containing salt, polymer, nanoparticles and bentonite in water-based fluid were prepared. These are:

- Titanium Oxide TiO_2 – Rutile structure fluid system
- Molybdenum disulfide (MoS_2) fluid system
- Graphene fluid system
- Titanium Nitride (TiN) fluid system

The thesis objective is to investigate the effect of various concentrations of the above listed nanoparticles in water based drilling fluids.

4.3 Effect of Molybdenum disulfide (MoS_2) nanoparticles

Molybdenum disulfide (MoS_2) is inorganic compound. It is composed of molybdenum and sulfur elements. Dilute acids and oxygen do not affect MoS_2 and it is relatively chemically unreactive. In appearance, molybdenum disulfide is similar to graphite. It is used a solid lubricant, since it has low friction properties. Therefore, in this this, the performance of the particle is tested in drilling fluid. Figure 4-6 shows the SEM photograph of MoS_2.

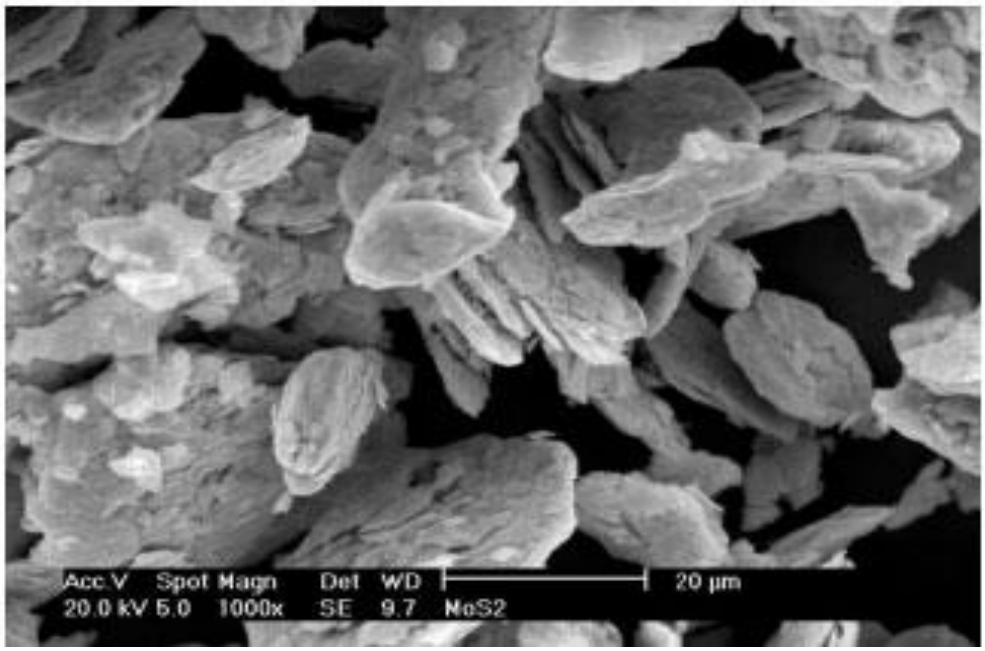

Figure 4-6 Morphology of MoS_2 particles – SEM photograph.

4.3.1 Drilling fluid development with Molybdenum disulfide (MoS_2) nanoparticles

As mentioned in the previous section, MoS_2 has lubricating effect and used as friction reducing particle. In drilling operation, the higher drag is the one it limits drilling from reaching a longer offset. It is demonstrated in the field that the application of drag reducing loss circulation material allowed to drilling an extended reach well for instance in Wytch farm [27]. Due to the lubricating property of the MoS_2, the MoS_2 treated bentonite drilling fluid has been developed. The systems are prepared in the presence of KCl salt and CMC polymer. Table 3.5 shows the fluid formulation.

The concentration of nano varied from 0.1 - 0.4gm and treated in 25gm bentonite water based fluid.

The fluids were mixed in the order:

500g H_2O + Xg Nano + 2,5g KCl + 0,5g CMC + 25g Bentonite

Table 4-1 Test matrix for nanosized MoS_2 in drilling fluid system

Test matrix for Nano - Molybdenum disulfide (MoS_2) in fluid system					
Ingredient	Ref Fluid	Fluid 1	Fluid 2	Fluid 3	Fluid 4
H2O[g]	500	500	500	500	500
Nano - MoS_2[g]	0	0,1	0,2	0,3	0,4
CMC[g]	0,5	0,5	0,5	0,5	0,5
KCl[g]	2,5	2,5	2,5	2,5	2,5
Bentonite[g]	25	25	25	25	25

4.3.2 Results and analysis of Molybdenum disulfide treated drilling fluid system

4.3.2.1 Rheology parameters, filtrate and pH results

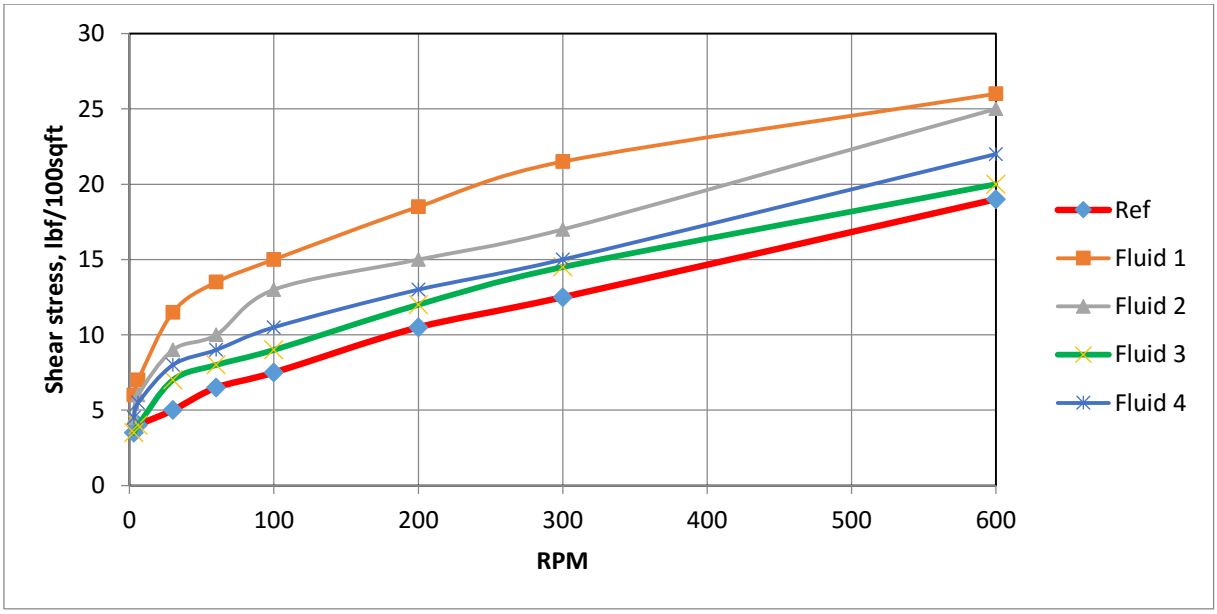

Figure 4-7 Rheology measurements for drilling fluid system containing MoS_2

The drilling fluids formulated in Table 4-1 are characterized through rheology, filtrate and pH measurement. Figure 4-7 Rheology measurements for drilling fluid system containing . Figure 4-7 visualises the Fann-35 Viscometer responses of Table 4-1 fluids.

The addition of MoS_2 shows a significant impact on the reference fluid. One can also observe that as the nano concentration increases, viscosity changes. As shown on the Figure 4-7, the addition 0.1g exhibits a higher impact, whereas increasing the concentration results in a different change in viscometer result relative to the reference fluid and Fluid 1. This shows that the effect of nano has not a non-linear effect on rheology and there exhibits an optimum concentration that works best in the water based drilling fluid. That has something to do with the disintegration/dispersed of the bentonite system and agglomerate/aggregate.

The drilling fluid behaviors are characterized in terms of their gel straight, flow resistance, filtrate and pH. The experimental results were applied in the Bingham- and Power Law model. Their parameters are calculated and shown in Figure 4-8 and Figure 4-9 respectively.

As displayed on Figure 4-8, the addition of nanosized MoS_2 has a great impact on the plastic viscosity (PV) when compared with the nano-free fluid system (reference). All MoS_2 modified fluid indicates a significant effect indicate a significant effect in terms of yield stress. The greatest improvement of YS, by 183%, is by the 0.1g MoS_2 modified system. The other modified systems show an increase of up to 50%.

In literature, it is documented that lower shear yield strength (LSYS) of drilling fluid is used to evaluate the barite sagging potential of a drilling fluid. Scott et al, [28] has analyzed sagging management and control issues. The authors have presented three field case studies in an attempt to investigate sag occurrence, suspected causes and treatment. From the presented case studies, the authors indicated that insufficient lower shear yield stress (LSYS) is the main cause for sagging. A very effective method to reduce sag tendencies is treating the fluid system to obtain desired LSYS recommended range [7-15lbf/100sqft]. The low shear yield stress (LSYS) is calculated from the lower shear rate readings as ($LSYS = 2\theta_3 - \theta_6$).

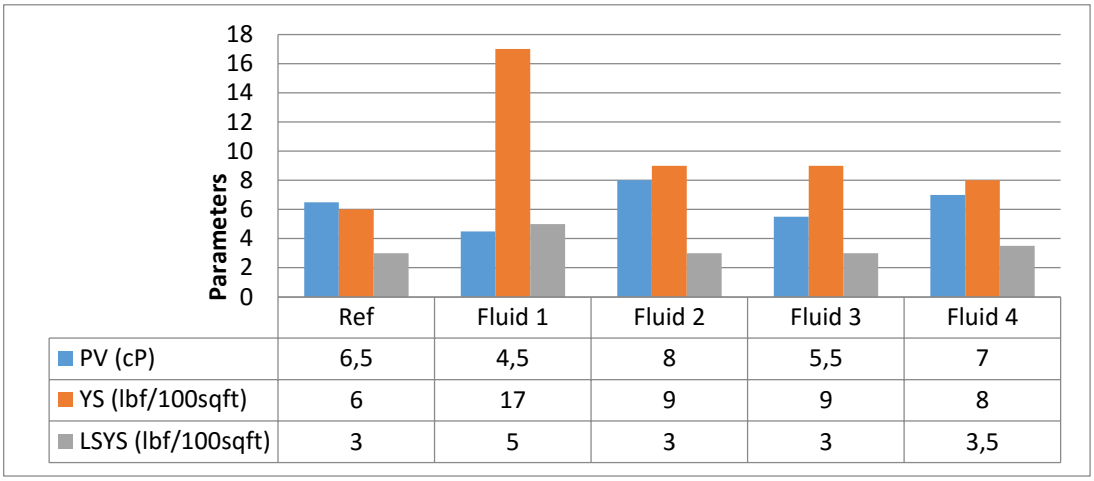

	Ref	Fluid 1	Fluid 2	Fluid 3	Fluid 4
PV (cP)	6,5	4,5	8	5,5	7
YS (lbf/100sqft)	6	17	9	9	8
LSYS (lbf/100sqft)	3	5	3	3	3,5

Figure 4-8 Presentation of PV, YS and LSYS results based on rheology measurements for MoS_2 drilling fluid system

The shear yield stress parameter (LSYS) is low in general for fluids with CMC polymer, compaired to Xanthan Gum effects. That is because it yields lower viscosity. That is not very good for particle settling, which should be avoided during drilling. As seen in Figure 4-8, the addition of very small increase in concentration of nanoparticles changes LSYS from 3 in the reference to 5.0 in 0.1g added MoS_2, to 3.0in 0.2g added additive, to 3.0 with 0.3g added MoS_2 and 3.5 for 0.4g added MoS_2 to the reference fluid formula. The addition of 0.1g seems to yield an optimum effect at this low concentration range.

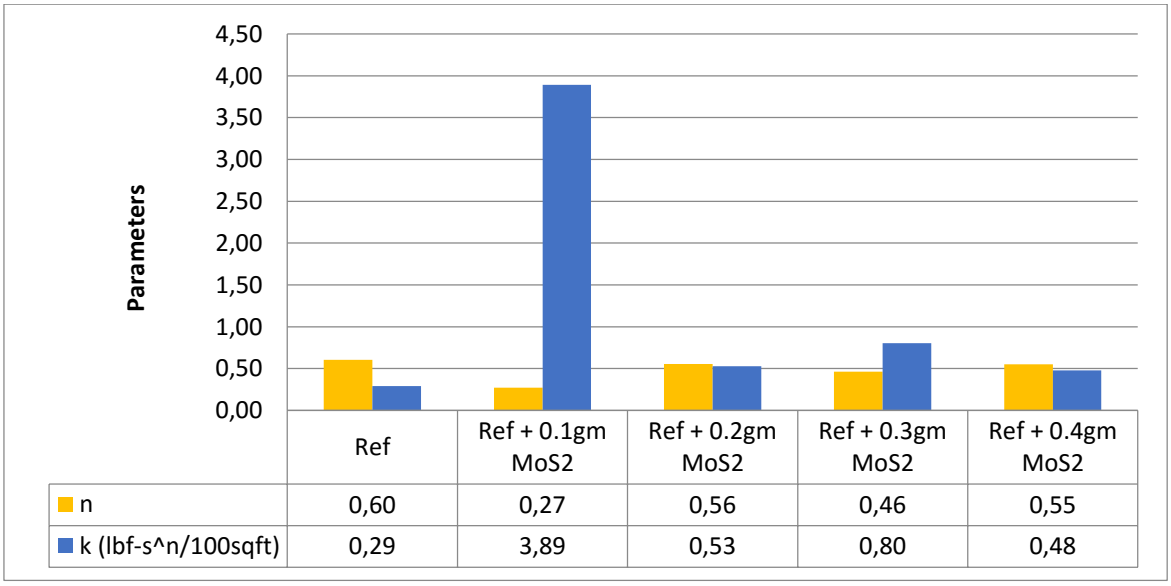

	Ref	Ref + 0.1gm MoS2	Ref + 0.2gm MoS2	Ref + 0.3gm MoS2	Ref + 0.4gm MoS2
n	0,60	0,27	0,56	0,46	0,55
k (lbf-s^n/100sqft)	0,29	3,89	0,53	0,80	0,48

Figure 4-9 Consistency index(k) and n-value for MoS_2 at different temperatures.

The Power Law model factors, n and k are shown in Figure 4-9. In all cases the n-value is below 1.0. That is an indication that the fluids express pseudoplastic behaviour. Since

all pseudoplastic fluids are shear thinning, viscosity is decreases when shear rate is increased. As we can see the n-value is fairly constant for set temperature and no effect from added nanoparticles can be observed, for most of the fluid samples. The fluid with +0.1g added MoS_2 yields an n-value of 0.27 compaired to 0.60 from nano-free fluid, meaning the fluid is more viscous, confirmed in Figure 4-7.

The Consistency Index, k, describes the average slope of the shear stress – shear rate curve. It is sometimes called the viscosity index. A higher value of k implies that a fluid has higher viscosity. The highest k value from the test of MoS_2 added fluids is the one with the least (+0.1g) added MoS_2 nanoparticles.

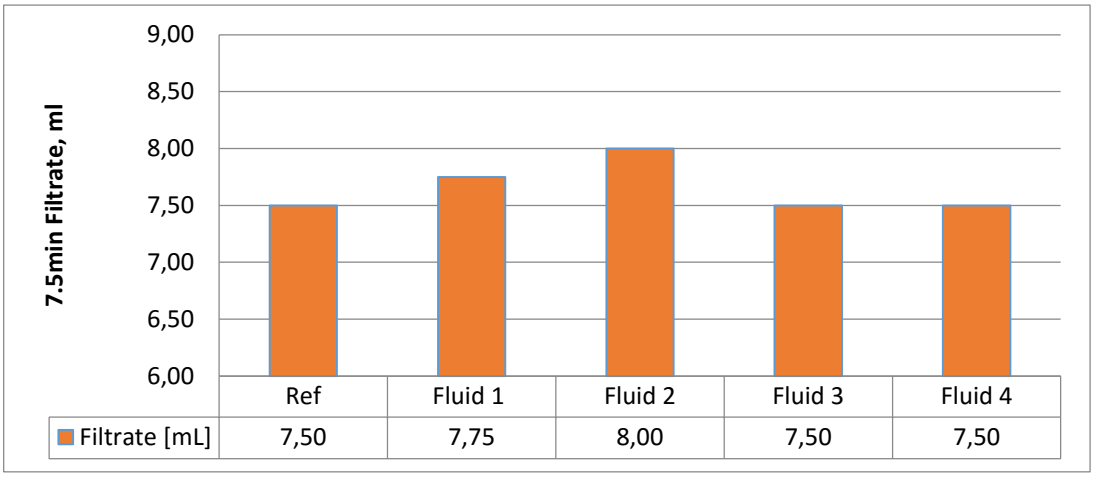

Figure 4-10 Diagram and data for filtrate loss of drilling fluid system containing MoS_2

As seen in Figure 4-10, the drilling fluid system containing CMC polymer for reduced filtration loss sets a reference filtrate loss of 7.50mL. The addition of 0.1g and 0.2g MoS_2 into the reference system results in increased filtrate loss to 7.75mL and 8.00mL respectively. Nonetheless, Fluid 3 and Fluid 4 with 0.3g and 0.4g added yield the same filtrate loss as the base fluid. That shows that there is no linear relationship with increasing filtrate loss with increased concentration of MoS_2 nanoparticles, since the filtrate loss is the same for fluid 3 and 4 as it is for the reference fluid.

As seen in Table 4-2 the pH is increased by 0.05 or 0.10 from the reference level of 8.95. The addition of MoS_2 nanoparticles seems to have no significant effect on the pH level of the base fluid, meaning that that the surface chemistry of the nanoparticles does not react with water to change the H^+ concentration of the fluid.

Table 4-2 pH measurements of MoS_2

Measurement	Ref fluid	Fluid 1	Fluid 2	Fluid 3	Fluid 4
pH	8,95	9,05	9,05	9.0	9,05

4.3.2.2 *Rheology modeling*

Table 4-3 describes the models with their function and its input parameters based on the MoS_2 reference fluid. The %-deviation from the actual measurement relative to the model predicted value is also given. With this, we can easily analyze which model predicts the fluid behavior the best. Blank fields mean that the model does not have the output parameter in question.

Table 4-3 Description of rheological models with MoS_2-reference fluid output parameters and %-deviation

		Parameters					
Model	Equation	τo,τy, A	k, C	n, B	μp, μ	%-Dev	cP
Herschel Bulkley	$0.0733*\gamma^{0.92310}+2.347$	3,4226	0,1234	0,7090		2,04	
Unified	$2.347+0.0731*\gamma^{0.9235}$	3,2010	0,2144	0,6223		3,10	
Power Law	$0.9594*\gamma^{0.5227}$		2,1289	0,2966		9,47	
Bingham	$0.0417*\gamma+3.307$	4,6456			0,0160	10,75	7,6608
Newtonian	$0.0464*\gamma$				0,0226	50,34	10,8209
Robertson and Stiff	$0.1078*(35.5807+\gamma)^{0.867}$ [3]	0,3775	55,6794	0,5666		2,67	

To get an idea about the relative accuracy of the models, Figure 4-11 and Figure 4-12 below display the models in practice. With the axes kept the same for both figures, it is obvious to see that the models in Figure 4-11 are much less accurate relative to those in Figure 4-12, seen below. The most accurate model for the reference fluid in this case is the Herschel Bulkley model, as the percent-deviation is as low as 2.04% (see Table 4-3). The least accurate is the Newtonian Model, which deviates by 50.34% from the original measurements. Figures and tables for all the other fluids with all models can be found in the Appendix A

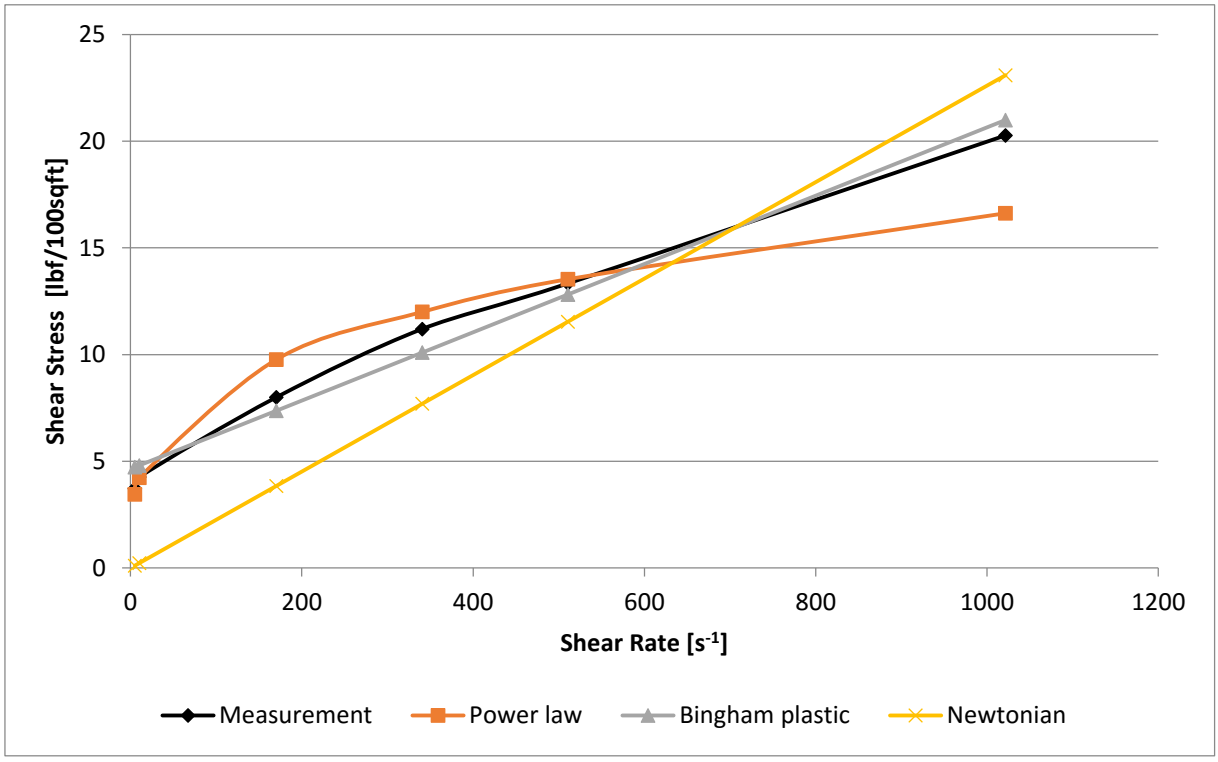

Figure 4-11 Rheology modelling for MoS_2 reference fluid with relatively bad model predictability

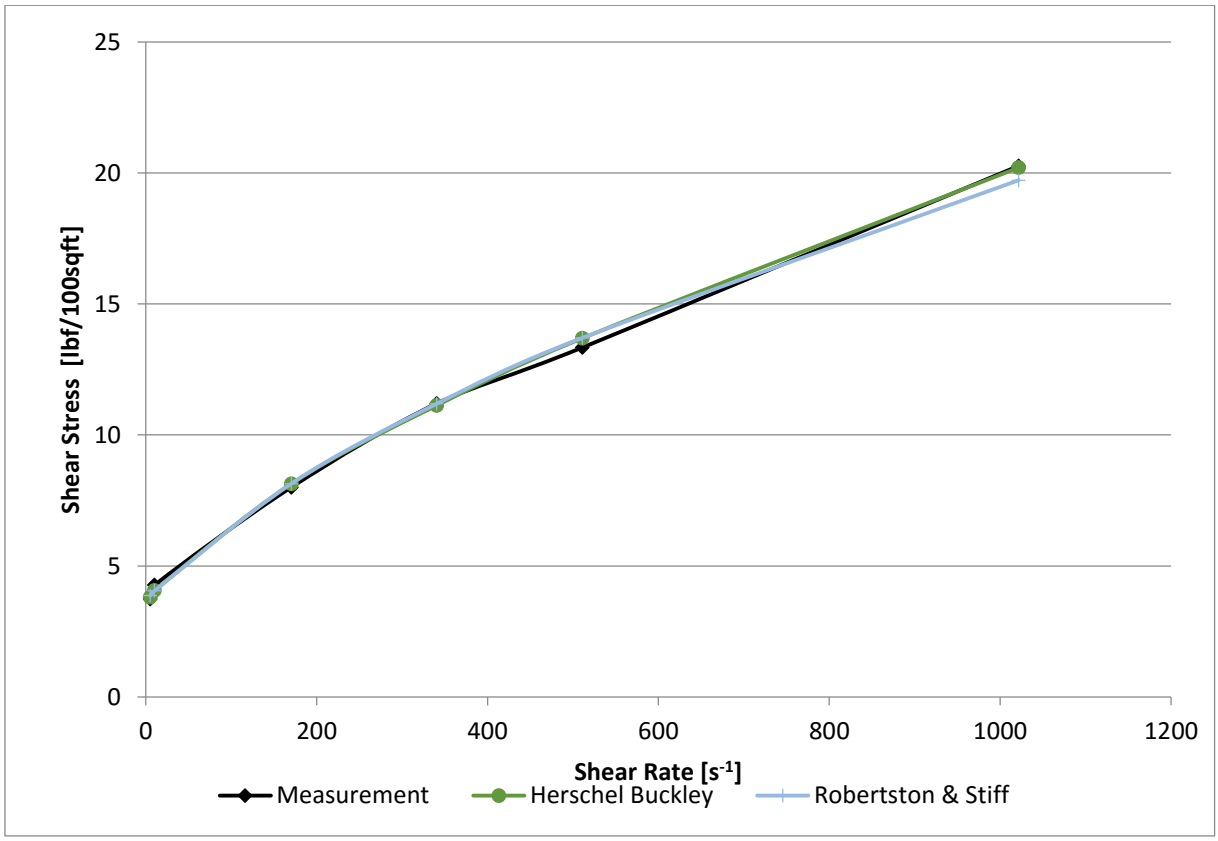

Figure 4-12 Rheology modelling for MoS_2 reference fluid with relatively good model predictability

Table 4-4 describes how each parameter in a rheological fluid model is affected by the addition of MoS_2 nanoparticles. Percentage-deviation from the reference fluid parameter has been included. For instance, the addition of 0.1g MoS_2 increases the Bingham plastic viscosity μp by 27.50 %, while reducing the H-B flow index (n) by 27,8 %. The models itself are included in Appendix A

Table 4-4 Rheology model parameters and percentage deviation from the reference fluid – MoS_2.

Model	Parameter	Ref	Ref + 0.1g MoS_2	Ref + 0.2g MoS_2	Ref + 0.3g MoS_2	Ref + 0.4g MoS_2
Herschel-Bulkley	τo	3,4226	4,8819	3,2334	3,1891	4,0094
	% deviation		**42,64**	**-5,53**	**-6,82**	**17,15**
	k	0,1234	0,7311	0,8722	0,2126	0,3950
	% deviation		**492,46**	**606,81**	**72,29**	**220,10**
	n	0,7090	0,5119	0,4696	0,6510	0,5580
	% deviation		**-27,80**	**-33,77**	**-8,18**	**-21,30**
Unified	τy	3,2010	5,3350	3,2010	3,2010	3,7345
	% deviation		**66,67**	**0,00**	**0,00**	**16,67**
	k	0,2144	0,4978	0,8911	0,2077	0,5381
	% deviation		**132,18**	**315,63**	**-3,13**	**150,98**
	n	0,6223	0,5704	0,4665	0,6547	0,9893
	% deviation		**-8,34**	**-25,04**	**5,21**	**58,97**
Power Law	k	8,1289	3,9718	3,0242	2,0693	2,9928
	% deviation		**-51,14**	**-62,80**	**-74,54**	**-63,18**
	n	0,2966	0,2778	0,2980	0,3210	0,2754
	% deviation		**-6,34**	**0,47**	**8,23**	**-7,15**

Bingham	**τy**	4,6456	9,6995	7,4163	5,3429	6,5083
	% deviation		**108,79**	**59,64**	**15,01**	**40,10**
	μp	0,0160	0,0204	0,0201	0,0171	0,0176
	% deviation		**27,50**	**25,63**	**6,88**	**10,00**
Newtonian	**μ**	0,0226	0,0342	0,0306	0,0247	0,0268
	% deviation		**51,33**	**35,40**	**9,29**	**18,58**
Robertson and Stiff	**A**	0,3775	2,4369	1,8906	0,7697	1,2375
	% deviation		**545,54**	**400,82**	**103,89**	**227,81**
	C	55,6794	11,6903	10,2228	23,7813	25,0756
	% deviation		**-79,00**	**-81,64**	**-57,29**	**-54,96**
	B	0,5666	0,3557	0,3730	0,4778	0,4153
	% deviation		**-37,22**	**-34,17**	**-15,67**	**-26,70**

4.3.2.3 Coefficient of friction

The lubricity of the drilling fluids has been measured using the CSM tribometer, shown in Figure 4-4 on p.39. The friction coefficient was measured on ball and plate surface contact in the presence of water based drilling fluid. The steel ball is an alloy of 6 chromium and 6mm diameter. At first, several tests were carried out in order to calibrate the test machine and get reliable results.

For all tests, a constant normal force of 10N was applied to the tribometer arm. The heater was set to maintain a ambient temperature so that the fluid system is exposed to a 22ºC. The testing was allowed to rotate for a linear distance of 20m and the test duration was ~8,33min. The linear speed was set to be 4 cm/s. For each testing, we only vary the surface radius. The test has been performed at three temperatures, namely 22°C, 50°C and 70°C. The average value of the experiments is used to generate temperature dependent coefficient of friction profile.

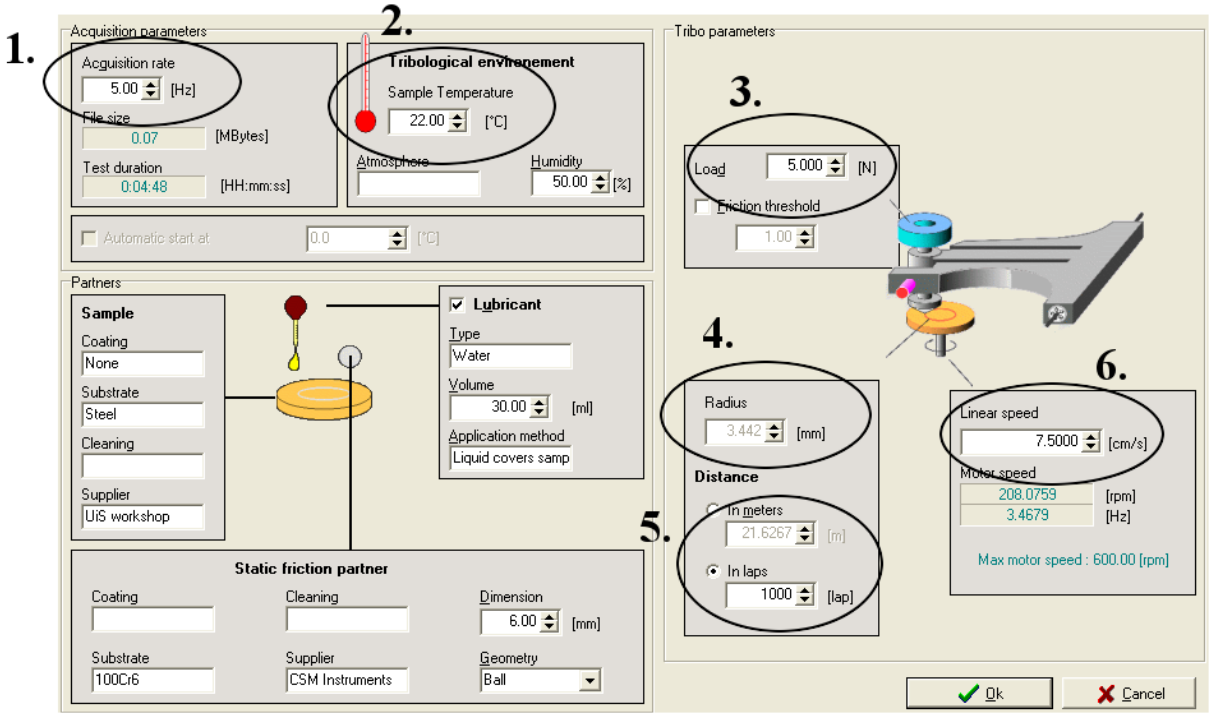

Figure 4-13 Testing panel of Tribometer

The testing interface panel is shown in Figure 4-13. The numbers shown on the figure are: Sampling rate (1), Heating device (2), Normal load applied on Tribometer arm (3), radius between the center and the tribometer ball pin (4) distance of testing (5), linear speed of sample with respect to tribometer arm (6)

Experiments on the tribometer were atleast repeated twice with the same fluid to ensure repeatability and reliability. The result considered acceptable if the friction coefficient (**μ)** did not deviate more than ±0.1 for all tests to ensure the quality of the result.

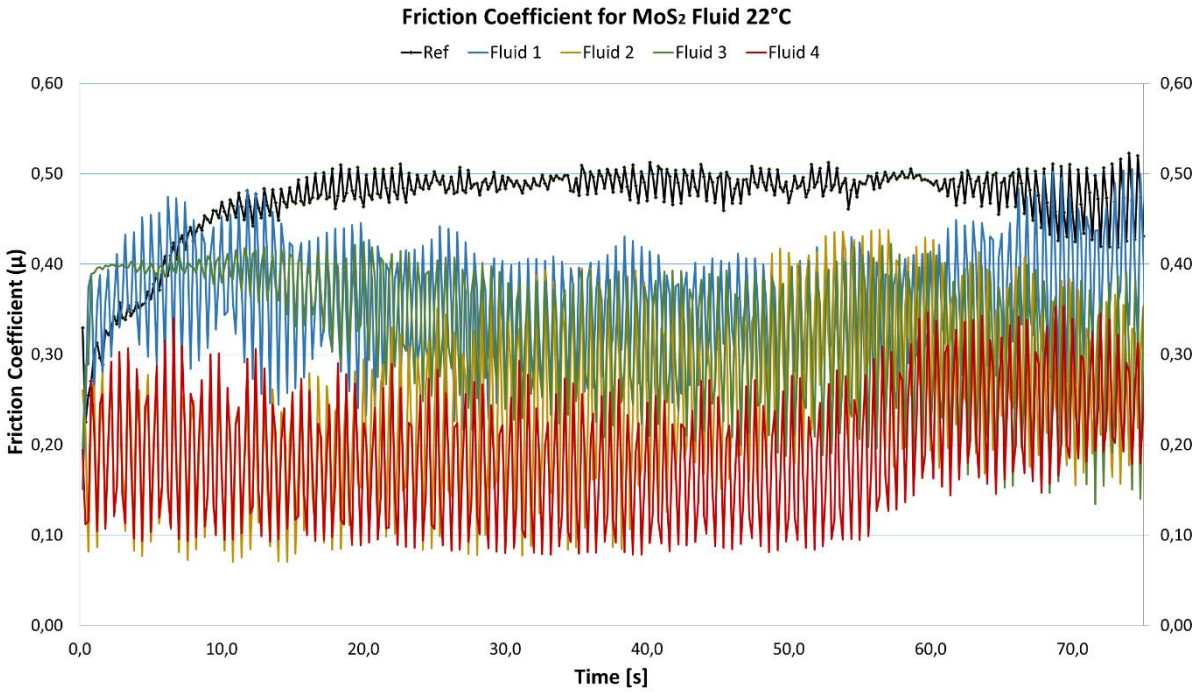

Figure 4-14 Friction Coefficient vs time for MoS_2 - 22°C

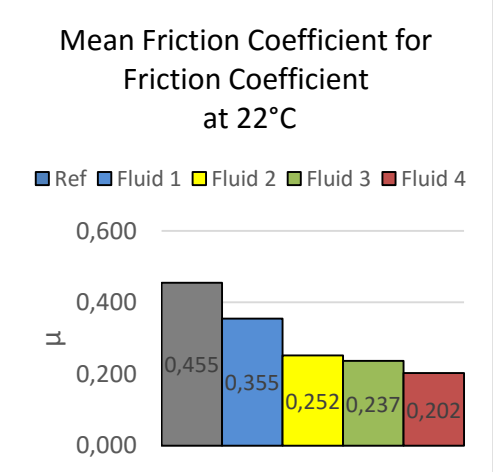

Figure 4-15 Mean Friction Coefficients for MoS_2

Figure 4-14 shows the raw friction coefficient measurement data of MoS_2 added fluid system with CMC polymer directly from the tribometer system. All fluids were measured at ambient temperature (22°C). The black line represents the reference (base) fluid and the colored lines different concentrations respectively, where Fluid 1 is 0,1g added nanoparticle, Fluid 2 is 0,2g etc. In Figure 4-15 we see the average values of μ for the MoS_2 added fluid system.

The results from these tests indicate that the addition of nanosized MoS_2 particles decreases μ with increased concentration in a constant manner. The lowest observed mean value for this experiment was 0,202. That represents a 56% reduction relative to the reference coefficient of 0,455. Table 4-5 compiles all relative percentage-differences of friction coefficients for all fluids.

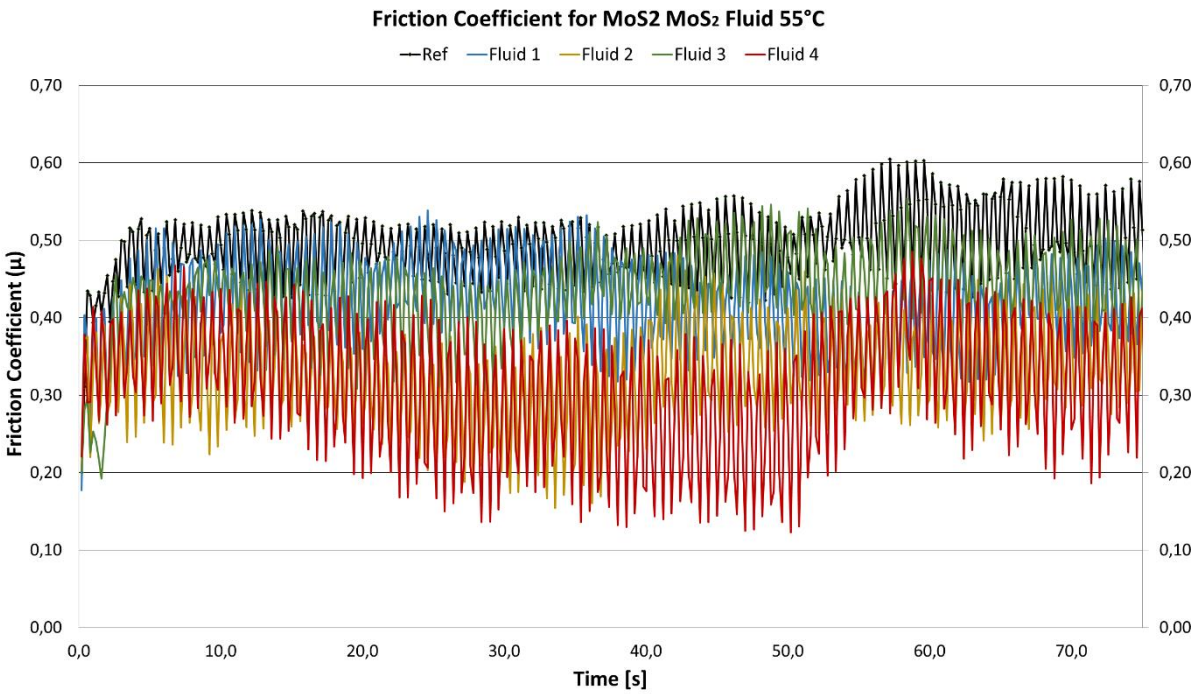

Figure 4-16 Friction Coefficient vs time for MoS_2 - 55°C

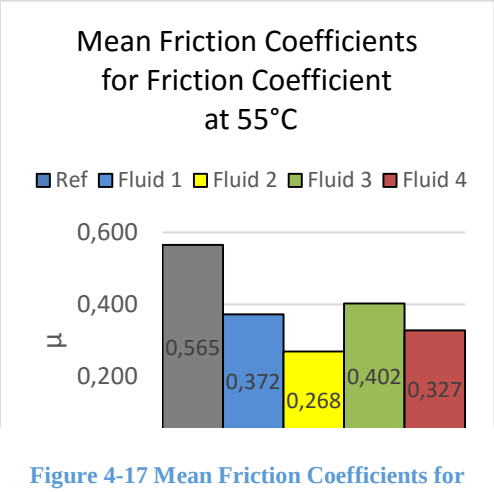

Figure 4-17 Mean Friction Coefficients for MoS_2 at 55°C

At 55°C (see Figure 4-16, Figure 4-17) the friction coefficient is notably elevated for all fluid samples. Yet the lubricating effect of MoS_2 nanoparticles can be clearly observed.

The constant reduction in friction coefficient by increased concentration of nanoparitcles that was observed at seems diminished as seen at 22°C, but the friction reduction is percentage wise higher now for lower concentration of added MoS_2, where Fluid 1 reduces friction by 34% at 55°C while at 22° the reduction was only by 22%. This time 0.2g added nano yields the most effect to decrease μ indicated as Fluid 2, resulting in a μ reduction by 53%.

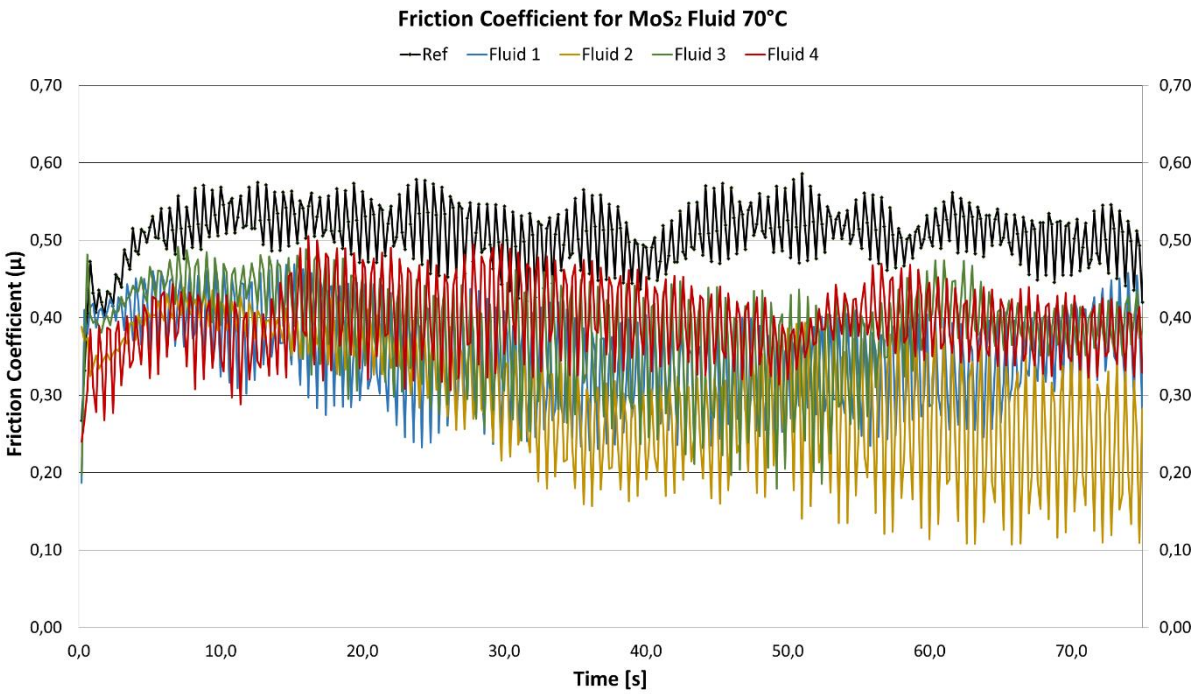

Figure 4-18 Friction Coefficient vs time for MoS_2 - 70°C

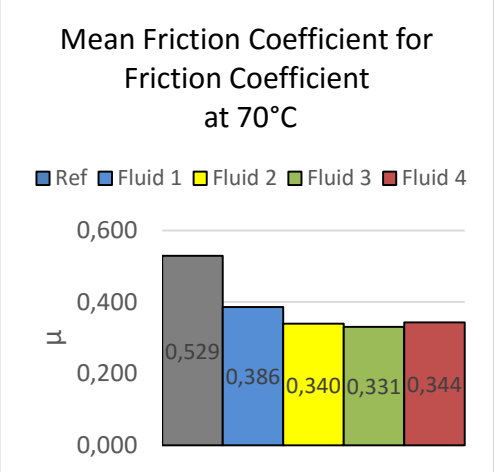

Figure 4-19 Mean Friction Coefficients for MoS_2 at 70°C

Increasing the temperature from 55°C to 70°C the friction increases again for all fluid samples except the reference fluid. This reduces the maximum friction reduction obtained from added MoS_2. As seen in Figure 4-19 all fluids with MoS_2 nano-additive have reduced friction. The lowest friction coefficient measured at 70°C is Fluid 3 has a reduced μ of 0.331(-38%) relative to 0.529 in the base fluid, resulting in a reduction by 38%.

As shown in those figures the addition of MoS_2 nanoparticles yield a major decrease in friction coefficient values for all concentrations and temperatures. Table 4-5 shows the percentage reduction for all fluids relative to the reference fluid. The numbers are based on the mean values shown in Figure 12, 14 and 16.

Table 4-5 µ-%Change associated with reference for MoS_2

µ-%Change associated with reference for MoS_2			
°C	22°	55°	70°
Fluid 1 (Ref +0,1g)	-22	-34	-27
Fluid 2 (Ref +0,2g)	-45	-53	-36
Fluid 3 (Ref +0,3g)	-48	-29	-38
Fluid 4 (Ref +0,4g)	-56	-42	-35

Based on the friction measurement data of fluid samples at different temperatures a model was generated in the form of a trend line. This is shown on Figure 4-20 and Table 4-6. Similarly Kårstad et al [29] have also measured linear function of temperature dependent coefficient of friction model. If R^2 is higher than 0.80 one can say that analysis behaving linearly. This table shows that some results fit quite well.

Table 4-6 Models for mean friction coefficient data as a function of temperature for MoS_2 added drilling fluid systems

Drilling fluids	**Friction measurement**			**Model**	**R^2**
	22°C	50 °C	70 °C		
Reference	0.455	0.565	0.529	y = 0,0018x + 0,4264	0.6440
Fluid 1	0.355	0.372	0.386	y = 0,0006x + 0,3400	0.9806
Fluid 2	0.252	0.268	0.340	y = 0.0016x + 0.2074	0.7200
Fluid 3	0.237	0.402	0.331	y = 0.0025x + 0.2027	0.5279
Fluid 4	0.202	0.327	0.344	y = 0.0031x + 0.1401	0.9592

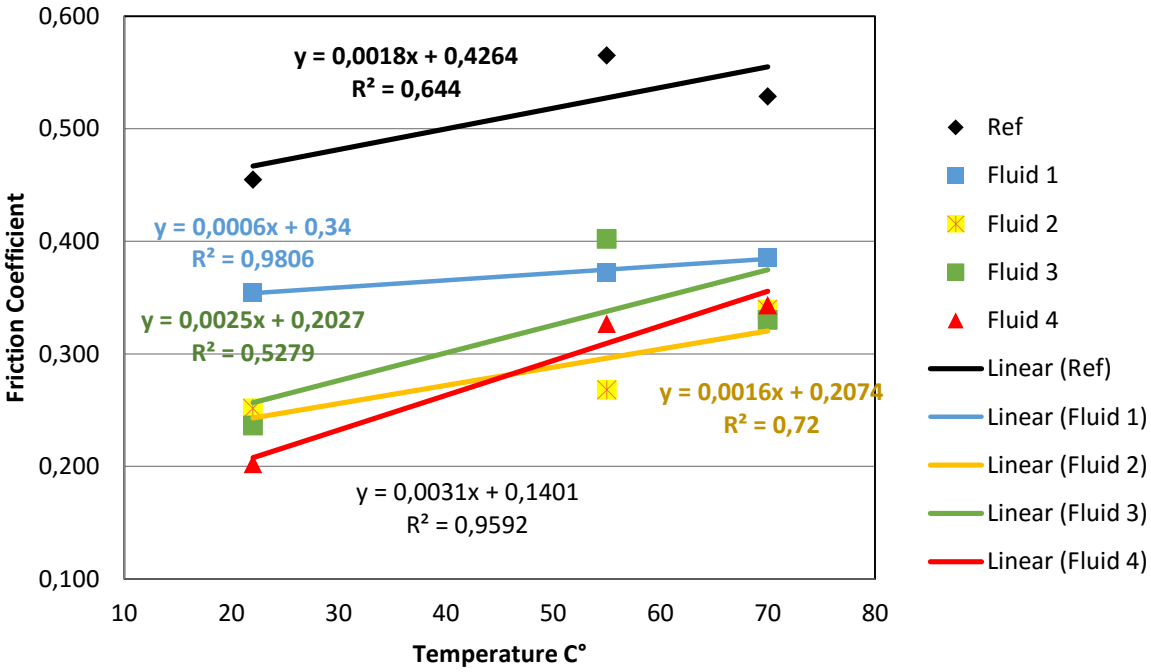

Figure 4-20 Mean Friction Coefficiens vs temperature with trendline for MoS_2

4.4 Effect of Titanium Oxide (TiO_2) nanoparticles

Titanium dioxide is an oxide of titanium, TiO_2. The particle occurs in nature as minerals rutile and Anatase. In this thesis, we tested both of the structures, but the results will be presented only of rutile structure based. The particle was purchased and tested in water based drilling fluid. A SEM picture of the of the particles is shown below. [30]

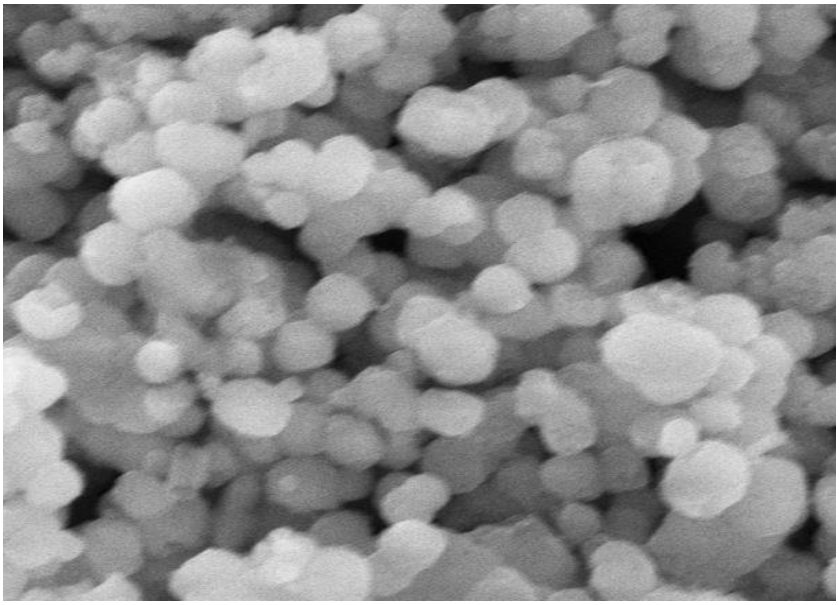

Figure 4-21 SEM picture of TiO_2 where a grain size is about ~20nm [31]

4.4.1 Drilling fluid development with Titanium Oxide TiO_2

The performance Titanium Oxide TiO_2 was evaluated in fluid system containing KCl and CMC. The concentration of Rutile-TiO_2 was varied from 0.1 - 0.4g per 25g bentonite water based mud. Table 4-7 shows the formulated test matrix.

The fluids were mixed in the order:

500g H_2O + Xg Nano + 2,5g KCl + 0,5g CMC + 25g Bentonite

Table 4-7 Test matrix for nanosized Rutile-TiO_2 drilling fluid system

Test matrix for nanosized Rutile-TiO_2 in fluid system					
Ingredient	Ref Fluid	Fluid 1	Fluid 2	Fluid 3	Fluid 4
H2O [g]	500	500	500	500	500
Rutile-TiO_2[g]	0	0,1	0,2	0,3	0,4
KCl[g]	2,5	2,5	2,5	2,5	2,5
CMC[g]	0,5	0,5	0,5	0,5	0,5
Bentonite[g]	25	25	25	25	25

4.4.2 Results and analysis of drilling fluid system containing nanosized TiO

4.4.2.1 Rheology, filtrate and pH results

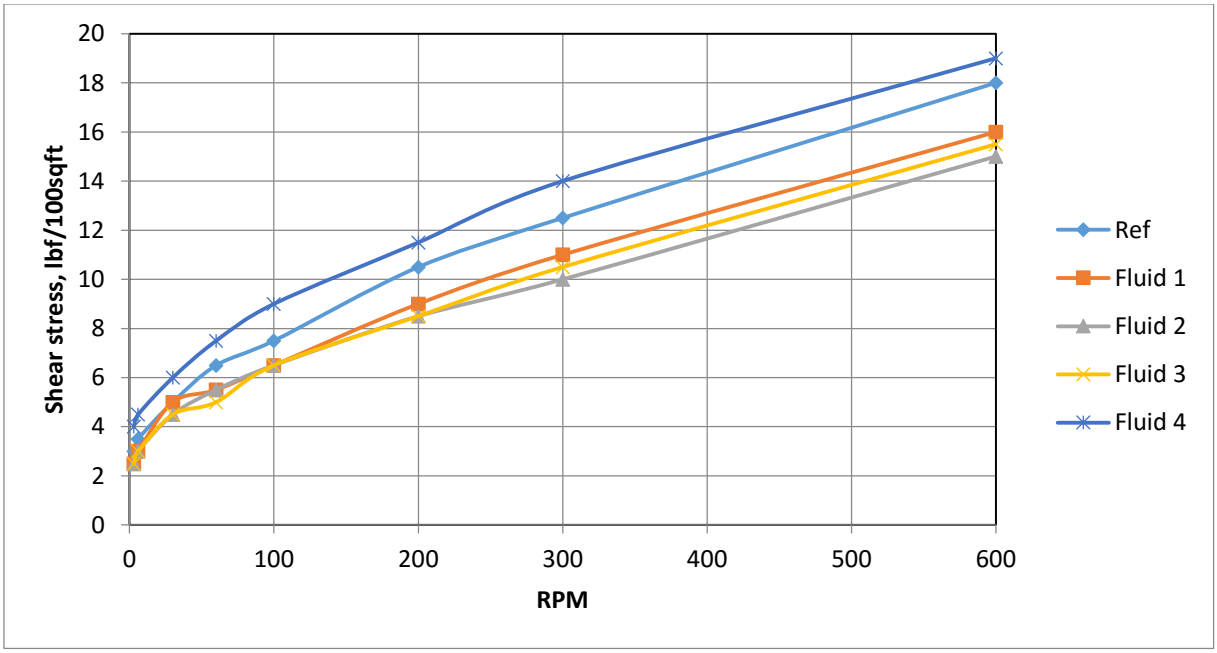

Figure 4-22 Viscometer response of drilling fluid system containing nano-sized Rutile-TiO_2

Figure 4-22 displays the Fann-35 Viscometer responses of fluids. The addition of TiO_2 shows a significant impact on the reference fluid. One can also observe that as the nanoparticles concentration increases, viscosity changes. We see that the addition 0.4g exhibits a higher impact in the form of increased viscosity, whereas other concentration result in a reduction in viscometer response compared to the reference fluid. This implies that the effect of nanoparticle concentration has a non-linear effect on rheology. Hence, the optimum concentration that works best in the water based drilling fluid has to be found empirically. That has something to do with the disintegration/dispersed and agglomeration/aggregation of the bentonite system.

The drilling fluid behaviors are characterized in terms of their gel straight, flow resistance, filtrate and pH. From this, the commonly used rheology models, the Bingham and Power law parameters are calculated and shown in Figure 4-23 and Figure 4-24 respectively.

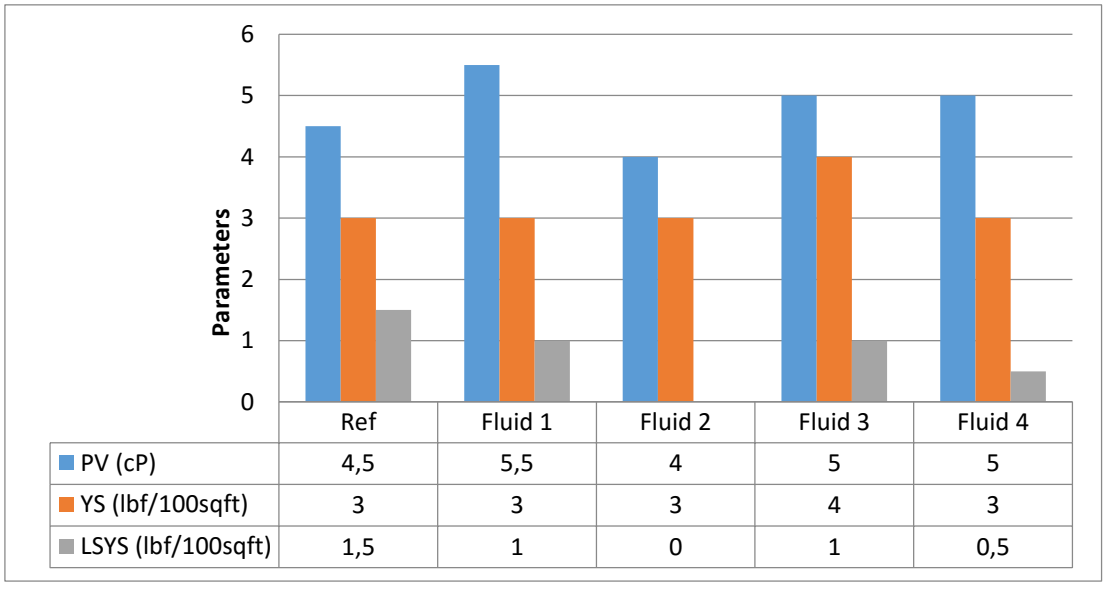

	Ref	Fluid 1	Fluid 2	Fluid 3	Fluid 4
PV (cP)	4,5	5,5	4	5	5
YS (lbf/100sqft)	3	3	3	4	3
LSYS (lbf/100sqft)	1,5	1	0	1	0,5

Figure 4-23 Presentation of PV, YS and LSYS results based on rheology measurements of nanosized Rutile-TiO_2 fluid

Figure 4-23 shows that Bingham plastic viscosity generally is not affected by addition of TiO_2. Naturally the PV would increase for added solids, but perhaps the amount added was not sufficient for this effect to be observed. Similarly, the yield stress (YS) also is not influenced by the nano-additive. As described in the literature study part, the electrostatic force among the charged particles causes yield stress. During this thesis work, the electrical resistivity of the particles mixed with 500gm water and the results shows no effect on the measurement.

The lower shear yield stress parameter (LSYS) is low in general for fluids with CMC polymer, because the viscosity is low. That is not very good for handling sagging (settling of particles). As Figure 4-23 states, the addition of very small increase in concentration of TiO_2 nanoparticles changes LSYS keeps all fluids at an LSYS of about 1.0, which is essentially an insignificant change in fluid parameters from added nanoparticles.

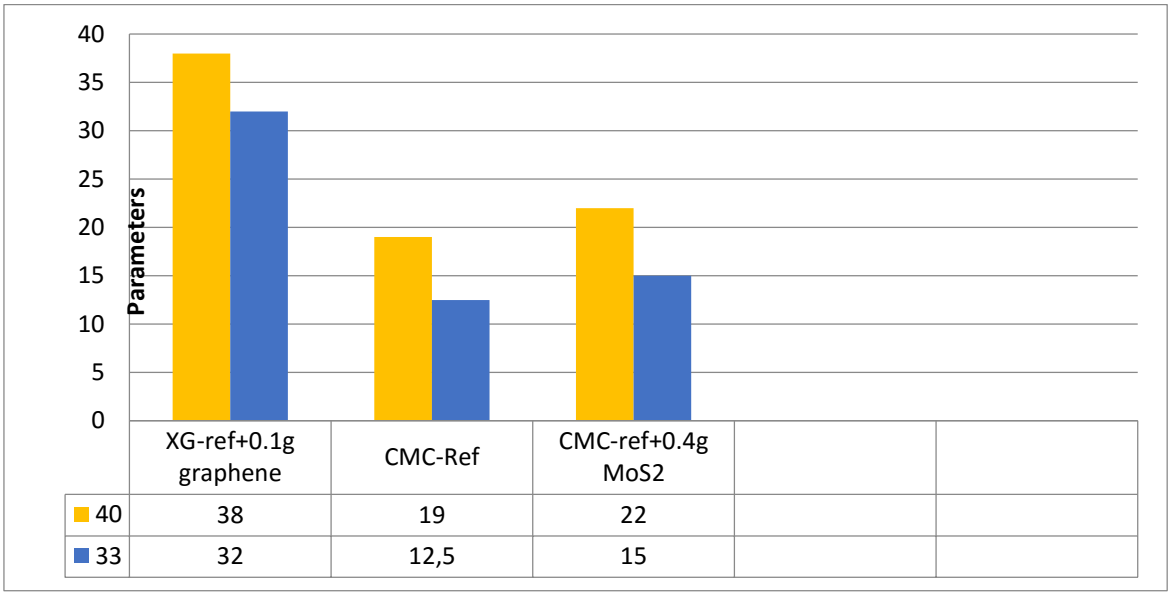

Figure 4-24 Consistency Index(k) and n-value for TiO_2 at different temperatures.

The Power Law parameters in Figure 4-24 show that in all cases the n-value is below 1.0. Only fluid 4 indicates a difference with a lowered n-value. The Consistency Index, k, is increased for fluid 4 resembling a higher viscosity, also proven in Figure 4-22 from the actual measurements.

Figure 4-25 shows the measured filtrate loss of the drilling fluids. Here also the addition of nano does not show any positive impact in improving the petro-physical property of the filter cake. That might have something to do with the ball-like structure og rutile-TiO_2; perhaps more flat shaped or elongated crystal structures work better. Therefore, all the fluid loss is almost equal to and even higher than the nano -free reference fluid system. For Fluid 1 and Fluid 4, 0.1g and 0.4g added TiO_2 nanoparticles increased the filtration loss from 7.5mL to 8.25mL(+10%) and 8.3mL(+10.7%) respectively.

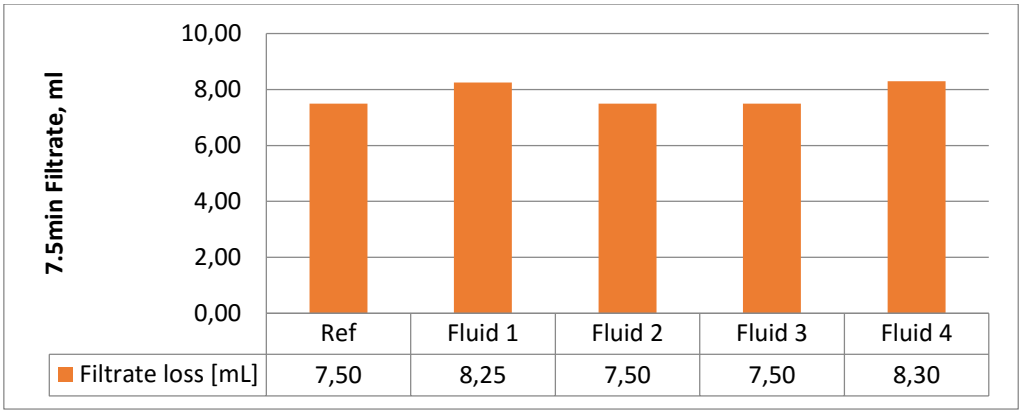

Figure 4-25 Diagram and data for filtrate loss of drilling fluid system containing TiO_2

As seen in Table 4-8, the addition of TiO_2 to the base fluid system seems to effect on the acidity/alkalinity on the reference fluid system, meaning that that the surface chemistry of the particles do not react with water to change the H+ concentration of the fluid.

Table 4-8 pH measurements for TiO_2

Measurement	Ref fluid	Fluid 1	Fluid 2	Fluid 3	Fluid 4
pH	8,95	8,95	8,9	8,85	8,85

4.4.2.2 Rheology modelling

Table 4-9 describes how each parameter in a rheological fluid model is affected by the addition of TiO_2 nanoparticles. Percentage-deviation from the reference fluid parameter has been included. For example μp-value for the Newtonian model experiences a -17,43% deviation (in the form of reduction because it is negative) for Ref+0.2g TiO_2 relative to the reference fluid, meaning the curve has less steeper slope i.e. a smaller gradient. The models itself are included in Appendix A

Table 4-9 Rheology model parameters and percentage deviation from the reference fluid – TiO_2.

Model	Parameter	Ref	Ref + 0.1g TiO_2	Ref + 0.2g TiO_2	Ref + 0.3g TiO_2	Ref + 0.4g TiO_2
Herschel-Bulkley	τo	2,790	2,292	2,249	2,272	3,757
	% deviation		-17,84	-19,38	-18,57	34,68
	k	0,1642	0,1561	0,1817	0,1684	0,2061
	% deviation		-4,93	10,66	2,56	25,52
	n	0,6704	0,6598	0,624	0,6405	0,6399
	% deviation		-1,58	-6,92	-4,46	-4,55
Unified	τy	2,668	2,134	2,134	2,134	3,735
	% deviation		-20,00	-20,00	-20,00	40,00
	k	0,2156	0,2249	0,2344	0,23	0,2158
	% deviation		4,31	8,72	6,68	0,09
	n	0,6278	0,6029	0,5846	0,5921	0,6328
	% deviation		-3,97	-6,88	-5,69	0,80
Power Law	k	1,7656	1,4262	1,5132	1,4896	2,5217
	% deviation		-19,22	-14,30	-15,63	42,82
	n	0,3244	0,3334	0,3183	0,3246	0,2831

	% deviation		**2,77**	**-1,88**	**0,06**	**-12,73**
Bingham	**τy**	4,4589	3,7540	3,7255	3,6950	5,7050
	% deviation		**-15,81**	**-16,45**	**-17,13**	**27,95**
	μp	0,0155	0,0139	0,0127	0,0133	0,0155
	% deviation		**-10,32**	**-18,06**	**-14,19**	**0,00**
Newtonian	**μ**	0,0218	0,0193	0,0180	0,0186	0,0236
	% deviation		**-11,47**	**-17,43**	**-14,68**	**8,26**
Robertson and Stiff	**A**	0,5188	0,4292	0,5417	0,4851	0,9141
	% deviation		**-17,27**	**4,41**	**-6,50**	**76,20**
	C	31,1452	30,0601	25,2747	27,6262	28,9688
	% deviation		**-3,48**	**-18,85**	**-11,30**	**-6,99**
	B	0,5177	0,5270	0,4811	0,5021	0,4436
	% deviation		**1,80**	**-7,07**	**-3,01**	**-14,31**

4.4.2.3 *Coefficient of friction result*

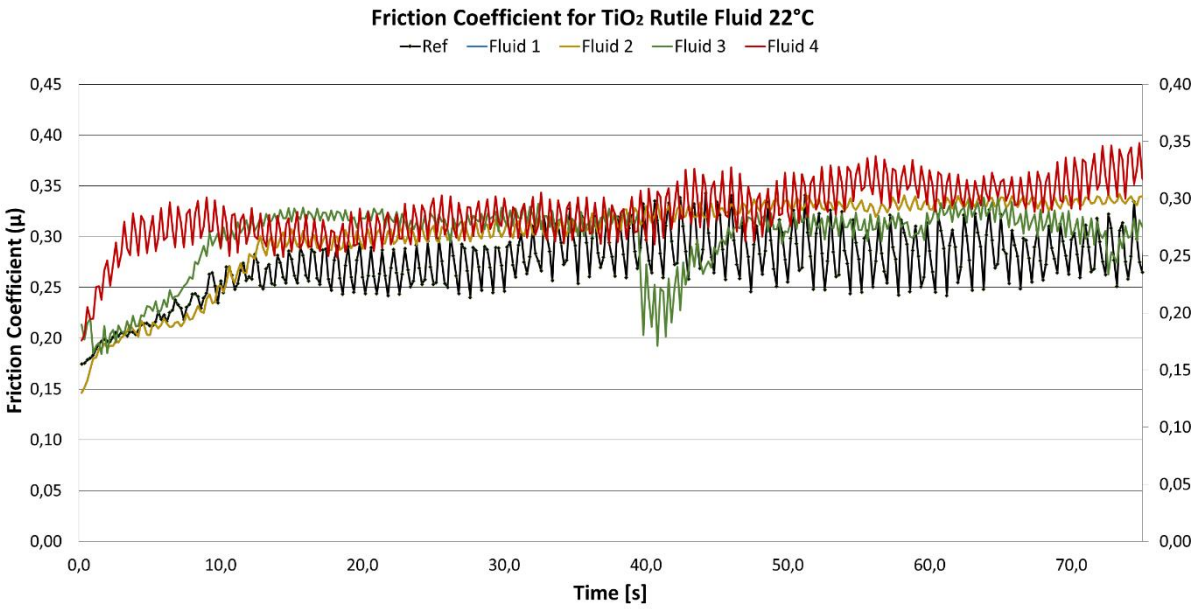

Figure 4-26 Friction coefficient tribometer measurement as a function of time - TiO_2 Rutile 22°C

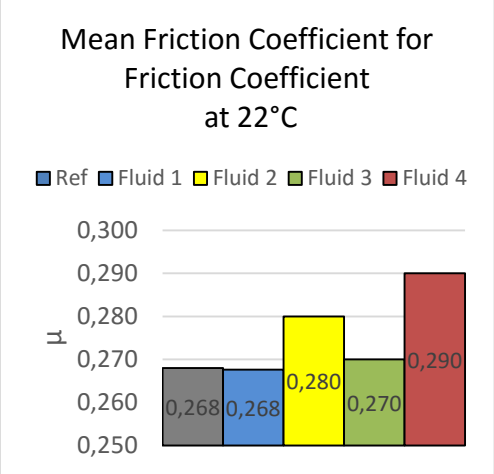

Figure 4-27 Mean Friction Coefficients for TiO_2 at 22°C

One might notice that the reference here is lower though the fluid is the same as for TiO_2. That's because the experiments were done with only 5N constant normal force for all TiO_2 fluids. Whereas, all the other experiments where done with 10N. Nonetheless the relative change in friction reduction due to added nanoparticles was expected to be visible if there is any.

Figure 4-27 shows that the reference the tribometer response yields a mean friction coefficient of 0,268. The addition of TiO_2 nanoparticles does not seems to affect the measurement in any positive way. Fluid 1 and Fluid 3 yield almost the same result as the base fluid, whereas Fluid 2 and Fluid 4 increase the friction coefficient to 0.28 and 0.29 respectively.

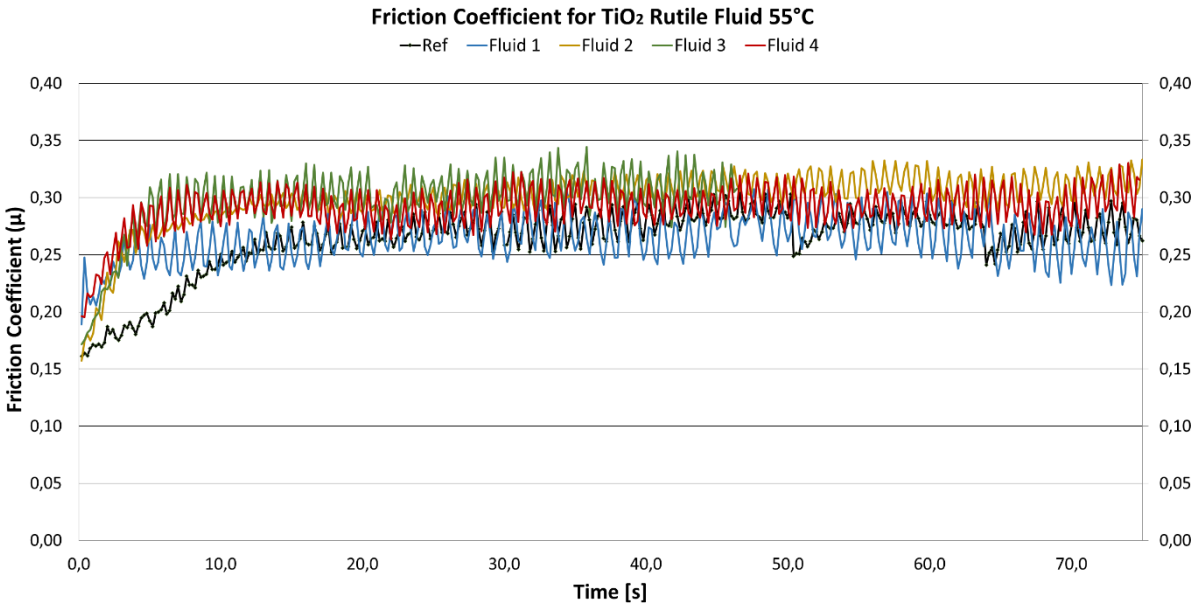

Figure 4-28 Friction coefficient tribometer measurement as a function of time - TiO_2 Rutile 55°C

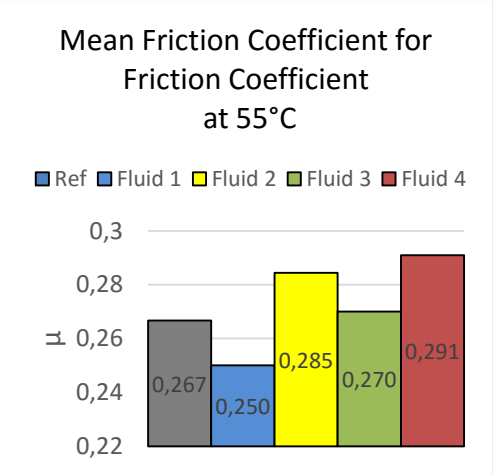

Figure 4-29 Mean Friction Coefficients for TiO_2 at 55°C

Tribometer yields a mean friction coefficient of 0.267 with the reference fluid. As shown further in Figure 4-29, Fluid 2,3 and 4 yield an increased μ at 55°C, while Fluid 1 has the lowest as 0.250. Increased temperature does not show a significant change in friction for those fluids as it did for TiO_2. It shall be noted that this experiment was done with only 5N in normal force, which might lead to less overall friction and make it harder to notice the lubricating effect of nanoparticle addition.

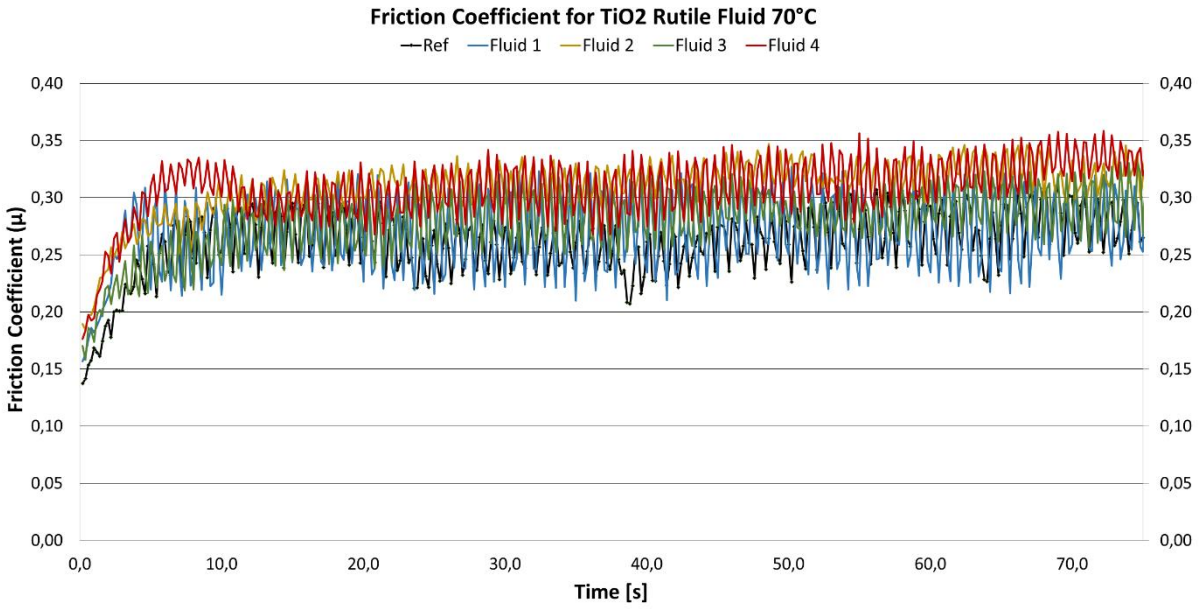

Figure 4-30 Friction coefficient tribometer measurement as a function of time - TiO_2 Rutile 70°C

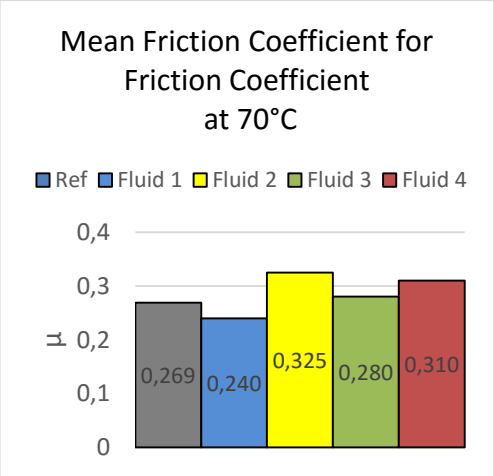

Figure 4-31 Mean Friction Coefficients for MoS_2 at 70°C

Temperature was increased to 70°C, which increased μ for all fluids. As seen in Figure 4-30 and Figure 4-31 the difference between all fluids is very low. The reference fluid without nano-additive yields a μ of 0.269, which is negligibly higher than the two at lower temperatures. The addition of 0.2g, 0.3g and 0,4g of TiO_2 to the reference fluid formulation yield 0.325(+21%), 0.280(+4%) and 0.310(+15%) respectively. Fluid 1, 0.1g added TiO_2, decreases friction to 0.240(-11%).

As seen in Table 4-10 below shows, Fluid 1 reduces friction as temperature increases. It would be interesting to see what other concentrations in that lower region of around 0.1g added nano might yield. No TiO_2 particle concentrations in this screeing show positive effect on friction testing. The relationship is non-linear in terms of concentration of nano-additive and mean friction coefficients. As shown in those figures the addition of TiO_2 nanoparticles yield only a small effect in friction coefficient values for all concentrations and temperatures. Table 4-10 shows the percentage change for all fluids relative to the reference fluid. The numbers are based on the mean values shown in Table 4-11, where we see the friction coefficient model as a function of temperature.

Table 4-10 µ-%Change associated with reference for TiO_2

µ-%Change associated with reference for			
°C	22°	55°	70°
Fluid 1 (Ref +0,1g)	0 %	-6 %	-11 %
Fluid 2 (Ref +0,2g)	+4 %	+7 %	+21 %
Fluid 3 (Ref +0,3g)	+1 %	+1 %	+4 %
Fluid 4 (Ref +0,4g)	+8 %	+9 %	+15 %

Based on the friction measurement data of fluid samples at different temperatures a model was generated in the form of a trend line. Displayed Figure 4-32 and Table 4-11 it one can observe 2 our of 5 fluids have an R^2 of 0.8 or above representing linear behavior. Fluid one is not increasing though.

Table 4-11 Models for mean friction coefficient data as a function of temperature for TiO_2 added drilling fluid systems

Drilling fluids	**Friction measurement**			**Model**	**R^2**
	22°C	50 °C	70 °C		
Reference	0.455	0.565	0.529	y = 0,0018x + 0,4264	0.6440

Fluid 1	0.355	0.372	0.386	y = -0,0006x + 0,2805	0.9970
Fluid 2	0.252	0.268	0.340	y = 0.0016x + 0.2074	0.7200
Fluid 3	0.237	0.402	0.331	y = 0.0025x + 0.2027	0.5279
Fluid 4	0.202	0.327	0.344	y = 0.0031x + 0.1401	0.9592

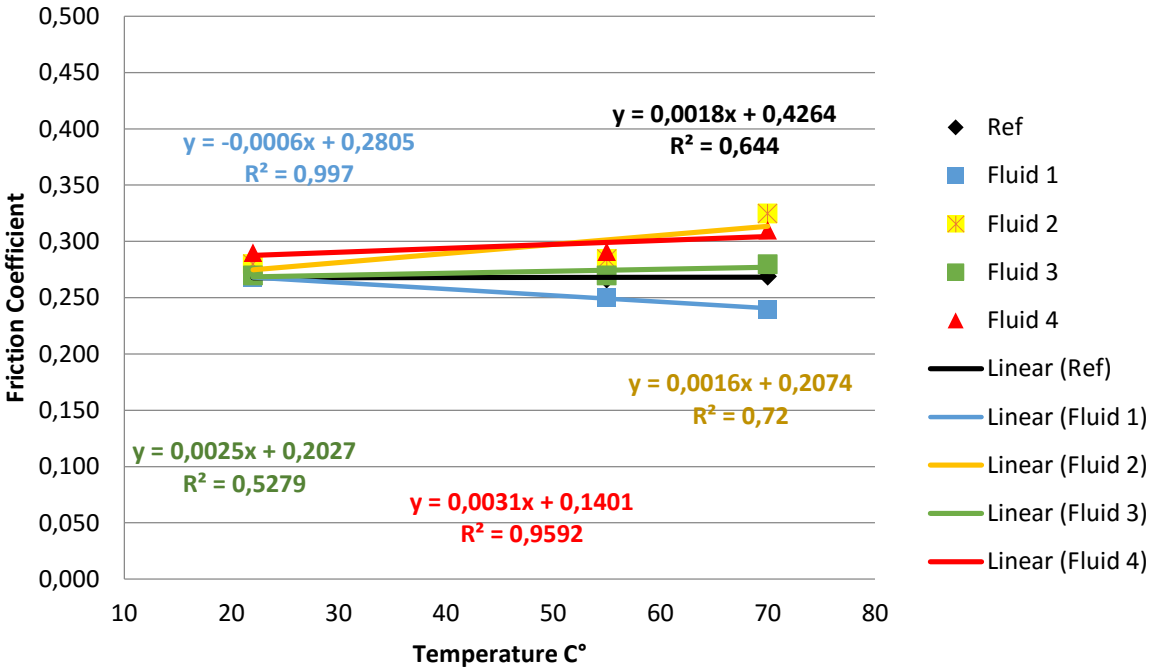

Figure 4-32 Mean Friction Coefficiens vs temperature with trendline for TiO_2

4.5 Effect of Graphene nanoparticles

Graphene is an allotrope of carbon. Figure 4-33 illustrate the two-dimensional form of graphene. In atomic scale, graphene has a honey-comb lattice. At each vertex, carbon atom forms.

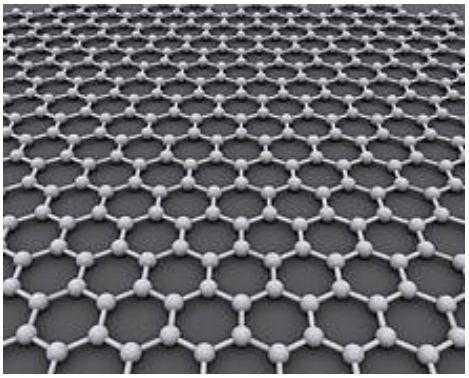

Figure 4-33 Illustration of graphene lattice [32]

Graphene has many amazing properties. It is a strong material. Recently its application in cement and drilling fluids has been documented. Figure 30 shows the SEM picture of nano graphane plates. [33]

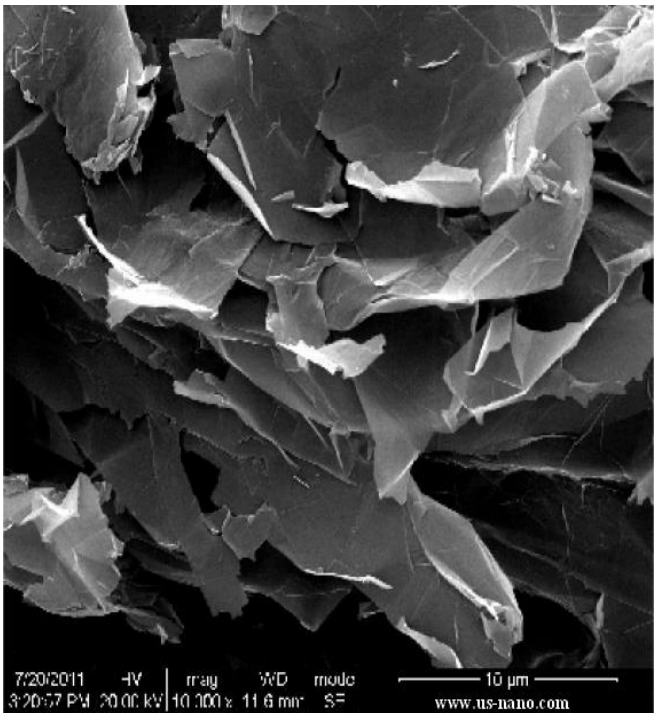

Figure 4-34 SEM picture of Graphene [33]

The performance of Graphene has been evaluated in the presence of Xanthan gum polymer and KCL salt.

Table 4-12 shows the graphene treated drilling fluid formulation.

The fluids were mixed in the order:

500g H_2O + Xg Nano + 2,5g KCl + 0,5g XG + 25g Bentonite

Table 4-12 Test matrix for nano - Grapehene in base drilling fluid system

Test matrix for Nano – Graphene in fluid system					
Ingredient	Ref Fluid	Fluid 1	Fluid 2	Fluid 3	Fluid 4
H2O	500	500	500	500	500
Nano - Graphene	0	0,1	0,2	0,3	0,4
KCl	2,5	2,5	2,5	2,5	2,5
XG	0,5	0,5	0,5	0,5	0,5
Bentonite	25	25	25	25	25

4.5.1 Results and analysis of drilling fluid system containing nanosized Graphene

4.5.1.1 Rheology, filtrate and pH results

The drilling fluids formulated in Table 4-12 are characterized through rheology, filtrate and pH measurement. Figure 4-35 is the Fann-35 Viscometer responses of Graphene fluids including the reference fluid. The addition of Graphene shows an impact on the reference fluid for the addition of 0.3g and 0.4g additive in 500mL drilling fluid. As shown on Figure 4-35, the addition 0.3g increases viscosity, whereas 0.4g results in a reduction in viscosity relative to the base system. This shows that the effect of nano has a non-linear effect on rheology and there exhibits an optimum concentration that works best in the water based drilling fluid, as it was for other fluids in this thesis as well.

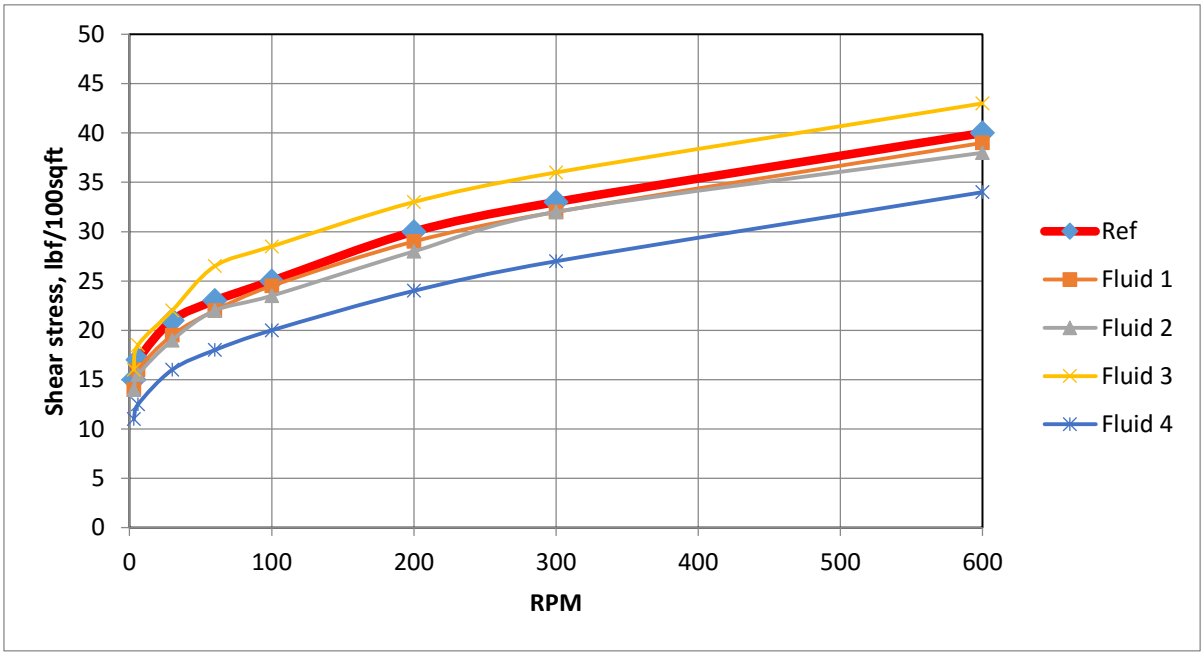

Figure 4-35 Rheology measurements for drilling fluid system containing Graphene

Based on the experimental data the Bingham and Power law parameters are calculated and shown in Figure 4-36 and Figure 4-37 respectively.

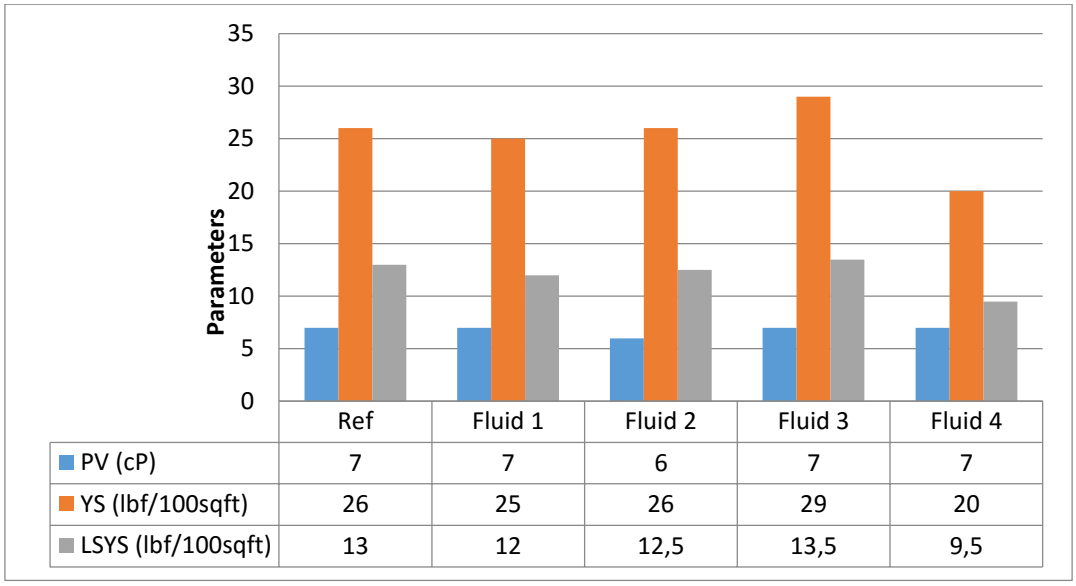

	Ref	Fluid 1	Fluid 2	Fluid 3	Fluid 4
PV (cP)	7	7	6	7	7
YS (lbf/100sqft)	26	25	26	29	20
LSYS (lbf/100sqft)	13	12	12,5	13,5	9,5

Figure 4-36 Presentation of PV, YS and LSYS results based on rheology measurements for Graphene added fluid system

The plastic viscosity (PV) is 7cP for all systems except for Fluid 2, yielding a measurement of 6cP. That means PV is unaffected by graphene based on our experimental data.

The yield strength (YS) parameter does not seem affected by the addition of of nanosized Graphene particles to the base fluid system. No linear trend can be observed by the linear increase of concentration. Figure 4-36 shows that the reference system had a Yield Strength of 26. Fluid 1 and Fluid 2 yield a measurement of 25 and 26 lbf/100sqft respectively. Fluid 3 and 4 with 0.3g and 0.4g added nano yield 29 and 20 lbf/100sqft respectively. This effect is not coherent with the small difference in concentration of nano-additive, but is arguably accepted as a result regardless.

The lower shear yield stress parameter (LSYS) is high in general for fluids with Xanthan Gum polymer. As seen in Figure 4-36, the addition of very small increase in concentration of Graphene nanoparticles changes LSYS from 12 in the reference to 12.0 in 0.1g added graphene, to 12.5 in 0.2g added graphene, to 13.5 with 0.3g added Graphene and 9.5 for 0.4g added Graphene to the reference fluid formula . That is essentially an insignificant change in fluid parameters from added nanoparticles. That means adding nanosized graphene in small concentrations does not affect sagging.

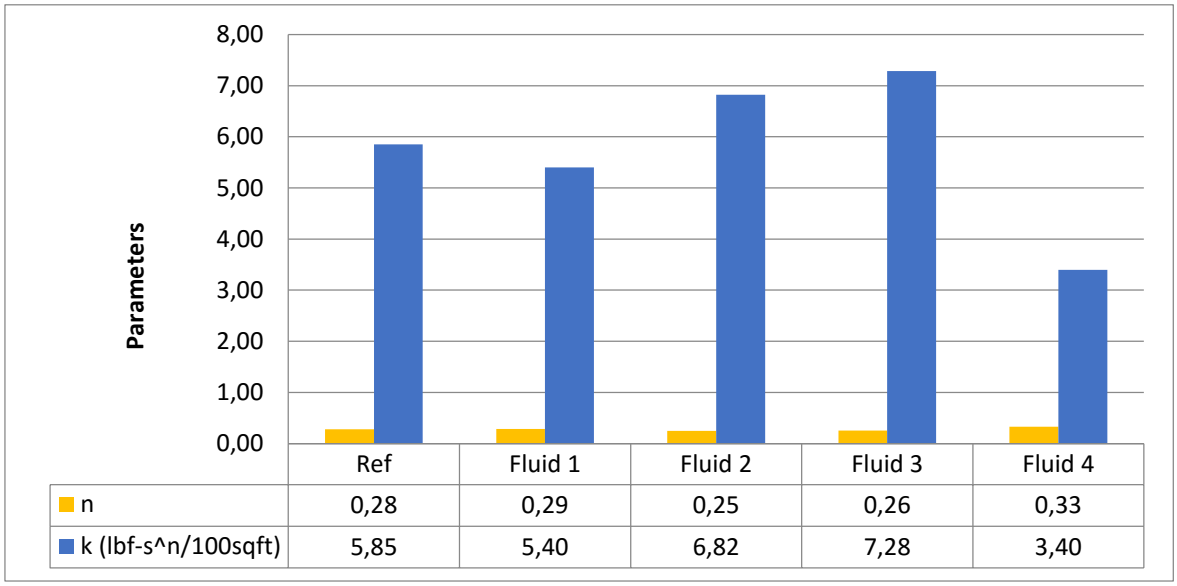

Figure 4-37 Consistency index(k) and flow index n - Graphene fluid systems

The flow and consistency index is displayed in Figure 4-37. As we can see the n-value is fairly constant for set temperature and no effect from added nanoparticles can be observed, for most of the fluid.

The consistency Index for Fluid 1, 2, 3 and 4 is 5.40, 6.82, 7.28 and 3.40 lbf-s^n/100sqft respectively. The reference fluid system yields 5.85 lbf-s^n/100sqft. The power law model shows the difference in consistency index between Fluid 3 and Fluid 4 very cleary.

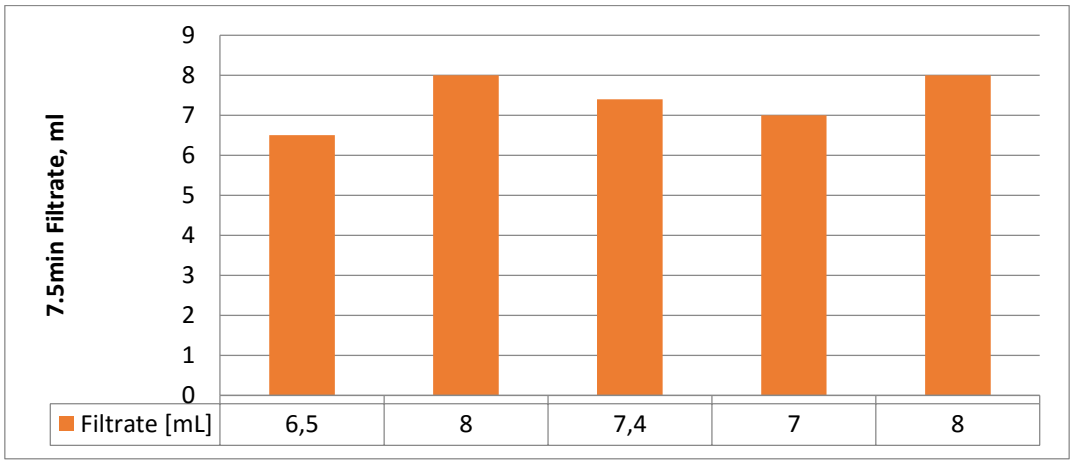

Figure 4-38 Diagram and data for filtrate loss of drilling fluid system containing Graphene

The filtrate loss, shown in Figure 4-38, is slightly increased from 6.5 in the base fluid system to 8.0 mL, 7.4 mL,7 mL and 8mL in Fluid 1,2,3 and 4 respectively. That

indicates that small amounts of added nanoparticles of Graphene might disrupt the pore-plugging bridging effect to reduce filtrate loss. Filtrate loss, like viscosity seems to exhibit an optimum concentration behavior and not a linear trend in correlation with concentration of nanoparticles in WBM.

Table 4-13 pH measurements for Graphene

Measurement	Ref fluid	Fluid 1	Fluid 2	Fluid 3	Fluid 4
pH	9.0	9.0	9.0	9.0	9.0

As seen in Table 4-13, the addition of Graphene to the base fluid system seems not to effect on the acidity/alkalinity on the reference fluid system.

4.5.1.2 Rheology modeling

Table 4-14 describes how each parameter in a rheological fluid model is affected by the addition of Graphene nanoparticles. Percentage deviation from the reference fluid parameter has been included. E.g. μ-value for for the Newtonian model experiences a -16.7% reduction for Ref+0.4g Graphene relative to the reference fluid, meaning the curve has a less steep slope i.e a smaller gradient. The models itself are included in Appendix A

Table 4-14 Rheology model parameters and percentage deviation from the reference fluid – Graphene.

Model	Parameter	Ref	Ref + 0.1g Graphene	Ref + 0.2g Graphene	Ref + 0.3g Graphene	Ref + 0.4g Graphene
Herschel-Bulkley	τo	14,130	12,863	13,412	14,029	10,277
	% deviation		-8,96	-5,08	-0,71	-27,27
	k	1,0399	1,159	0,7712	1,8087	0,7563
	% deviation		11,45	-25,84	73,93	-27,27
	n	0,484	0,4692	0,5237	0,9856	0,5157
	% deviation		-3,06	8,20	103,64	6,55
Unified	τy	13,8710	12,8040	13,3375	14,4045	10,1365
	% deviation		-7,69	-3,85	3,85	-26,92
	k	1,1899	1,1937	0,8111	1,5740	0,8327
	% deviation		0,32	-31,83	32,28	-30,02
	n	0,4641	0,4648	0,5161	0,4404	0,5012
	% deviation		0,15	11,20	-5,11	7,99
Power Law	k	11,8480	10,9440	10,7920	12,7730	8,2450
	% deviation		-7,63	-8,91	7,81	-30,41
	n	0,1746	0,1830	0,1812	0,1775	0,2012
	% deviation		4,81	3,78	1,66	15,23
Bingham	τy	19,8120	18,8760	18,4190	21,9430	14,8740
	% deviation		-4,72	-7,03	10,76	-24,92
	μp	0,0252	0,0251	0,0246	0,0267	0,0232
	% deviation		-0,40	-2,38	5,95	-7,94

Newtonian	**μ**	0,0533	0,0519	0,0507	0,0579	0,0444
	% deviation		**-2,63**	**-4,88**	**8,63**	**-16,70**
Robertson and Stiff	**A**	6,3651	6,3031	5,5821	8,4406	4,1850
	% deviation		**-0,97**	**-12,30**	**32,61**	**-34,25**
	C	28,9323	23,2748	29,6904	16,7646	26,8374
	% deviation		**-19,55**	**2,62**	**-42,06**	**-7,24**
	B	0,2727	0,2704	0,2853	0,2434	0,3085
	% deviation		**-0,84**	**4,62**	**-10,74**	**13,13**

4.5.1.3 *Coefficient of friction*

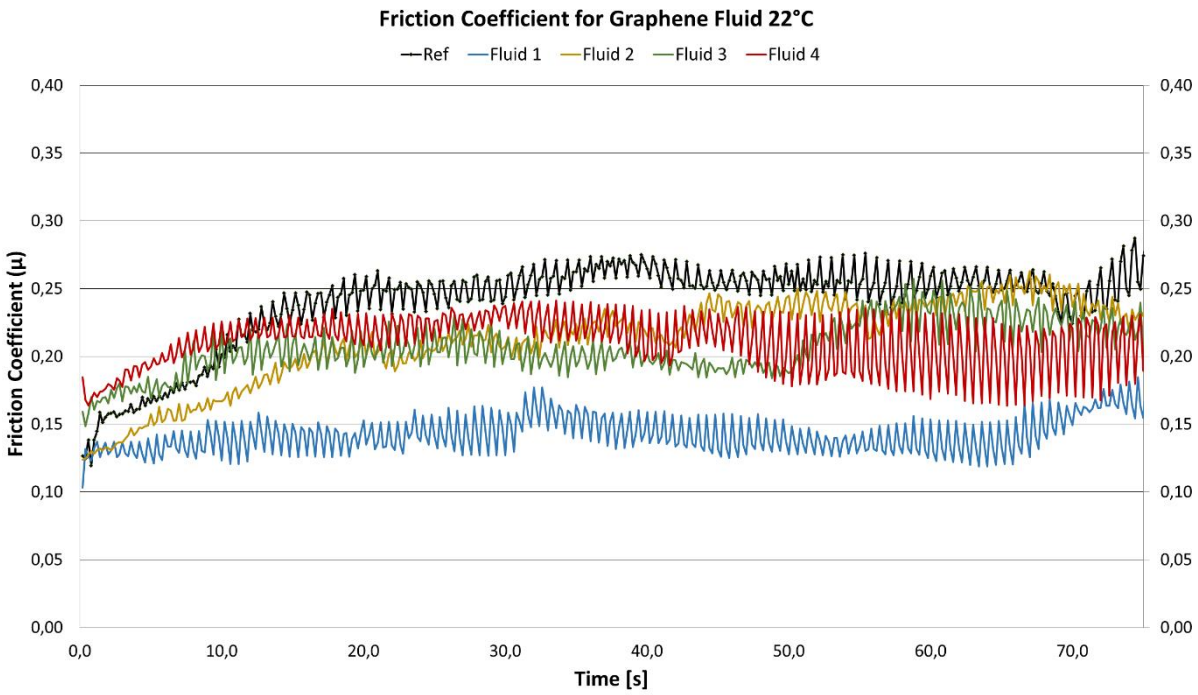

Figure 4-39 Friction coefficient tribometer measurement as a function of time - Graphene 22°C

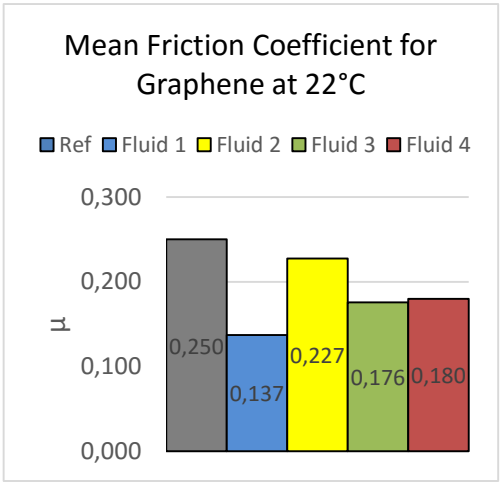

Figure 4-40 Mean Friction Coefficients for Graphene at 22°C

Figure 4-39 shows the raw friction coefficient measurement data of Graphene added fluid system with Xantham Gum polymer from the tribometer system. All fluids were measured at 22°C. In Figure 4-40 we see the average values of μ for all the Graphene added fluid system measured at 22°C

The results from these tests indicate that adding nanosized Graphene particles to the reference fluid decreases μ with concentration not in a constant manner. The lowest observed mean value for this test was 0,137, which represents a 31% reduction from the reference coefficient of 0,250. Further, below Table 4-15 shows all percentage changes in friction for all fluids compiled.

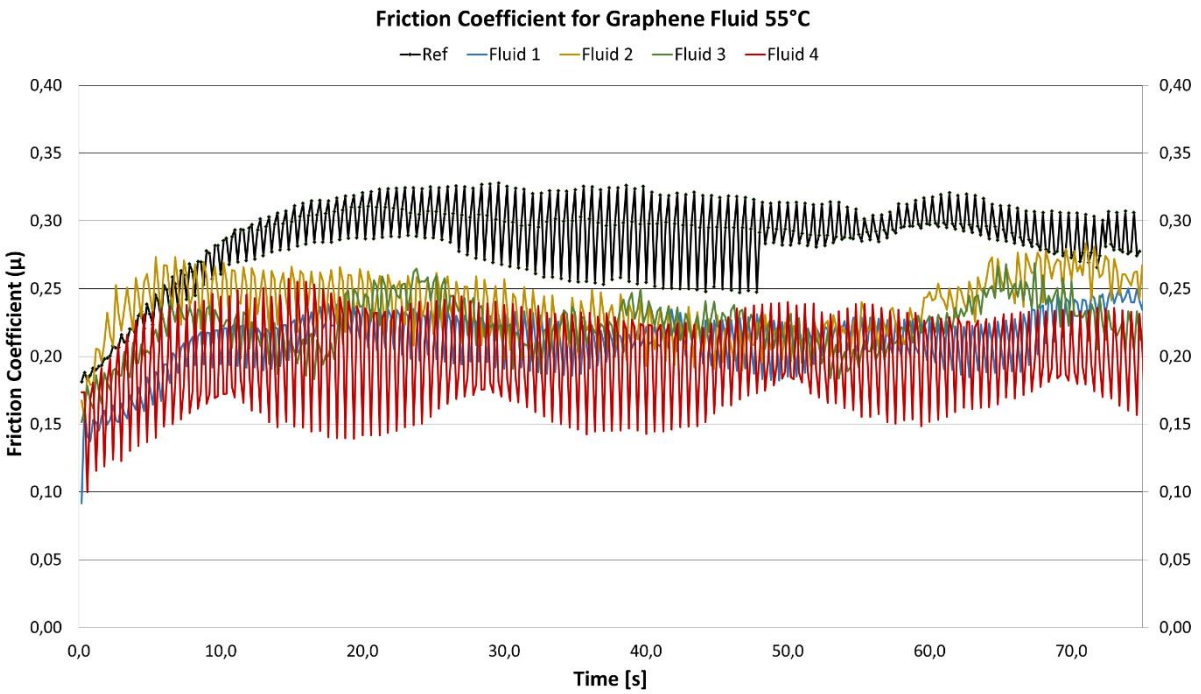

Figure 4-41 Friction coefficient tribometer measurement as a function of time - Graphene 55°C

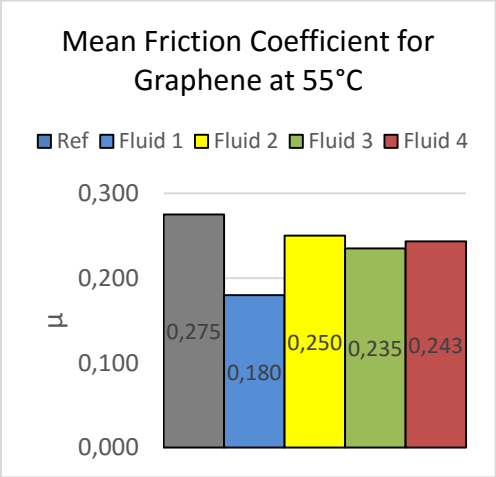

Figure 4-42 Mean Friction Coefficients for Graphene at 55°C

For 55°C, Figure 4-41 and Figure 4-42 graphene-modified fluids indicate increased lubricity, by decreased μ. The optimum amount was 0.1g at this temperature, whereas higher amounts slightly increased friction. The lowest observed mean value for this test was 0,180 which represents a 56% reduction from the reference coefficient of 0,250.

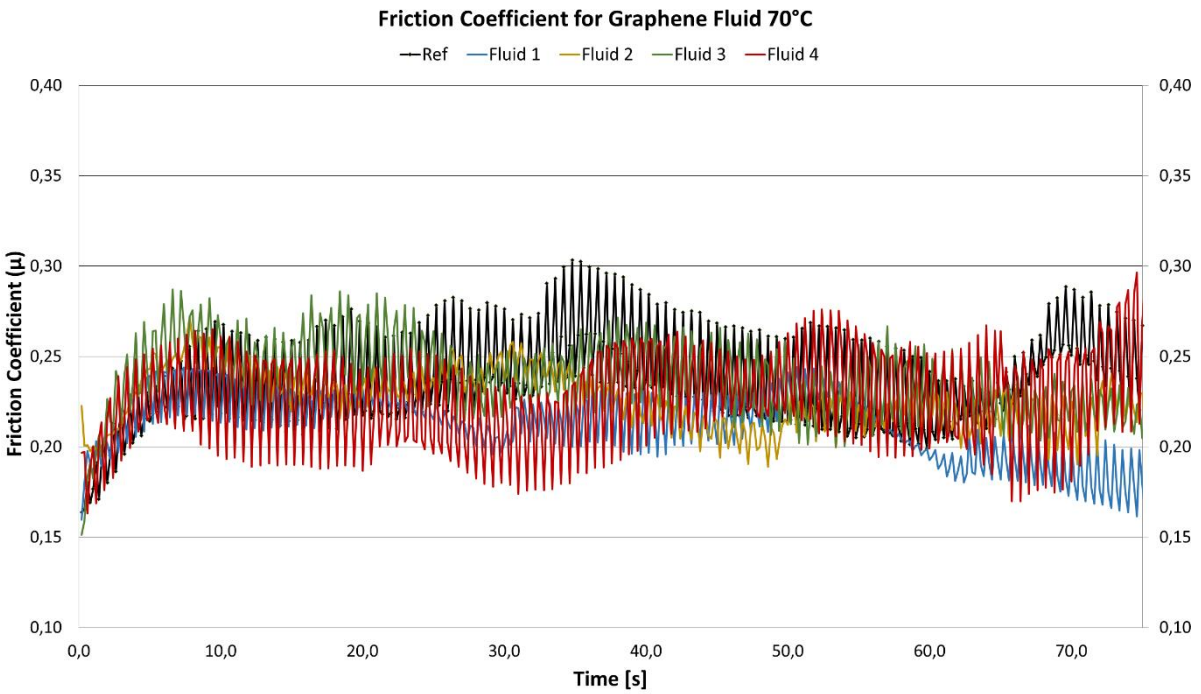

Figure 4-43 Friction coefficient tribometer measurement as a function of time - Graphene 70°C

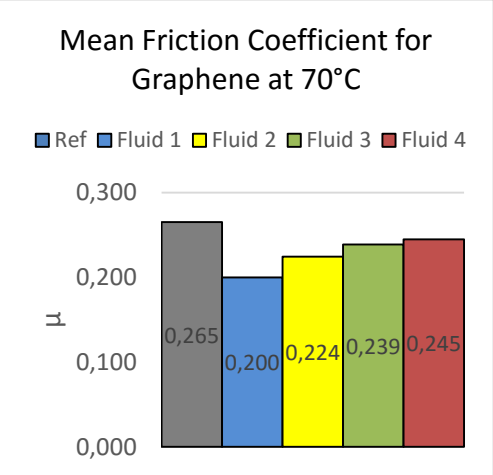

Figure 4-44 Mean Friction Coefficients for Graphene at 70°C

Figure 4-43 shows the raw friction coefficient measurement data of Graphene added fluid system directly from the tribometer system. All these fluids were measured at temperature of 70°C.

From Figure 4-44 displays that graphene-modified fluids have higher lubricity also at 70°C, relative to the reference system. The lowest observed mean value for this test was 0,200 for 0.1g added graphene which represents a 27% reduction from the reference friction coefficient of 0,250.

For comparison purpose the percentage - reduction of coefficient friction due to the nano graphene additive is calculated with respect to the reference nano free drilling fluid (see Table 4-15.)

Table 4-15 µ-%Change with respect to reference

µ-%Change with respect to the reference			
°C	22°	55°	70°
Fluid 1 (Ref +0,1g)	-56 %	-42 %	-27 %
Fluid 2 (Ref +0,2g)	-11 %	-11 %	-17 %
Fluid 3 (Ref +0,3g)	-37 %	-18 %	-11 %
Fluid 4 (Ref +0,4g)	-35 %	-14 %	-8 %

The addition of Graphene nanoparticles yields an increase in lubricity all additions tested and also in all temperatures measured.

Table 4-16 Models for mean friction coefficient data as a function of temperature for Graphene added drilling fluid systems

Drilling fluids	**Friction measurement**			**Model**	**R^2**
	22 ºC	50 ºC	70 ºC		
Reference	0,250	0,275	0,265	y = 0,0018x + 0,4264	0,6440
Fluid 1	0,137	0,180	0,200	y = 0,0013x + 0,1084	1,0000
Fluid 2	0,227	0,250	0,224	y = 0,0016x + 0,2074	0,7200
Fluid 3	0,176	0,235	0,239	y = 0,0025x + 0,2027	0,5279
Fluid 4	0,180	0,243	0,245	y = 0,0031x + 0,1401	0,9592

The mean of the measured data for all temperatures is summarized in this table and illustrated with trendlines in Figure 4-45. The figure displays that as temperature increases the coefficient of friction becomes higher. R^2 indicates the accuracy between the trendline and the measured data. For Fluid 1 R^2 is exactly 1, indicating 100% correlation.

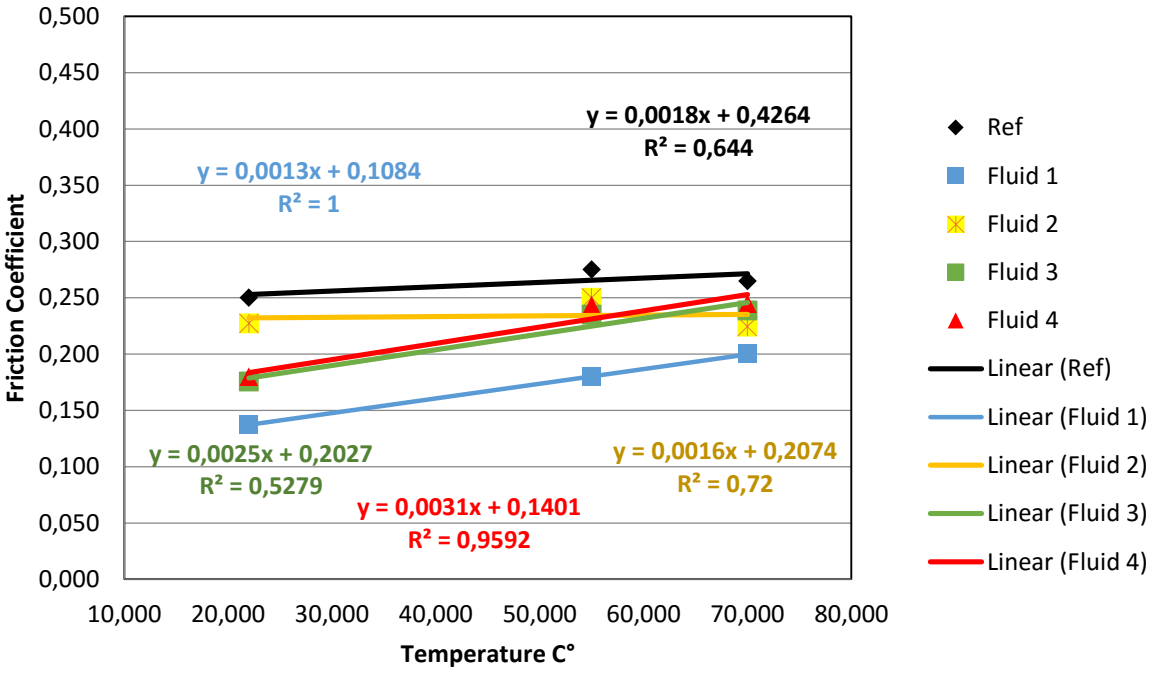

Figure 4-45 Mean Friction Coefficiens vs temperature with trendline for Graphene

4.6 Effect Titanium Nitride (TiN) nanoparticles

The melting point of nano-titanium nitride is 2950 °C. Other properties of TiN are it has high hardness, high-temperature chemical stability and very good thermal conductivity properties.

It is widely used as barrier layer in contact and interconnect metallization, as well as Wear-resistant coating can be mentioned as example. However, up to the author knowledge, it is not documented its application in drilling fluid. This thesis considered the particle to evaluate its performance in drilling fluid

Figure 4-46 shows SEM the photograph picture of the particle [34]

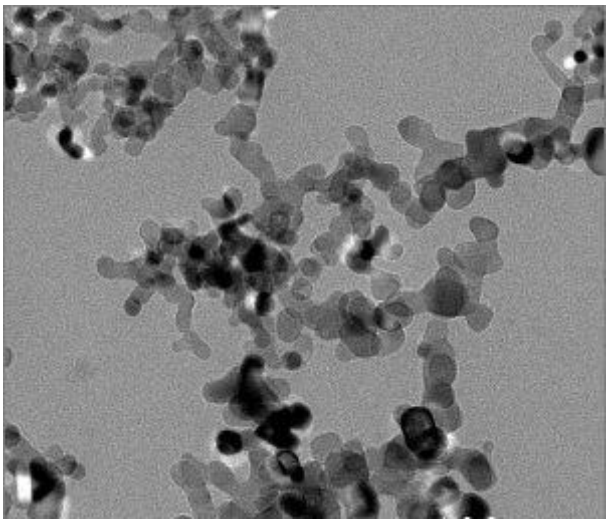

Figure 4-46 SEM photograph of TiN particles. [34]

4.6.1 Drilling fluid system containing TiN nanoparticles

The fluid system containing PAC was prepared and added nano - TiN in order to evaluate the properties gained from nanoparticles combined with KCl and PAC. The fluids are listed in Table 4-17.

The fluids were mixed in the order:

500g H_2O + Xg Nano + 2,5g KCl + 0,5g PAC + 25g Bentonite

Table 4-17 Test matrix for drilling fluid system with added TiN

Test matrix for Nano – Titanium Nitride (TiN) in fluid system					
Ingredient	Ref Fluid	Fluid 1	Fluid 2	Fluid 3	Fluid 4
H2O	500	500	500	500	500
Bentonite	25	25	25	25	25
PAC	0,5	0,5	0,5	0,5	0,5
KCl	2,5	2,5	2,5	2,5	2,5
Nano - TiN	0	0,1	0,2	0,3	0,4

4.6.2 Results and analysis of drilling fluid system containing TiN

4.6.2.1 Rheology, filtrate and pH results

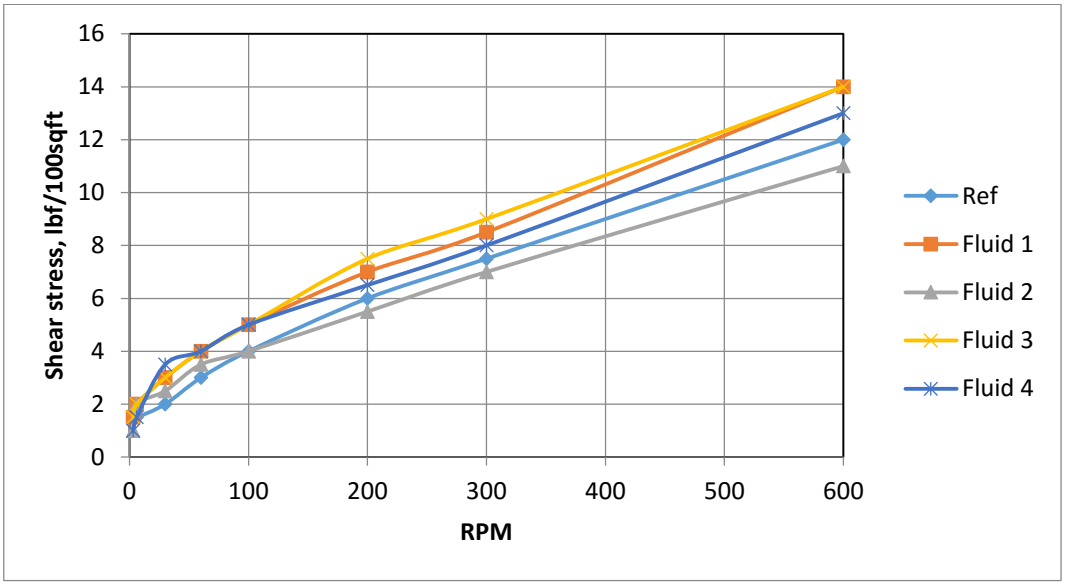

Figure 4-47 Rheology measurements for drilling fluid system containing TiN

Figure 4-47 displays the Fann-35 Viscometer responses of the measured drilling fluids. These experimental are further studied in the Bingham and Power law models. Their plot and parameters are shown in Figure 44 and Figure 45 respectively.

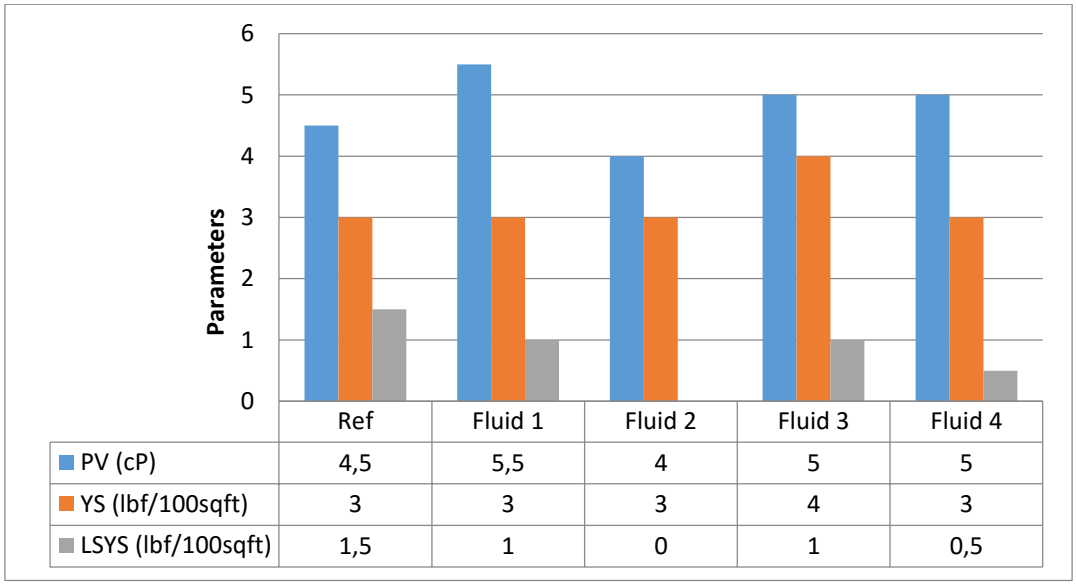

	Ref	Fluid 1	Fluid 2	Fluid 3	Fluid 4
PV (cP)	4,5	5,5	4	5	5
YS (lbf/100sqft)	3	3	3	4	3
LSYS (lbf/100sqft)	1,5	1	0	1	0,5

Figure 4-48 Presentation of PV, YS and LSYS results based on rheology measurements for TiN added fluid system

In Figure 4-48 we see that he plastic viscosity (PV) between 4cP and 5.5 cP for all systems. The yield strength (YS) parameter does not seem affected by the addition of nanosized TiN.

The lower shear yield stress (LSYS) parameter is very low in general for fluids with PAC polymer, hence only a slight change can be observed from 1.5 to 0. That is essentially an insignificant change in fluid parameters from added TiN nanoparticles.

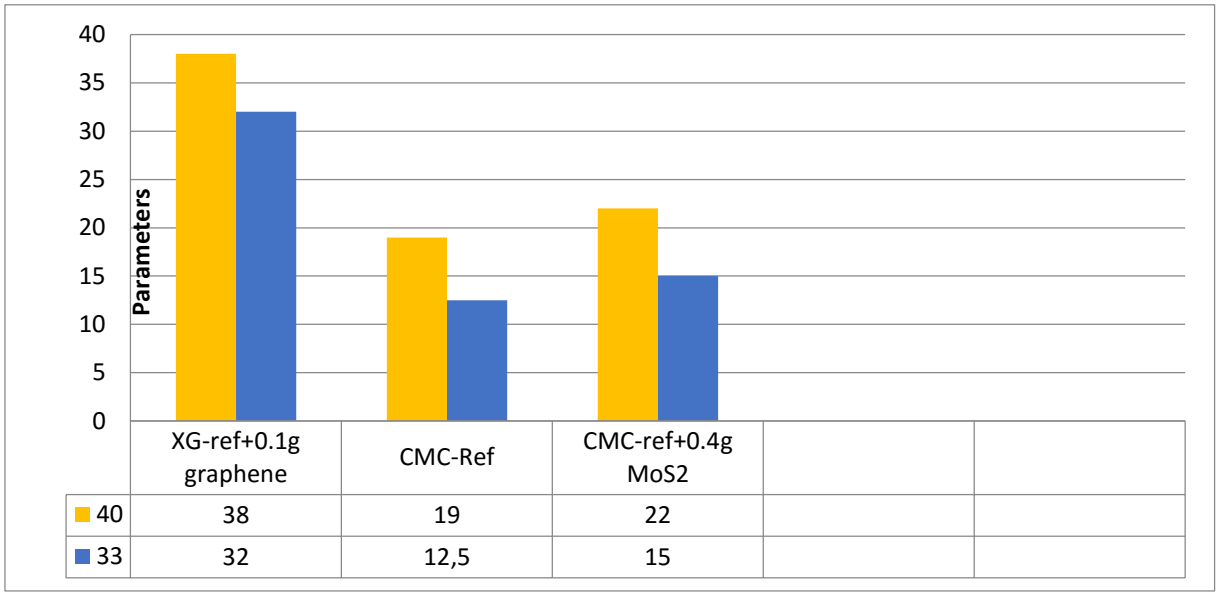

Figure 4-49 Consistency index(k) and n-value for TiN fluid systems at different temperatures.

Figure 4-49 displays the consistency and flow index for the Power Law model. As we can see the n-value is fairly constant and no effect from added nanoparticles can be observed, ranging from 0.10 to 0.17, where the reference fluid system yields 0.11.

The Consistency Index, k, describes the average slope of the shear stress – shear rate curve. The highest k value from the test of TiN added fluids is the one with the least (+0.3g) added TiN nanoparticles. That is why that fluid has also the highest viscosity, but the difference is very low.

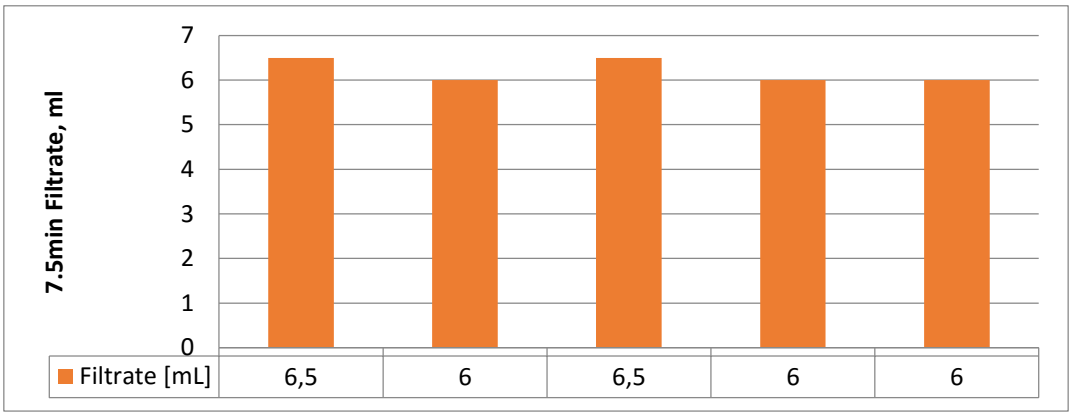

Figure 4-50 Diagram and data for filtrate loss of drilling fluid system containing TiN_2

As seen in Figure 4-50 the reference system is not affected by the addition of nanoparticles in terms of filtrate loss, as they all respond with very little deviation from the reference fluid. A slight reduction of -0.5mL can be observed for fluid 1, 3 and 4.

Table 4-18 pH measurements for TiN

Measurement	Ref fluid	Fluid 1	Fluid 2	Fluid 3	Fluid 4
pH	6,5	6.0	6,5	6.0	6.0

As seen in Table 4-18, the addition of TiN to the base fluid system seems to effect on the acidity/alkalinity on the reference fluid system.

4.6.2.2 Rheology modeling

Table 4-19 describes how each parameter in a rheological fluid model is affected by the addition of Graphene nanoparticles. Percentage deviation from the reference fluid parameter has been included. E.g. μp-value for the Bingham model experiences a 23.26% deviation (in the form of reduction because it is negative) for Ref+0.2g TiN relative to the reference fluid, meaning the curve has a less steep slope i.e. a smaller gradient.

Table 4-19 Rheology model parameters and percentage deviation from the reference fluid – TiN.

Model	Parameter	Ref	Ref + 0.1g TiN	Ref + 0.2g TiN	Ref + 0.3g TiN	Ref + 0.4g TiN
Herschel-Bulkley	τo	1,427	1,279	0,546	1,279	0,623
	% deviation		-10,38	-61,76	-10,38	-56,32
	k	0,0669	0,1398	0,3215	0,1379	0,1979
	% deviation		108,97	380,57	106,13	195,81
	n	0,7677	0,6552	0,4968	0,9870	0,6027
	% deviation		-14,65	-35,29	28,57	-21,49
Unified	τy	1,1737	1,0670	0,0000	1,0670	0,5335
	% deviation		-9,09	-100,00	-9,09	-54,55
	k	0,1656	0,2354	0,6574	0,2322	0,2401
	% deviation		42,15	296,98	40,22	44,99
	n	0,6250	0,5743	0,3928	0,5824	0,5729
	% deviation		-8,11	-37,15	-6,82	-8,34
Power Law	k	0,7657	0,8194	0,6574	0,8097	0,5182
	% deviation		7,01	-14,14	5,75	-32,32

	n	0,4011	0,3922	0,3928	0,3993	0,4580
	% deviation		**-2,22**	**-2,07**	**-0,45**	**14,19**
Bingham	**τy**	2,4033	2,3899	2,0121	2,5270	2,0660
	% deviation		**-0,56**	**-16,28**	**5,15**	**-14,03**
	μp	0,0129	0,0127	0,0099	0,0128	0,0121
	% deviation		**-1,55**	**-23,26**	**-0,78**	**-6,20**
Newtonian	**μ**	0,0163	0,0161	0,0128	0,0164	0,0151
	% deviation		**-1,23**	**-21,47**	**0,61**	**-7,36**
Robertson and Stiff	**A**	0,0711	0,2543	0,3553	0,2467	0,2952
	% deviation		**257,67**	**399,72**	**246,98**	**315,19**
	C	57,1269	22,8380	10,2342	22,8380	7,5275
	% deviation		**-60,02**	**-82,09**	**-60,02**	**-86,82**
	B	0,7716	0,5778	0,4909	0,5877	0,5481
	% deviation		**-25,12**	**-36,38**	**-23,83**	**-28,97**

4.6.2.3 Coefficient of friction

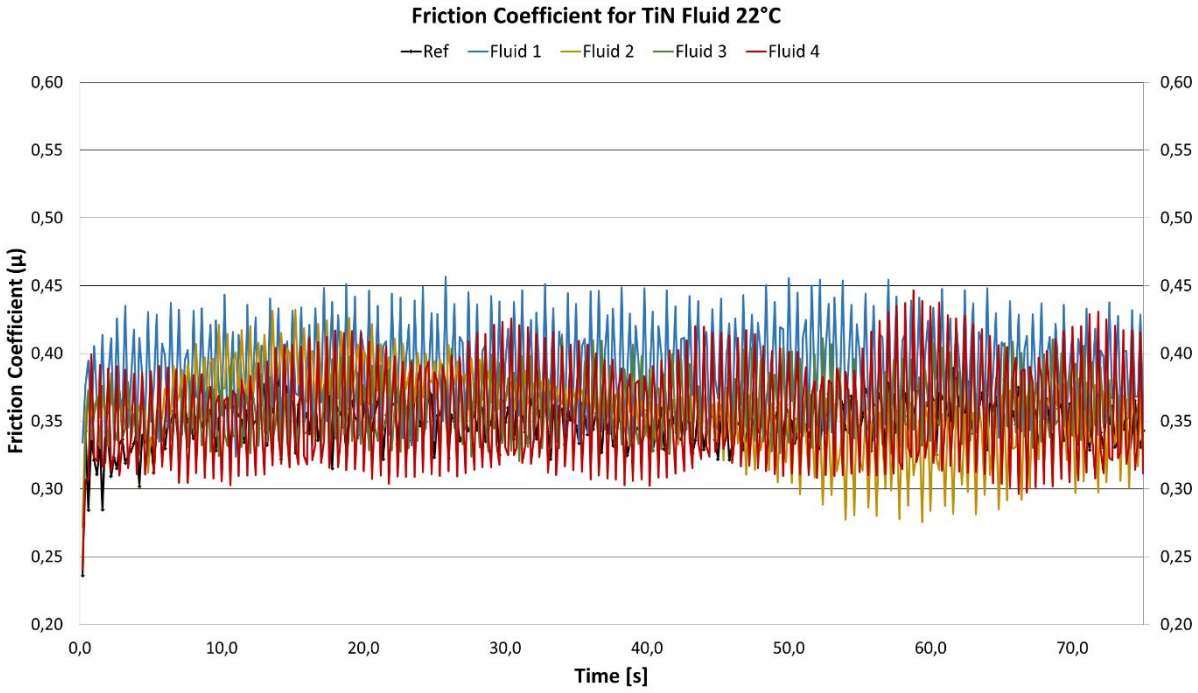

Figure 4-51 Friction coefficient tribometer measurement as a function of time for TiN 22°C

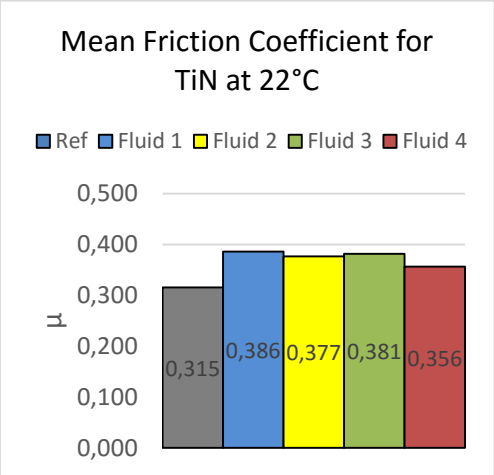

Figure 4-52 Mean Friction Coefficients for TiN at 22°C

Figure 4-51 shows the raw friction coefficient measurement data of base fluids with Titanium Nitride (TiN) from the tribometer apparatus. All these fluids were measured at ambient temperature at 22°C. In Figure 4-52 we can observe the average values of μ for all the TiN added fluid system measured at 22°C.

The results from these tests indicate that adding nanosized TiN particles to the reference fluid does not change very much μ at ambient temperature, compared to many other tests. As seen inFigure 4-52, the lowest observed mean value for this test was a μ of 0.315, which is from the reference fluid. The addition of TiN yields a slight increase in friction up to a μ of 0.386 (+22%) for 0.1g

added TiN nanoparticles. Table 4-20 on page 93 displays the other %-changes relative to its reference fluids.

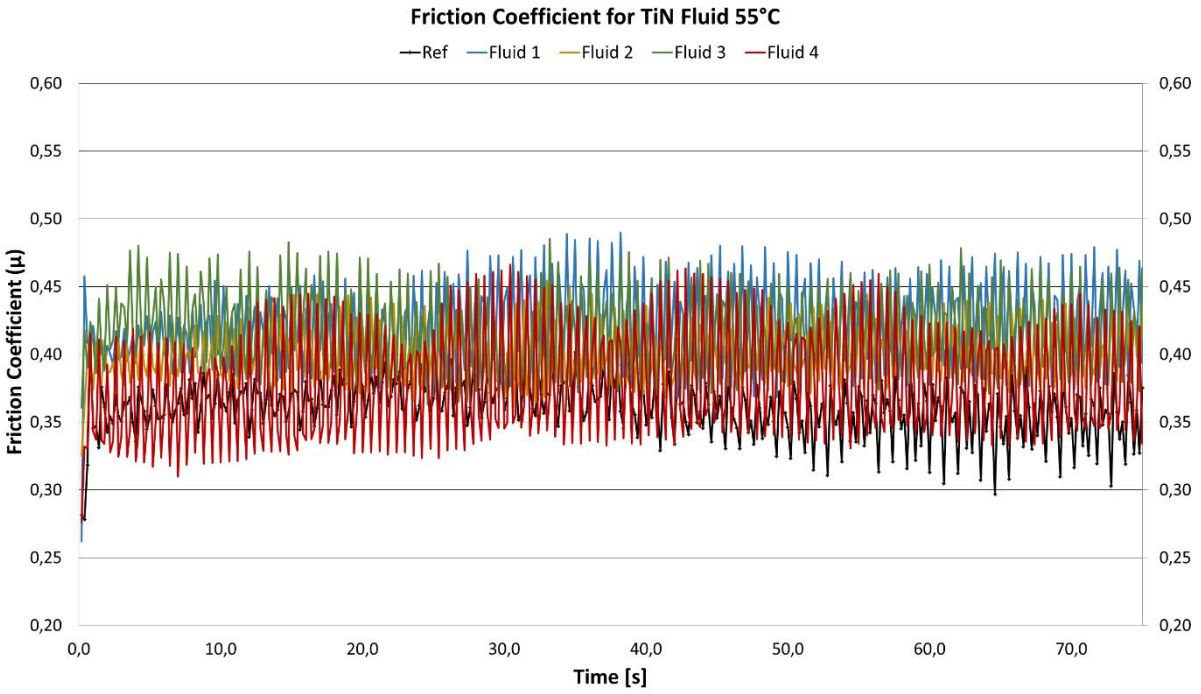

Figure 4-53 Friction coefficient tribometer measurement as a function of time for TiN 55°C

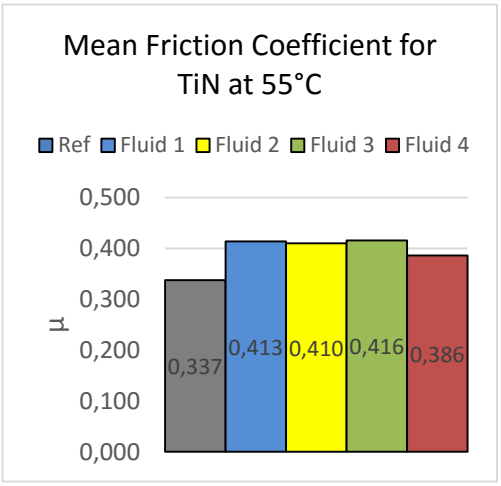

Figure 4-54 Mean Friction Coefficients for TiN at 55°C

Figure 4-53 shows the raw friction coefficient measurement data of base fluids with Titanium Nitride (TiN) from the tribometer apparatus. All these fluids were measured at 55°C. From Figure 4-54 it can be observed that adding nanosized TiN particles to the reference fluid does not affect the lubricity at 55°C. The lowest observed mean value for this test was a μ of 0.337, which is from the reference fluid. The addition of TiN yields a slight increase in friction coefficient up to 0.416 (+23%) for 0.3g added TiN nanoparticles. Relatively the result is very similar to the one taken at 22°C. Table 4-20 on page 93 displays the other %-changes relative to its reference fluids.

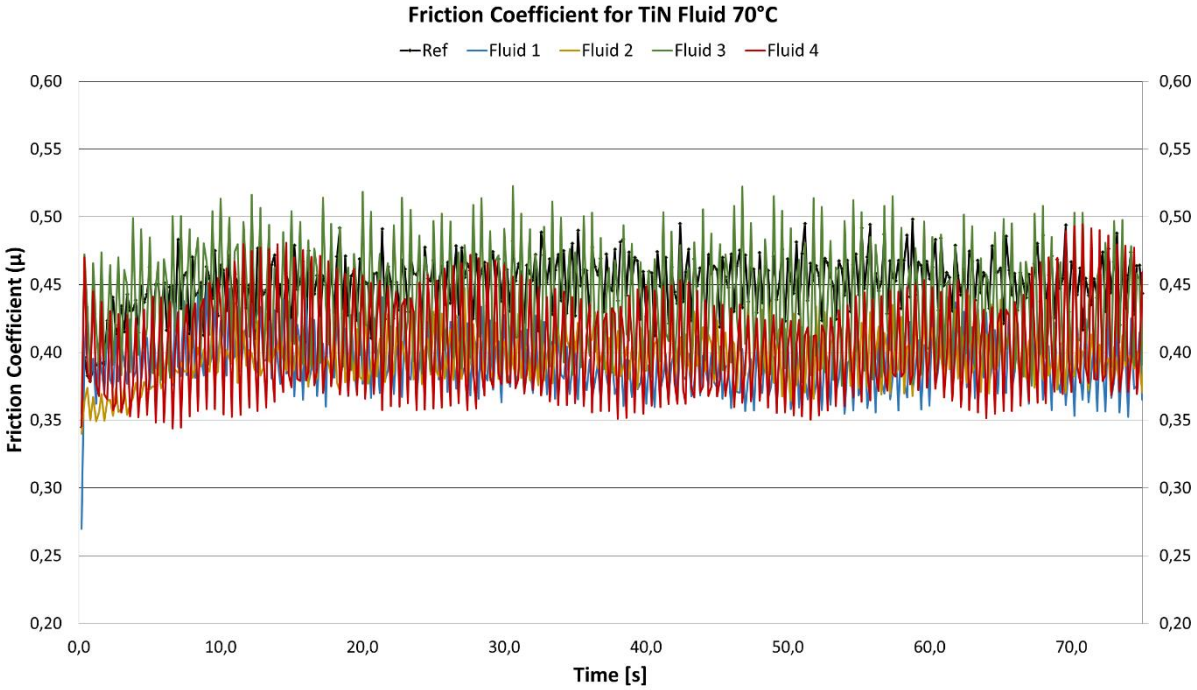

Figure 4-55 Friction coefficient tribometer measurement as a function of time for TiN 70°C

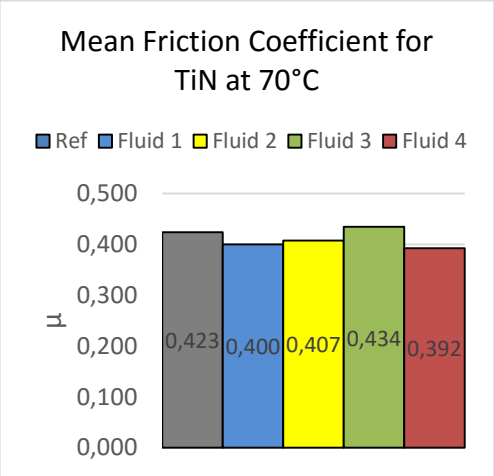

Figure 4-56 Mean Friction Coefficients for TiN at 70°C

Figure 4-55 and Figure 4-56 indicate that adding nanosized TiN particles to the reference fluid does not affect μ at 70°C temperature. The lowest observed mean value for this test was a μ of 0.392(-7%), which is from 0.4g added nanoparticles, which is a reduction of mew from 0.423 given from the reference fluid. The fluids in this temperature area seem to respond all almost with the same value.

Table 4-20 µ-%Change associated with reference for TiN

µ-%Change associated with reference for TiN			
°C	22°	55°	70°
Fluid 1 (Ref +0,1g)	+22 %	+23 %	-6 %
Fluid 2 (Ref +0,2g)	+19 %	+21 %	-4 %
Fluid 3 (Ref +0,3g)	+21 %	+23 %	+13 %
Fluid 4 (Ref +0,4g)	+13 %	+14 %	-7 %

Based on experiments with TiN-modified drilling fluid system, no no lubricating effect could be observed..

Table 4-21 Models for mean friction coefficient data as a function of temperature for TiN added drilling fluid systems

Drilling fluids	**Friction measurement**			**Model**	**R^2**
	22 °C	50 °C	70 °C		
Reference	0,315	0,337	0,423	y = 0,002x + 0,2612	0,7331
Fluid 1	0,386	0,413	0,400	y = 0,0004x + 0,3812	0,4655
Fluid 2	0,377	0,410	0,407	y = 0,0018x + 0,4264	0,8669
Fluid 3	0,381	0,416	0,434	y = 0,0011x + 0,3570	0,9981
Fluid 4	0,356	0,386	0,392	y = 0,0008x + 0,3400	0,9764

Figure 4-57 shows that as temperature increases the coefficient of friction becomes higher as well. The addition of TiN nanoparticles does not reduce the coefficient of friction profile below the nanofree system for our screening case. Still, R^2 is above 0.8 for 3 out of 5 fluid representing the linear relationship.

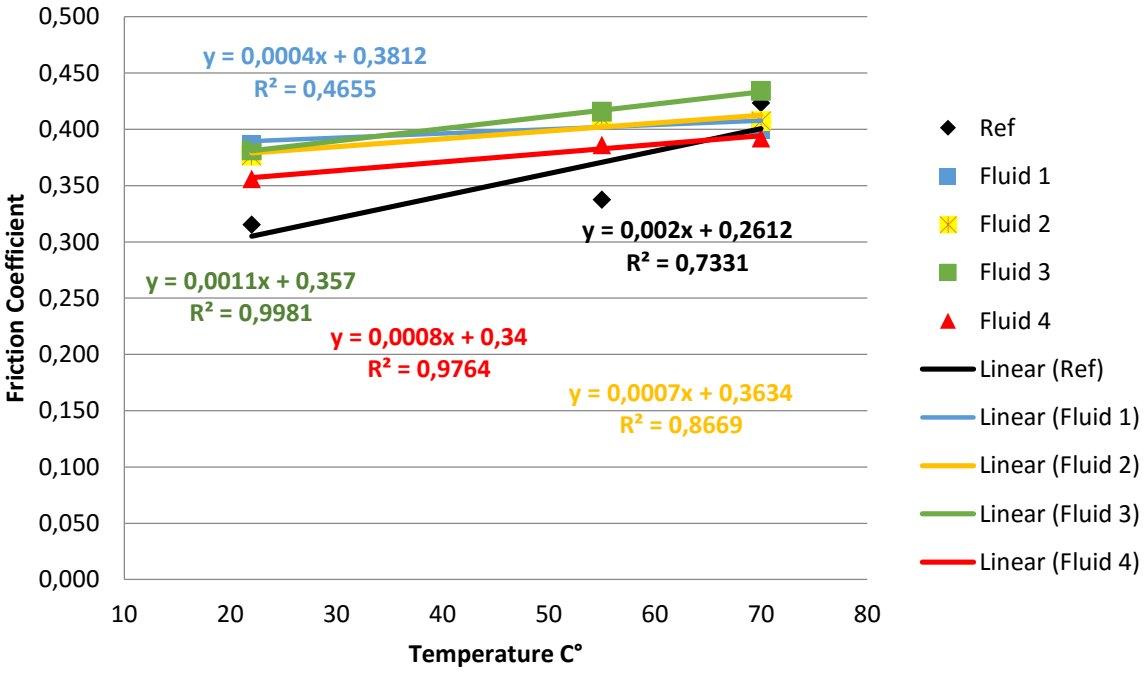

Figure 4-57 Mean Friction Coefficiens vs temperature with trendline for TiN

4.7 Viscoelasticity – Oscillatory test: Amplitude Sweep

Drilling fluids can display viscous and elastic responses during deformation. The elastic property has an effect on the flow behavior and pressure drop during circulation of drilling fluid. The measure of viscoelastic properties of drilling fluids allow for the evaluation of the gel strength of drilling fluid. MoS_2- modified systems showed great effect on rheology and lubricity it have been selected for an amplitude sweep analysis. Additionally, fluids containing graphene have been tested as well. To classify viscoelastic behavior of fluids one can investigate the yield point or the flow point. In this thesis, we use the flow point to evaluate viscoelastic properties.

Figure 4-58 shows the phase angle vs the shear stress obtained from the experiment. The bar diagram in Figure 4-59 displays the results, where we clearly see energy absorbed by the fluid is at least doubled for the MoS_2 modified fluids. That indicates an improvement in terms of hydraulics and barite sagging.

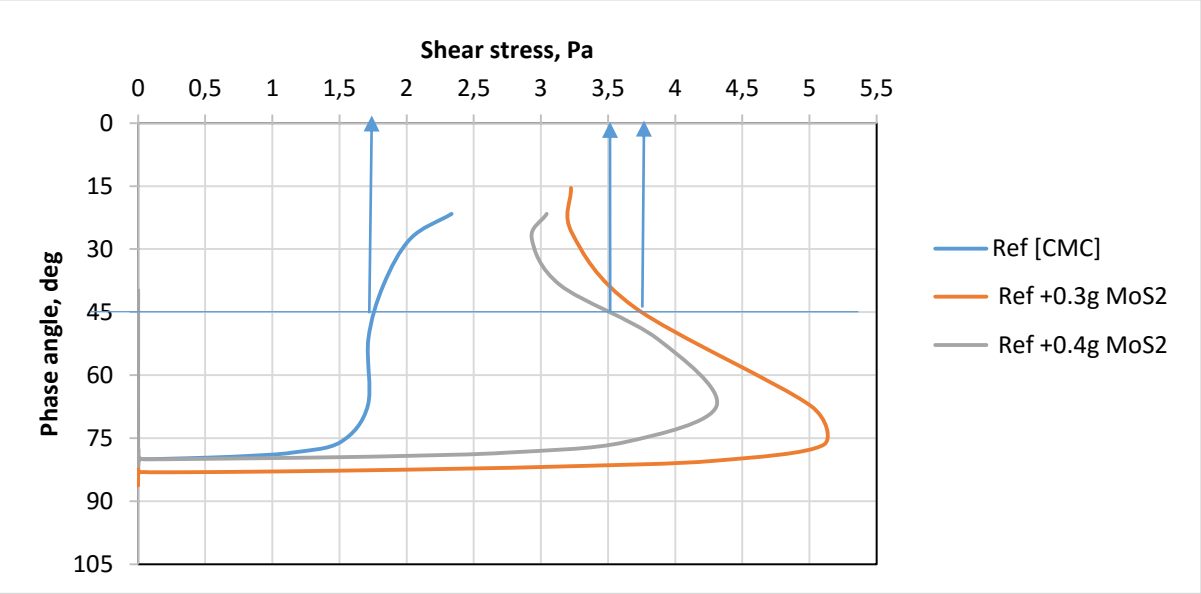

Figure 4-58 Shear stress absorbed vs phase angle – MoS_2 fluids

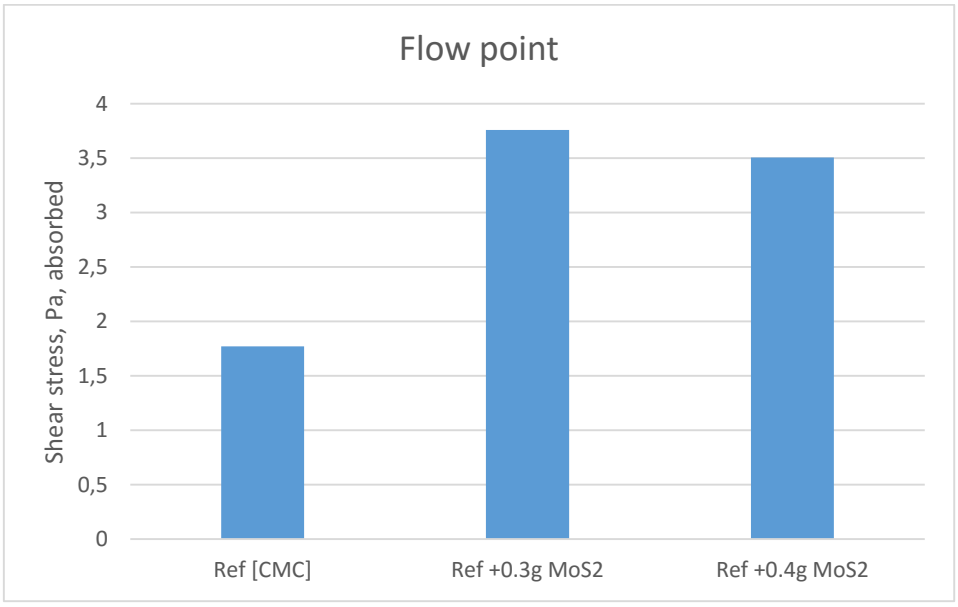

Figure 4-59 Flow point comparison for MoS_2 added system

The phase angle vs the shear stress obtained from the experiment is displayed in Figure 4-60. As seen in Figure 4-61 the addition of graphene did not improve the viscoelastic properties of drilling fluids.

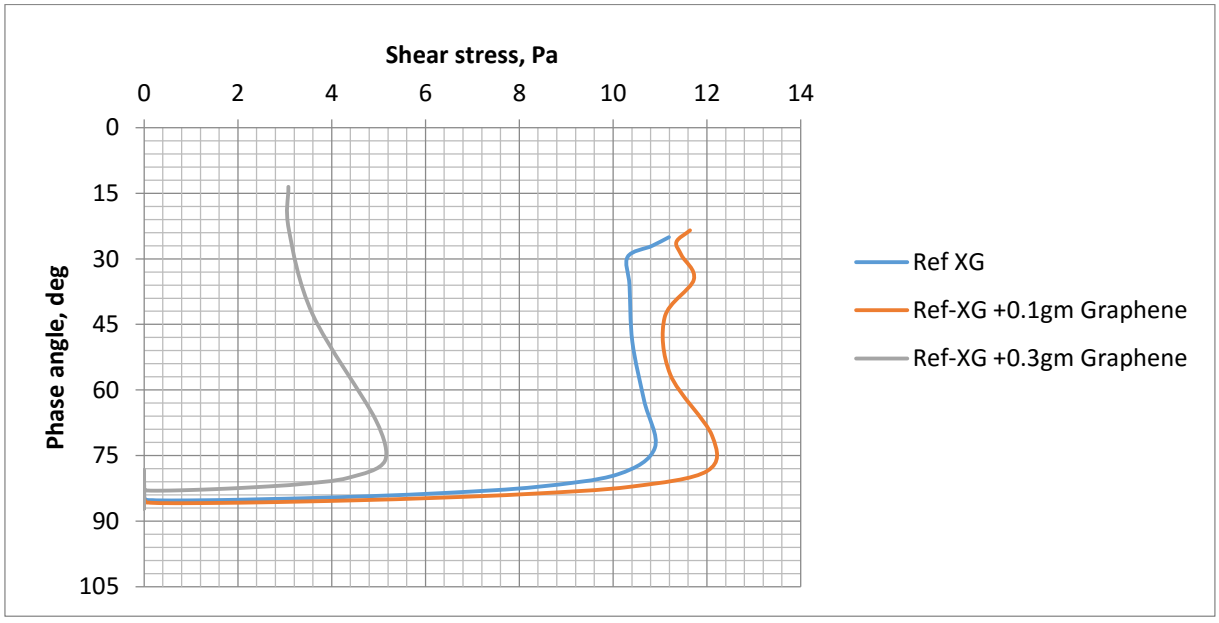

Figure 4-60 Shear stress absorbed vs phase angle - Graphene

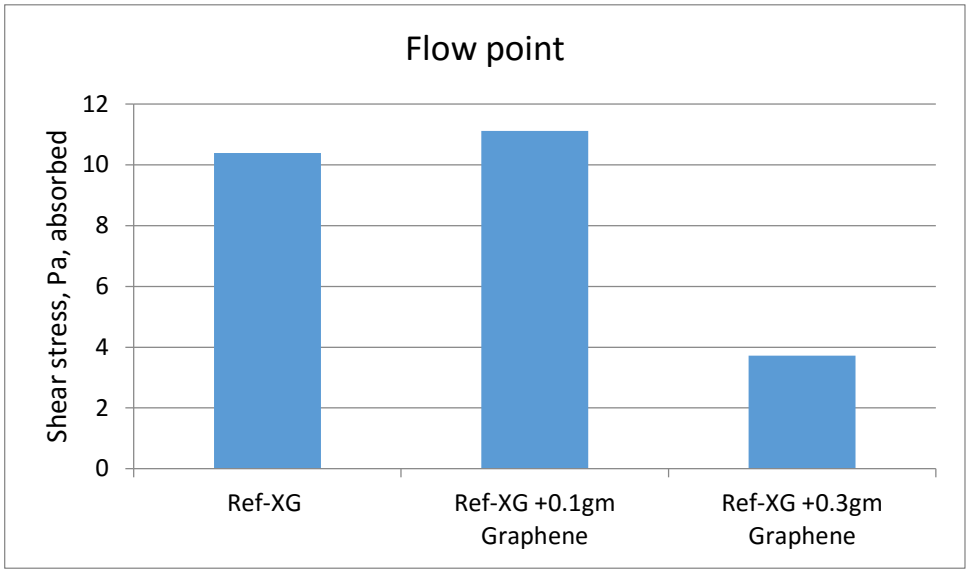

Figure 4-61 Flow point comparison for Graphene added system

5 Performance simulation studies

This chapter presents the improved drilling fluid performance in a simulated well scenario. The study evaluates the hydraulics, ECD of the selected nano-added fluid comparing with its nano-free reference fluid system.

5.1 Hydraulic simulation

Drilling fluid is an integral part of the drilling operation. Among other functions, drilling fluids main function is to maintain a stable bottomhole pressure to avoid well instability. The pressure exerted by the drilling fluid is determined by flowrate and its physical & rheological properties.

In this section, the hydraulic responses of the drilling fluids will be investigated by simulation in a specific well. The evaluation is based on the ECD and the pump pressures for various flow rates. Previous studies have shown that the Unified model (eq. 13 p.26) predicts more accurately than the Herschel-Bulkley model, therefore it used for the simulation. [24]

5.1.1 Simulation arrangement

Figure 5-1 illustrates a 10000ft deep experimental well considered for the simulation. The inner diameter of the well is 8.75'' casing and 8.5 '' well. The inner and outer diameter of the pipe is 5'' and 4'' respectively.

To simplify the experimental setup, the BHA is not considered. The drill string is connected with a bit contain three 28/32-in sized nozzles.

The discharge line is connected with the top of the pipe and therefore, we assume that we do not have surface pressure losses due to surface equipment.

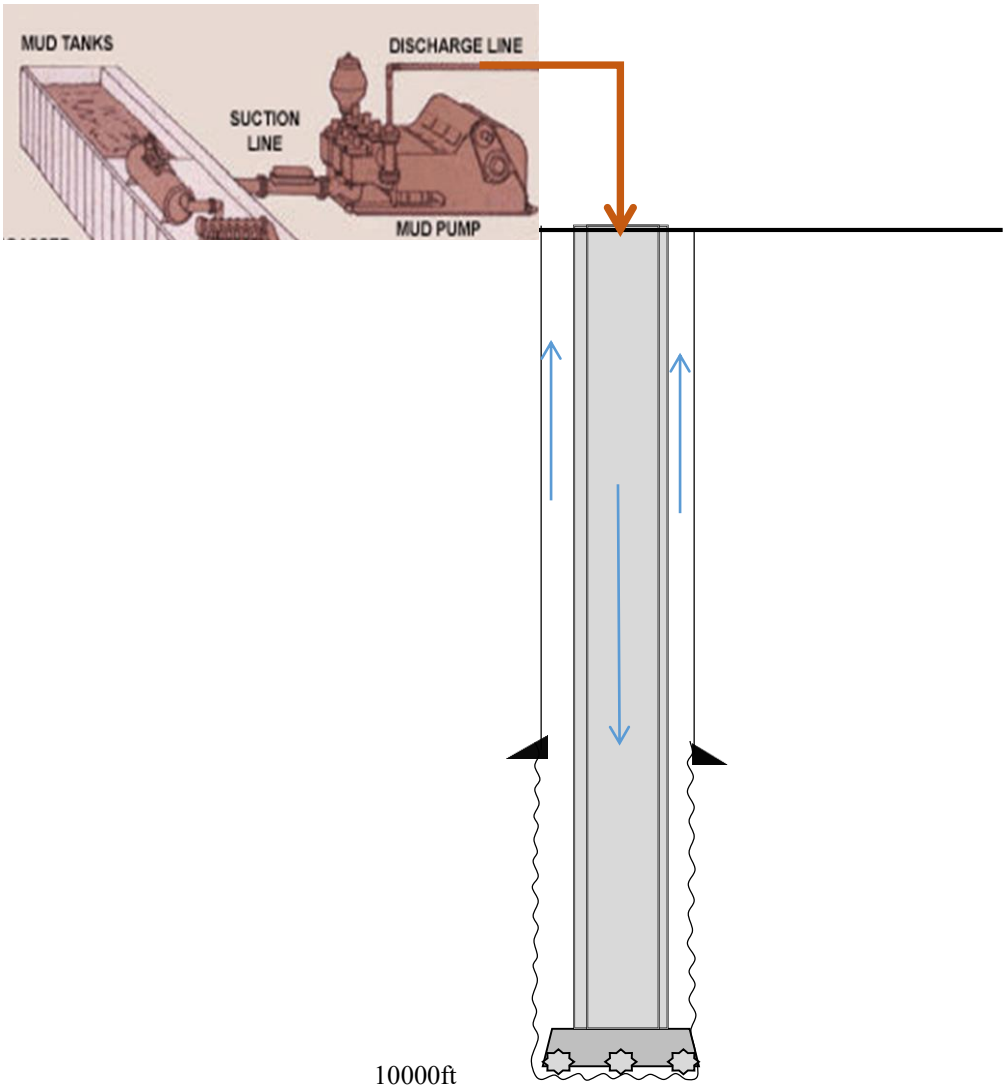

Figure 5-1 Sketch of hydraulic simulation well

5.1.2 Effect of graphene-modified fluid on ECD and Pump Pressure simulation results

The viscometer data of nano-graphene-modified drilling fluid that were used for the simulation, are given in Figure 4-35 on p.71. These fluids have been applied in the simulation well at the rate of 5 gpm to 600 gpm.

Figure 5-2 shows the simulated ECD as a function of flow rates. Notice that as the flow rate increases, the ECD increase as well. That is due to the increase in friction pressure loss, i.e. the fluid experiences more resistance to flow. The fluid containing 0.3g nano-graphene yields a higher ECD, while the 0.4g added nano-Graphene yields the lowest ECD.

Figure 5-3 displays the total pressure loss for each fluid in the well. As seen in Figure 5-4 the difference between the reference fluid, the 0.1g and 0.2 graphene-modified fluid is negligible. Depending on what is desired, adding 0.3g or 0.4g nano-sized graphene particles can have a great impact on the fluid system. Figure 5-4 displays the %-difference related to the reference fluid, pointing out the tremendous effects of graphene nanoparticles on pump pressure loss.

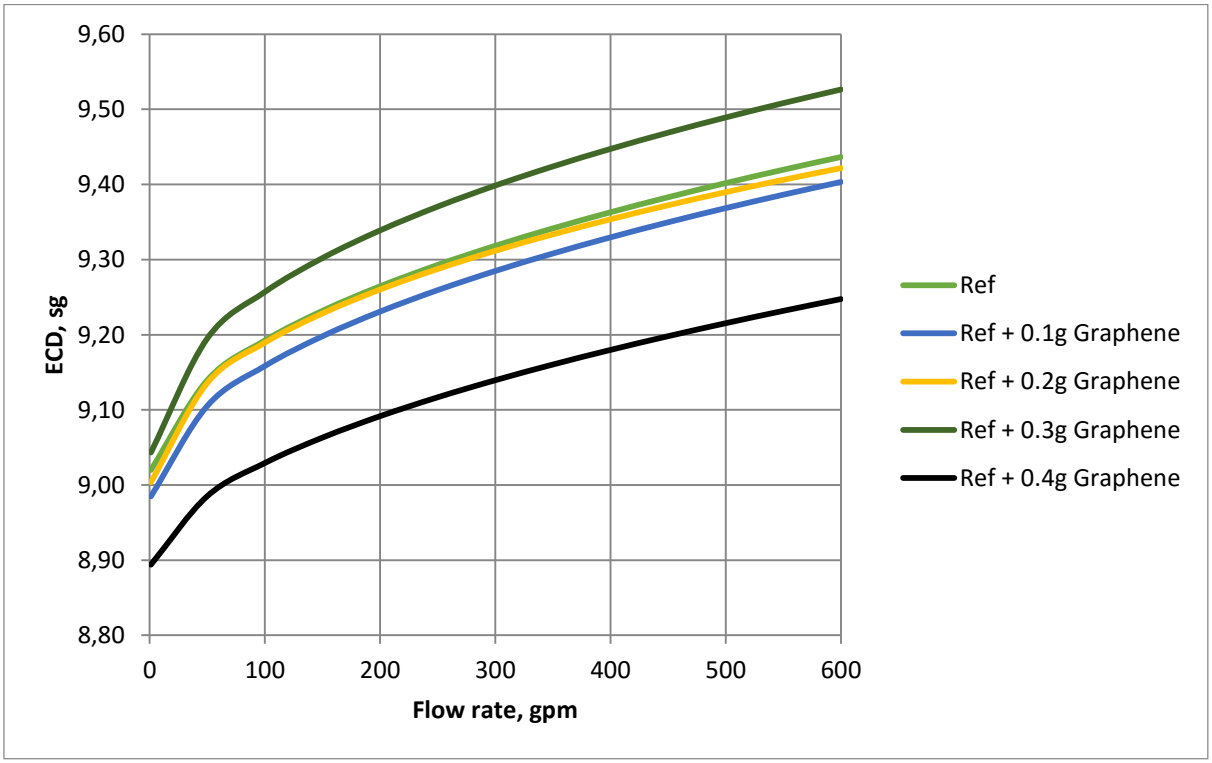

Figure 5-2 ECD of the drilling fluid systems including Graphene from the Unified hydraulics model

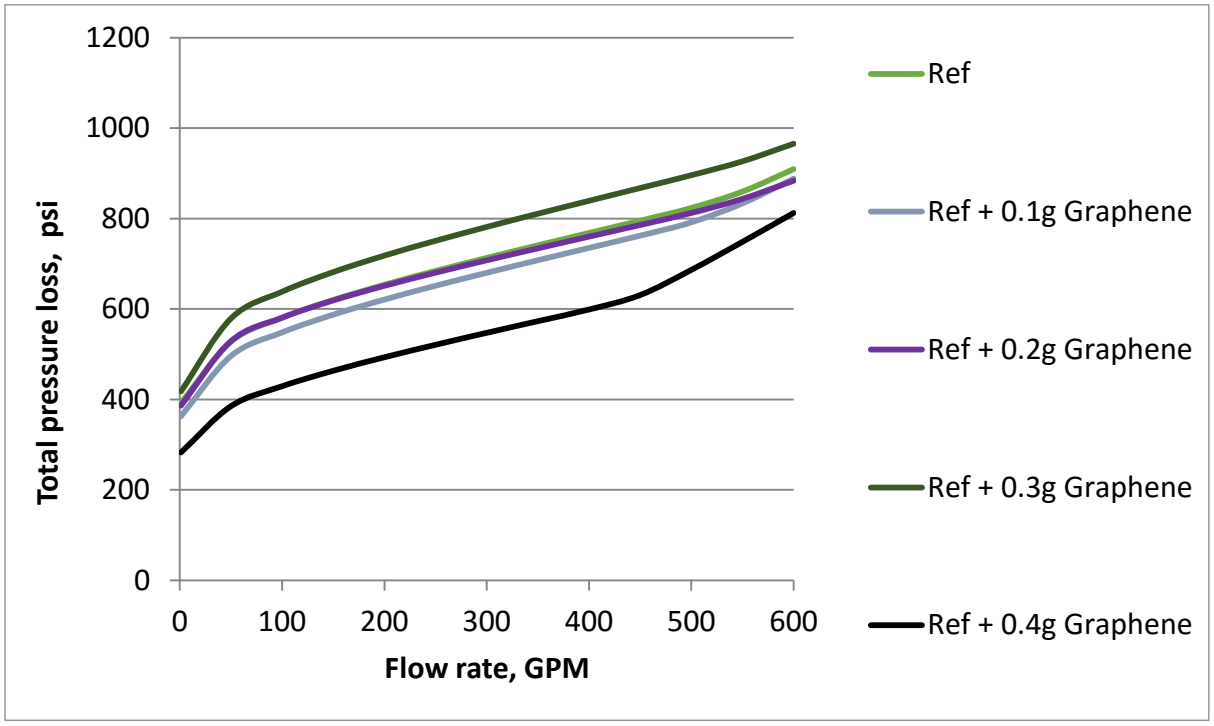

Figure 5-3 Total pressure loss of the fluid systems for graphene from the Unified hydraulics model

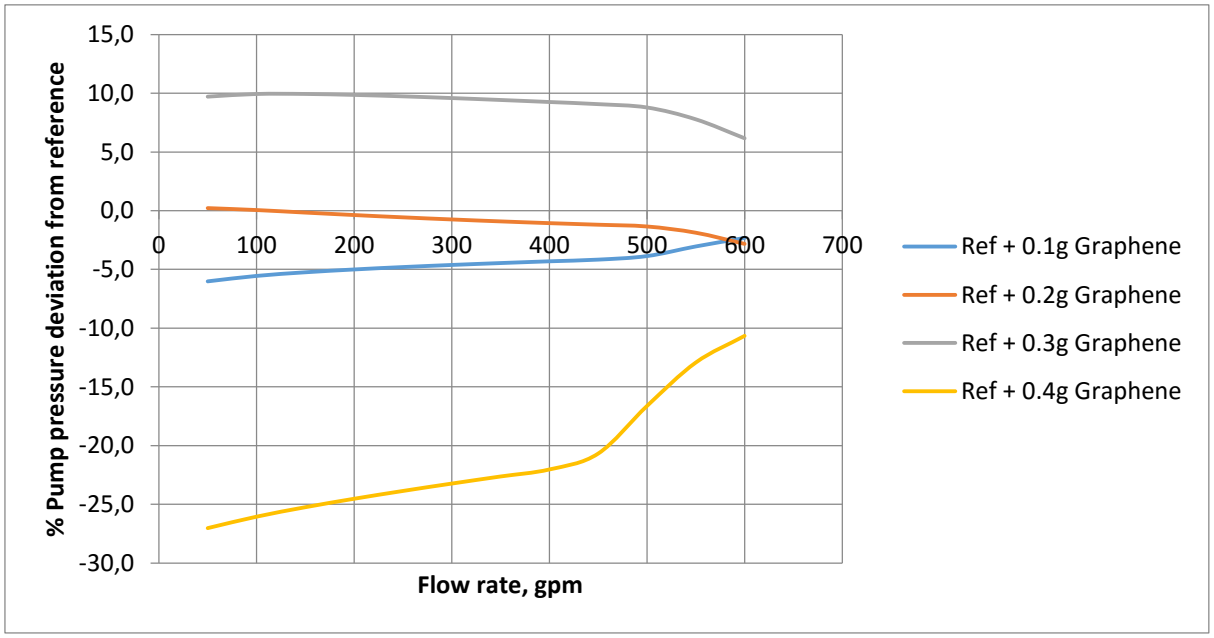

Figure 5-4 Pump pressure %-deviation from reference for Graphene added fluids

5.1.3 Effect of MoS_2-modified fluid on ECD and Pump pressure simulation results

Similarly, the effect of MoS_2 treated drilling fluids have been simulated. The viscometer data of drilling fluids are given on p.43 in Figure 4-7. The fluids are pumped at the rate ranging from 5 gpm to 600 gpm. Figure 5-6 and Figure 5-7 display that the 0.1gm MoS_2 modified fluid yields a significant increment in ECD and pump pressure loss. The other fluids do not differentiate a lot from each other, but all of them are slightly above the reference fluid in terms of ECD and pump pressure loss.

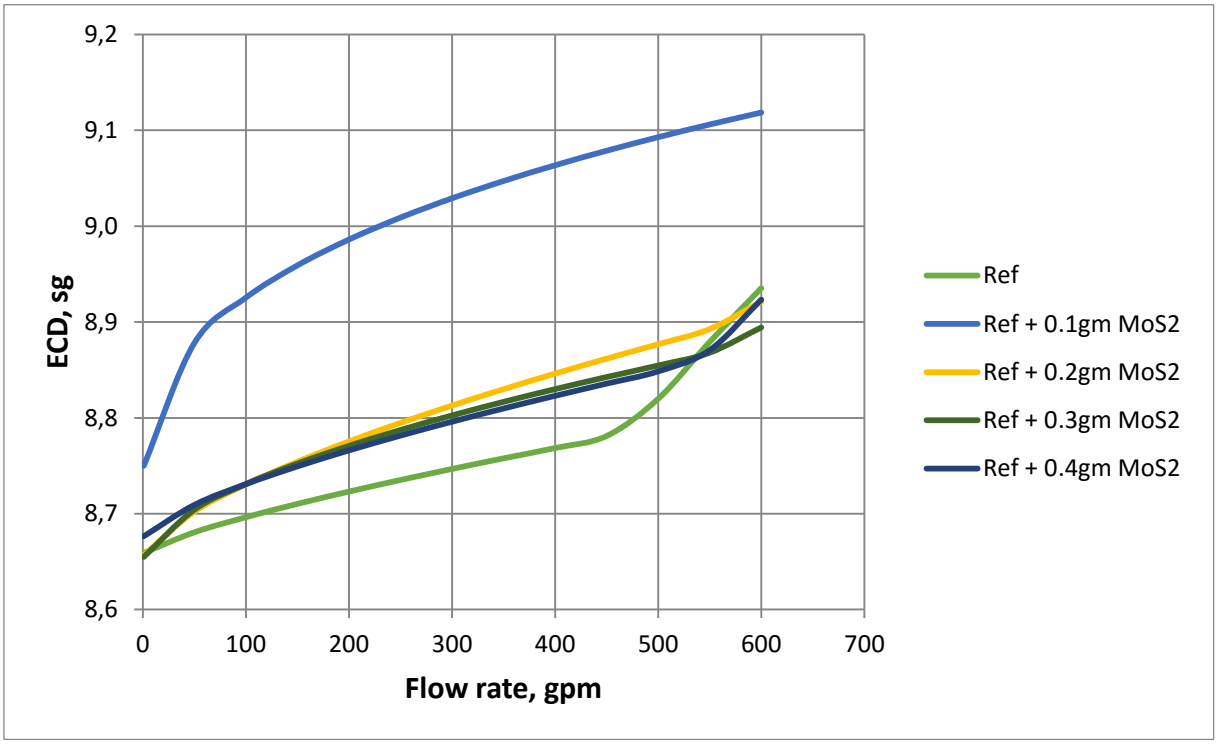

Figure 5-5 ECD of fluid systems including MoS_2 nanoparticles

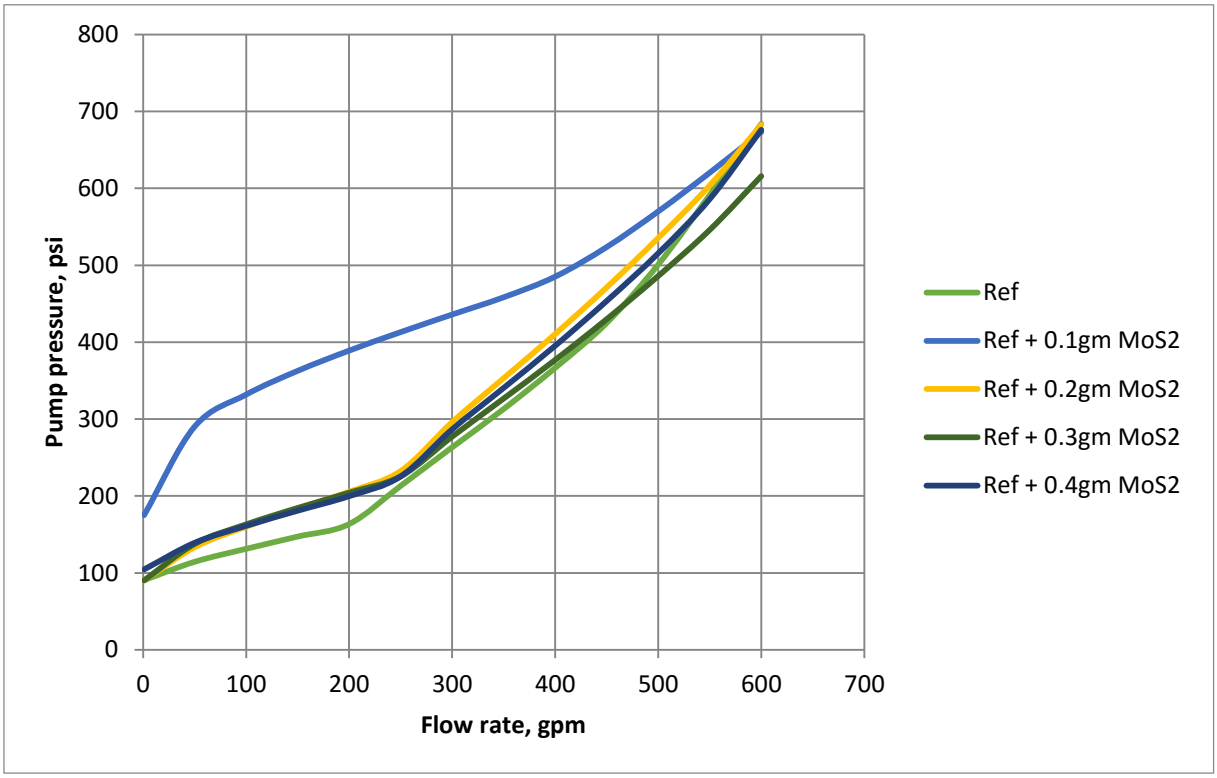

Figure 5-6 **Simulated pump pressure for MoS_2 nanoparticles**

5.2 Cuttings transport simulation

Hole cleaning is also an important issue during drilling operation. The cutting lifting capacity of drilling fluids depends on its physical and rheological parameters. [35] [36]

The best nano-modified systems, in terms on lubricity developed in Section 4, were further evaluated in a cutting transport efficiency simulation. As always, each nano-modified fluid will be compared to its respective nano-free drilling fluid.

The higher flow rate is positive to lift cutting out of the well. However, the higher flow rate increases ECD and stress in drilling string. if the flow rate is not optimized, in the worst case scenario, it may case well instability and drill string damage. During simulation the lower minimum flow rate to transport cutting is indirectly interpreted as drilling fluid has good properties.

5.2.1 Simulation setup

The cutting transport property of the considered drilling fluid has been simulated in a deviated well and 12000ft long well. The well has been drilled in 12.615'' open hole and on the top, it was cased with intermediate 13 3/8'' casing.

During drilling a 5''OD and 4.86'' ID drilling pipe was used. The BHA components are presented in Appendix B. The well is constructed in Landmark/Wellplan^{TM} software [37]. The well structure is shown on Figure 5-1.

5.2.2 Drilling fluids

The data in Table 5-1 represent the Fann 35 viscometer data measured at the given set RPM for the fluids. These data are used for the borehole cuttings transport simulation.

Table 5-1 Fann35 Rheometer data for Graphene and MoS2 with their reference fluids

RPM	XG-Ref	XG-ref+0.1g graphene	CMC-Ref	CMC-ref+0.4g MoS2
600	40	38	19	22
300	33	32	12,5	15
200	30	28	10,5	13
100	25	23,5	7,5	10,5
60	23	22	6,5	9
30	21	19	5	8
6	17	15,5	4	5,5
3	15	14	3,5	4,5

5.2.3 Transport parameters

The transport data consists of operational parameters and cutting parameter. The transport efficient of the drilling fluid to lift 0.125in size and 2.5sg density of cutting were analyzed by pumping at the rate of 450ppg.

Cuttings are generated while drilling a formation at the rate of 60ft/hr. In order to have good borehole cleaning performance, i.e. avoid bedding of particles, the cutting particles have to be at least kept in suspension in the drilling fluid and ultimately lifted to surface. Therefore, the drill string is set to be rotating at the rate of 90 revolutions per minute. A picture of the cuttings transport parameters is shown in Figure 5-7.

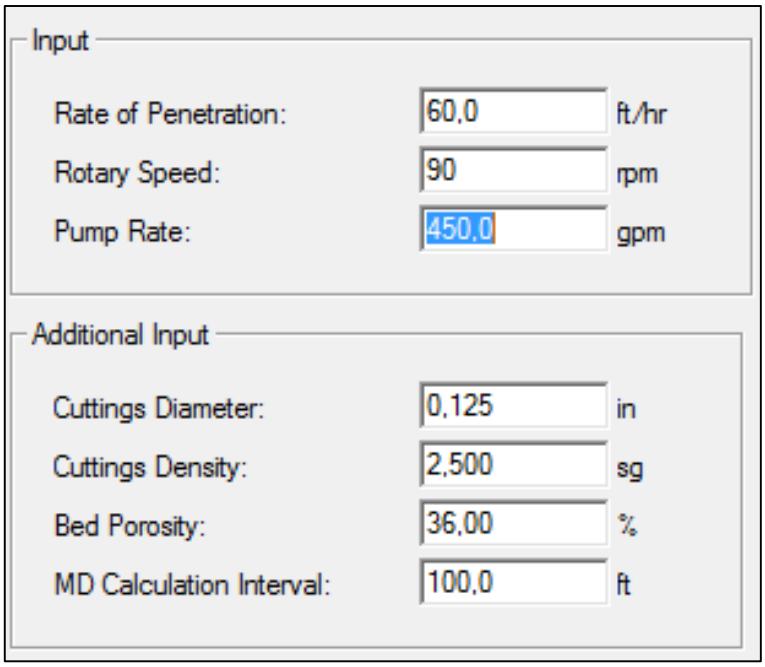

Figure 5-7 Cutting transport analysis data

5.2.4 Simulation result and discussion

The drilling fluids cutting carrying capacity were evaluated base on the simulation parameters considered above. The analysis cutting bed height at the 450gpm, which is the typical circulation rate. Cutting accumulation in wellbore deteriorate drilling operation. Among others, it will cause drill string sticking, modify well pressure and hence may cause desired wellbore instability and increase torque and drag [36]

As shown in Figure 5-8 and Figure 5-9, the in the vertical section up to 5000ft, has no cutting deposition. Below that depth inclination of wellbore increases allowing cuttings to settle and cause bedding. Increased inclination increases bedding troubles, i.e. increasing bed height.

Figure 5-9 shows the simulation results obtained from using the MoS_2 added fluid system and its reference fluid. The results show that the addition of MoS_2 nanoparticles for the considered flow rate reduced the cutting bed height from 3.8in to 2.2in, about 42%. This is due to the impact of nano-additive on the rheology property of the drilling fluid.

Figure 5-8 displays the hole cleaning performance of Graphene added fluid compared to its reference fluid system. Figure 5-8 indicates that the 0.1 gram graphene-modification does not have any impact on borehole cleaning. The main reason is shown on the

viscometer data (Figure 4-35), as the additive does not modify the fluid rheology properties.

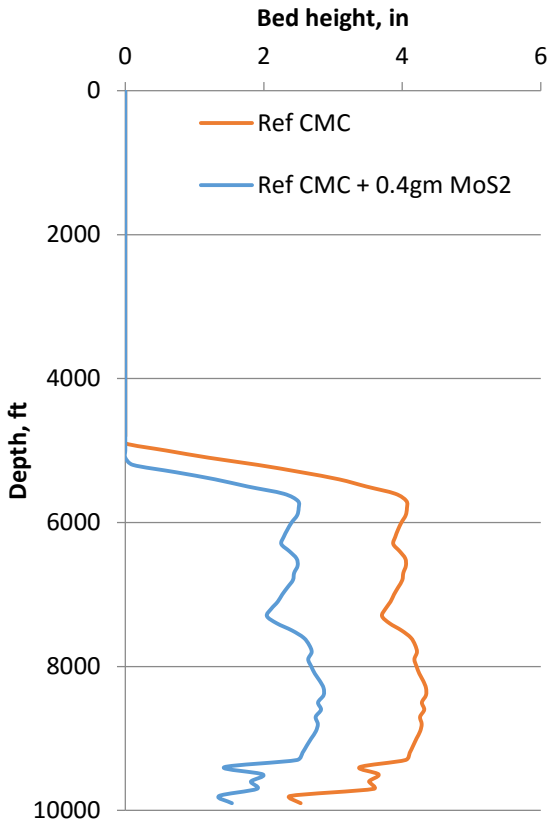

Figure 5-9 Simulation results illustrating drilling depth vs bed height with nanofree and nanoadded CMC base fluid.

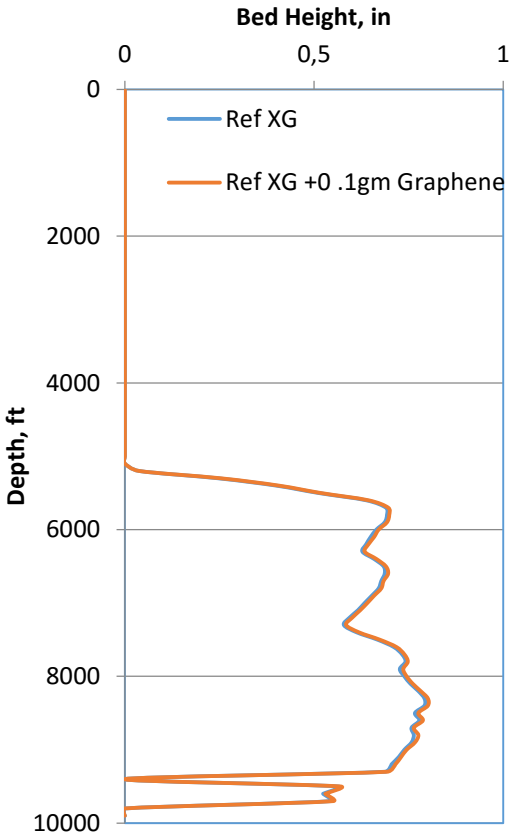

Figure 5-8 Simulation results illustrating drilling depth vs bed height with nanofree and nanoadded Xantham Gum base fluid

6 Drill string mechanics simulation

During petroleum exploration and production, drilling operation costs the oil industry a lot. The drilling industry is trying to develop new methods and technologies to drill a well more efficiently and quicker to save time. This indirectly reduces drilling cost.

Since the introduction of petroleum exploration, the industry is improving recovery. Among others, well placement in the reservoir contribute a lot. Recently the drilling in horizontal direction and a longer offset improves productivity. This indirectly also reduced the number of well required be drilling for optimum reservoir production, since the horizontal wells are exposed a larger part of the reservoir drainage area when the wells are drilled further. Drilling a longer offset is limited by high torque and drag. The longest extended reach drilling well I located in Russia, which is a measure depth of 12,700meters. Figure 6-1 shows the current extended reach drilling envelope drilling with the current technology [38]

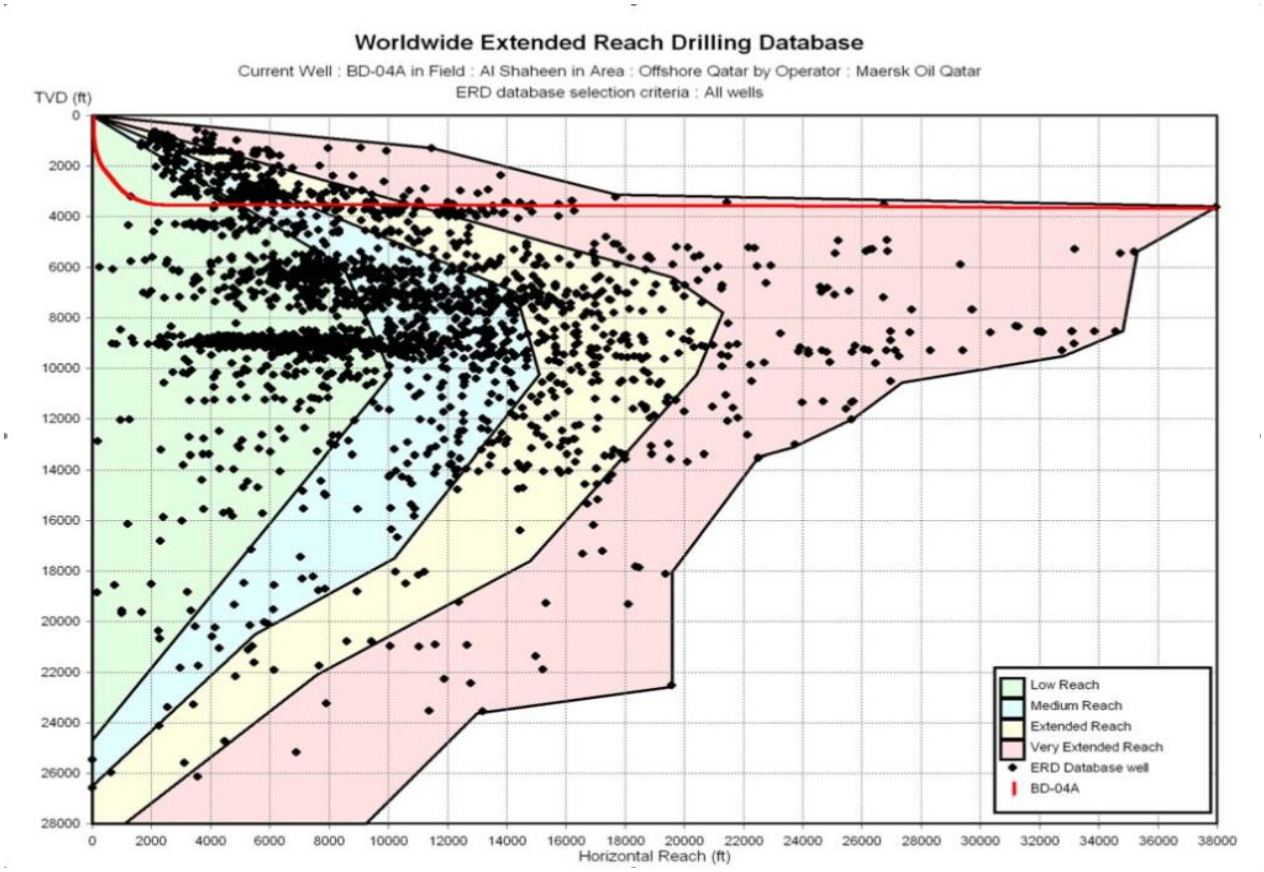

Figure 6-1 ERD envelope of drilled wells [38]

6.1 Description of fluids

As mentioned earlier, the current drilling envelope has been drilling the conventional drilling fluid and method. To analyze the questions addressed in section 1.2, this part will present the effect of nanoparticles by evaluating the potentially extended reach drilling.

For torque and drag simulation studies, best nano-modifying fluids in terms of lubricity were selected. The selection was based on the friction test results presented in section 4. Table 6-1 and Table 6-2 are the fluid systems. The average coefficient of frictions are calculated from measured friction at the three temperatures.

Table 6-1 Cofficients of frictions from experiments averaged for T&D simulation – MoS_2

Drilling fluids	Coefficient of frictions			
	20^0C	55^0C	70^0C	Average
Ref CMC	0.455	0.565	0.529	0.5160
Ref CMC+0.4g MoS_2	0.202	0.327	0.344	0.2910

Table 6-2 Cofficients of frictions from experiments averaged for T&D simulation – Graphene

Drilling fluids	Coefficient of frictions			
	20^0C	55^0C	70^0C	Average
Ref XG	0.2500	0.2750	0.2650	0.2630
Ref XG+0.1gm Graphene	0.1372	0.1800	0.2000	0.1724

6.1.1 Torque and drag simulation setup

Rotating at bottom, drilling and two tripping operations, in and out were considered to characterize the effect of nano-additive treated fluid. The drilling fluids have been pumped in the simulation well at the rate of 500gpm. Figure 6-2 shows the operational parameters.

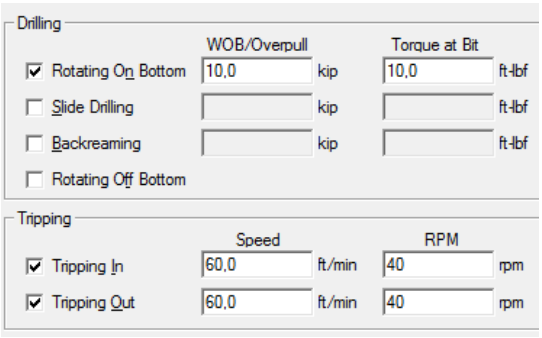

Figure 6-2 Drilling and tripping simulation parameters

The drillstring properties, casing and well size is shown in Appendix B. The well inclination and the azimuth is also shown in Appendix B. Figure 6-3 displays the torque and drag simulation well. The maximum well inclination is 36deg. The rheology of the MoS_2 treated drilling fluids and the Graphene treated drilling fluids are provided in Table 4-1 p.43 and Table 4-7 p.58 respectively.

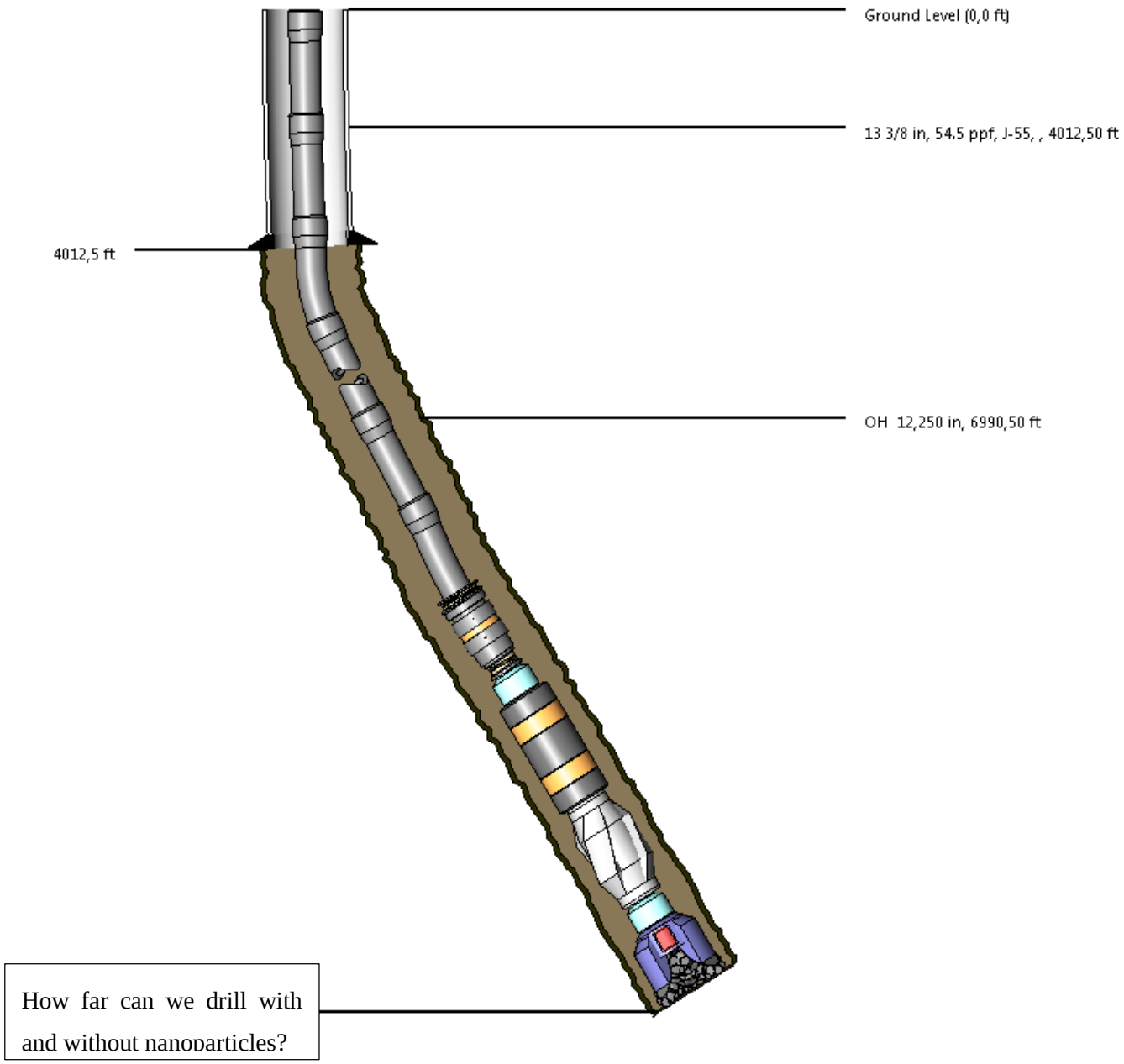

Figure 6-3 Drilling simulation setup

6.2 Simulation result

As mentioned earlier, the drilling and tripping operations has been simulated. These are torque and drag, torque and Von-Mises stress. Simulation were desinged with the objectivie of find if the loads and the stesses are with in a safe operational window for maximum drilling length. The simulation results are attached in Appendix B. The summary of the results are shown in Table 6-3 and Table 6-4

Table 6-3 shows the summary of the simulation results obtained from MoS_2 nano fluid. Displayed is a comparison between nano free drilling fluid (Ref CMC) and fluid with the addition of 0.4g nano MoS_2 (i.e 0.023%wt) which extends the maximum drilling length with about 26.3% additional length.

Similarly the effect of nano grapane in driling the reference drilling fluid yields a longer offset which we also simulated and the results are summarized in Table 6-4. As shown, the addition of 0.1g Graphene (+0,05%) improved the drilling length by 7.7%.

The results presented here illlstrate the huge potential of nano technology in improving drilling performance and hence crossing the current ERD envelope.

Table 6-3 Comparison of Ref CMC and Ref CMC + 0.4g MoS_2 drilling fluids on maximum drilling length

Drilling fluid	Maximum drilling length, ft	Change in length,ft	% Change
Ref CMC	9900	2600	26.3
Ref CMC + 0.4 gm MoS_2	12500		

Table 6-4 Comparison of Ref XG and Ref XG + 0.1g Graphene drilling fluids on maximum drilling length

Drilling fluid	Maximum drilling length,ft	Change in length,ft	% Change
Ref XG	13000	1000	7.7
Ref XG + 0.1g Graphene	14000		

For illustration the simulation results obtained from torque and drag of the MoS_2 based drilling fluids has been compared and presented in the following; (more illustrative data in Appendix C)

Figure 6-4 and Figure 6-5 shows the simulation of Drag for *Ref CMC* and *Ref CMC + 0.4g* MoS_2 respectably. Similarly, the corresponding torque loads are shown in Figure 6-6 and Figure 6-7.

Analyzing Figure 6-4, at hook load (purple line) at the surface of 314.9 kip seem allow to drill further as the tension limit is 400 kip. However, the corresponding torque shown in Figure 6-6 is right at the limit, implying that maximum drilling depth within the safe operational window is reached. Hence, the maximum drilling depth to drill with the reference drilling fluid is 9900ft.

The operation window for drag and torque for the nano-treated drilling fluid system, see Figure 6-5 and Figure 6-7 respectively, allows us a maximum drilling length of 12500ft, as mentioned above yielding a 26.3% increase in length.

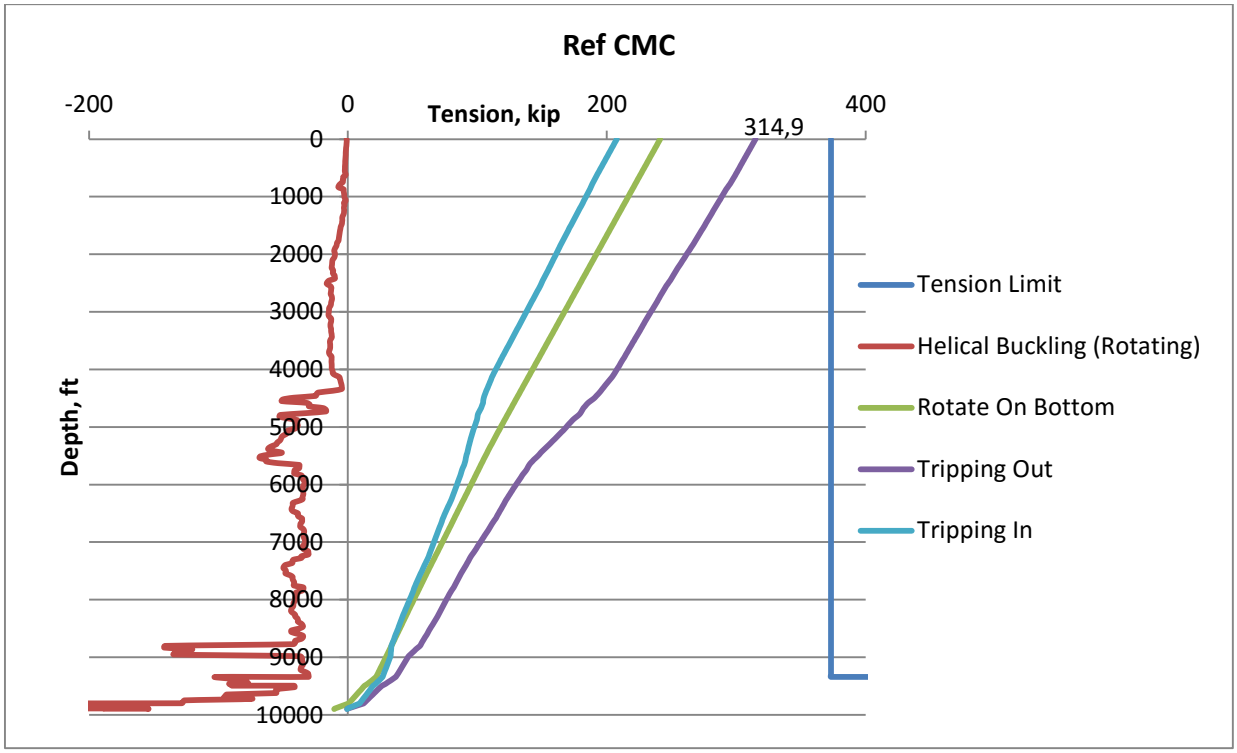

Figure 6-4 Drilling and Tripping loads with nano free -reference drilling fluid (Ref CMC)

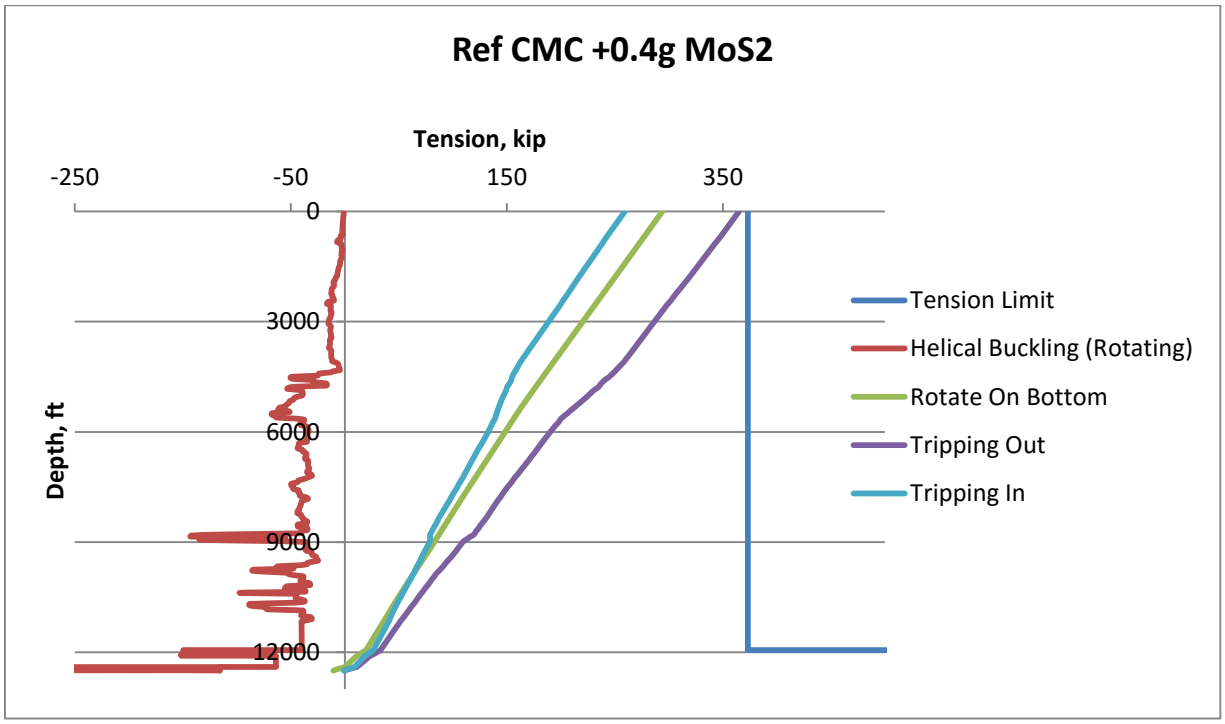

Figure 6-5 Drilling and Tripping loads with nano treared drilling fluid (Ref CMC+0.4gm MoS_2)

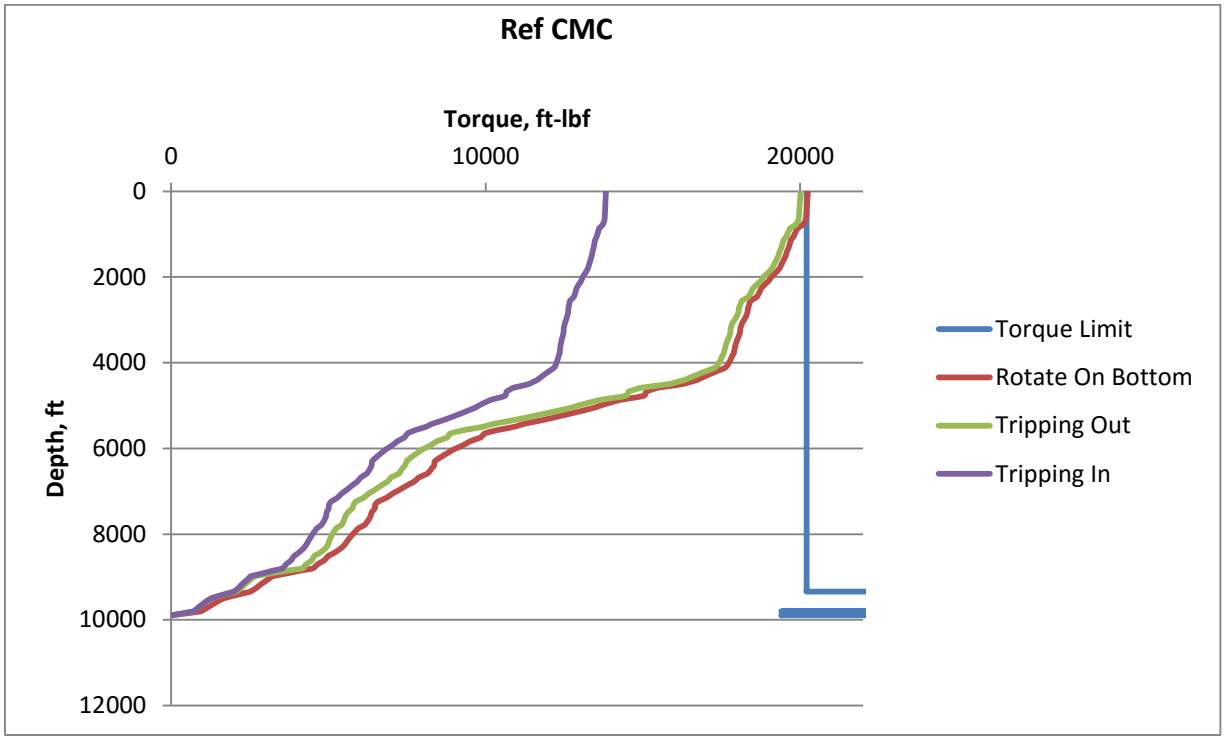

Figure 6-6 Torque loads with nano-free reference drilling fluid (Ref CMC)

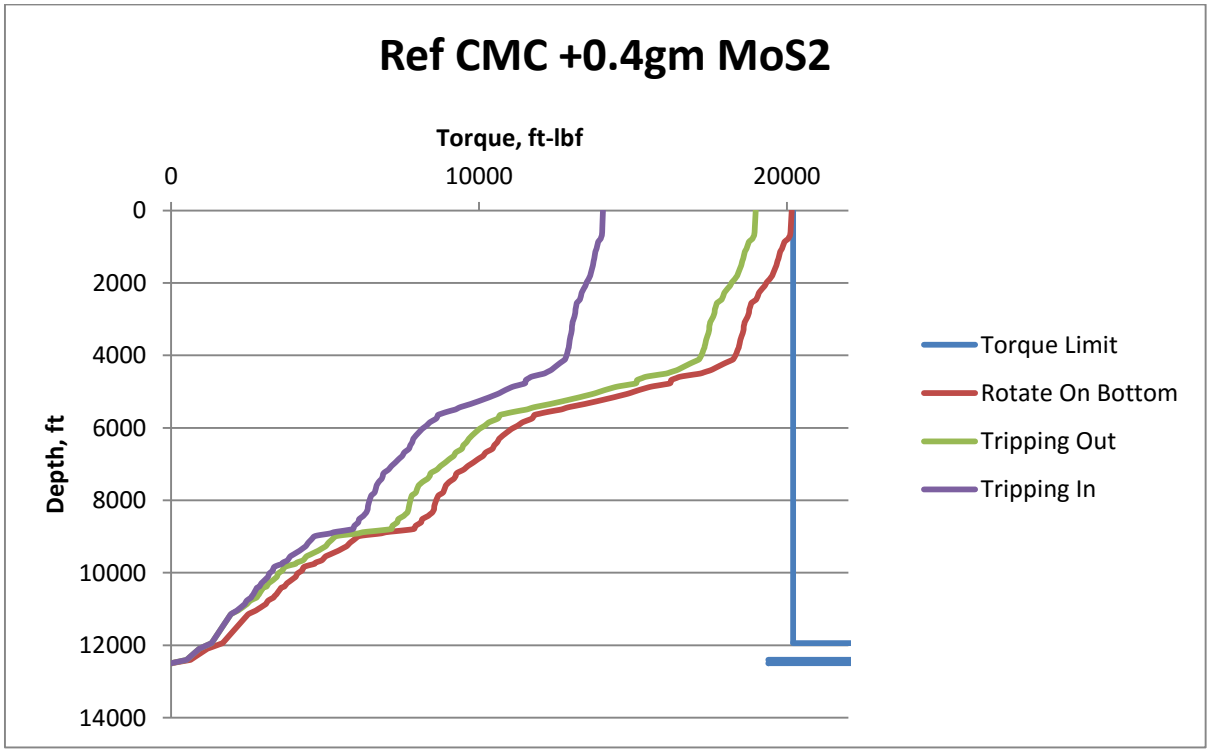

Figure 6-7 Torque loads with nano treated drilling fluid (Ref CMC+0.4gm MoS_2)

7 Summary and Discussion

Experiments performed in the thesis conclude that the nano-additives can affect physical, rheological and lubricating parameters. The crystalline structure of the nanosized particles, their surface chemistry, their grain size distribution and synergy with other ingredients in the water based drilling mud system can affect the fluid properties in both positive and negative ways. Therefore each type of nanoparticles has to be discussed by itself.

7.1 Effect of Molybdenum disulfide (MoS_2) nanoparticles

Rheological measurements show that adding 0.1g MoS_2 increased Bingham YS by 183%, while an additive range from 0.2g to 0.4g only yielded an increment of about 50% in yield strength compared to the base system. Additionally, the 0.1g MoS_2 added fluid displays an increased LSYS as it increased from 3 lbf/100sqft in the reference system to 5 lbf/100sqft, while the other concentrations barely show an increment. In addition, the filtrate loss slightly increased, suggesting that the addition of MoS_2 may turn the system into a more flocculated system. PV is unaffected.

Flow behavior index (n) indicates fluids tendency to shear thin. Consistency index (k) serves as a viscosity index. The addition of MoS_2 nanoparticles increases k and decreases n. All fluids in this thesis display pseudoplastic behavior, i.e. all fluids are shear thinning. The system with 0.1g additive stands out with a significantly increased k, from 0.29 to 3.89, meaning that viscosity is significantly increased.

The pH value barely changes by the addition of MoS_2 additive. Perhaps, the slight increment can lead to a more dispersed/aggregated system, but nothing has been observed.

Based ambient temperature experiments and model analysis, one can therefore conclude that 0.1g additive gives the best improvement on fluid rheological properties at ambient temperature.

For all fluid the tribological analysis was conducted at three different temperatures (20, 55, 70°C). A linear increase of friction was expected and satisfied based on work of Kårstad et al. [29]

As MoS_2 reduces friction at all temperatures and for all concentration by at least 22% and maximum 53%. Hence, we can conclude that it increases the lubricity of the developed water based drilling fluid. The most optimal addition for MoS_2 was 0.2g considered at elevated temperatures, as it yielded the highest reduction in friction coefficient relative to the reference fluid system.

The measure of viscoelastic properties allow for the evaluation of gel strength of drilling fluids. Since MoS_2 showed great effect on rheology and friction it has been selected for an amplitude sweep analysis. The only other fluid investigated is with graphene additive discussed later. To classify viscoelastic behavior of fluids one can either look for the yield point or the flow point. In this thesis we use the flow point to evaluate and compare fluid viscoelasticity. As discussed in the results, the energy absorbed is doubled for the additive treated fluids including MoS_2. That means the addition of MoS_2 nanoparticles strengthens the gel structure, which enhances the fluids ability to keep cuttings in suspension when fluid circulation is paused. In other words, the fluid system is better dispersed and has improved stability. [39]

7.2 Effect of Titanium Oxide (TiO_2) nanoparticles

Rheological measurements show that adding TiO_2 barely affects the Bingham properties.

The rheological Power law model indicates that the flow behavior indexes and consistency indexes are positively affected by 0.4g added TiO_2 nanoadditive, by increasesing k from 0.47 to 0.90 and decreasing n 0.53 to 0.44. That indicates increased viscosity for that fluid system. The other samples display reduced k and slightly increased n values, hence the slightly reduced viscosity.

Filtrate loss is either unchanged or increased for these low concentrations. Perhaps increasing the concentration of TiO_2 beyond what is done in this thesis might create a more flocculated system.

The pH value is unaffected by the addition of TiO_2 additive.

The tribology measurements do not vary as much for TiO_2 as it did for MoS_2. The friction coefficient change is between being at the most reduced by 11% or increased by 21%, representing a narrow change for difference concentrations and temperatures. Unlike for the rheology evaluation, the lowest concentration improves the lubricity the most. Making difficult to find an optimum concentration for an overall enhancement for a water based drilling fluid system.

7.3 Effect of Graphene nanoparticles

Based on the rheology measurements, the Bingham PV and YS show that the fluids are little affected by the addition of nanosized graphene particles. Whether the addition flocculates or deflocculates the system is also unclear, because the addition of 0.3g graphene yields maximum viscosity and gel while the addition of 0.4g generates the minimum of both attributes.

The Power Law indexes display similar tendencies, where 0.3g additive slightly reduces n and increases k, while the fluid with 0.4g additive generates the opposite.

Filtrate loss is increased for all tested samples, by 0.9 to 1.5mL, except for one sample. Perhaps the most interesting find is that the best filter-cake next to the reference fluid is the one with 0.3g additive. Rarely an additive can increase viscosity, while keeping the filter-cake quality almost the same.

The pH value completely unaffected by the addition of graphene particles.

Graphene is interesting in terms of being a good lubricity agent. The friction coefficient is reduced at all temperatures and for all concentration by at least 8% and maximum 56%. The highest lubricity gain is for 0.1g added nanoparticles. Perhaps when intending to increase viscosity and lubricity of a fluid at the same time, the fluid with 0.3g graphene additive seems to satisfy both wishes.

The flow point from the amplitude sweep measurement for graphene added fluids show very different results compared to molybdenum disulfide. The addition of 0.1g graphene slightly increases the flow point, while adding 0.3g reduces the shear stress absorbed to reach the flow point by almost ca 60%. Therefore, 0.3g additive reduces the elastic property (gel) and makes the fluid system more easily viscous than elastic.

7.4 Effect of Titanium Nitride (TiN) nanoparticles

Based on the rheology measurements, the Bingham and Power law Rheology Model it seems that TiN has almost no effect at all on rheological properties.

Interestingly, the filtrate loss is slightly reduced for all added amounts of TiN, with the exception of 0.2g added particles, which has the same 6.5mL filtrate loss as the base fluid. The amount for the other fluids is not more reduced than 0.5mL in the 7.5min filtration test, meaning only a minor filter-cake improvement.

The pH is decreased to from 6.5 in the base fluid to 6.0 in the other fluid samples. Fluid 2 is the only fluid resembling the reference fluid, as it was for the filtrate test.

TiN seems to be a bad lubricity agent, since the friction coefficient is increased, ranging from +13% to +23%, for all concentrations at 22°C and 55°C. At 70°C a slightly lubricating effect can be observed, thought it is below 7% for all fluids. The addition of 0.3g never displays increased lubricity.

Overall TiN in our PAC water based fluid system does not seem to show improvements of significance at these low concentrations.

7.5 Simulation results

7.5.1 Hydraulic Simulation

Hydraulic simulations of drilling fluids are necessary for drilling operations. They yield important information about fluid behavior for cutting transport efficiency and ECD management. The Unified rheology model was selected to be used for these calculations as it gives a very low error rate and based the evualtion of Jeyhun [24]

Simulation shows that the 0.4g graphene-modified fluid yields a 21% reduction in pump pressure loss at 450 gpm, while 0.3g modification increases the pump pressure loss by 9%.

0.1g modified MoS_2 system has greatly increased pump pressure loss and ECD for rates below 450gpm. Simulation displays a 77% ECD and increased pump loss at 200gpm.

None of the other developed fluid systems show a significant effect ECD or pump pressure loss at any flow rate.

7.5.2 Cuttings transport Simulation

Wellplan simulation software was applied to investigate the cutting transport quality of nano-modified drilling fluids. The fluids were selected based on their enhanced lubricity. The simulation well had an inclination where cuttings would accumulate, leading to a build up of bed height. The analysis the drillings fluids affect on bed height at the 450gpm, which is a typical circulation rate.

The results show that the addition of MoS_2 nanoparticles for the considered flow rate reduced the cutting bed height from 3.8in to 2.2in, about 42%. This is due to the impact of nano-additive on the rheology property of the drilling fluid.

On the contrary, the 0.1 gram graphene nano-additive does not have impact on borehole cleaning. That is because the 0.1g additive had no significant affect on rheological properties either.

7.5.3 Torque and Drag Simulation

Torque and Drag simulations in Wellplan provide necessary information about the well parameters to optimize the design of drilling fluid and drillstring. It calculates the limits to drilling, allowing to see how far one can drill. One can use this information to optimize well positioning for optimized drainage of a reservoir. The length of a well is usually limited by either torque or drag. Torque and drag are friction dependent entities. Since he application of nano-additives in water based drilling fluids can vastly increase lubricity, T&D simulations were conducted. Nano-additives with their concentration yielding the highest percentage reduction in coefficient of friction have been selected to be applied in the simulation studies for T&D.

In the simulation, the reference fluid system allowed the maximum length of 9900ft, while the addition of 0.4g MoS_2 into the reference fluid increased the maximum drilling length by 26.3%, to 12500ft.

In the simulation for the XG-reference fluid system, the reference drilling system yields high lubricity to begin with. It allowed a drilling length of 13000ft. Although, the coefficient of friction for the graphene modified fluid system is 34.5% lower, the addition of 0.1g nanosized graphene increased the maximum drilling length only by 7.7% to 14000ft.

8 Conclusion

The objective of this thesis work was to test different nano-additives in conventional water based drilling fluid systems, and find out whether drilling fluid performance could be enhanced. The best fluids were selected based on rheology and friction parameters and have been tested in different models and simulations to give a better understanding of the impact nano-additives have on the overall drilling operation.

Rheological experiments can conclude that addition of 0.1 g MoS_2 per 500 ml at ambient temperature, improved the Bingham Yield Strength (YS) of the drilling fluid by 183 % relative to the reference fluid, while addition of Graphene, TiO_2 and TiN did not have a significant impact on the fluid rheological properties.

Viscoelastic experiments show up to 100% increased storage and loss modulus for MoS_2 nano-modified drilling fluid compared to nano-free fluid, which indicates improved stability and a more dispersed fluid.

WellPlan™ and Unified hydraulic model simulations were carried out. Cuttings transportation, total pressure drop across the well and ECD effects have been simulated to evaluate the performance of nano-treated systems relative to the nano-free reference systems. Simulations together with experiments in this thesis can conclude that effects given by nanoparticles are;

- Increased lubricity of drilling fluid by MoS_2 and Graphene additives yielded up to 26.3% extended drilling reach.
- Improved borehole cleaning capacity by decreasing bed height due to reduced flow behaviour index for 0.4g added MoS_2 per 500mL drilling fluid.
- That MoS_2 additive could impact pumping ECD, potential increasing or reducing the annular pressure compared to the reference system.
- Improved hydraulic properties by decreasing pressure loss and ECD for 0.1g and 0.4g Graphene nano-additive per 500mL drilling fluid.

The results evaluating the impact of nanoparticles on filtrate loss were inconclusive, suggesting that further analysis is required to evaluate the effect on filter-cake quality.

9 References

[1] S. Azar.J.J., Drilling Engineering". PennWell Corporation. Tulsa, Oklahoma, 2007.]..

[2] J. Cook, "Stabilizing the Wellbore to Prevent Lost Circulation". Oilfield Review Winter 2011/2012: 23, no. 4., 2011.

[3] G. Stjern, Local rock mechanical knowledge proves drilling performance in fractured formations at the Heidrun field." Journal of Petroleum Science and Engineering 38(3-4): 83-96, 2003..

[4] Wang, Dr. Wei-Min Liu and Dr. Xiao-Bo, Nanoparticle-based lubricant additives. Springer-Verlag Berlin Heidelberg 2012, 10, 2 April 2012.], 2012.

[5] H. R. Samuel, Friction factors: What are they for torque, drag, vibration, bottom hole assembly and transient surge/swab analyses? IADC/SPE 128059, 11:11, 2010.

[6] Kutty, Kulliyev , Well Performance Improvement Using Complex Nano Fluids SPE-177831-MS CESI chemical, Flotek company, SPE, 2015.

[7] Norazly Mohd Taha and Sean Lee,, Nano graphene application improving drilling fluid performance IPTC-18539-MS, Scomi KMC, 2015.

[8] J. Messenger, "Lost Circulation", Pennwell Publishing Company. Tulsa, Oklahoma, 1981, ISBN: 978-0878141753, 1981.

[9] A. Kristensen, "Flow properties of water-based drilling fluids". Norwegian University of Science and Technology, 2013.

[10] M. X. Zhen Xiuhua, Drilling Fluids School of Engineering and Technology China University of Geosciences (Beijing) 29 Xueyuan Road Beijing, 100083 P.R.China.

[11] Caenn, R., , Darley, H.C.H. and Gray. G, “Composition and Properties of drilling and Completion Fluids”, 6th edition 2012.]., 2012.

[12] F. Outubuddin, Outubuddin and Fu 2002, Ray and Okamoto 2003.

[13] MiSwaco, Drilling Fluids Engineering Manual, Polymer chemistry and Applications”. Chapter 6, 1998, 1198.

[14] K. B. Adel Benchabane, “Rheological properties of carboxymethyl cellulose (CMC) solutions”. Colloid Polym Sci, 2008. DOI: 10.1007/s00396-008-1882-2]..

[15] Khaled. and Abdelbaki., Rheological and electrokinetic properties of carboxymethylcellulose-water dispersions in the presence of salts”. International Journal of Physical Sciences Vol. 7(11). DOI: 10.5897/IJPS11.1779. 9 March, 2012.]..

[16] M. Economides, L. Watters and S. Dunn-Norman, “Petroleum Well Construction”, 1998 ISBN 0-471-96938-9.].

[17] C. M. O'Brien D.E., Stabilizing Sensitive Shales with Inhibited Potassium-Based Drilling Fluids," Journal of Petroleum Technology 25, no. 9 (September 1973): 1089-1100.]..

[18] G. Kolle and R. Mesel,, Brønnvæsker: for VK1 brønnteknikk, Vett & Viten,, 1998.

[19] Okafor, M.N. and J.F. Evers, Experimental Comparison of Rheology Models for Drilling fluids SPE-24086-MS, 1992.

[20] S. Strand, Øvinger i bore- og brønnvæsker, Høgskolen i Stavanger, Stavanger. 1998.

[21] M. Ochoa, Analysis of Drilling Fluid Rheology and Tool Joint Effect to Reduce Errors in Hydraulics Calculations, [PhD Thesis], Texas A&M University, p.99, 2006.

[22] O. Skjeggestad, Boreslamteknologi: teori og praksis, Bergen: Alma Mater forlag., 1989.

[23] API RP 13-B1, Recommend Practice for Field Testing Water-Based Drilling Fluids, third edition. 2003. Washington, DC: API..

[24] J. Sadigov, Comparisons of rheology and hydraulics prediction of mud systems in concentric and eccentric well geometry / MSc thesis, UiS, 2013.

[25] Binh, B. , Saasen, A. and Maxey, J. et al., Viscoelastic Properties of Oil-Based Drilling Fluids" Annual Transactions of the Nordic Rheology Society. Vol 20., 2012.

[26] T. Mezger, The Rheology Handbook. Hanover: European, 2011.

[27] N. Robertson, Effective Torque Management of Wytch Farm Extended-Reach Sidetrack Wells SPE-95430-MS, 2005.

[28] P. Z. M. Scott, Scott, P.D., Zamora, M // Barite-Sag Management: Challenges, Strategies, Opportunities //SPE-87136-MS IADC/SPE Drilling Conference, 2-4 March, Dallas, Texas 2004.

[29] Eirik Kårstad, Bernt S. Adnøy and T. Fjelde, A study of temperature dependent friction in wellbore fluids// SPE/IADC drilling conference and exhibition held in Amsterdam , The Netherlands, 17-19 March 2009, 2009.

[30] "nanoshell," 2016. [Online]. Available: https://www.nanoshel.com/product/degussa-p25-TiO2/.

[31] http://www.nanoshel.com/wp-content/uploads/2014/03/Titanium-Oxide-SEM.jpg, 2016.

[32] Wikipedia, https://en.wikipedia.org/wiki/Graphene ; Illustration of graphene lattice, Wikipedia, 2016.

[33] us-nano, http://s.b5z.net/i/u/10091461/i/US1059-SEM-Graphene_Nanoplatelets.jpg http://www.us-nano.com/inc/sdetail/28009, 2016.

[34] us-nano, http://www.us-nano.com/inc/sdetail/201), 2016.

[35] A. Bourgoyne, M. K. Jr., M. Chenevert and F. Young J, , "Applied Drilling Engineering", SPE Textbook Series Vol. 2, 1991. Richardson, Texas (ISBN: 978-1-55563-001-0)., 1991.

[36] Nazari, Hareland and Azar, ,"Review of Cuttings Transport in Directional Well Drilling: Systematic Approach", SPE 132372, SPE Western Regional Meeting, 27-29 May 2010, Anaheim, California, U.S.A., 2010.

[37] H. WellPlan (Landmark)TM Software, WellPlan (Landmark)TM Software, Halliburton., 2016.

[38] M. &. M. R. Walker, Sakhalin-1: Technologies to Efficiently Drill and Develop Resources While Expanding the ERD Envelope. Moscow, World Petroleum Congress, p. 4., 2014.

[39] T. G. Mezger., "The Rheology Handbook", 2002. ISBN 3-87870-745-2..

10 Appendix – A - Rheology Models with %-deviation

10.1 MoS2

10.1.1.1 Reference Fluid – +0.0g MoS2

Table 5 Description of rheological models with MoS2-reference fluid output parameters and %-deviation

		Parameters					
Model	Equation	τo,τy, A	k, C	n, B	μp, μ	%-Deviate	cP
Herschel Bulkley	$0.0733*\gamma^{0.92310}+2.347$	3,4226	0,1234	0,7090		2,04	
Unified	$2.347+0.0731*\gamma^{0.9235}$	3,2010	0,2144	0,6223		3,10	
Power Law	$0.9594*\gamma^{0.5227}$		2,1289	0,2966		9,47	
Bingham	$0.0417*\gamma+3.307$	4,6456			0,0160	10,75	7,6608
Newtonian	$0.0464*\gamma$				0,0226	50,34	10,8209
Robertson and Stiff	$0.1078*(35.5807+\gamma)^{0.8673}$	0,3775	55,6794	0,5666		2,67	

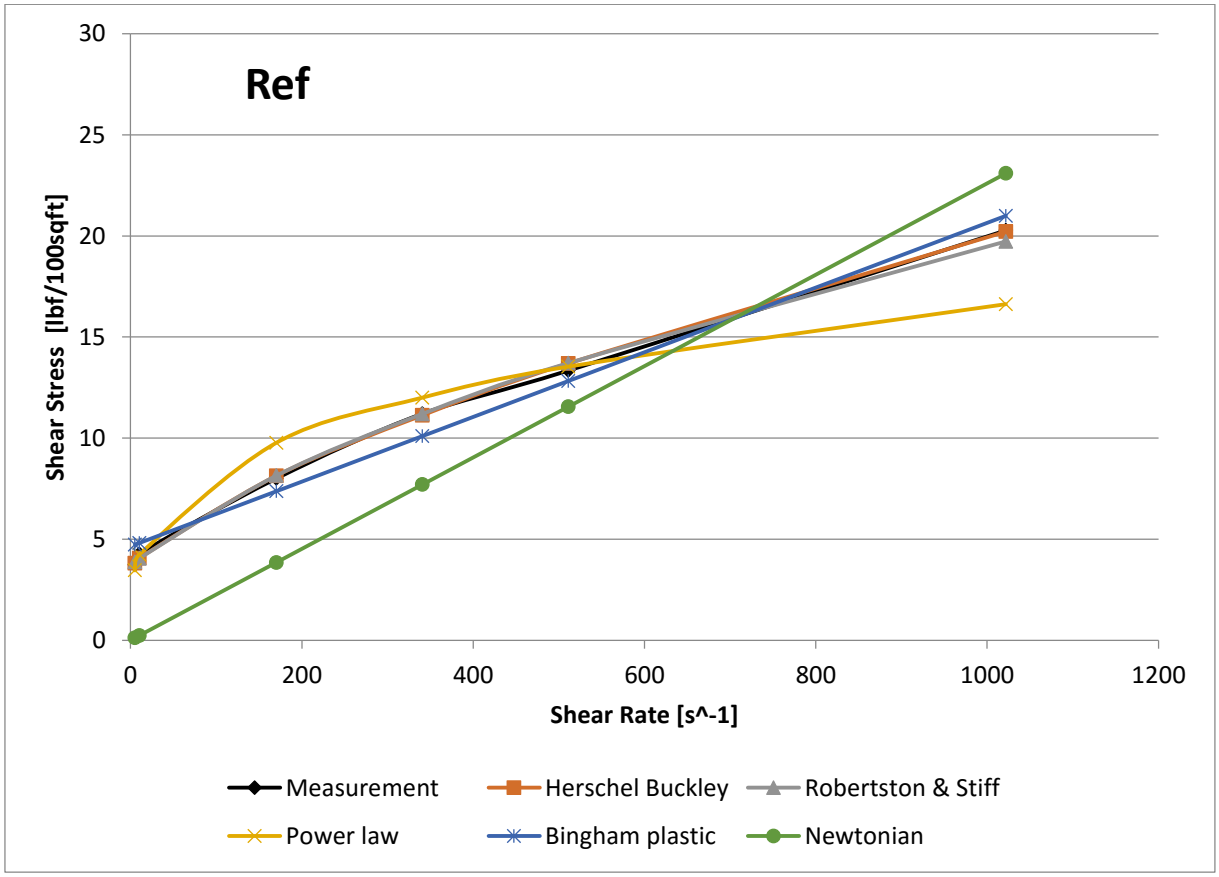

10.1.1.2 Reference Fluid +0.1g MoS_2

Table 6 Description of rheological models with MoS2-reference fluid output parameters and %-deviation

		Parameters					
Model	Equation	τo,τy, A	k, C	n, B	μp, μ	%-Deviate	cP
Herschel Bulkley	$0.0733*\gamma^{0.92310}+2.347$	4,882	0,7311	0,51190		3,90	
Unified	$2.347+0.0731*\gamma^{0.9235}$	5,335	0,4978	0,5704		5,17	
Power Law	$0.9594*\gamma^{0.5227}$		3,9718	0,2778		2,14	
Bingham	$0.0417*\gamma+3.307$	9,700			0,0204	23,59	9,76752
Newtonian	$0.0464*\gamma$				0,0342	57,83	16,375
Robertson and Stiff	$0.1078*(35.5807+\gamma)^{0.8673}$	2,4369	11,6903	0,3557		2,50	

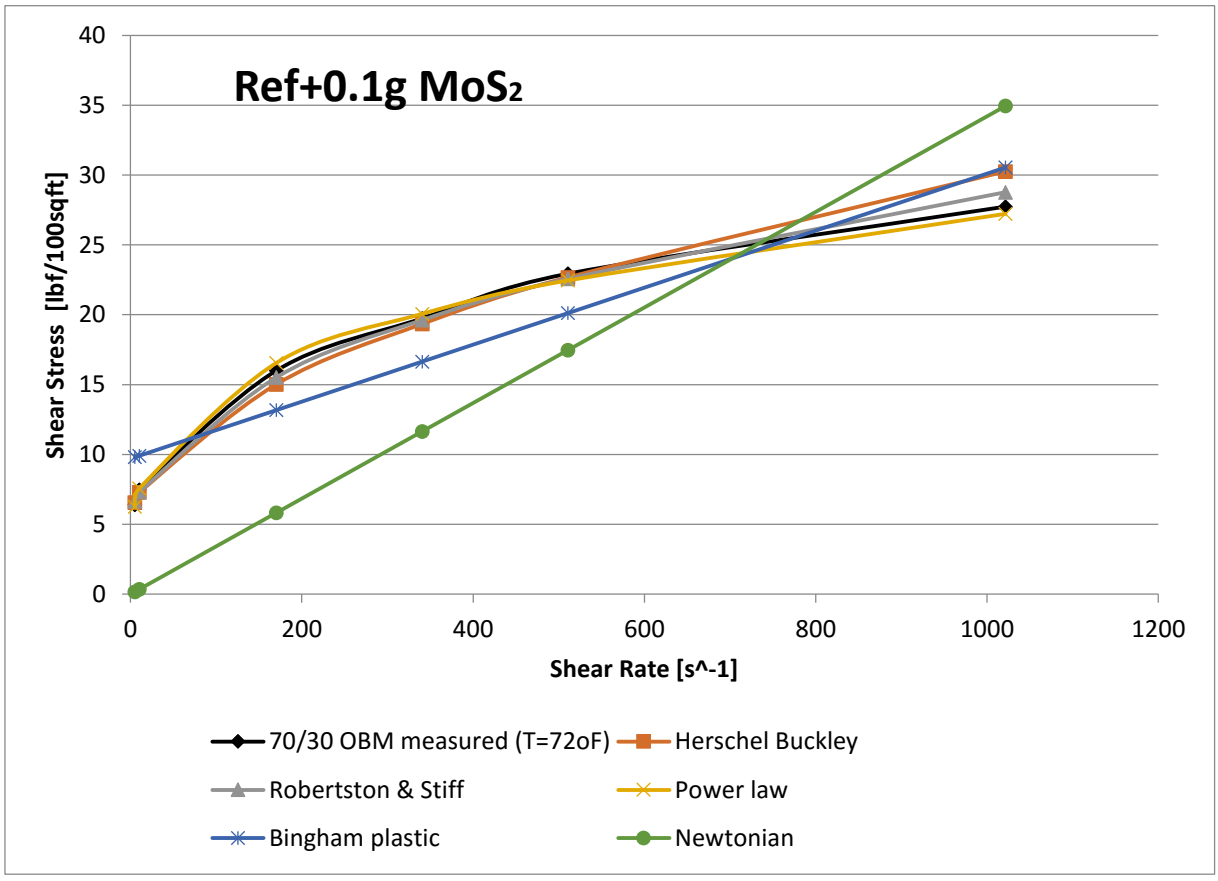

10.1.1.3 Reference Fluid +0.2g MoS_2

Table 7 Description of rheological models with MoS2-reference fluid output parameters and %-deviation

		Parameters					
Model	Equation	τo,τy, A	k, C	n, B	μp, μ	%-Deviate	cP
Herschel Bulkley	$0.0733*\gamma^{0.92310}+2.347$	3,233	0,8722	0,46960		6,20	
Unified	$2.347+0.0731*\gamma^{0.9235}$	3,201	0,8911	0,4665		6,20	
Power Law	$0.9594*\gamma^{0.5227}$		3,0242	0,298		5,62	
Bingham	$0.0417*\gamma+3.307$	7,416			0,0201	19,28	9,62388
Newtonian	$0.0464*\gamma$				0,0306	53,37	14,6513
Robertson and Stiff	$0.1078*(35.5807+\gamma)^{0.8673}$	1,8906	10,2228	0,373		6,94	

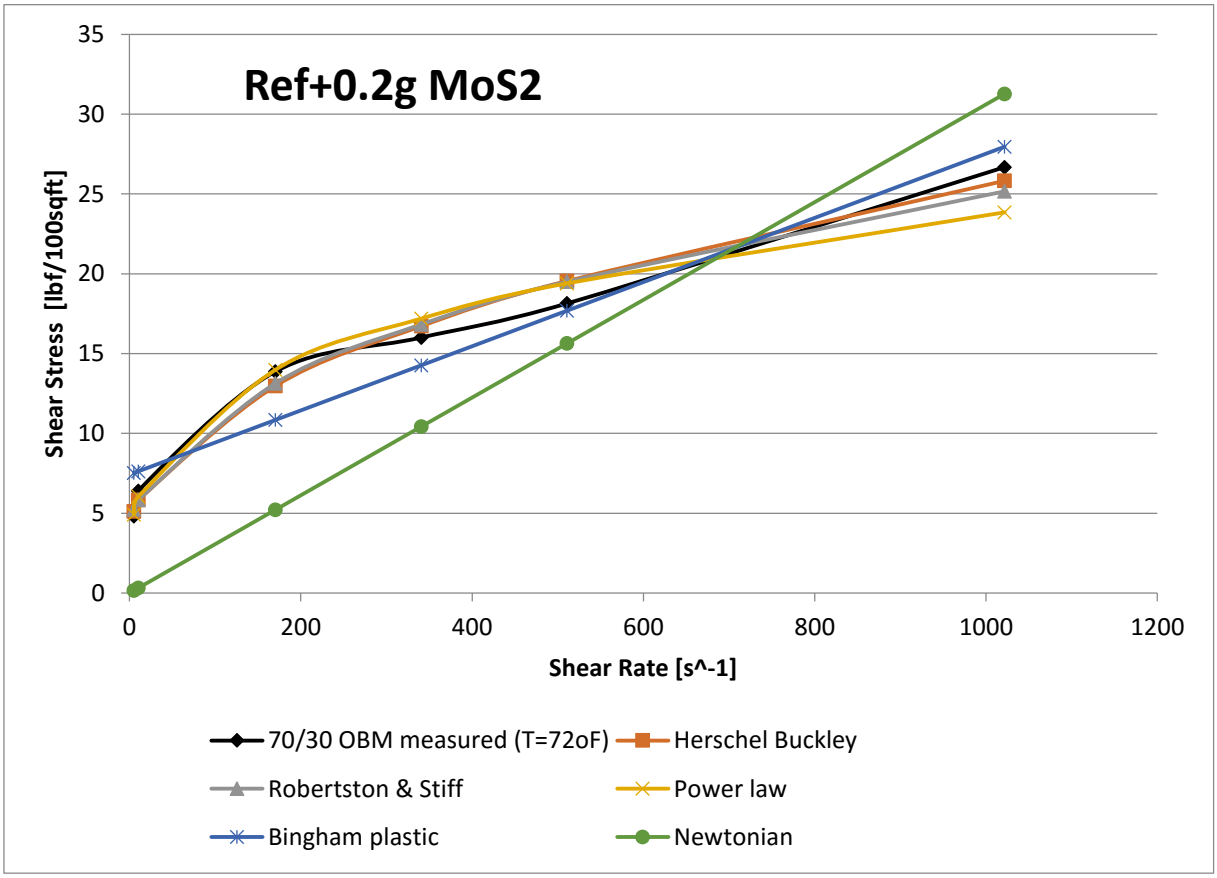

10.1.1.4 Reference Fluid +0.3g MoS_2

Table 8 Description of rheological models with MoS2-reference fluid output parameters and %-deviation

		Parameters					
Model	Equation	τo,τy, A	k, C	n, B	μp, μ	%-Deviate	cP
Herschel Bulkley	$0.0733*\gamma^{0.92310}+2.347$	3,189	0,2126	0,65100		2,60	
Unified	$2.347+0.0731*\gamma^{0.9235}$	3,201	0,2077	0,6547		2,70	
Power Law	$0.9594*\gamma^{0.5227}$		2,0693	0,321		6,19	
Bingham	$0.0417*\gamma+3.307$	5,343			0,0171	19,57	8,18748
Newtonian	$0.0464*\gamma$				0,0247	52,98	11,8264
Robertson and Stiff	$0.1078*(35.5807+\gamma)^{0.8673}$	0,7697	23,7813	0,4778		1,17	

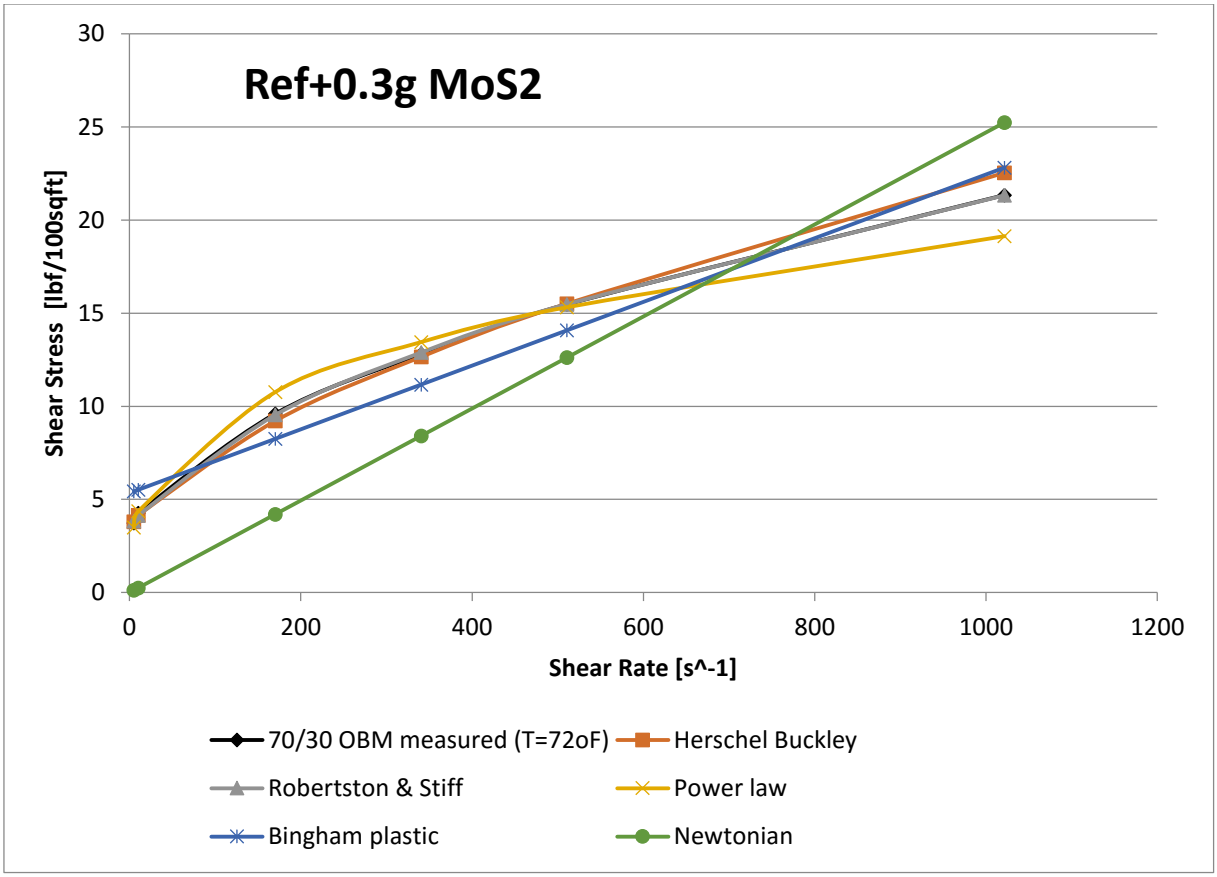

10.1.1.5 Reference Fluid +0.4g MoS_2

Table 9 Description of rheological models with MoS2-reference fluid output parameters and %-deviation

		Parameters					
Model	Equation	τo,τy, A	k, C	n, B	μp, μ	%-Deviate	cP
Herschel Bulkley	$0.0733*\gamma^{0.92310}+2.347$	4,009	0,395	0,55800		3,92	
Unified	$2.347+0.0731*\gamma^{0.9235}$	3,735	0,5381	0,5111		3,87	
Power Law	$0.9594*\gamma^{0.5227}$		2,9928	0,2754		6,87	
Bingham	$0.0417*\gamma+3.307$	6,508			0,0176	13,98	8,42688
Newtonian	$0.0464*\gamma$				0,0268	52,84	12,8318
Robertson and Stiff	$0.1078*(35.5807+\gamma)^{0.8673}$	1,2375	25,0756	0,4153		4,78	

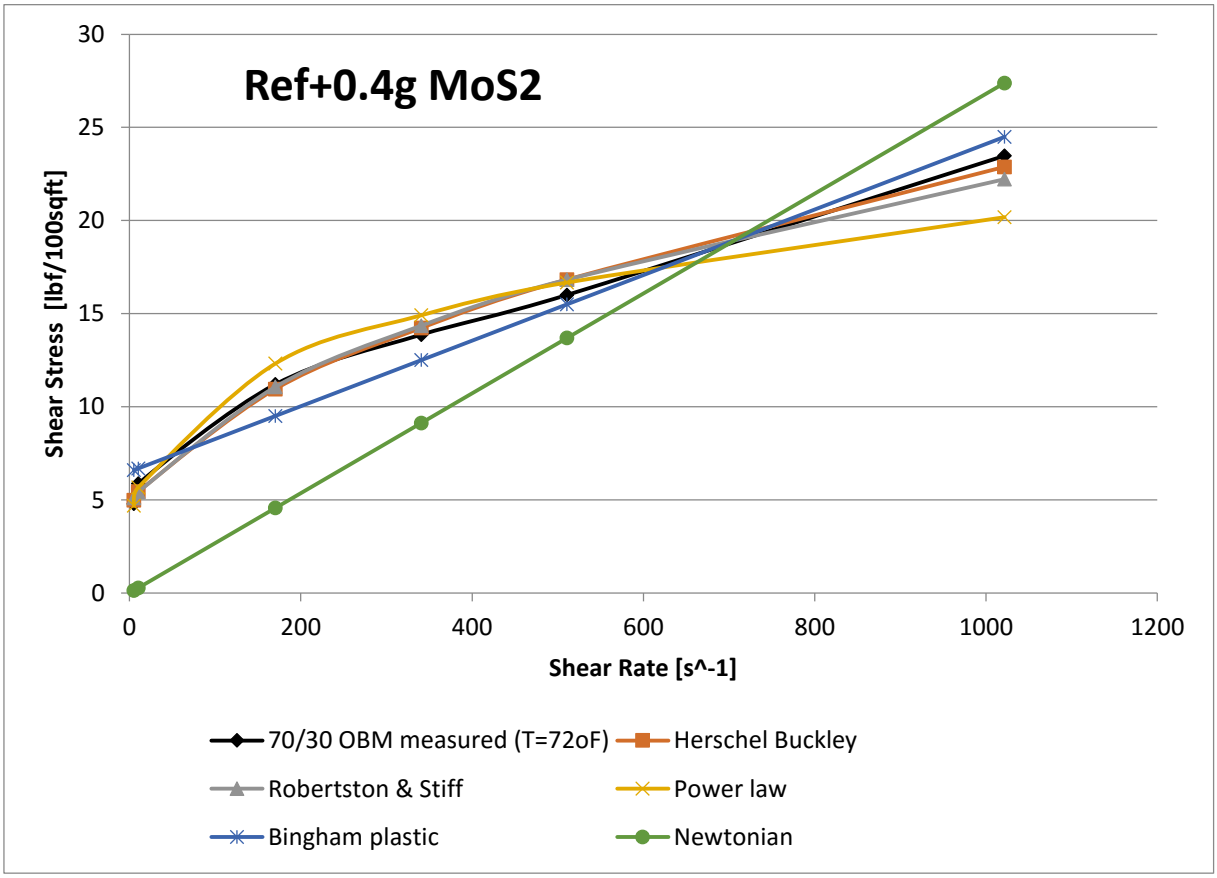

10.2 TiO_2

10.2.1.1 Reference Fluid

Table 10 Description of rheological models with MoS2-reference fluid output parameters and %-deviation

		Parameters					
Model	Equation	τo,τy, A	k, C	n, B	μp, μ	%-Deviate	cP
Herschel Bulkley	$0.0733*\gamma^{0.92310}+2.347$	2,790	0,1642	0,6704		2,46	
Unified	$2.347+0.0731*\gamma^{0.9235}$	2,668	0,2156	0,6278		1,71	
Power Law	$0.9594*\gamma^{0.5227}$		1,7656	0,3244		6,87	
Bingham	$0.0417*\gamma+3.307$	4,459			0,0155	17,11	7,4214
Newtonian	$0.0464*\gamma$				0,0218	51,73	10,4378
Robertson and Stiff	$0.1078*(35.5807+\gamma)^{0.8673}$	0,5188	31,145	0,5177		2,10	

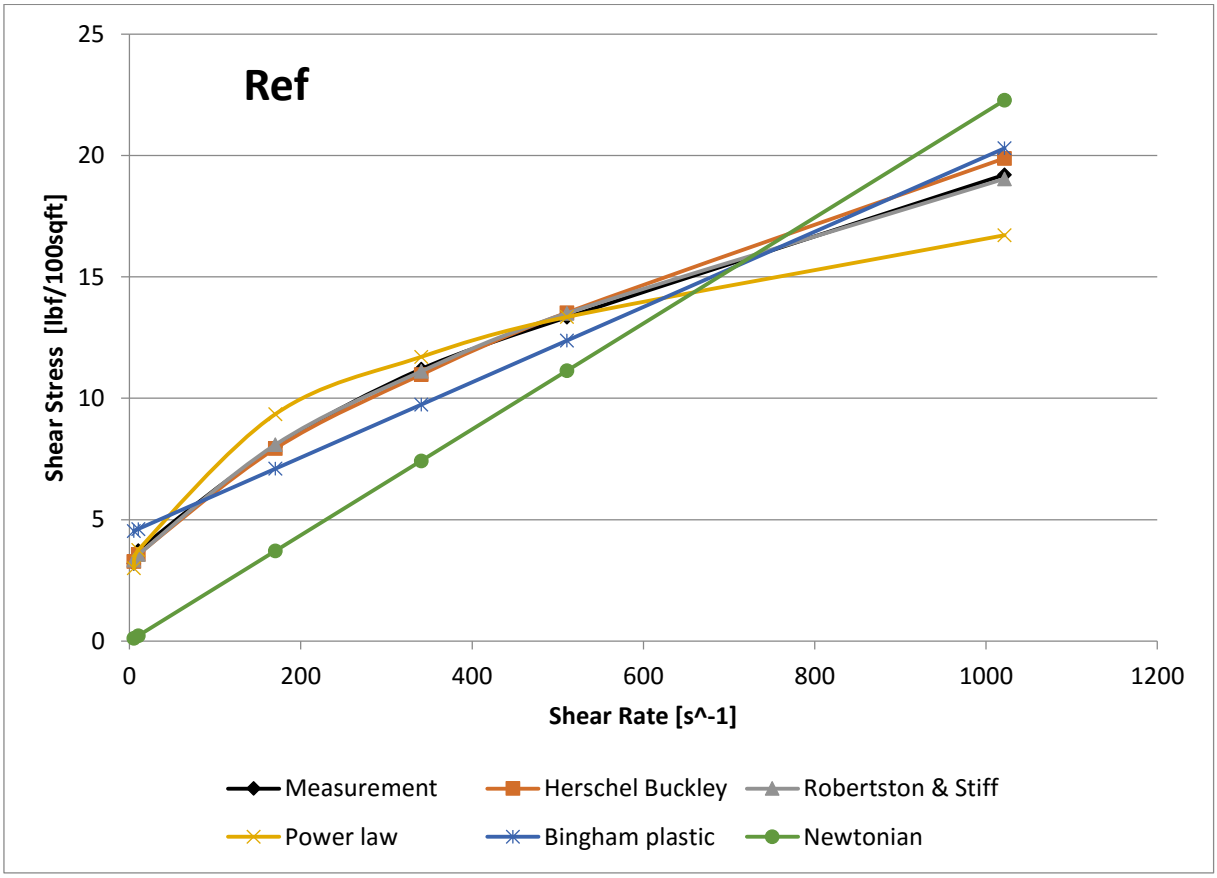

10.2.1.2 Reference Fluid +0.1g TiO_2

Table 11 Description of rheological models with MoS2-reference fluid output parameters and %-deviation

		Parameters					
Model	Equation	τo,τy, A	k, C	n, B	μp, μ	%-Deviate	cP
Herschel Bulkley	$0.0733*\gamma^{0.92310}+2.347$	2,790	0,1642	0,6704		2,46	
Unified	$2.347+0.0731*\gamma^{0.9235}$	2,668	0,2156	0,6278		1,71	
Power Law	$0.9594*\gamma^{0.5227}$		1,7656	0,3244		6,87	
Bingham	$0.0417*\gamma+3.307$	4,459			0,0155	17,11	7,4214
Newtonian	$0.0464*\gamma$				0,0218	51,73	10,4378
Robertson and Stiff	$0.1078*(35.5807+\gamma)^{0.8673}$	0,5188	31,145	0,5177		2,10	

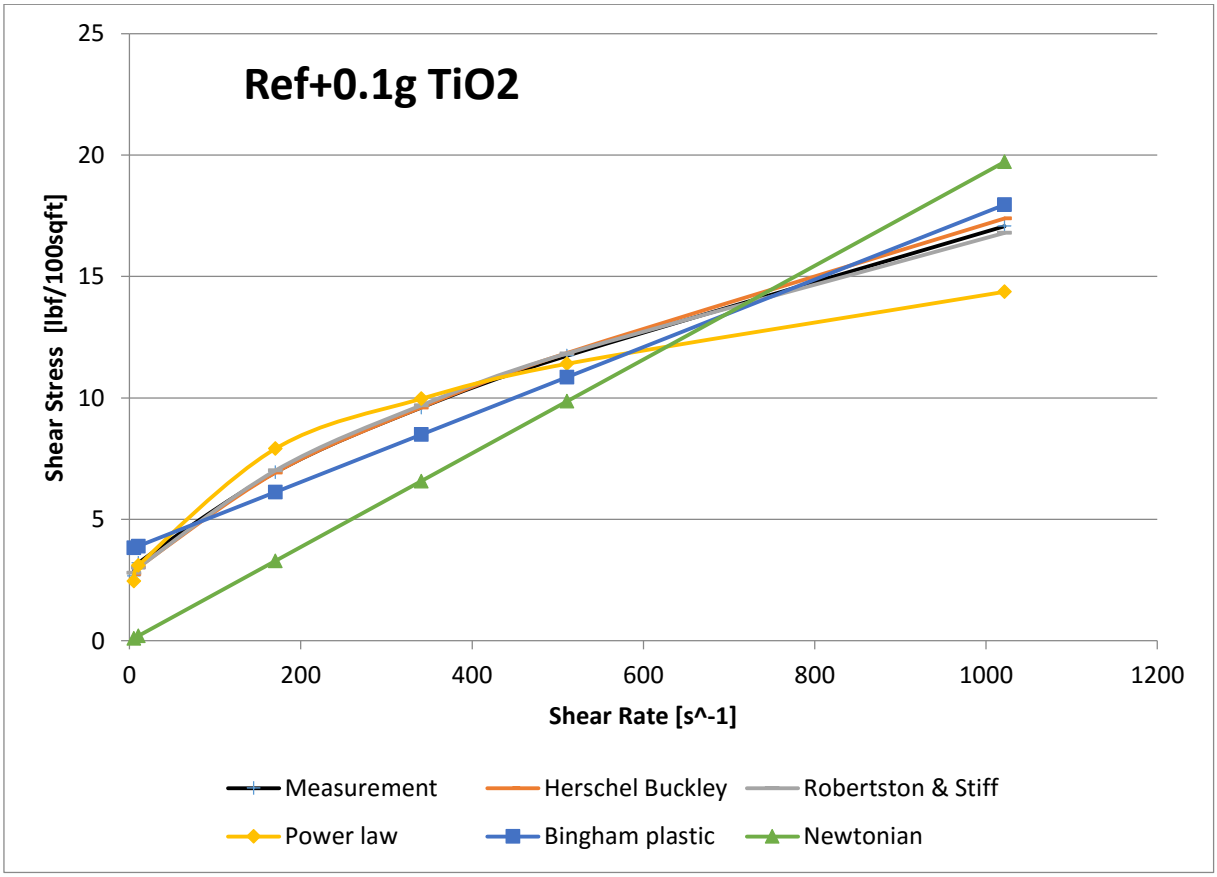

10.2.1.3 Reference Fluid +0.2g TiO_2

Table 12 Description of rheological models with MoS2-reference fluid output parameters and %-deviation

		Parameters					
Model	Equation	τo,τy, A	k, C	n, B	μp, μ	%-Deviate	cP
Herschel Bulkley	$0.0733*\gamma^{0.92310}+2.347$	2,790	0,1642	0,6704		2,46	
Unified	$2.347+0.0731*\gamma^{0.9235}$	2,668	0,2156	0,6278		1,71	
Power Law	$0.9594*\gamma^{0.5227}$		1,7656	0,3244		6,87	
Bingham	$0.0417*\gamma+3.307$	4,459			0,0155	17,11	7,4214
Newtonian	$0.0464*\gamma$				0,0218	51,73	10,4378
Robertson and Stiff	$0.1078*(35.5807+\gamma)^{0.8673}$	0,5188	31,145	0,5177		2,10	

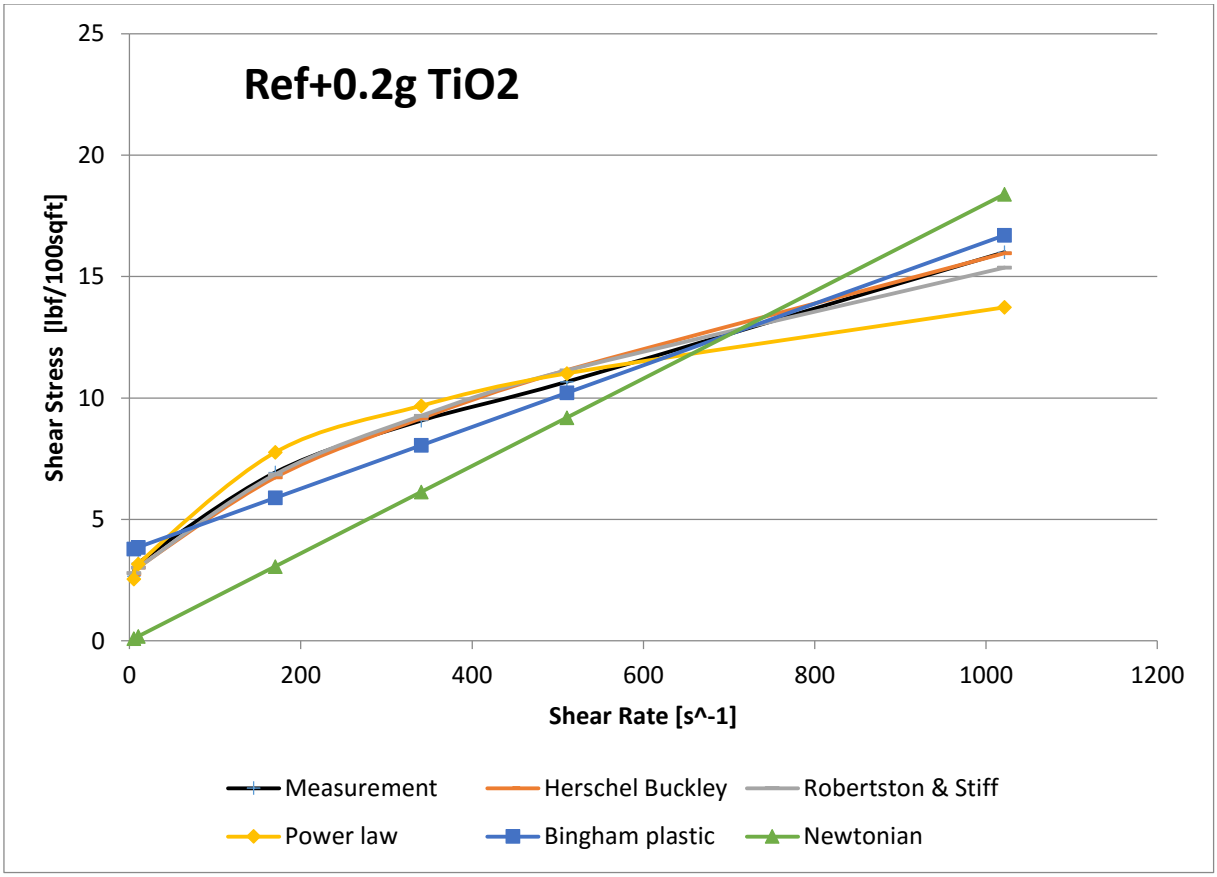

10.2.1.4 Reference Fluid +0.3g TiO_2

Table 13 Description of rheological models with MoS2-reference fluid output parameters and %-deviation

		Parameters					
Model	Equation	τo,τy, A	k, C	n, B	μp, μ	%-Deviate	cP
Herschel Bulkley	$0.0733*\gamma^{0.92310}+2.347$	2,790	0,1642	0,6704		2,46	
Unified	$2.347+0.0731*\gamma^{0.9235}$	2,668	0,2156	0,6278		1,71	
Power Law	$0.9594*\gamma^{0.5227}$		1,7656	0,3244		6,87	
Bingham	$0.0417*\gamma+3.307$	4,459			0,0155	17,11	7,4214
Newtonian	$0.0464*\gamma$				0,0218	51,73	10,4378
Robertson and Stiff	$0.1078*(35.5807+\gamma)^{0.8673}$	0,5188	31,145	0,5177		2,10	

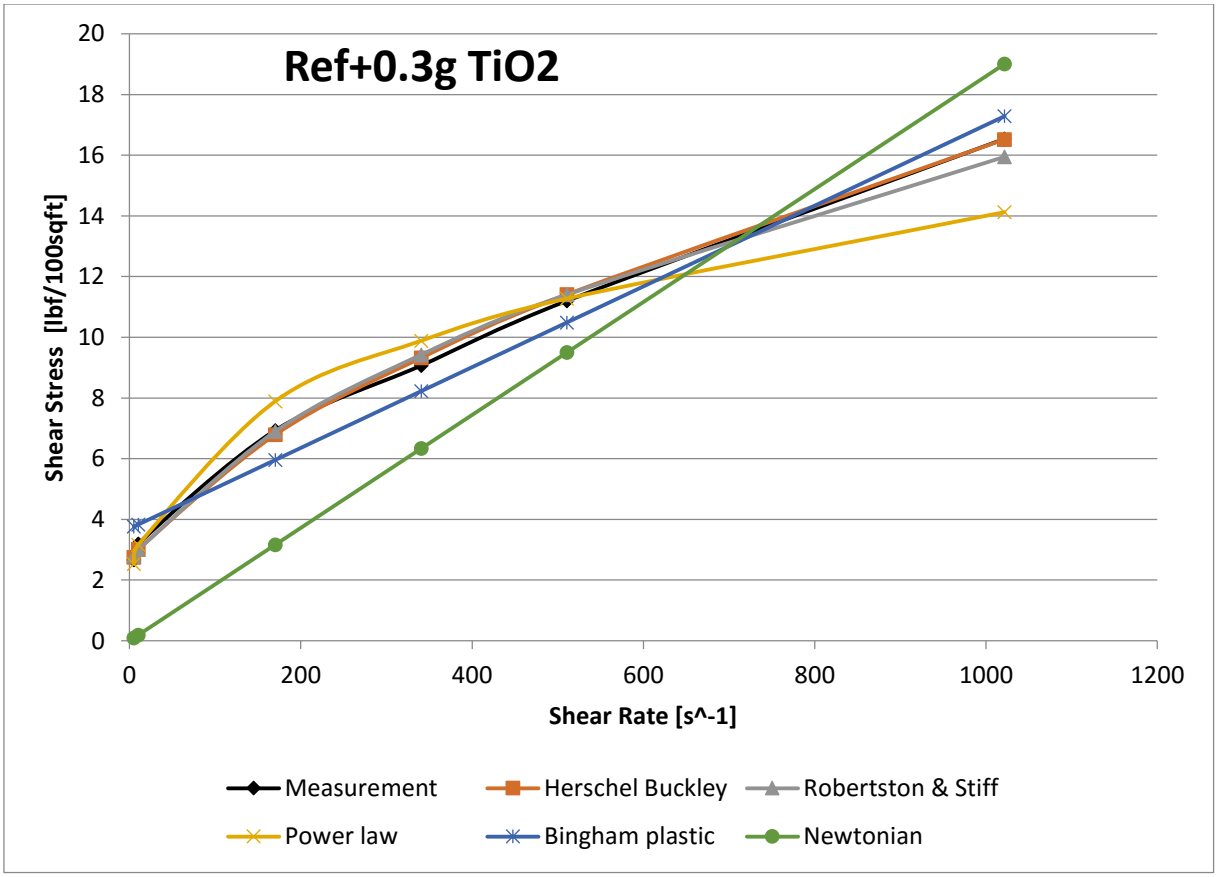

10.2.1.5 Reference Fluid +0.4g TiO_2

Table 14 Description of rheological models with MoS2-reference fluid output parameters and %-deviation

		Parameters					
Model	Equation	τo,τy, A	k, C	n, B	μp, μ	%-Deviate	cP
Herschel Bulkley	$0.0733*\gamma^{0.92310}+2.347$	2,790	0,1642	0,6704		2,46	
Unified	$2.347+0.0731*\gamma^{0.9235}$	2,668	0,2156	0,6278		1,71	
Power Law	$0.9594*\gamma^{0.5227}$		1,7656	0,3244		6,87	
Bingham	$0.0417*\gamma+3.307$	4,459			0,0155	17,11	7,4214
Newtonian	$0.0464*\gamma$				0,0218	51,73	10,4378
Robertson and Stiff	$0.1078*(35.5807+\gamma)^{0.8673}$	0,5188	31,145	0,5177		2,10	

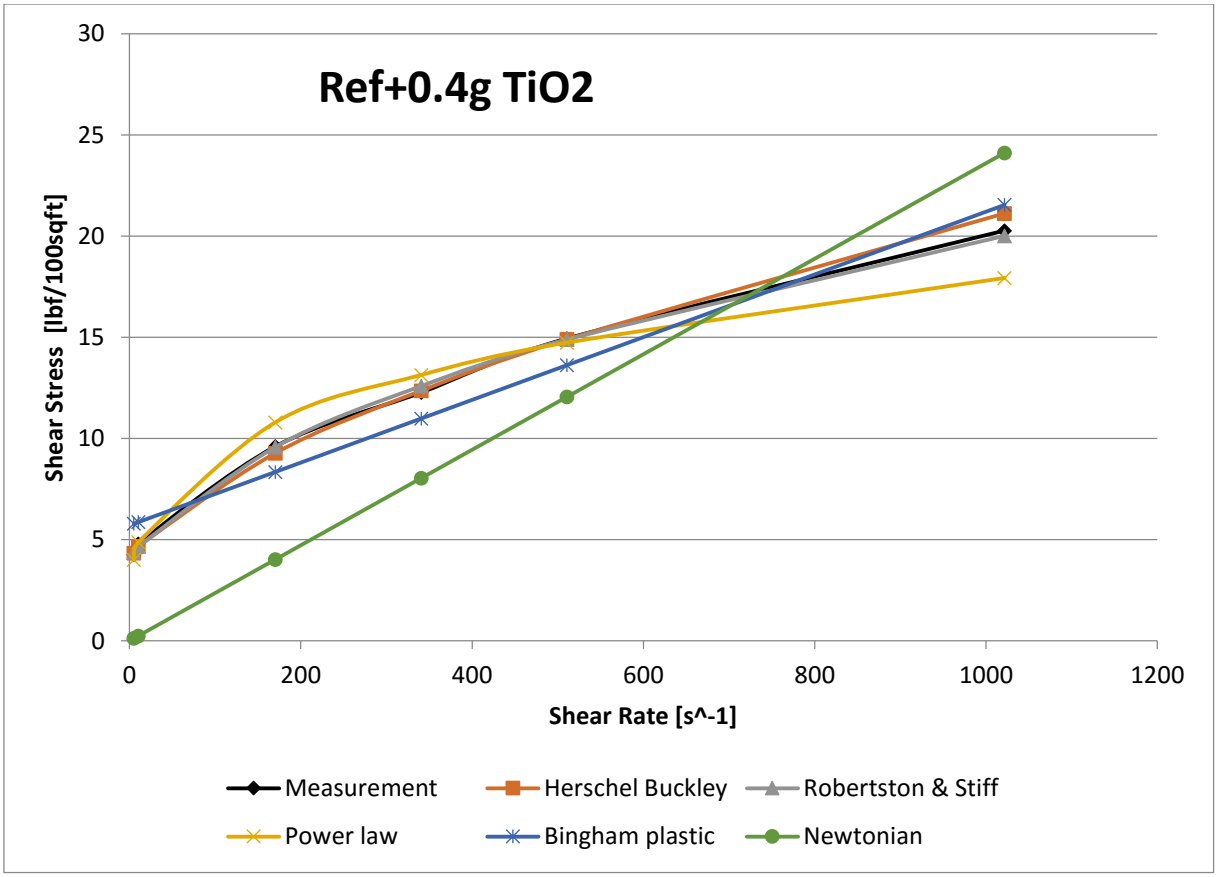

10.3 Graphene

10.3.1.1 Reference Fluid

Table 15 Description of rheological models with MoS2-reference fluid output parameters and %-deviation

		Parameters					
Model	Equation	τo,τy, A	k, C	n, B	μp, μ	%-Deviate	cP
Herschel Bulkley	$0.0733*\gamma^{0.92310}+2.347$	14,130	1,0399	0,48400		1,97	
Unified	$2.347+0.0731*\gamma^{0.9235}$	13,871	1,1899	0,4641		1,77	
Power Law	$0.9594*\gamma^{0.5227}$		11,848	0,1746		3,65	
Bingham	$0.0417*\gamma+3.307$	19,812			0,0252	11,68	12,0658
Newtonian	$0.0464*\gamma$				0,0533	59,14	25,5200
Robertson and Stiff	$0.1078*(35.5807+\gamma)^{0.8673}$	6,3651	28,9323	0,2727		1,86	

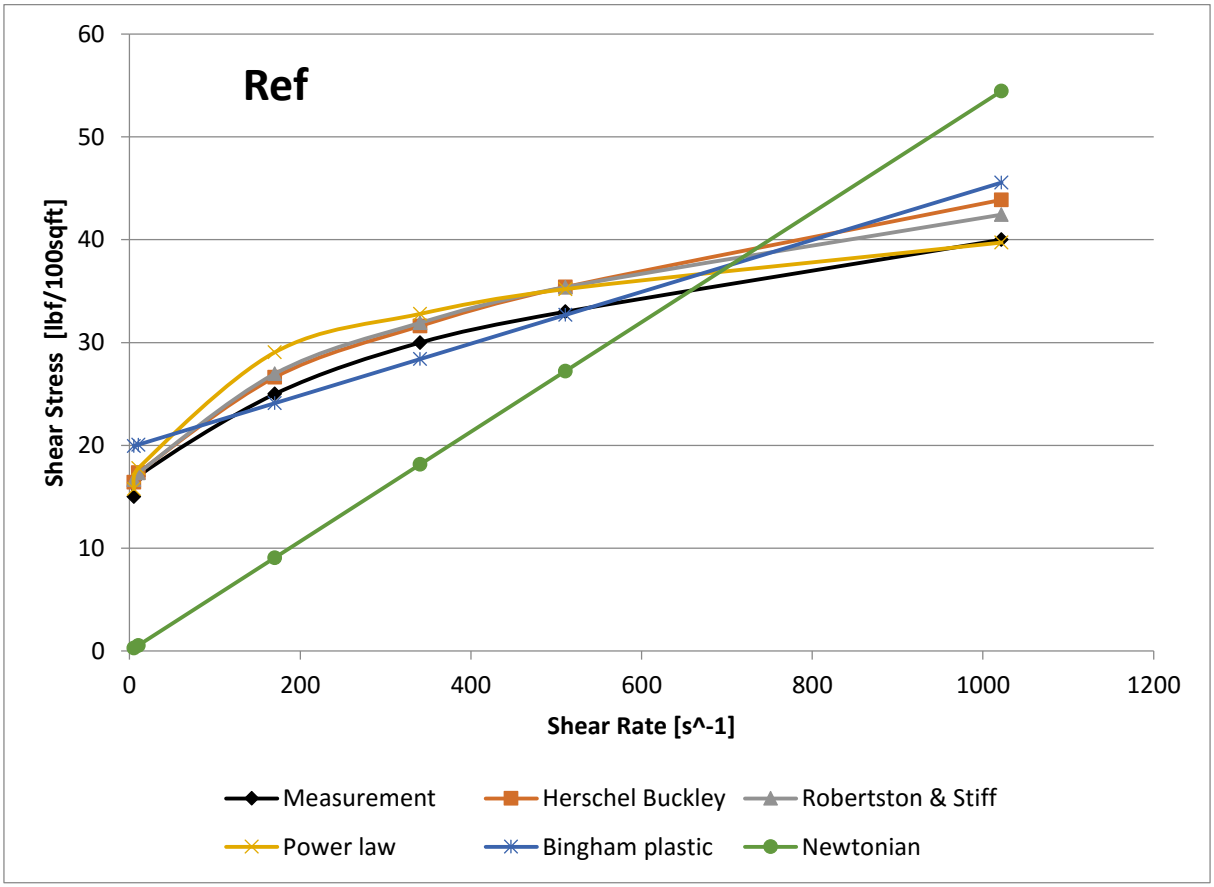

10.3.1.2 Reference Fluid +0.1g Graphene

Table 16 Description of rheological models with MoS2-reference fluid output parameters and %-deviation

		Parameters					
Model	Equation	τo,τy, A	k, C	n, B	μp, μ	%-Deviate	cP
Herschel Bulkley	$0.0733*\gamma^{0.92310}+2.347$	12,863	1,159	0,46920		2,19	
Unified	$2.347+0.0731*\gamma^{0.9235}$	12,804	1,1937	0,4648		2,11	
Power Law	$0.9594*\gamma^{0.5227}$		10,944	0,183		3,34	
Bingham	$0.0417*\gamma+3.307$	18,876			0,0251	12,71	12,0179
Newtonian	$0.0464*\gamma$				0,0519	58,99	24,8497
Robertson and Stiff	$0.1078*(35.5807+\gamma)^{0.8673}$	6,3031	23,2748	0,2704		1,83	

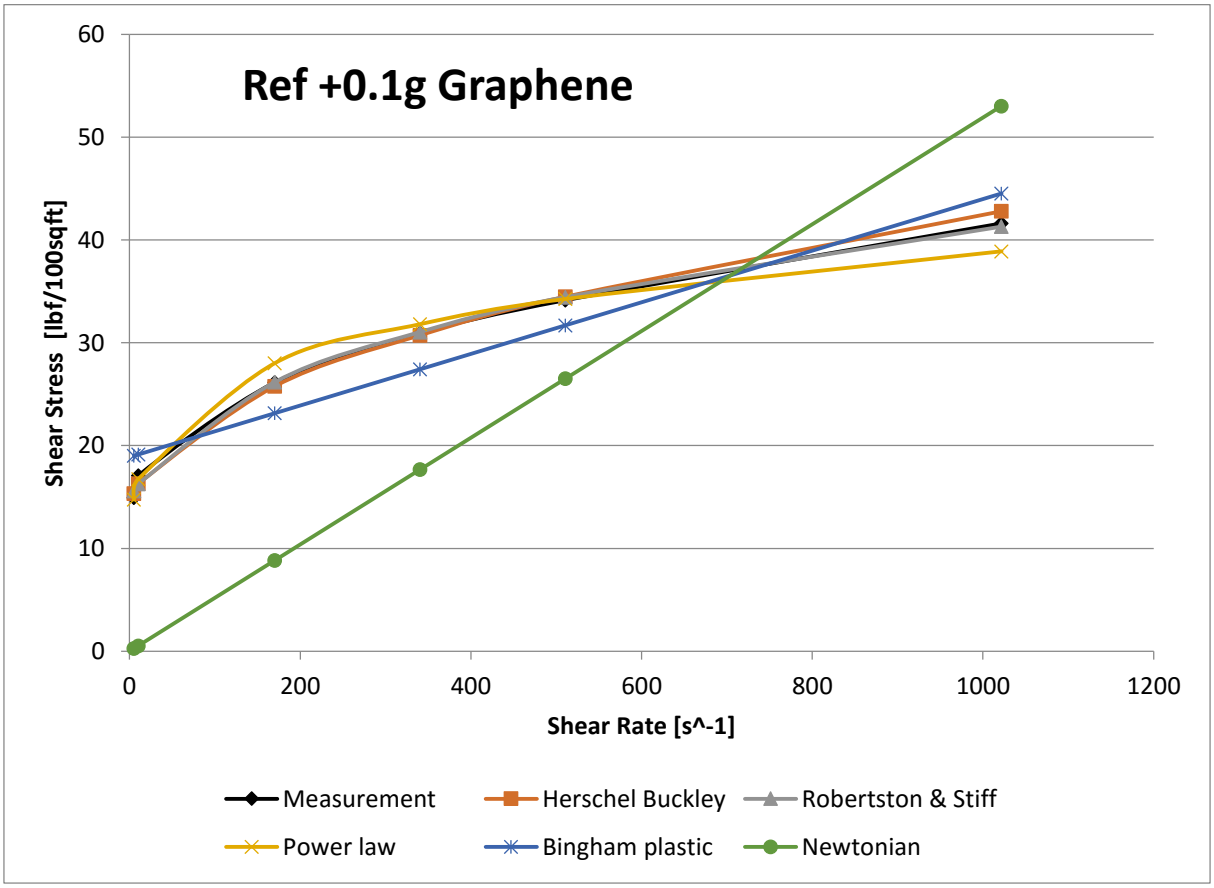

10.3.1.3 Reference Fluid +0.2g Graphene

Table 17 Description of rheological models with MoS2-reference fluid output parameters and %-deviation

		Parameters					
Model	Equation	τo,τy, A	k, C	n, B	μp, μ	%-Deviate	cP
Herschel Bulkley	$0.0733*\gamma^{0.92310}+2.347$	13,412	0,7712	0,52370		2,15	
Unified	$2.347+0.0731*\gamma^{0.9235}$	13,338	0,8111	0,5161		2,03	
Power Law	$0.9594*\gamma^{0.5227}$		10,792	0,1812		4,22	
Bingham	$0.0417*\gamma+3.307$	18,419			0,0246	12,31	11,7785
Newtonian	$0.0464*\gamma$				0,0507	59,13	24,2752
Robertson and Stiff	$0.1078*(35.5807+\gamma)^{0.8673}$	5,5821	29,6904	0,2853		1,66	

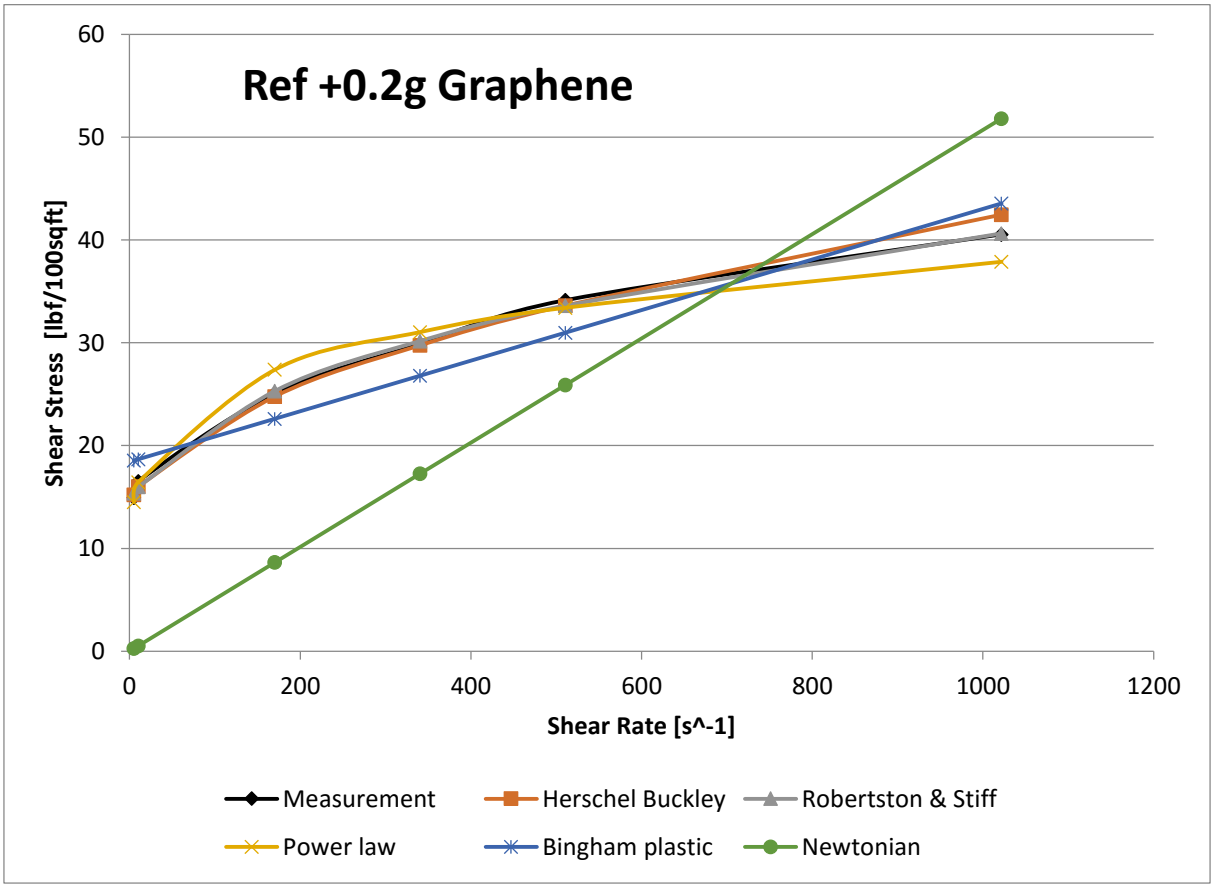

10.3.1.4 Reference Fluid +0.3g Graphene

Table 18 Description of rheological models with MoS2-reference fluid output parameters and %-deviation

		Parameters					
Model	Equation	τo,τy, A	k, C	n, B	μp, μ	%-Deviate	cP
Herschel Bulkley	$0.0733*\gamma^{0.92310}+2.347$	14,029	1,8087	0,42020		2,51	
Unified	$2.347+0.0731*\gamma^{0.9235}$	14,405	1,574	0,4404		2,86	
Power Law	$0.9594*\gamma^{0.5227}$		12,773	0,1775		2,39	
Bingham	$0.0417*\gamma+3.307$	21,943			0,0267	13,55	12,7840
Newtonian	$0.0464*\gamma$				0,0579	59,80	27,7225
Robertson and Stiff	$0.1078*(35.5807+\gamma)^{0.8673}$	8,4406	16,7646	0,2434		1,97	

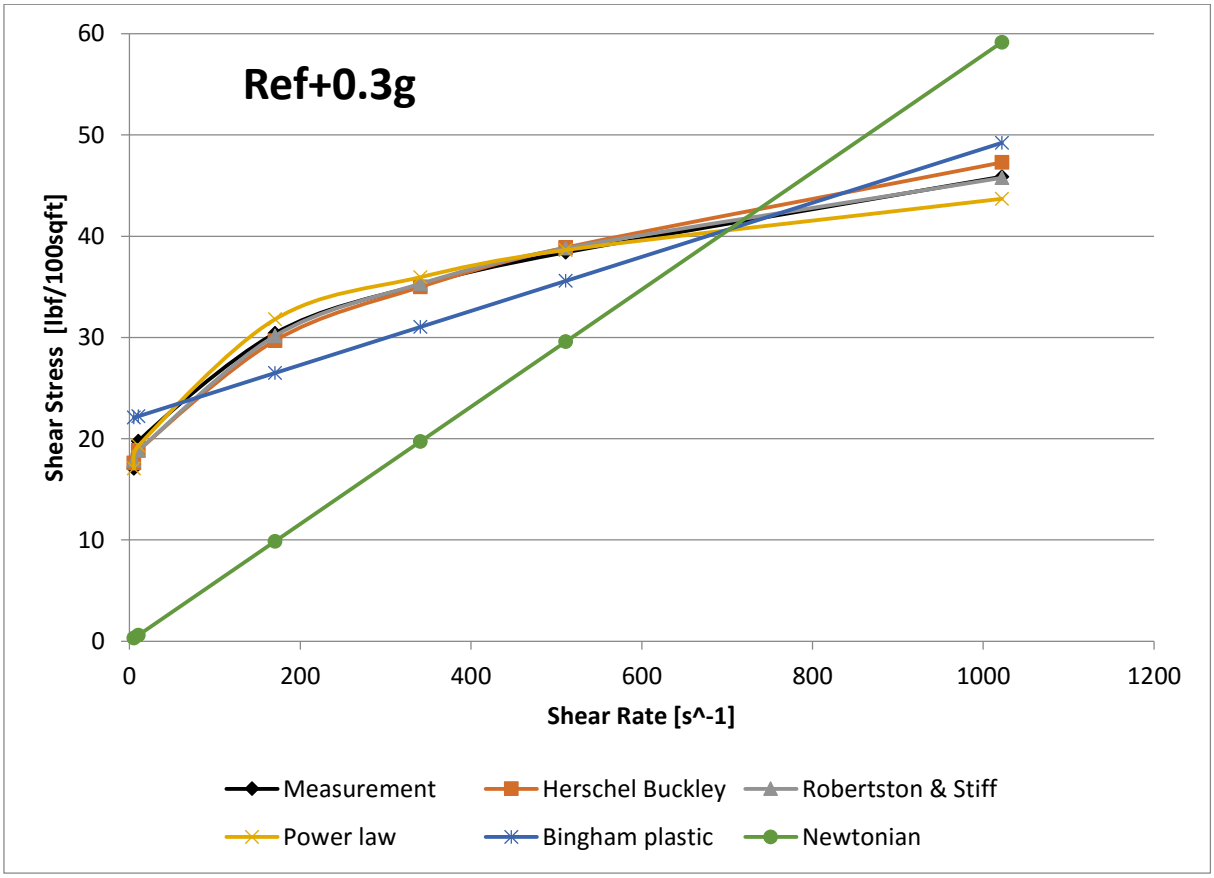

10.3.1.5 Reference Fluid +0.4g Graphene

Table 19 Description of rheological models with MoS2-reference fluid output parameters and %-deviation

		Parameters					
Model	Equation	τo,τy, A	k, C	n, B	μp, μ	%-Deviate	cP
Herschel Bulkley	$0.0733*\gamma^{0.92310}+2.347$	10,277	0,7563	0,51570		2,04	
Unified	$2.347+0.0731*\gamma^{0.9235}$	10,137	0,8327	0,5012		1,77	
Power Law	$0.9594*\gamma^{0.5227}$		8,245	0,2012		4,20	
Bingham	$0.0417*\gamma+3.307$	14,874			0,0232	12,91	11,1082
Newtonian	$0.0464*\gamma$				0,0444	57,75	21,2587
Robertson and Stiff	$0.1078*(35.5807+\gamma)^{0.8673}$	4,185	26,8374	0,3085		1,97	

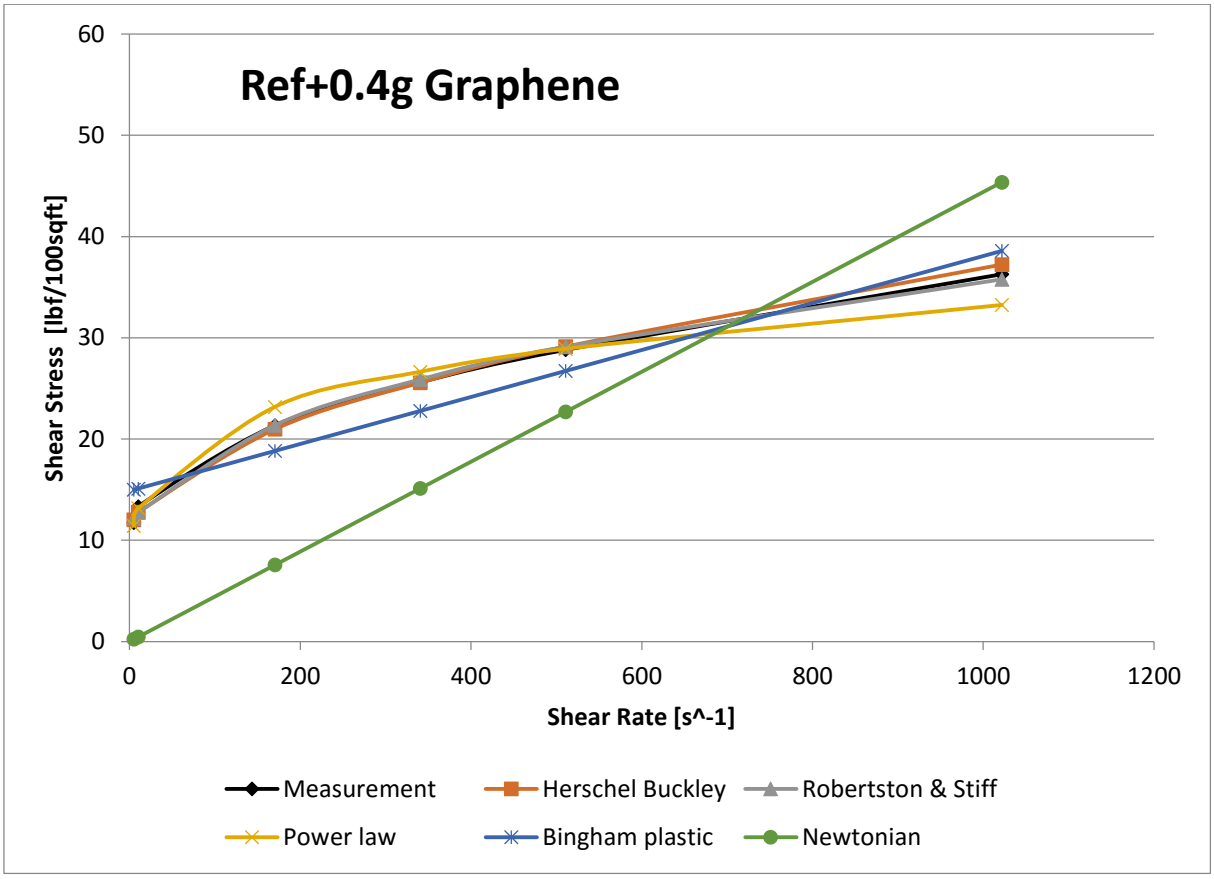

10.4 TiN

10.4.1.1 Reference Fluid

Table 20 Description of rheological models with MoS2-reference fluid output parameters and %-deviation

		Parameters					
Model	Equation	τo,τy, A	k, C	n, B	μp, μ	%-Deviate	cP
Herschel Bulkley	$0.0733*\gamma^{0.92310}+2.347$	1,427	0,0669	0,76770		12,87	
Unified	$2.347+0.0731*\gamma^{0.9235}$	1,174	0,1656	0,625		13,02	
Power Law	$0.9594*\gamma^{0.5227}$		0,7657	0,4011		19,17	
Bingham	$0.0417*\gamma+3.307$	2,403			0,0129	22,56	6,17652
Newtonian	$0.0464*\gamma$				0,0163	48,31	7,80444
Robertson and Stiff	$0.1078*(35.5807+\gamma)^{0.8673}$	0,0711	57,1269	0,7716		12,95	

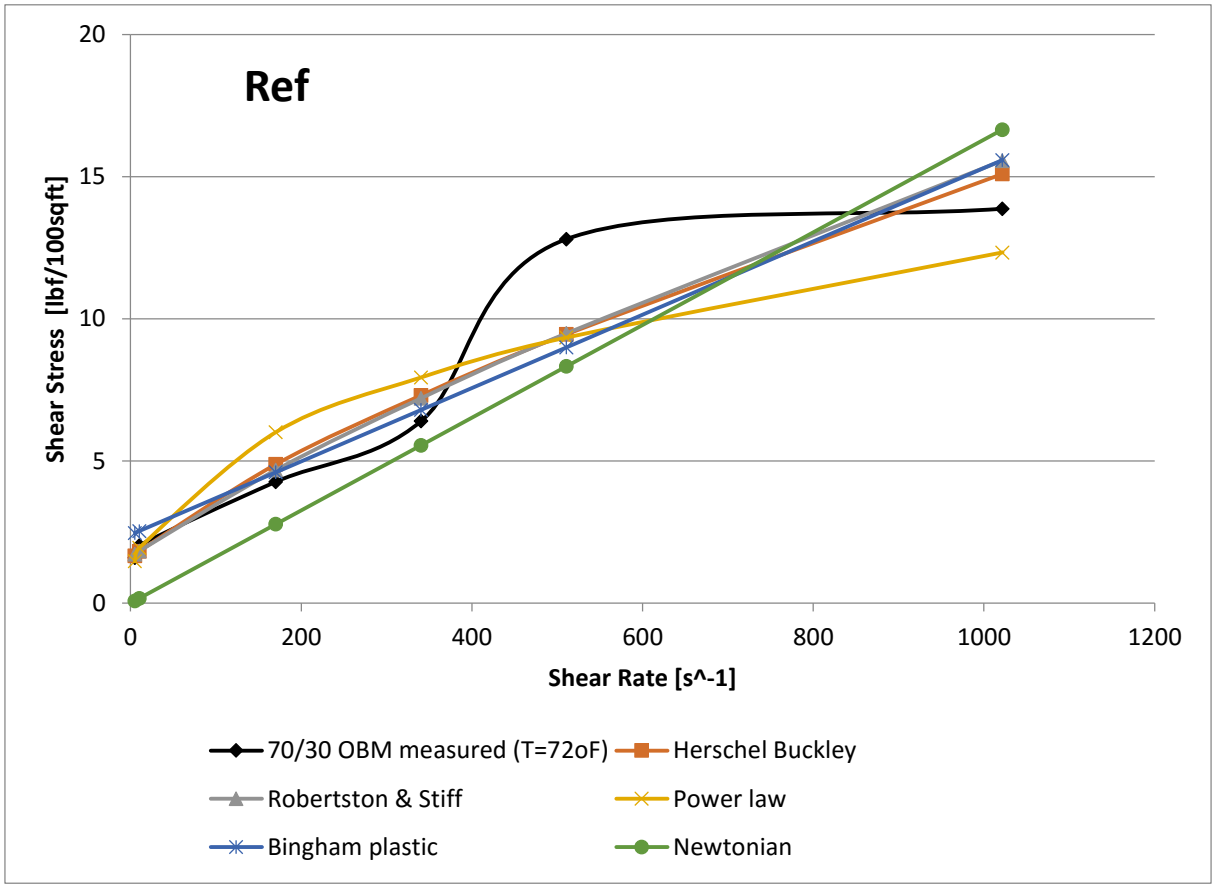
Ref
Shear Stress [lbf/100sqft]
Shear Rate [s^-1]
0
5
10
15
20
0
200
400
600
800
1000
1200
70/30 OBM measured (T=72oF)
Herschel Buckley
Robertston & Stiff
Power law
Bingham plastic
Newtonian

10.4.1.2 Reference Fluid +0.1g TiN

Table 21 Description of rheological models with MoS2-reference fluid output parameters and %-deviation

		Parameters					
Model	Equation	τo,τy, A	k, C	n, B	μp, μ	%-Deviate	cP
Herschel Bulkley	$0.0733*\gamma^{0.92310}+2.347$	1,279	0,1398	0,65520		4,59	
Unified	$2.347+0.0731*\gamma^{0.9235}$	1,067	0,2354	0,5743		5,70	
Power Law	$0.9594*\gamma^{0.5227}$		0,8194	0,3922		8,63	
Bingham	$0.0417*\gamma+3.307$	2,390			0,0127	16,86	6,08076
Newtonian	$0.0464*\gamma$				0,0161	46,96	7,70868
Robertson and Stiff	$0.1078*(35.5807+\gamma)^{0.8673}$	0,2543	22,8380	0,5778		5,48	

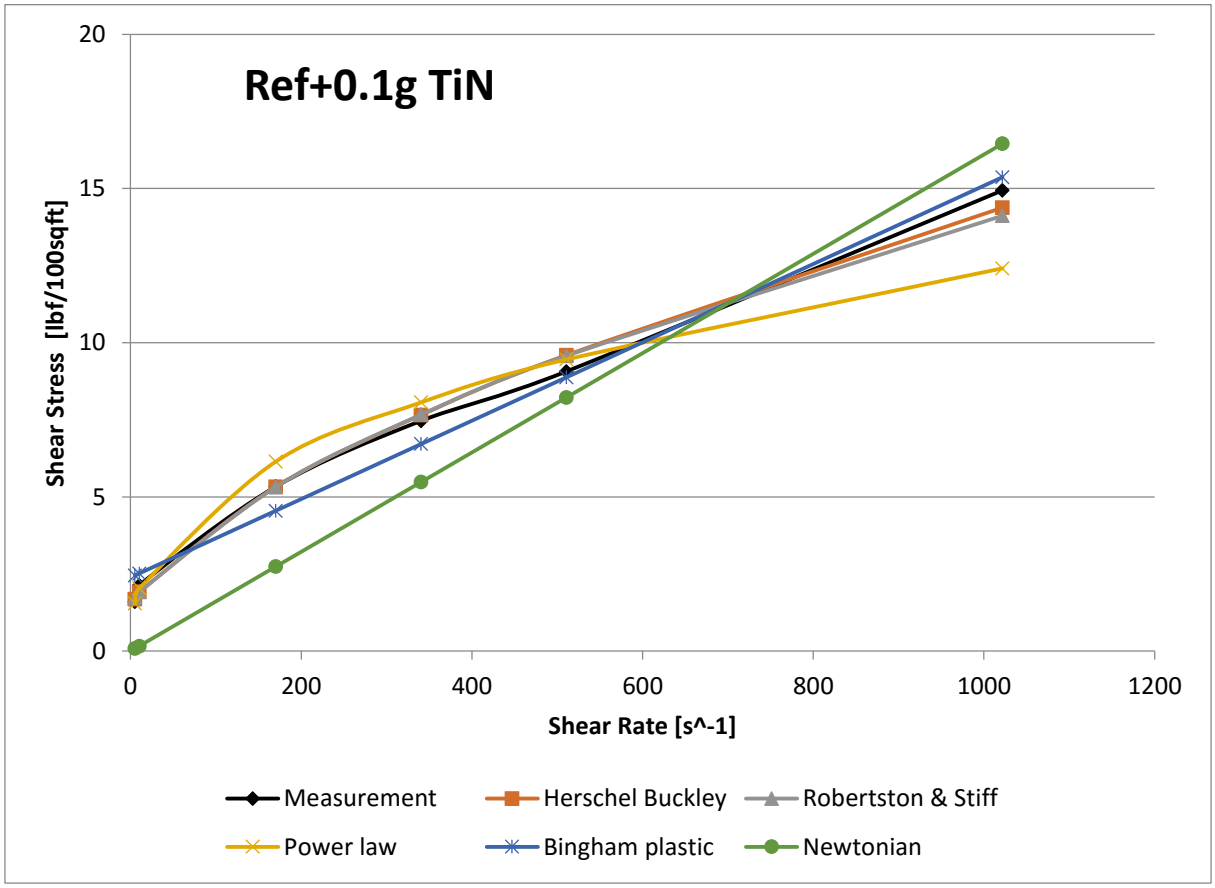

10.4.1.3 Reference Fluid +0.2g TiN

Table 22 Description of rheological models with MoS2-reference fluid output parameters and %-deviation

		Parameters					
Model	Equation	τo,τy, A	k, C	n, B	μp, μ	%-Deviate	cP
Herschel Bulkley	$0.0733*\gamma^{0.92310}+2.347$	2,790	0,1642	0,6704		2,46	
Unified	$2.347+0.0731*\gamma^{0.9235}$	2,668	0,2156	0,6278		1,71	
Power Law	$0.9594*\gamma^{0.5227}$		1,7656	0,3244		6,87	
Bingham	$0.0417*\gamma+3.307$	4,459			0,0155	17,11	7,4214
Newtonian	$0.0464*\gamma$				0,0218	51,73	10,4378
Robertson and Stiff	$0.1078*(35.5807+\gamma)^{0.8673}$	0,5188	31,145	0,5177		2,10	

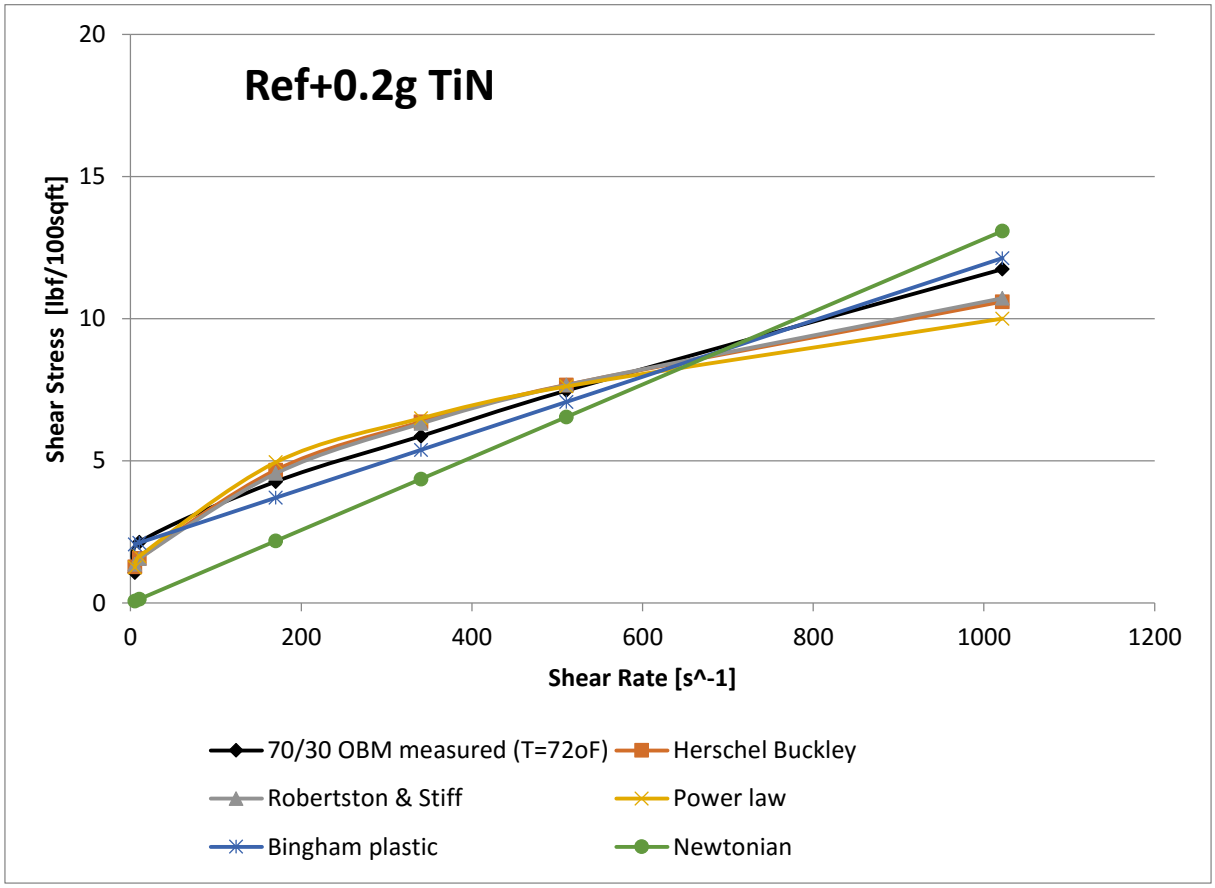

10.4.1.4 Reference Fluid +0.3g TiN

Table 23 Description of rheological models with MoS2-reference fluid output parameters and %-deviation

		Parameters					
Model	Equation	τo,τy, A	k, C	n, B	μp, μ	%-Deviate	cP
Herschel Bulkley	$0.0733*\gamma^{0.92310}+2.347$	1,279	0,1379	0,66350		3,72	
Unified	$2.347+0.0731*\gamma^{0.9235}$	1,067	0,2322	0,5824		4,38	
Power Law	$0.9594*\gamma^{0.5227}$		0,8097	0,3993		7,39	
Bingham	$0.0417*\gamma+3.307$	2,527			0,0128	20,38	6,12864
Newtonian	$0.0464*\gamma$				0,0164	48,28	7,85232
Robertson and Stiff	$0.1078*(35.5807+\gamma)^{0.8673}$	0,2467	22,8380	0,5877		4,49	

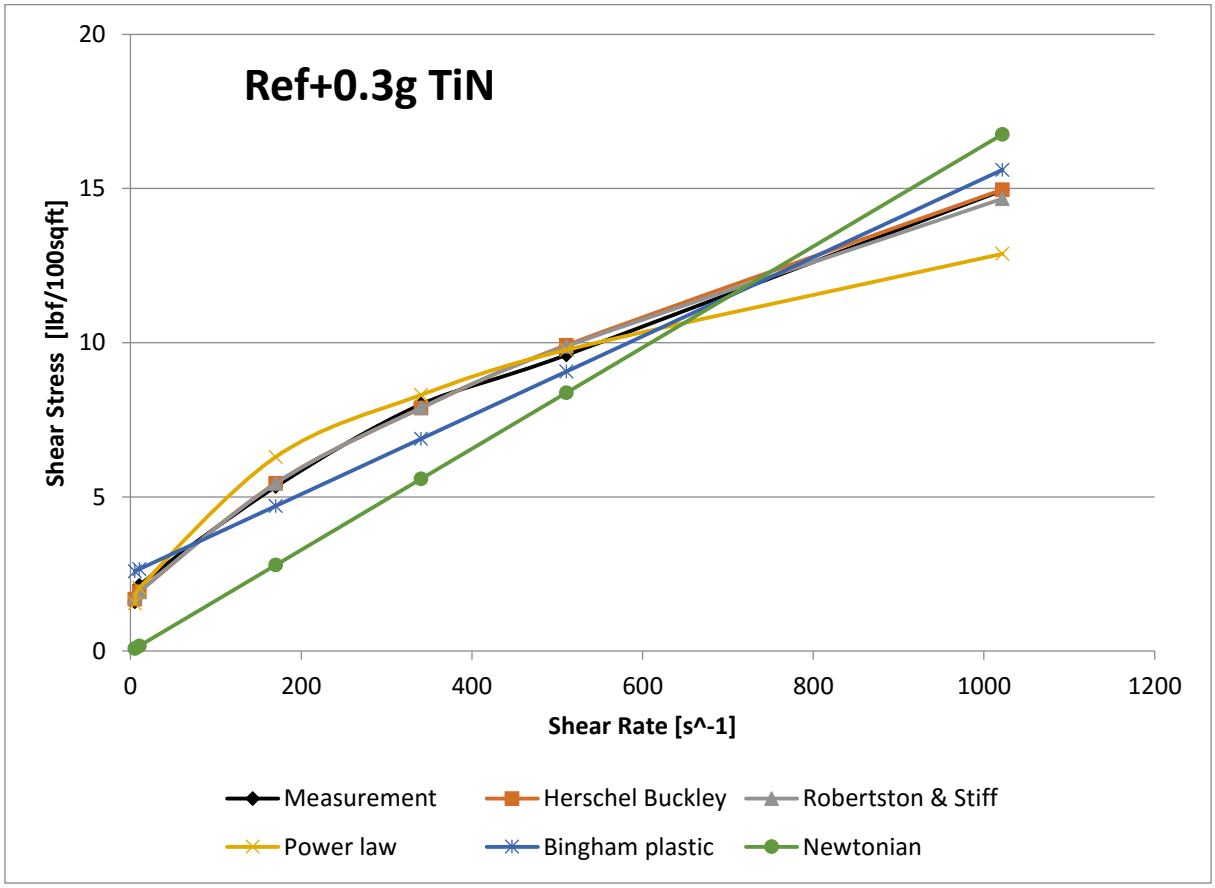

10.4.1.5 Reference Fluid +0.4g TiN

Table 24 Description of rheological models with MoS2-reference fluid output parameters and %-deviation

		Parameters					
Model	Equation	τo,τy, A	k, C	n, B	μp, μ	%-Deviate	cP
Herschel Bulkley	$0.0733*\gamma^{0.92310}+2.347$	0,623	0,1979	0,60270		6,55	
Unified	$2.347+0.0731*\gamma^{0.9235}$	0,534	0,2401	0,5729		6,34	
Power Law	$0.9594*\gamma^{0.5227}$		0,5182	0,458		5,84	
Bingham	$0.0417*\gamma+3.307$	2,066			0,0121	29,51	5,79348
Newtonian	$0.0464*\gamma$				0,0151	46,94	7,22988
Robertson and Stiff	$0.1078*(35.5807+\gamma)^{0.8673}$	0,2952	7,5275	0,5481		7,25	

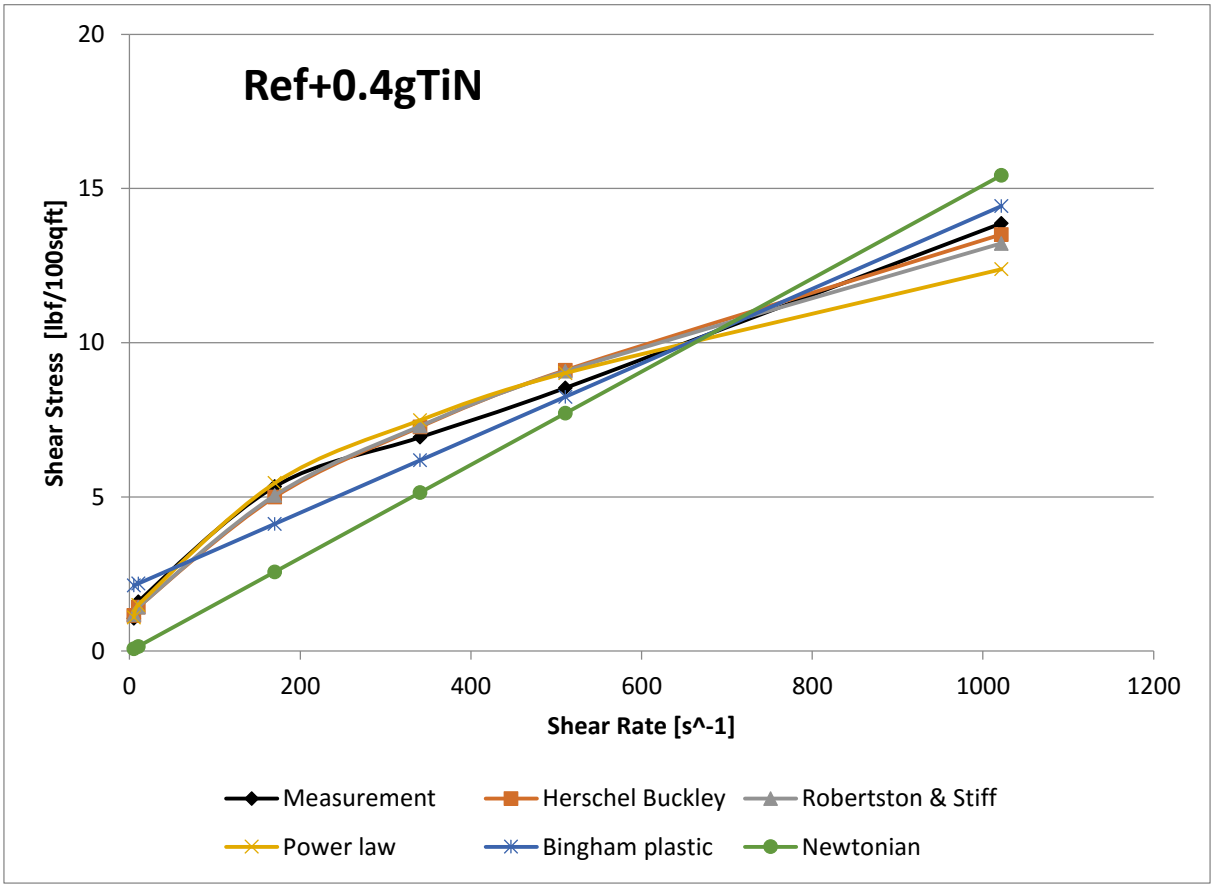

Appendix B Well construction parameters.

Drill string data

String Editor

String Initialization — String Name: Assembly; String (MD): 13523,0 ft; Specify: Top to Bottom; Import String

Library — Export; Import

	Section Type	Length (ft)	Measured Depth (ft)	OD (in)	ID (in)	Weight (ppf)	Item Description
1	Drill Pipe	12964,00	12964,0	5,000	4,000	28,26	Drill Pipe 5 in, 25.60 ppf, E, 5 1/2 FH, P
2	Heavy Weight	120,00	13084,0	6,625	4,500	70,50	Heavy Weight Drill Pipe Grant Prideco, 6 5/8 in, 70.50 ppf
3	Jar	33,00	13117,0	6,500	2,750	91,79	Hydraulic Jar Dailey Hyd., 6 1/2 in
4	Heavy Weight	305,00	13422,0	5,000	3,000	49,70	Heavy Weight Drill Pipe Grant Prideco, 5 in, 49.70 ppf
5	Sub	5,00	13427,0	6,000	2,400	79,51	Bit Sub 6, 6 x 2 1/2 in
6	MWD	85,00	13512,0	8,000	2,500	154,36	MWD Tool 8 , 8 x 2 1/2 in
7	Stabilizer	5,00	13517,0	6,250	2,000	93,72	Integral Blade Stabilizer 8 1/2" FG, 6 1/4 x 2 in
8	Sub	5,00	13522,0	6,000	2,400	79,51	Bit Sub 6, 6 x 2 1/2 in
9	Bit	1,00	13523,0	10,625		166,00	Tri-Cone Bit, 0,589 in²

Hole data

Hole Section Editor

Hole Name: Hole Section; Import Hole Section

Hole Section Depth (MD): 13523,0 ft; Additional Columns

	Section Type	Measured Depth (ft)	Length (ft)	ID (in)	Drift (in)	Effective Hole Diameter (in)	Friction Factor	Linear Capacity (bbl/ft)	Item Description
1	Casing	4012,5	4012,50	12,615	12,459	12,615	0,52	0,1547	13 3/8 in, 54.5 ppf, J-55,
2	Open Hole	13523,0	9510,50	12,615		12,615	0,52	0,1546	
3									

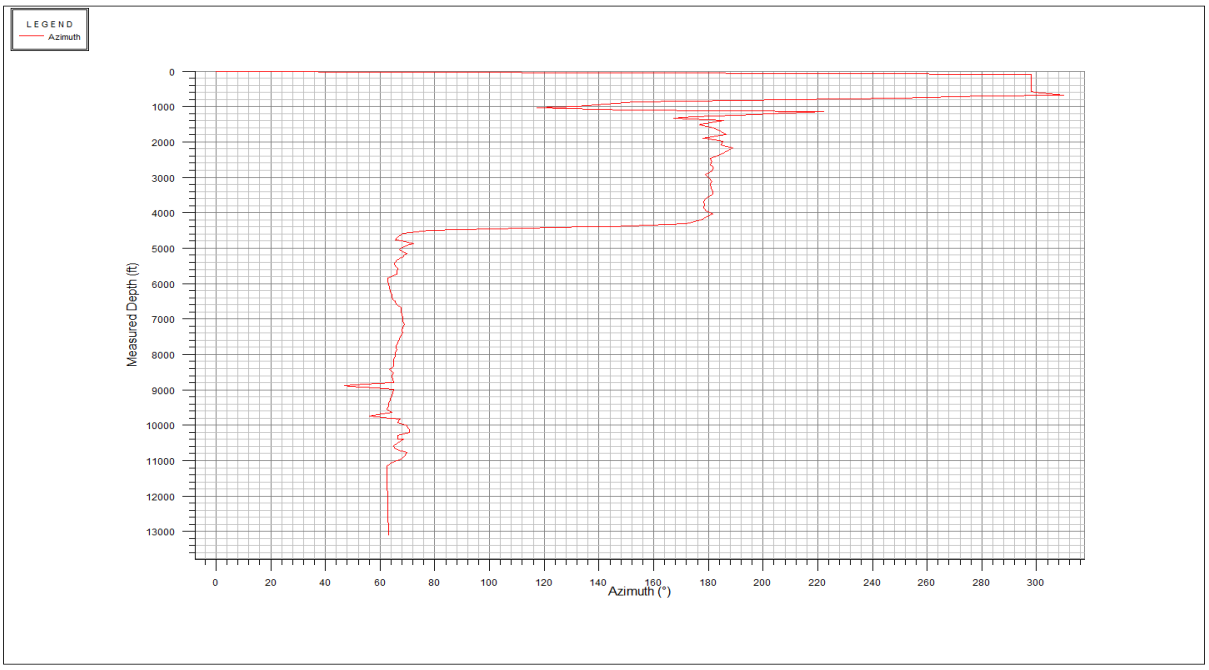
LEGEND
Azimuth
Measured Depth (ft)
0
1000
2000
3000
4000
5000
6000
7000
8000
9000
10000
11000
12000
13000
0
20
40
60
80
100
120
140
160
180
200
220
240
260
280
300
Azimuth (°)

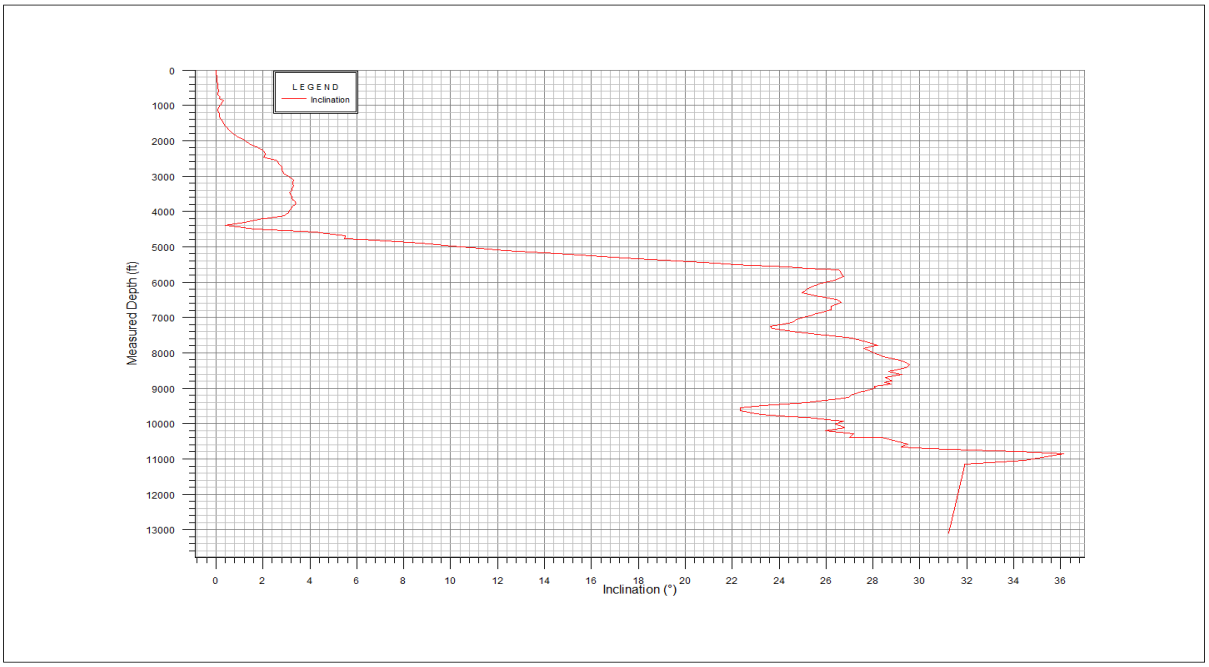
LEGEND
Inclination
Measured Depth (ft)
0
1000
2000
3000
4000
5000
6000
7000
8000
9000
10000
11000
12000
13000
0
2
4
6
8
10
12
14
16
18
20
22
24
26
28
30
32
34
36
Inclination (°)

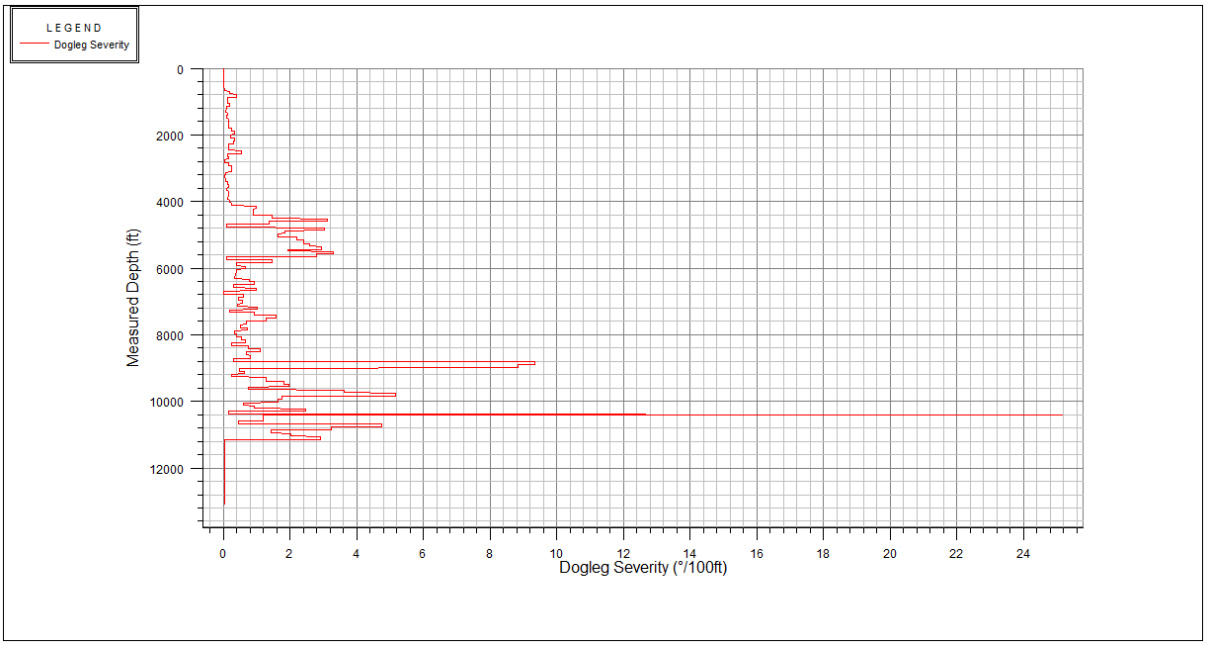
LEGEND
Dogleg Severity
Measured Depth (ft)
0
2000
4000
6000
8000
10000
12000
0
2
4
6
8
10
12
14
16
18
20
22
24
Dogleg Severity (°/100ft)

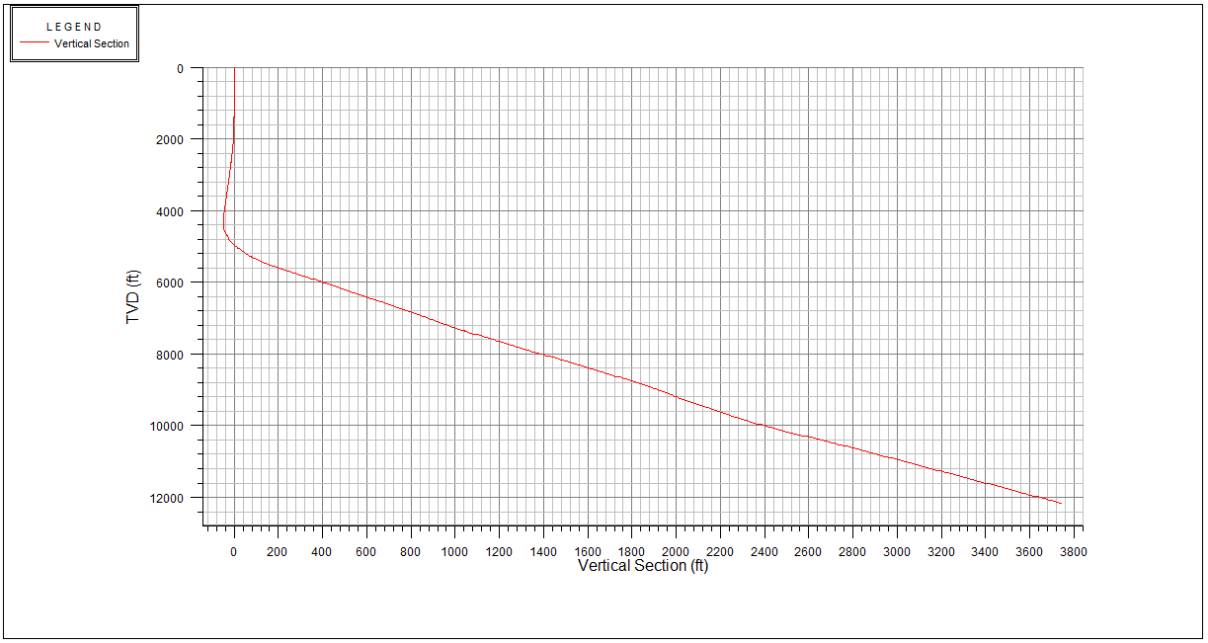
LEGEND
Vertical Section
TVD (ft)
0
2000
4000
6000
8000
10000
12000
0
200
400
600
800
1000
1200
1400
1600
1800
2000
2200
2400
2600
2800
3000
3200
3400
3600
3800
Vertical Section (ft)

Appendix C:

10.5 Effect of nano free (Ref CMC) and Ref CMC +0.4tm MoS2

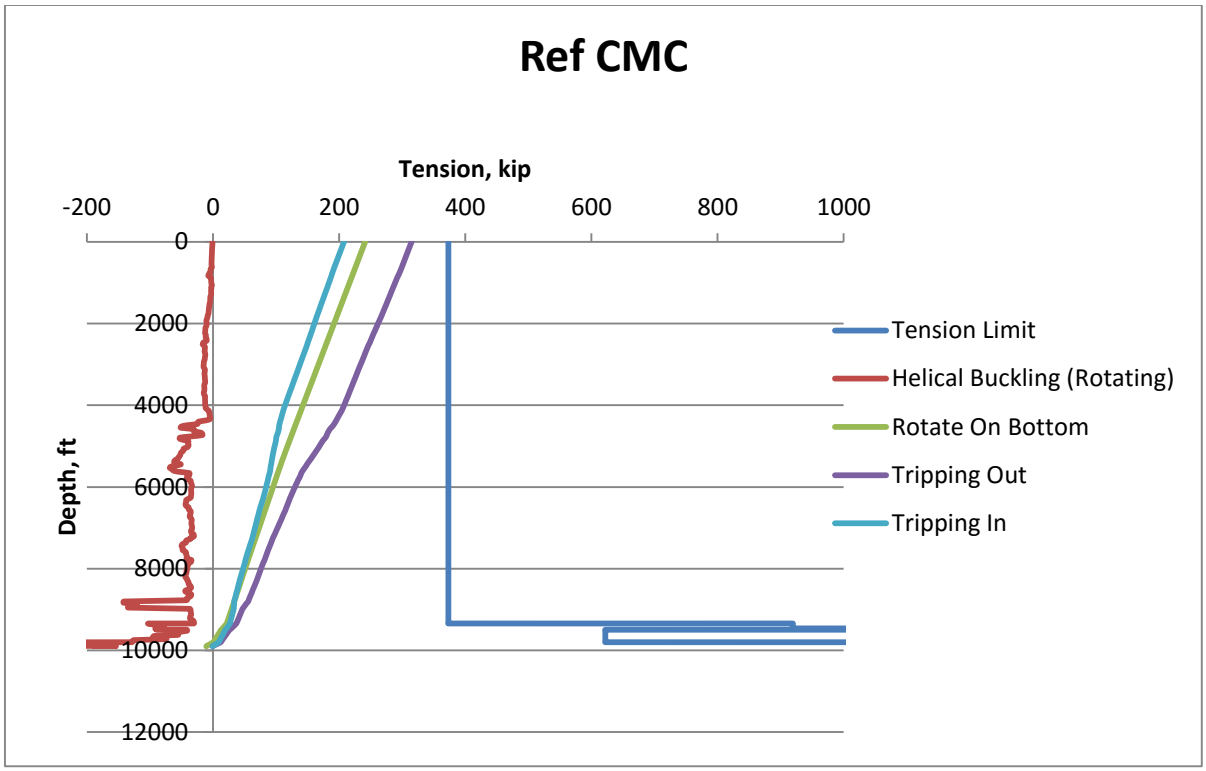

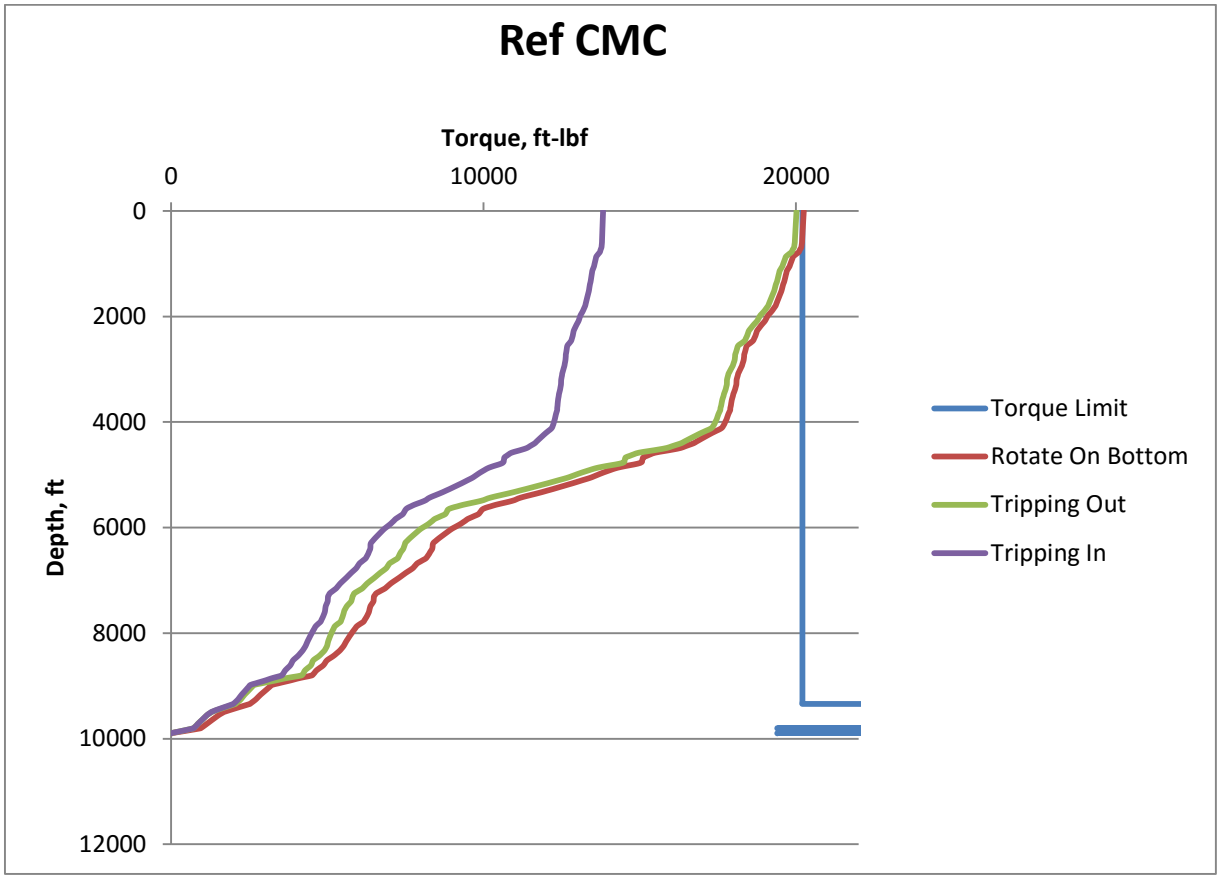
Ref CMC
Torque, ft-lbf
0
10000
20000
Depth, ft
0
2000
4000
6000
8000
10000
12000
Torque Limit
Rotate On Bottom
Tripping Out
Tripping In

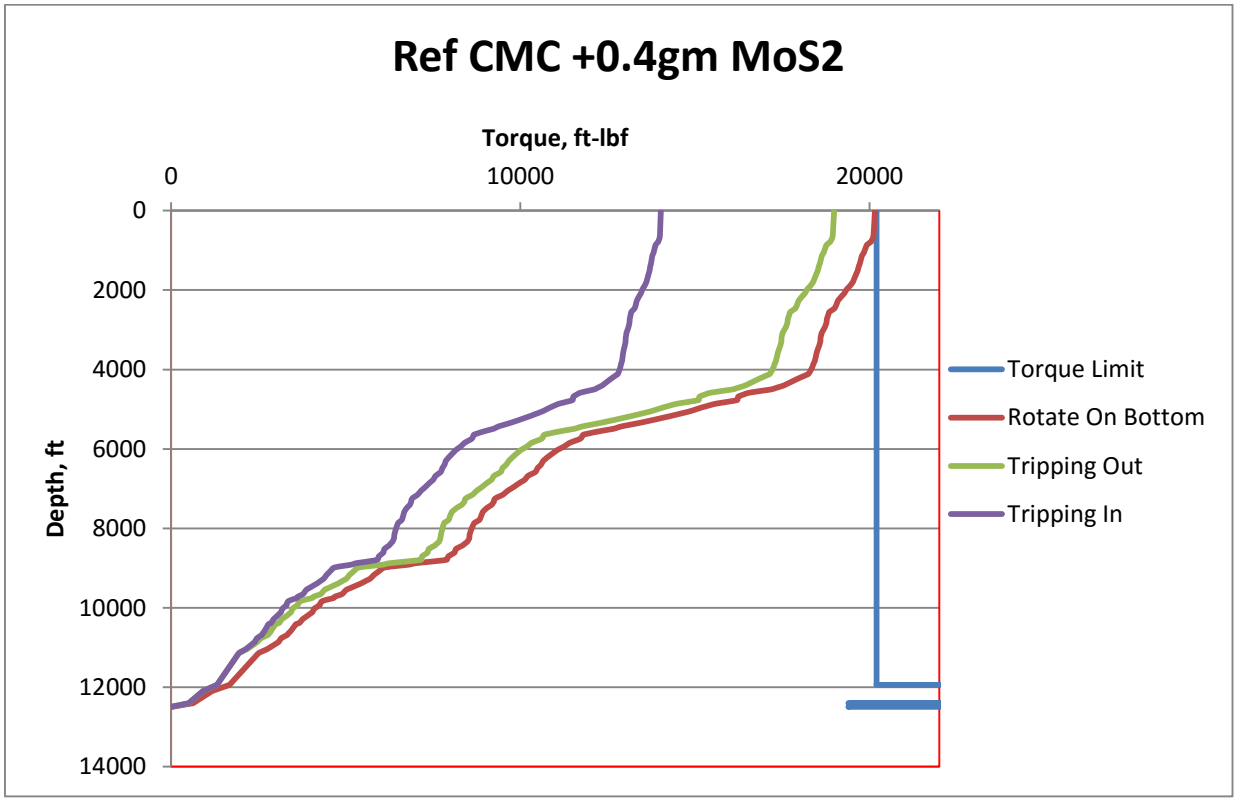
Ref CMC +0.4gm MoS2
Torque, ft-lbf
0
10000
20000
Depth, ft
0
2000
4000
6000
8000
10000
12000
14000
Torque Limit
Rotate On Bottom
Tripping Out
Tripping In

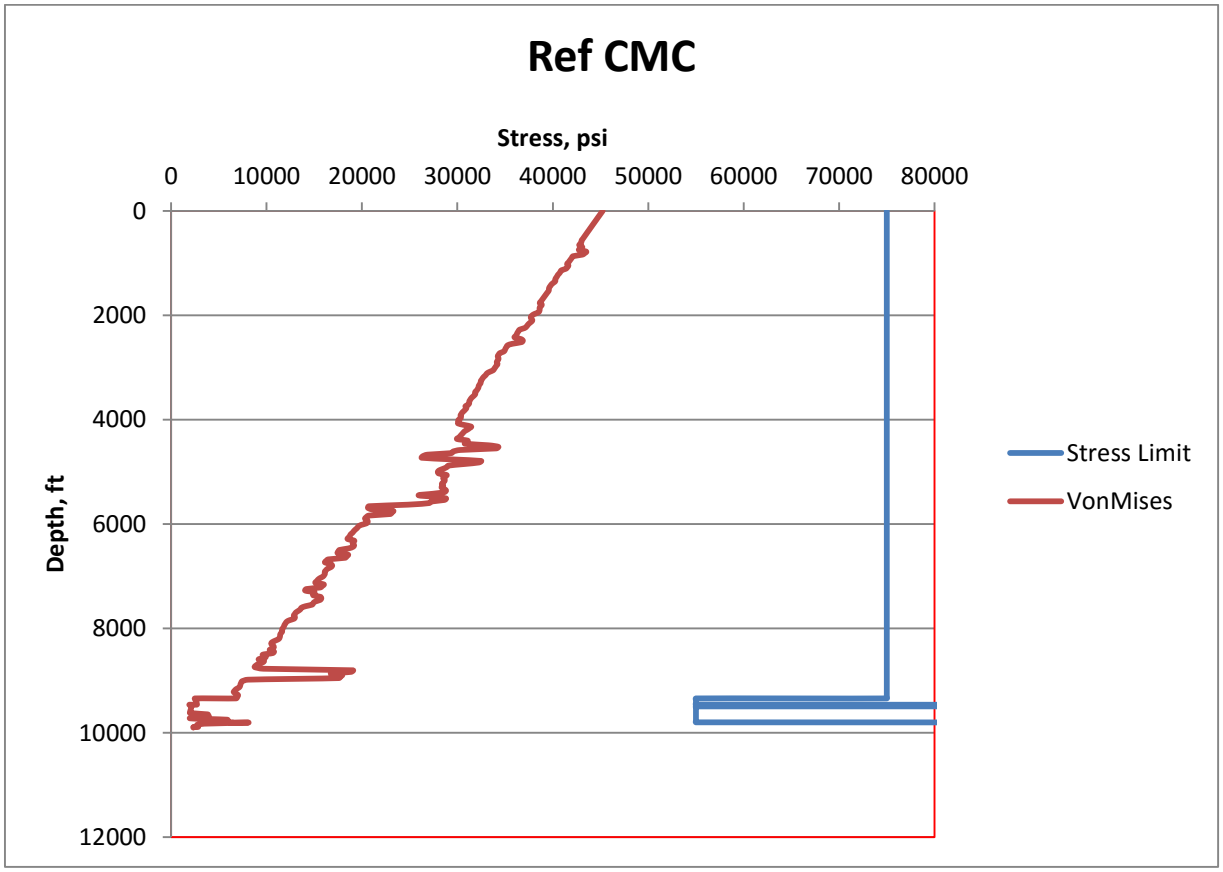
Ref CMC
Stress, psi
0
10000
20000
30000
40000
50000
60000
70000
80000
Depth, ft
0
2000
4000
6000
8000
10000
12000
Stress Limit
VonMises

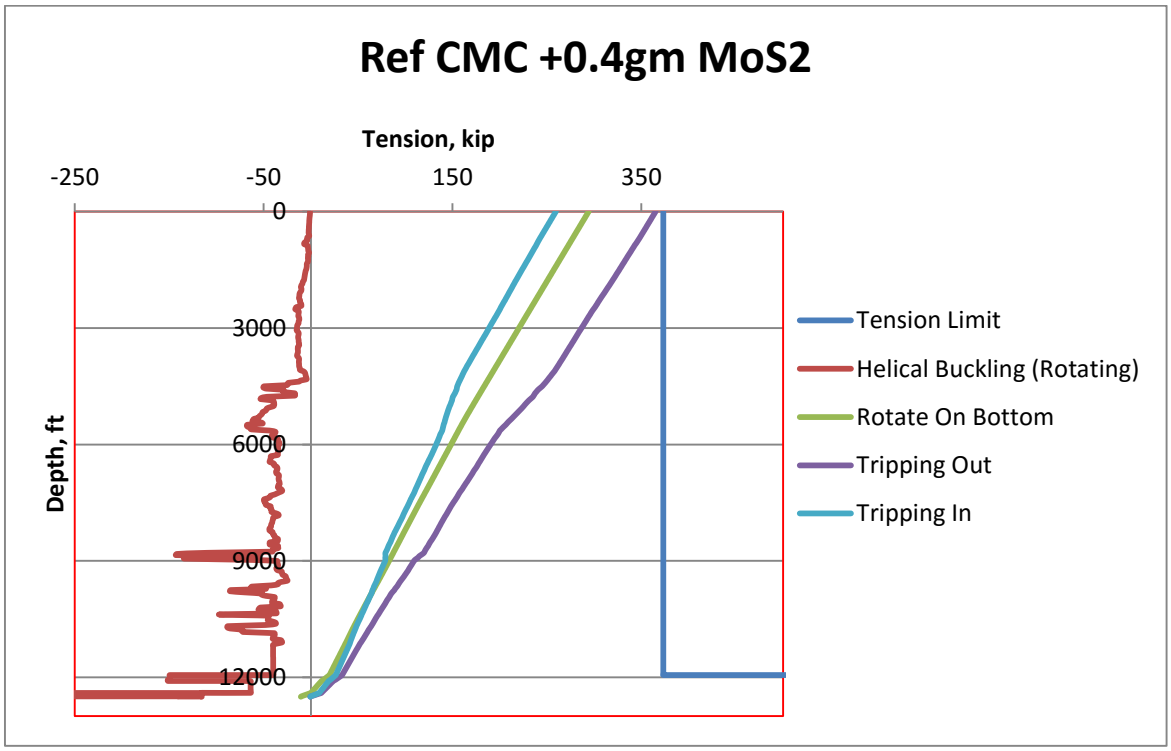
Ref CMC +0.4gm MoS2
Tension, kip
-250
-50
150
350
Depth, ft
0
3000
6000
9000
12000
Tension Limit
Helical Buckling (Rotating)
Rotate On Bottom
Tripping Out
Tripping In

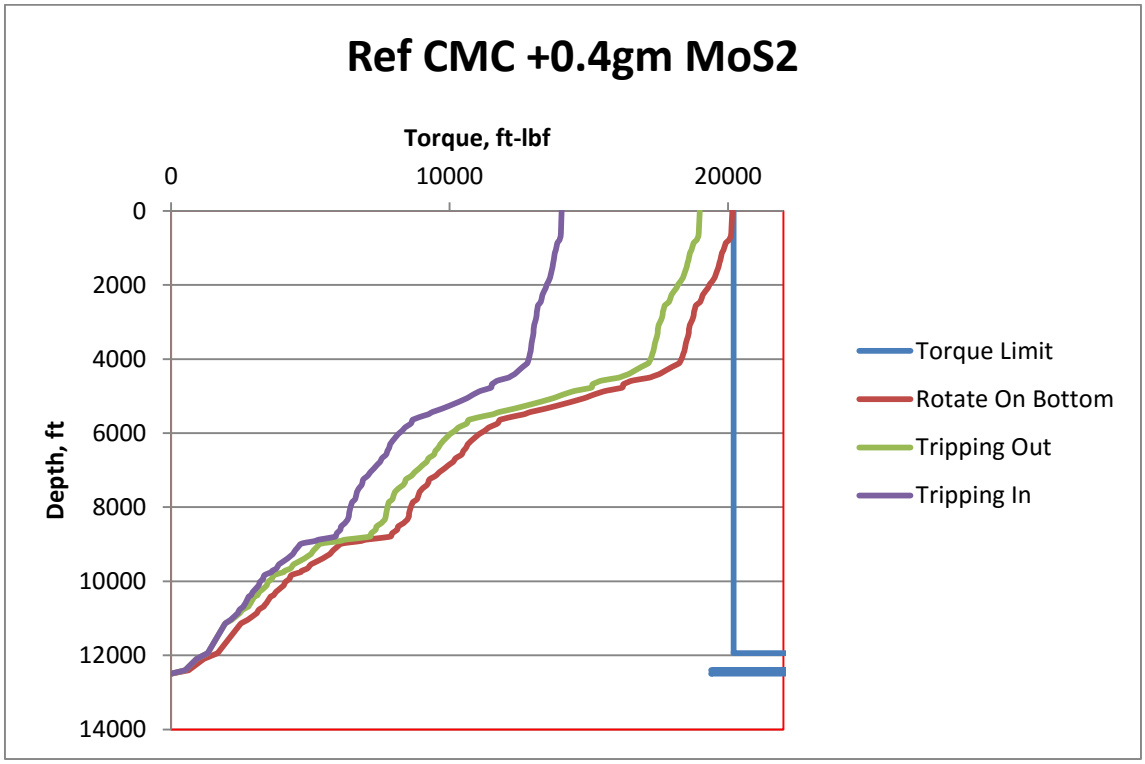

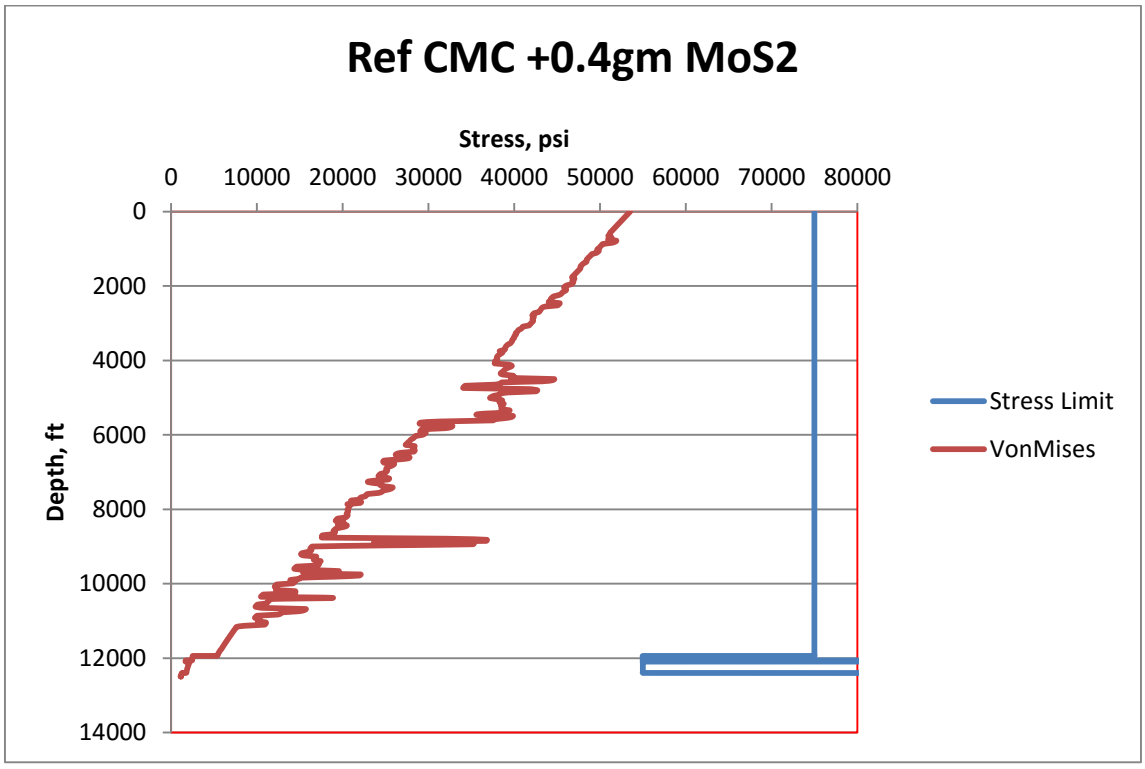

10.6 Effect of nano free (Ref XG) and Ref XG +0.1tm Graphene

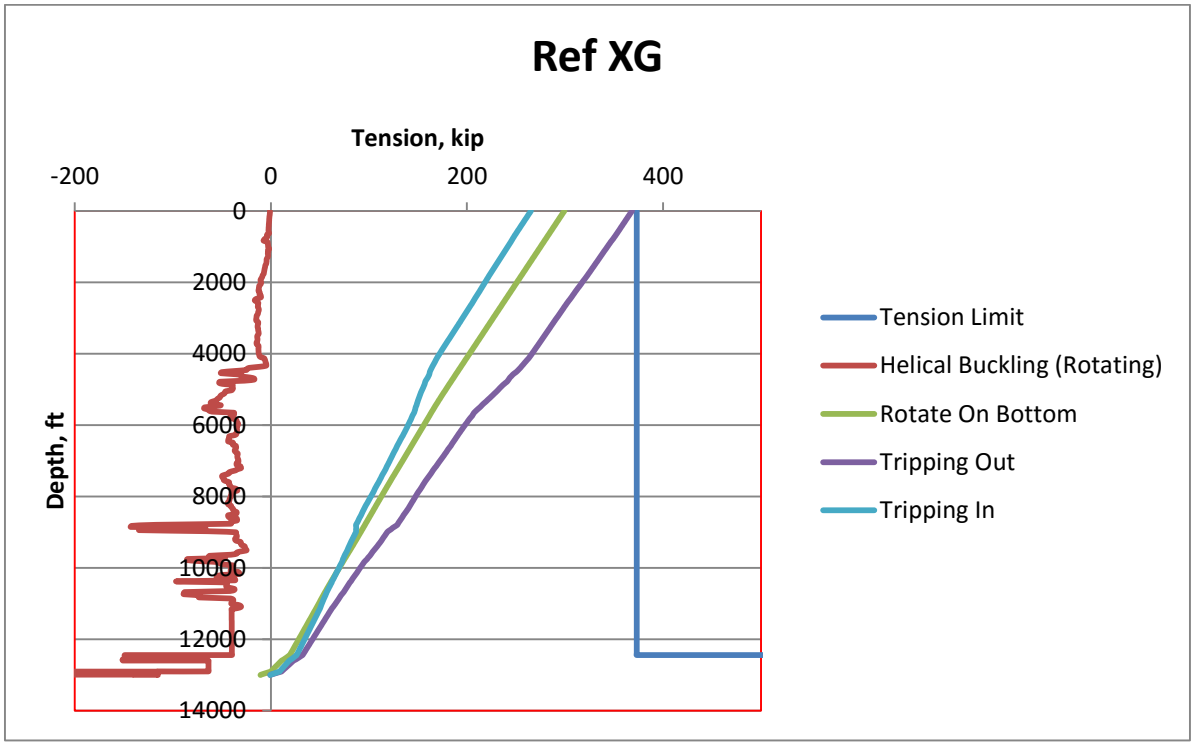
Ref XG
Tension, kip
-200
0
200
400
Depth, ft
0
2000
4000
6000
8000
10000
12000
14000
Tension Limit
Helical Buckling (Rotating)
Rotate On Bottom
Tripping Out
Tripping In

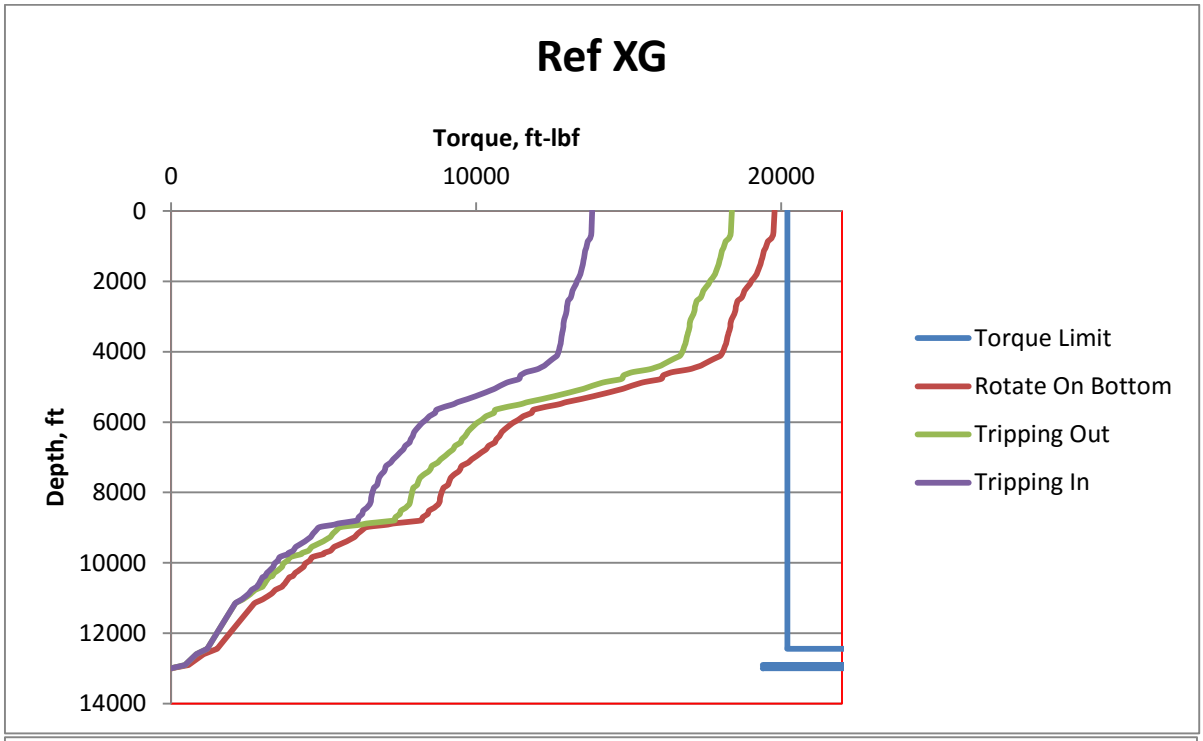
Ref XG
Torque, ft-lbf
0
10000
20000
0
2000
4000
6000
8000
10000
12000
14000
Depth, ft
Torque Limit
Rotate On Bottom
Tripping Out
Tripping In

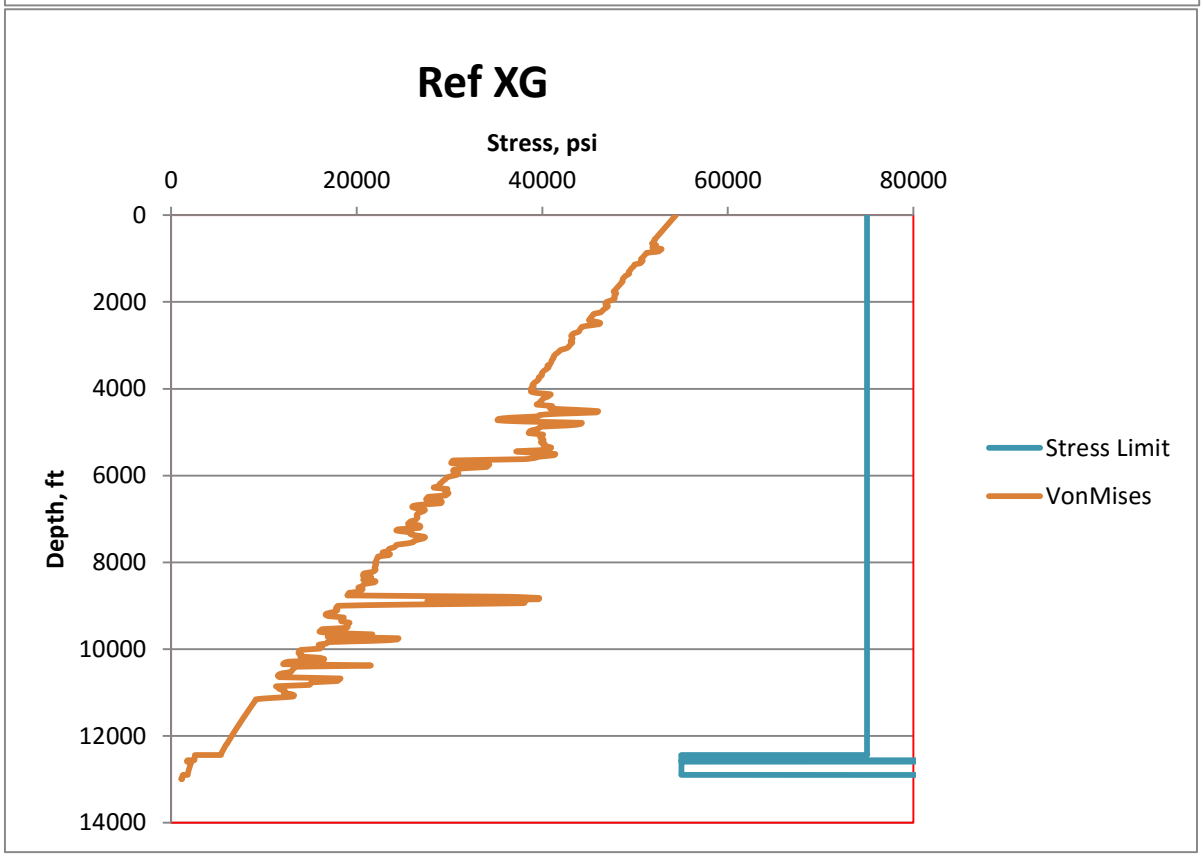
Ref XG
Stress, psi
0
20000
40000
60000
80000
0
2000
4000
6000
8000
10000
12000
14000
Depth, ft
Stress Limit
VonMises

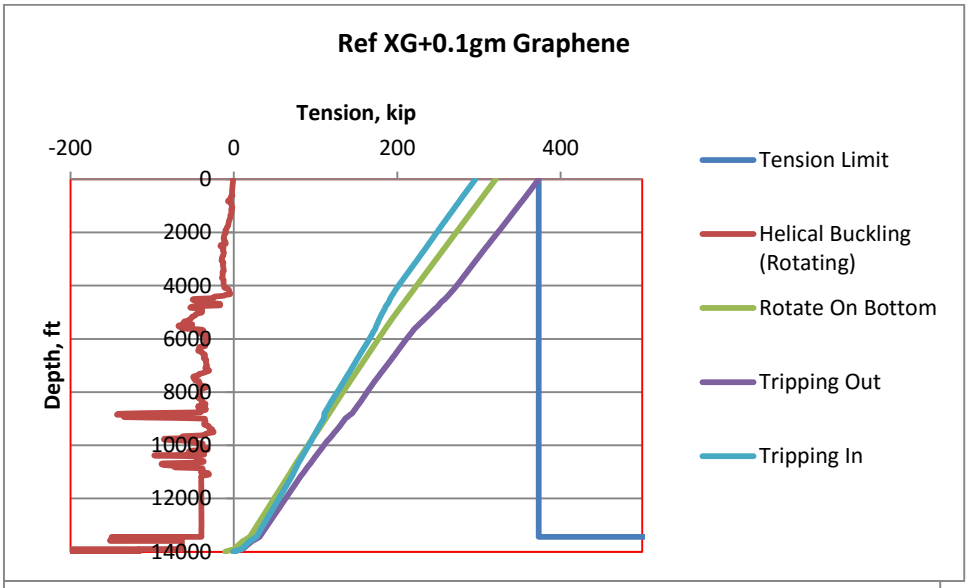
Ref XG+0.1gm Graphene
Tension, kip
-200
0
200
400
0
2000
4000
6000
8000
10000
12000
14000
Depth, ft
Tension Limit
Helical Buckling (Rotating)
Rotate On Bottom
Tripping Out
Tripping In

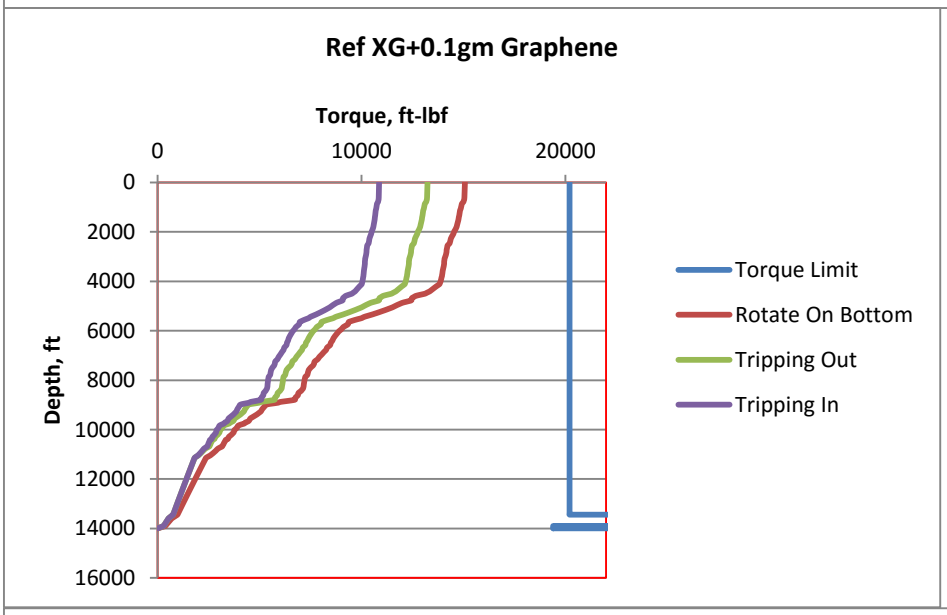
Ref XG+0.1gm Graphene
Torque, ft-lbf
0
10000
20000
0
2000
4000
6000
8000
10000
12000
14000
16000
Depth, ft
Torque Limit
Rotate On Bottom
Tripping Out
Tripping In

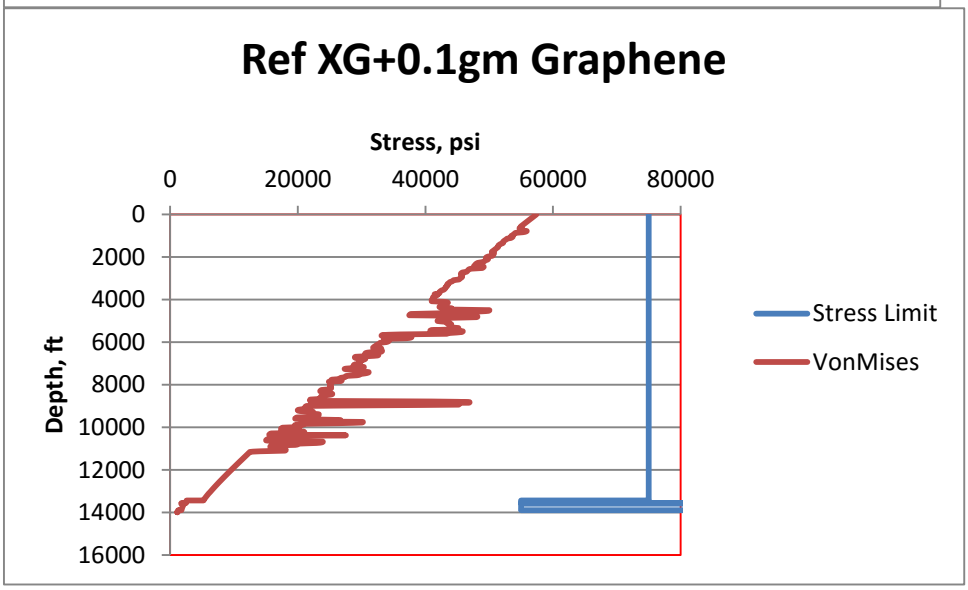
Ref XG+0.1gm Graphene
Stress, psi
0
20000
40000
60000
80000
0
2000
4000
6000
8000
10000
12000
14000
16000
Depth, ft
Stress Limit
VonMises

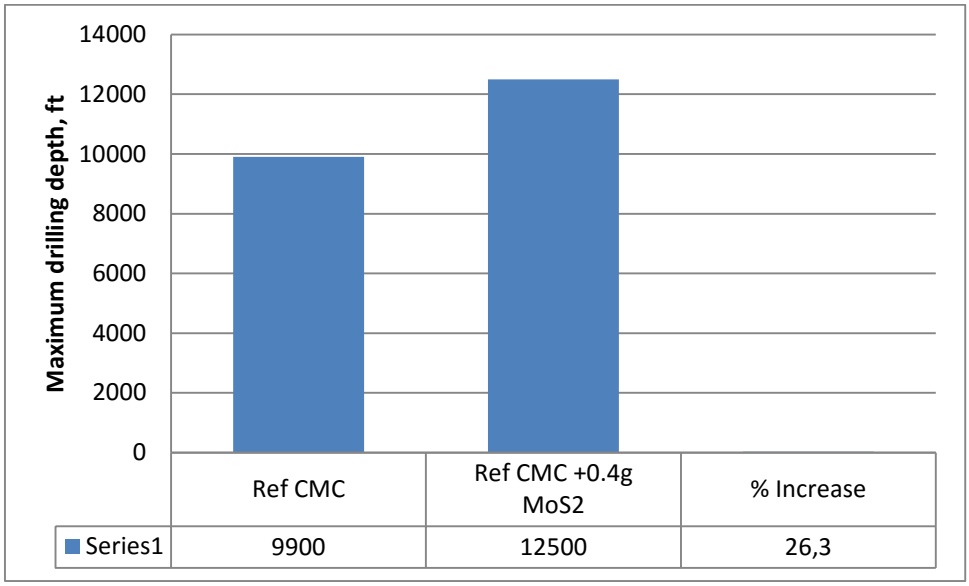
Maximum drilling depth, ft
14000
12000
10000
8000
6000
4000
2000
0
Ref CMC
Ref CMC +0.4g MoS2
% Increase
Series1
9900
12500
26,3

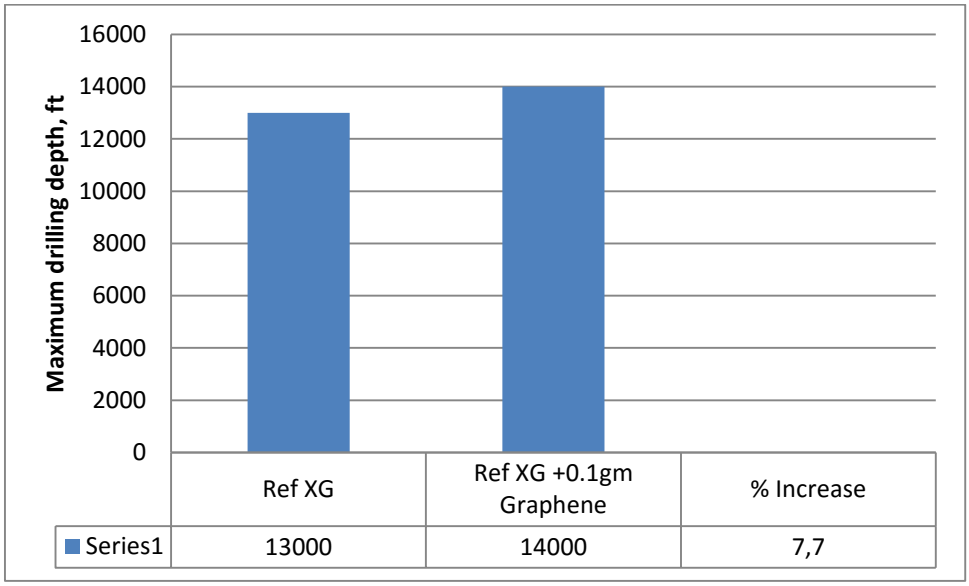
Maximum drilling depth, ft
16000
14000
12000
10000
8000
6000
4000
2000
0
Ref XG
Ref XG +0.1gm Graphene
% Increase
Series1
13000
14000
7,7

List of Symbols

C	Robertson and Stiff stain correction, 1/s
C_d	Bit discharge coefficient which is normally set equal to 0.95.
D	Hydraulic diameter of the pipe, m
G'	Elastic/storage modulus, Pa
G"	Loss /Viscous modulus, Pa
h_{mc}	Thickness of mud cake
k	Consistency factor, lbf/100sqft
μ	Friction coefficient
n	Flow index, a power law exponent.
ΔP_a	Pressure loss, Pa
k	Permeability of mud cake,
ΔP	Differential pressure across mud cake, Pa
t	time of filtrate testing, s
V_C	Cumulative filtrate volume per unit area, cm^3/cm^2
Vsp	Spurt loss, ml
$\bar{V}$	Mean fluid velocity, m/s
μ	Dynamic viscosity of the fluid (Pa·s or N·s/m² or kg/m·s)
ρ	Density of the fluid (kg/m^3)
ρ_{st}	Static mud density (ppg)
γ	Shear rate , 1/s
τ	Shear stress, lbf/100sqft
τ_y	Yield point, lbf/100sqft
μ_p	Plastic viscosity, cP
δ	Phase angle (degree)

Nomenclature

E&P	Exploration and Production
EOR	Enhanced Oil Recovery
HTHP	High Temperature High Pressure
OBM	Oil Based Drilling Mud
NCS	Norwegian Continental Shelf
WBM	Water Based Drilling Mud
ECD	Equivalent Circulating Density
PV	Plastic Viscosity
RPM	Revolutions per minute
SEM	Scanning Electron Microscopy
TVD	True Vertical Depth
XG	Xanthan Gum
YP	Yield Point
AP	Apparent viscosity
YS	Yield Stress
YP -	Yield Point
API -	American Petroleum Institute
CMC	Carboxymethyl Cellulose
ECD	Equivalent circulation density
LVER	Linear Viscoelastic Region
PAC	Polyanionic cellulose
PV	Plastic viscosity
YS	Yield stress
LSYS	Lower shear yield stress
ROP	Rate of Penetration
ppb	Pounds per (oil) Barrel
ppg	Pounds per gallon
gpm	Gallon per minut

List of Figures

List of Tables